Distribution Agreement

In presenting this thesis or dissertation as a partial fulfillment of the requirements for an advanced degree from Emory University, I hereby grant to Emory University and its agents the non-exclusive license to archive, make accessible, and display my thesis or dissertation in whole or in part in all forms of media, now or hereafter known, including display on the world wide web. I understand that I may select some access restrictions as part of the online submission of this thesis or dissertation. I retain all ownership rights to the copyright of the thesis or dissertation. I also retain the right to use in future works (such as articles or books) all or part of this thesis or dissertation.

Signature:

_____ _____

Christopher Edwards May 1st 2025

Primates, Probes, and Protection: Preclinical Evaluation of Antibodies to HIV-1 and SARS-CoV-2 in Rhesus Macaques

By

Chris Edwards

B.A., Washington University, 2018

Program in Immunology and Molecular Pathogenesis
Graduate Division of Biological and Biomedical Sciences

Steven Bosinger, Ph.D.
Advisor

Rama Amara, Ph.D.
Committee Member

Matthew Gardner, Ph.D.
Committee Member

Rui Kong, Ph.D.
Committee Member

Jens Wrammert, Ph.D.
Committee Member

Accepted:

Kimberly Jacob Arriola, Ph.D, MPH
Dean of the James T. Laney School of Graduate Studies

Date

Primates, Probes, and Protection: Preclinical Evaluation of Antibodies to HIV-1 and SARS-CoV-2 in Rhesus Macaques

By

Chris Edwards

B.A., Washington University, 2018

Advisor: Steven Bosinger, Ph.D.

An abstract of
A dissertation submitted to the Faculty of the
James T. Laney School of Graduate Studies at Emory University
In partial fulfillment of the requirements for the degree of
Doctor of Philosophy

Program in Immunology and Molecular Pathogenesis
Graduate Division of Biological and Biomedical Sciences

2025

Abstract

Primates, Probes, and Protection: Preclinical Evaluation of Antibodies to HIV-1 and SARS-CoV-2 in Rhesus Macaques

By Chris Edwards

Broadly neutralizing antibodies (bNAbs) exhibit protective efficacy against HIV-1 infection making them an ideal archetype for HIV-1 vaccine design. Presently, no vaccine candidate has induced bNAbs against neutralization-resistant tier 2 viruses. However, the development of stabilized, native-like envelope (Env) trimers such as BG505.SOSIP.664 has marked a significant advancement in vaccine design, due to their ability to elicit tier 2 neutralizing antibodies (NAbs) in rhesus macaques (RM). NAb development against tier 2 immunogens in RM remains poorly understood, with hypothesized contributions from genetic variation at the IG loci, naive B cell repertoire, and differential gene expression in B cell lineages. To address these knowledge gaps, we have developed a set of BG505.SOSIP.644 probes capable of recovering paired clonotype identity, antigen specificity, and gene expression of B cells in a high throughput fashion. These probes were constructed by conjugating biotinylated BG505.SOSIP.644 to streptavidin covalently linked to both sc-RNA-Seq compatible DNA oligonucleotides and flow cytometry compatible fluorophores. Using these reagents, we isolated and sequenced BG505.SOSIP.644 specific memory B cells from an RM developing high titers of neutralizing antibodies. To benchmark the accuracy of our technology, we compared our recovered heavy and light chain sequences to those identified from the same animal using conventional methodology and successfully recovered 100% of previously identified NAbs. We then applied this technology to recover BG505.SOSIP.644 specific memory B cells from 5 additional vaccinated RMs, and cloned 34 antibodies for functional characterization. Our approach will allow for high-throughput analysis of the evolution of Env specific lineages in both RM and humans in response vaccination with HIV-1 Env immunogens, including BG505.SOSIP.644.

The continued evolution of SARS-CoV-2 variants capable of subverting vaccine and infection-induced immunity suggests the advantage of a broadly protective vaccine against betacoronaviruses (β-CoVs). Recent studies have isolated monoclonal antibodies (mAbs) from SARS-CoV-2 recovered-vaccinated donors capable of neutralizing many variants of SARS-CoV-2 as well as other β-CoVs. Many of these mAbs target the conserved S2 stem region of the SARS-CoV-2 spike protein, rather than the receptor binding domain contained within S1 primarily targeted by current SARS-CoV-2 vaccines. One of these S2-directed mAbs, CC40.8, has demonstrated protective efficacy in small animal models against SARS-CoV-2 challenge. As the next step in the pre-clinical testing of S2-directed antibodies as a strategy to protect from SARS-CoV-2 infection, we evaluated the *in vivo* efficacy of CC40.8 in a clinically relevant non-human primate model by conducting passive antibody transfer to RM followed by SARS-CoV-2 challenge. CC40.8 mAb was intravenously infused at 10mg/kg, 1mg/kg, or 0.1mg/kg into groups (n = 6) of RM, alongside one group that received a control antibody (PGT121 10mg/kg). We observed a significant reduction in viral loads, inflammatory cytokines, and inflammatory

macrophages within the lower airway of animals infused with 10mg/kg and 1mg/kg doses of CC40.8, and viral genome sequencing revealed a lack of escape mutations in the CC40.8 epitope. These data demonstrate the protective efficiency of broadly neutralizing S2-targeting antibodies against SARS-CoV-2 infection within the lower airway while providing critical preclinical work necessary for the development of pan–β-CoV vaccines.

Collectively, the results of these studies highlight the power of high-resolution immunoprofiling tools and non-human primate models to advance rational vaccine for two major global pathogens, HIV-1 and SARS-CoV-2, and underscore the potential of broadly neutralizing antibodies to inform next-generation strategies for preventing infection by highly variable viruses.

Primates, Probes, and Protection: Preclinical Evaluation of Antibodies to HIV-1 and SARS-CoV-2 in Rhesus Macaques

By

Chris Edwards

B.A., Washington University, 2018

Advisor: Steven Bosinger, Ph.D.

A dissertation submitted to the Faculty of the
James T. Laney School of Graduate Studies at Emory University
In partial fulfillment of the requirements for the degree of
Doctor of Philosophy

Program in Immunology and Molecular Pathogenesis
Graduate Division of Biological and Biomedical Sciences

Acknowledgements:

This work is dedicated to the countless scientists who came before me, who dared to chip away at the unknown even when the world chipped away at them.

I want to thank my parents, Peggy Sutko and Don Edwards, who fostered a love of learning that I will carry with me forever. Your love and support throughout my education has been invaluable.

To my sibling Ethan, I am so inspired by your courage and your kind heart. I am endlessly proud to be your brother.

I want to thank my friends, especially Yuzuka, Jeff, Graham, Ben, and Ayesha. You've each taught me to find joy in so many areas of my life- a skill graduate school could never come close to teaching me. I am so grateful for every one of my friends- I carry each of you with me no matter how far apart we are.

I would like to thank all of the Bosinger Lab members, past and present, especially Thang, Curtis, Kirti, Elijah, Michelle, Stacey, Amit, Nagarajan, and Sydney. Amit and Nagarajan, this work would not have been possible without your patient mentorship and expertise. Michelle, thank you for being my first mentor during my training. I am constantly inspired by your approach to science, and I am grateful for every bit of knowledge and every skill I have gleaned from you. Stacey, thank you for fostering a welcoming, organized, and fun environment in the lab, it has been a privilege being your coworker and more importantly, your friend. Kirti and Elijah, I am so proud of the work we did together, and I can't imagine being part of a better team. Thang and Curtis- thank you for bringing so much laughter to every day we shared in (and outside of) lab, I am lucky to call you each my friend.

Finally, I would like to thank my advisor, Steve. Your mentorship the last 4 years has been transformative for me. Thank you for being my biggest advocate and for giving me so many opportunities to learn and grow. Your dedication to both science and your team are a rare combination we are lucky to be a part of. It is an honor to be your first graduate student and I am so proud of the work I have done under your mentorship.

Table of Contents

Chapter One: Introduction – SARS-CoV-2 | HIV

1.1. Thesis Introduction
1.2. Human Immunodeficiency Virus (HIV-1) and acquired immunodeficiency syndrome (AIDS)
  1.2.1. Virology Overview
  1.2.2. Transmission, Pathogenesis and Progression to AIDS
  1.2.3. HIV-1 Envelope Glycoprotein (Env)
    1.2.3.1. Synthesis, Transport, and Glycosylation
    1.2.3.2. Structure
    1.2.3.3. Function
  1.2.4. Immune Responses to HIV-1
    1.2.4.1. Innate Responses
    1.2.4.2. T cell Responses
      1.2.4.2.1. CD8+ T Cell Responses
      1.2.4.2.2. CD4+ T Cell Responses
    1.2.4.3. Antibody and B cell Responses
      1.2.4.3.1. Broadly Neutralizing Antibodies (bNAbs)
        1.2.4.3.1.1. Target Epitopes
        1.2.4.3.1.2. bNAb Memory B cells
  1.2.5. Anti-Retroviral Therapy and Pre-Exposure Prophylaxis (PreP)
  1.2.6. HIV-1 Vaccine Approaches
    1.2.6.1. CD4 Binding Site
    1.2.6.2. V3
    1.2.6.3. V2
    1.2.6.4. Membrane Proximal External Region (MPER)
    1.2.6.5. Fusion Peptide
    1.2.6.6. Glycans
    1.2.6.7. Combined T + B Cell Vaccines
    1.2.6.8. BG505 SOSIP
1.3. Severe acute respiratory syndrome coronavirus 2 (SARS-CoV-2)
  1.3.1. Origin Transmission and Pathogenesis
  1.3.2. Virology
    1.3.2.1. Replication Cycle
    1.3.2.2. Spike Glycoprotein (S)
      1.3.2.2.1. Neutralizing Epitopes of S
  1.3.3. Immune Responses to SARS-CoV-2
    1.3.3.1. IFN Responses
    1.3.3.2. Macrophage Responses in COVID-19
      1.3.3.2.1. Tissue Resident Macrophages
        1.3.3.2.1.1. Alveolar Macrophages
        1.3.3.2.1.2. Interstitial Macrophages
      1.3.3.2.2. Recruited Monocytes and Macrophages
      1.3.3.2.3. Antibody Dependent Enhancement
    1.3.3.3. Adaptive Immune responses
      1.3.3.3.1. T cell Responses
      1.3.3.3.2. B cell Responses
      1.3.3.3.3. Antibody Responses
  1.3.4. SARS-CoV-2 Vaccines
  1.3.5. Summary

1.1. Thesis Introduction

As globalization increases, the rate at which we respond to infectious disease outbreaks with preventative measures must also increase. Since the rapid spread of SARS-CoV-2 began in the winter of 2019, over 770 million cases have been reported and over 7 million people have died[1]. In response to the global COVID-19 pandemic, the biomedical research community focused on the rapid production of a vaccine, which yielded the revolutionary mRNA-based vaccines in record timing with 95% efficacy[2,3]. But as time progresses, variants of concern have arisen after accumulating key mutations in the spike protein- the sole target of neutralizing antibodies[4]. As these variants arise, we must be able to quickly identify the epitopes of antigen specific B cells and verify the neutralizing ability of their associated antibodies.

Conversely, since the start of the HIV-1 pandemic in 1981 there have been no HIV-1 vaccines that have successfully prevented infection in humans above a modest efficacy[5-8]. In 2023 an estimated 1-1.7 million people became newly infected with HIV, highlighting the urgent need for a prophylactic vaccine to combat the ongoing health crisis[9]. This thesis will illustrate how recent developments in single cell barcoding technologies can be used to investigate the development of potent neutralizing antibodies against HIV-1 envelope immunogens in rhesus macaques (RMs), the gold standard preclinical model for studying HIV-1[10]. It will also investigate the *in vivo* efficacy of coronavirus bNAb CC40.8 in a clinically relevant non-human primate model by conducting passive antibody transfer to RMs followed by SARS-CoV-2 challenge. These studies will inform the design of vaccine constructs, help us gain a deeper understanding of antibody

responses to viral proteins, and demonstrate the effectiveness of antigen barcoding techniques in streamlining the identification and evaluation of neutralizing antibodies.

1.2. Human Immunodeficiency Virus (HIV) and Acquired Immunodeficiency Syndrome (AIDS)

1.2.1. Virology Overview

HIV-1 is a retrovirus that consists of 2 copies of its single stranded RNA (ssRNA) genome encased in a protein capsid within a spherical envelope[11-13]. The conical capsid is formed from around 1200 subunits of the capsid protein (CA) and contains the reverse transcriptase (RT) and integrase (IN) enzymes[14,15]. The capsid connects with the matrix (MA) protein which forms a discontinuous shell associated with the inner leaflet of the infected host cell derived lipid envelope[16]. This envelope is acquired during budding of virions and contains approximately 10 trimers of the only external viral envelope protein, Env[17-19], as well as host derived cell surface proteins. The viral proteins Vpr, Nef, and the precursors to Gag have been shown to associate with components of the virion during packaging[20-23].

After initial contact between host adhesion molecules and Env trimers, the gp120 domains of Env trimers on virions make contact with CD4 surface receptors. CD4 is most commonly expressed on the surface of CD4+ T cells, with certain macrophages and other myeloid lineage subsets also expressing the receptor[24-26]. Upon binding, the gp120 subunits undergo a confirmational change that exposes the coreceptor binding site[27,28]. Once exposed, this site can bind primarily either CCR5 or CXCR4 surface receptors, with several other chemokine receptors serving as alternative receptors[29-32]. Binding of the coreceptor to the coreceptor binding site leads to another confirmational change in the

gp41 subunit, resulting in insertion of a fusion peptide into the cell membrane, and subsequently, the fusion of the viral and host cell membranes[33]. Fusion of these 2 membranes results in the release of the viral capsid, which uncoats in the nucleus, releasing the viral genome and the viral RT and IN enzymes[34-37].

In the cytosol, the RT enzyme produces a complimentary DNA strand from the genomic viral RNA, forming an RNA-DNA hybrid. RT then degrades the remaining RNA strand and generates a corresponding, complimentary DNA strand. The DNA polymerase activity of RT enzyme is highly error prone, with 0.1-1 mutations introduced each time the genome is replicated[38]. The now double stranded DNA (dsDNA) proviral genome associates with both host and viral factors to form the pre-integration complex (PIC), including both IN and Vpr[39-42]. IN and Vpr each contain nuclear localization sequences, which direct the PIC to the nucleus while Vpr also induces arrest of the cell cycle[43,44]. Once in the nucleus, IN facilitates the integration of the dsDNA proviral genome nonspecifically, and the latency phase of the viral replication cycle can begin, with memory CD4+ T cells forming the largest reservoir of latently infected cells[45-47]. During latency, the virus will remain transcriptionally silent until the memory T cell is activated, with the factors that reverse latency are still under investigation[48].

Once viral transcription has been initiated by recruitment of RNA polymerase II (RNA Pol II) to the 5' long terminal repeat (LTR) of the integrated viral genome, inefficient transcription leads to very few full-length viral mRNA transcripts capable of undergoing splicing[49]. Expression of the viral protein Tat from the few complete transcripts that are formed during this phase allows for stabilization of the viral mRNA elongation by recruitment of elongation factors and stabilization of RNA Pol II[50]. The increase in viral

mRNA increases the number of transcripts that undergo both partial and complete splicing[51]. Completely spliced mRNAs are exported to the cytoplasm where they are translated into viral proteins including Rev, which mediate export of the unspliced and partially spliced viral mRNA transcripts[52]. The unspliced transcripts are translated into Gag-Pol polyproteins, while the partially spliced transcripts are translated into Vpu and Env[53] at the ER, where Env will be heavily glycosylated and undergo trimer formation[54,55]. Gag polyproteins will associate at the cell surface membrane, where they associate with unspliced viral genomic RNA and facilitate budding[56-58]. Viral factors Nef and Vpr associate with the budding virion, and following scission, the viral protease (PR) acts on the polyproteins within envelope in a process called maturation[20,59]. During maturation the capsid is formed around the viral genome following rearrangement of the internal viral proteins, resulting in a complete, infectious particle[60,61].

1.2.2. Transmission and Pathogenesis

Viremic individuals can harbor HIV-1 in blood, semen, vaginal secretions, and breastmilk- which has resulted in several known routes of transmission. HIV-1 is primarily transmitted to uninfected individuals via sexual contact at mucosal surfaces with infected individuals or through exposure to infected blood while less common transmission can occur during either childbirth or breastfeeding[11,62-65]. Heterosexual intercourse between HIV-1 positive and negative individuals has around a 0.1% chance for viral transmission, a rate which can be affected by factors such as male circumcision and the presence of genital ulcers[66,67]. Additional factors affecting transmission include the viral load of the infected individual and integrity of the mucosae at the site of exposure, with most infections occurring from either cell free or cell associated virions[68,69].

HIV-1 infection is typically established by one or by a few quasi-species within the wide genetic range of viruses present during chronic infection[70-72]. These founder viruses preferentially use CCR5 as their coreceptor, compared to the CXCR4 tropic viruses that often dominate later during the onset of AIDS[73-75]. Dendritic cells present at the site of infection are often the first cells to make contact with transmitted/founder (T/F) viruses[76], driven by associations between cell surface molecule DC-sign and the gp120 trimers[25,77]. These dendritic cells can disseminate the virus by carrying it to the draining lymphoid tissues, where the virus can infect reservoirs of CCR5+ CD4+ T cells[28,78]. After the initial CD4+ T cell infection by T/F viruses, the virus disseminates systemically through the lymphatics within 6 to 7 days[79]. During this period, the virus can replicate in CD4+ memory T cells present within the gut associated lymphatic tissue (GALT). Depletion of GALT CD4+ memory T cells is observed in both in rhesus macaques infected with SIV and humans with HIV-1[80,81]. The chronic immune activation, infection, and depletion CD4+ memory T cells results in rapid establishment of latent HIV-1 reservoirs within memory T cells and yields the infected individual vulnerable to opportunistic infections at later points during chronic infection[82]. During this acute phase, the infected individual often experiences flu like symptoms but remains PCR negative for detectable virus anywhere from 7 to 21 days following infection[83,84]. At around 21-28 days, the viral load peaks and then settles to what is referred to as the “set point,” which the virus can maintain for up to several years[85]. Only around 0.5% of people living with HIV-1 are able to self-limit the viral load to less than 50 viral copies per mL in peripheral blood, which allows them to maintain their CD4+ T cell counts and prevent the progression to AIDS[86]. These individuals are known as “elite controllers.”

During the chronic phase of infection in non-elite controllers, the virus continues to replicate within CD4+ T cells until less than 200 CD4+ T cells per uL of plasma remain- the clinical threshold for the onset of AIDS[87]. The speed at which this threshold is reached is correlated inversely with magnitude of the viral set point[88], and is also affected by HLA type[89,90] and age[91]. The onset of AIDS is associated with opportunistic infections, virally associated cancers, and shift from CCR5 to CXCR4 tropic viral quasispecies[92-98].

1.2.3. HIV-1 Envelope Glycoprotein (Env)

1.2.3.1. Synthesis, Transport, and Glycosylation

Env is produced as a polyprotein precursor within the endoplasmic reticulum (ER) known as gp160, which is later separated via protease cleavage to the receptor binding subunit, gp120, and membrane spanning subunit, gp41[99,100]. After oligomerizing in the ER[101], gp160 is trafficked through the golgi to the cell surface via a signal peptide at its N terminus[102], where it is cleaved by cellular furin proteases to gp120 and gp41[103-105]. Env undergoes heavy N-linked glycosylation, leading to a glycan shield of high mannose and complex N glycans that contribute to approximately half of its molecular weight[106,107]. The mechanism of Env incorporation into budding virions is still under investigation, as there is evidence of passive incorporation[108-110], direct incorporation through gp41 Gag interactions[111], and indirect incorporation via host adaptor protein binding to Gag and Env[112]. Studies have also revealed that HIV-1 virions incorporate host molecules at the membrane or at the cytoplasmic sites, in some cases with maintained biological activity[113-116].

1.2.3.2. Structure

A fully functional Env trimer contains 3 heterodimers of the receptor binding domain (RBD) containing subunit gp120, and the membrane spanning base subunit gp41 held together via noncovalent interactions[117]. gp120 can be broken down into 5 regions of conserved amino acid sequence noted as C1-C5, with 5 variable regions found in-between, V1-V5[118,119]. The gp120 structure can also be broken down into the inner core and outer loops, which are largely formed by the constant and variable regions respectively[120,121]. The C and N termini of gp120 form a beta sheet that mediates the noncovalent binding to gp41[122]. The trimer apex is formed by the V1/V2 hypervariable loop, with the V3 loop making contact with the V2 of adjacent heterodimers[123]. The CD4 binding site is located below these V loops, and contains highly conserved, discontinuous sequences within gp120[124,125]. Disulfide bonds maintain much of both the gp120 core structure as well as the V1-V4 loops[120]. The Env trimer fluctuates between a stable closed confirmation and an open conformation that is unstable in the absence of CD4 and subsequent coreceptor binding[126-128]. Such shifts are mediated by the movement of 3 mobile regions of the inner domain of gp120[122], which occlude the conserved epitopes of the CD4 binding site when in the closed confirmation[129]. The gp41 subunit of Env is made up of 3 distinct regions: the ectodomain that associates with gp120 ($gp41_{ecto}$), the transmembrane (TM) domain, and the cytoplasmic tail (CT) domain[130]. The N terminus of the $gp41_{ecto}$ contains the hydrophobic fusion peptide as well as a heptad repeat that helps facilitate trimerization[131] and membrane fusion[132].

1.2.3.3. Function

The balance of high mannose N-linked glycans and complex N-linked glycans of gp120 facilitate binding to DC-Sign on the surface of dendritic cells without

internalization[133], so that the dendritic cells may disseminate the virus particles to target CD4+ cells without being endocytosed or degraded[134]. The binding of CD4 by Env stabilizes its open conformation, allowing for further conformational changes that expose the coreceptor binding site near the V3 loop[121,135]. Once a coreceptor is engaged at this site, additional conformational changes mediate insertion of the fusion peptide into the target cell membrane, which allows the heptad repeats of the $gp41_{ecto}$ domain to pull the virus envelope and cell membrane into close proximity[132,136]. Upon fusion the viral capsid is passed into the cytosol where it is uncased, beginning the processing of viral replication[137].

1.2.4. Immune Responses to HIV-1

1.2.4.1. Innate Responses

The first systemic signs of an innate immune response to infection occur around days 5-7 prior to detection of the virus in plasma. Sentinel cells including plasmacytoid dendritic cells (pDCs) release anti-HIV-1 cytokines after detecting the virus via PRRs such as TLR7[138]. Activation of the innate immune system results in elevated levels of acute phase proteins such as serum amyloid A[139]. The inflammatory cascade of IL-15 and type I IFN activates antiviral NK cells, which are among some of the first cells to respond to the infection[140]. NK cells have shown to be active and highly cytolytic during this phase, with elite controllers exhibiting higher levels of NK cell reactivity and killing[141,142]. Several HLA alleles associated with control of HIV-1 infection show preferential binding to activating receptors on the surface of NK cells[143].

Macrophages are susceptible to HIV-1 infection, forming alternative viral reservoirs and contributing to inflammation following infection[144]. These macrophages exhibit

dysfunction and are resistant to killing via granzyme release by NK and CD8+ T cells[145]. Tissue resident macrophages form an early viral reservoir, and have been shown to drive viral rebound following cessation of ART in humanized mice[146]. HIV-1 has been detected within several tissue macrophage subsets of virologically suppressed individuals, including the brain, lung, and urethral tract[147-151]. Proinflammatory cytokines from macrophages and circulating monocytes can prime NK cells for stronger anti-HIV-1 responses, including IL-23, IL-18, IFN-B and IL-15[152].

1.2.4.2. T cell Responses

1.2.4.2.1. CD8+ T Cell Responses

Activated HIV-1 specific CD8+ T cells with upregulated perforin and granzyme b are detectable within the blood around 3 days post infection, their numbers increasing in magnitude during the following 2 weeks[153-155]. While this peak in CD8+ T cell responses results in reductions of overall viral load, it also serves as the first selective pressure on the population of viral quasi species, resulting in escape mutants capable of evading the concurrently activated CD8+ T cell subsets[156-158]. While acute phase CD8+ T cell responses target Nef and Env, subsets targeting Gag and Pol are arise later during the chronic phase and maintain the viral set point[159]. This set point has also been found to correlate with certain HLA types[154]. During the chronic phase, the repertoire of the CD8+ T cell responses diversifies and becomes enriched with T cells targeting epitopes more conserved across quasispecies[160]. The potency and speed of the CD8+ T cell responses targeting such epitopes has been found to correlate with better viral control resulting in a lower magnitude of the viral set point[161].

The progressive dysfunction and exhaustion of CD8+ T cells during chronic infection is driven by the persistence of antigen[162]. The first signs of CD8+ T cell exhaustion arise during the acute phase of infection, characterized by an impaired ability to proliferate in response to antigen and reduced expression of activation and degranulation markers[163]. The upregulation of exhaustion marker PD-1 on HIV-1 specific CD8+ T cells can also be quantified during acute infection[164]. During chronic infection, cytolytic activity of these cells is further diminished, which is thought to drive progression of HIV-1 infection[153,165,166]. However, while their ability to kill infected cells may be dysfunctional, CD8+ T cells have also been shown to suppress active HIV-1 replication via non-cytolytic mechanisms, such as cytokine expression[167-170]. CD8+ T cell dysfunction is intertwined with the simultaneous CD4+ dysfunction that occurs during infection, yielding inadequate helper T cell functions during both acute and chronic phases.

1.2.4.2.2. CD4+ T Cell Responses

During acute HIV-1 infection, the cytokine storm prompted first by DCs and then monocytes, macrophages, NK cells, and T cells likely contribute to the irreversible depletion of CD4 T lymphocytes from the lymphoid tissues of the gastrointestinal tract[171,172]. During this phase, the intense inflammation due to viral replication in the large CD4+ T cell reservoirs of the gut can lead to damage of the mucosal barriers, promoting leakage of bacterial products that further induce immune activation and CD4+ T cell death[173]. Despite drops in viral load within the blood during the end of acute infection, the virus still actively replicates into the chronic phase in CD4+ T cells within the lymphoid tissue[174]. Within the lymph node (LN), CD4+ regulatory T cells accumulate in response to the widespread inflammation, and drive collagen deposition. This fibrosis reduces the

production of survival signals such as IL-7, fueling a feedback loop that diminishes the levels numbers of naive T cells in the LNs and circulation which drives further loss of IL-7 producing cells[175,176]. The generalized immune activation simultaneously drives expansion of CD4+ follicular helper T cells (TFHs) within the LN, which have been identified as a major HIV-1 reservoir as CD8+ T cells are excluded from the germinal center[177-179]. Compared to non-TFH CD4+ cells, TFHs have higher levels of associated HIV-1 mRNA and DNA[178], and in RM, following CD8+ depletion of elite SIV controllers, TFHs redistribute the virus to non-TFH CD4+ cells, triggering viral rebound[180]. Despite the contributions to the viral reservoir, the frequency and functionality of antigen specific TFH cells correlates with bNAb development[181]. However, as most patients do not develop bNAbs, and exhibit dysfunctional B cell responses to non-HIV-1 antigens, CD4+ TFHs exhibit continued dysfunction from acute through chronic infection[182].

1.2.4.3. Antibody and B cell Responses

B cell dysfunction has been documented in both acute and chronic phases of HIV-1 infection. During acute infection, the widespread activation of CD4+ T cells can lead to hypergammaglobulinemia[183], while the frequency and functionality of memory B cells responding to non-HIV-1 pathogens are altered during the chronic phase[184]. Anti-gp41 non-neutralizing antibodies are first detected within virion-IgM/IgG immune complexes around 1 week following detection of virus within the plasma[185]. IgM and IgG3 antibodies with low frequencies of SHM are enriched within the early anti-HIV-1 antibody repertoire, suggesting a germinal center (GC) independent mechanism of short-lived plasma cells[186-188]. The altered repertoires observed during acute infection are likely due to the destruction of the lymphoid tissue where GC formation would occur[189]. Additionally, highly

mutated non-neutralizing antibodies specific for gp41 were found to be produced by plasma cells circulating in the blood[190]. These plasma cells derive from gut microbiota specific memory B cells residing in the terminal ileum[191]. This phenomenon is theorized to drive antigenic sin during HIV-1 vaccine studies away from protective antibody development[192].

1.2.4.3.1. Broadly Neutralizing Antibodies (bNAbs)

Because of the rapid evolution of env epitopes driven by the high mutation rate of HIV-1 genome replication, mutations that escape host neutralizing antibody responses continually arise, preventing viral control in the majority of infected individuals[193-197]. In addition to point mutations, the hypervariable V1-V5 regions of Env are prone to indels and can vary greatly in length even within chronic infection stemming from a singular founding virus[198]. Only an estimated 15-30% of individuals develop bNAbs capable of neutralizing over 90% of circulating viruses, and typically only arise over a year following infection[193]. Interestingly, infants and children living with HIV-1 seem to develop bNAbs that arise more quickly and with fewer mutations from germline than adults, although the mechanism is still under investigation[199,200]. When individuals do develop serum with broad neutralizing capacity, the breadth can largely be attributed to one or two antibody specificities[201-205].

bNAb development in chronically infected and viremic individuals likely results at least in part from altered phenotypes of memory B cells and TFHs. Studies have found correlations between higher viral loads during infection and the neutralizing breadth of the generated antibody repertoire, despite the loss and altered function of CD4+ T cells[206-208]. bNAbs also exhibit higher rates of polyreactivity (reacting to self and non self-

antigens) than non-neutralizing antibodies[209], which has been theorized to contribute to the difficulty in generating bNAbs via vaccination in healthy individuals[210-212]. HIV-1 infection has been shown to alter the immune tolerance mechanisms reigning in auto and polyreactive B cells, lending a broader B cell repertoire containing bNAb precursors [213,214].

Another difficulty of bNAb generation lies in both the magnitude and frequency of mutations required for their maturation from germline. During GC responses, antigen specific B cells undergo successive rounds of clonal expansion, affinity maturation, and selection[215-220]. Within GCs, activation-induced cytidine deaminase (AID) introduces somatic hypermutation (SHM) in immunoglobulin (Ig) genes, leading to the generation of B cells with higher-affinity antibodies through selection by follicular dendritic cells and T follicular helper cells[221]. Mutations within Ig genes have varying degrees of "intrinsic mutability," meaning certain mutations within an Ig gene have higher likelihood of arising due to the activity of AID[222-225]. bNAbs often require highly improbably mutations during their maturation, likely contributing to their difficult elicitation[222]. Studies have shown that these improbable mutations can be selected for with the correct ligand, providing foundational support for the rational design of germline and B cell lineage targeting vaccine strategies[226,227].

1.2.4.3.1.1. Target Epitopes

bNAbs can be roughly divided into 7 classes depending on the region of the target epitope within Env: the V1V2 trimer apex (containing the V2 glycan site), the V3 high-mannose patch, the CD4 binding site (CD4bs), the gp120-gp41 interface, and the membrane proximal region (MPER), the fusion peptide, and the silent face [228,229]. These epitope regions exhibit varying degrees of accessibility, impacting the characteristics of

the corresponding binding class of bNAbs. For comparably accessible epitopes such as the V3 mannose patch, bNAbs exhibit a range of binding angles and sub-epitopes and are more common amongst people living with HIV-1[229-232]. The gp120-gp41 interface similarly contains many sub-epitopes for bNAb binding[233-235]. However, other epitopes such as the CD4 binding site constrict bNAb diversity through constrained angles and deep epitope pockets[236-238]. The long glycan chains present on the V1V2 apex select for bNAbs with long CDRH3 containing anionic residues, while MPER directed mAbs often contain hydrophobic surfaces and long variable looks capable of interacting with epitopes contained within lipid membranes[239-247]. Serological analysis of patients with highly neutralizing antibody activity against HIV-1 also revealed that the majority of bNAbs mapped to epitopes dependent on the presence of glycans [229]. These epitopes include the trimer apex, the high-mannose patch, and the gp41-gp120 interface. V1V2 apex binding bNAbs typically exhibit unusually long, anionic CDRH3[248,249]. While the CD4 binding site does elicit bNAbs, these often require heavy SHM, arising several years into chronic infection[228]. More information on each target epitope and associated bNAbs can be found in section 1.2.6.

1.2.4.3.1.2. bNAb Memory B cells

A vast majority of identified bNAbs to date have been isolated from the memory B cells of people living with HIV-1 that were designated as slow clinical progressors[250-252]. During chronic infection, the majority of circulating HIV-1 specific B cells express either a tissue-like memory phenotype (CD27-, $CD21^{low}$) or an activated memory phenotype (CD27+, $CD21^{low}$), in contrast to the resting memory phenotype of most circulating B cells in HIV-1 infected individuals on ART or in elite controllers[253]. Isolation and subsequent

analysis of bNAb producing B cells from an individual living with HIV-1 with several potent bNAbs revealed that these tissue-like memory B cells were not the source of the bNAbs[254]. Other studies have report similar phenotypes of memory B cells producing bNAbs[204,255,256], which are consistent with the finding that tissue-like memory B cells have lower SHM on average than resting memory B cells[255]. Lineage tracing studies reveal shared clonal lineages between tissue-like memory and resting memory B cell populations, but the forces driving these phenotypes remain to be clearly identified[255].

1.2.5. Anti-Retroviral Therapy and Pre-Exposure Prophylaxis (PreP)

Anti-retroviral agents (ARVs) are therapeutics developed to suppress HIV-1 replication at various points in the viral life cycle. These agents can be combined into a daily regimen to treat people living with HIV-1 called anti-retroviral therapy (ART) and lower the viral load below detectable levels[257,258]. While ART has proven to be highly effective at reducing negative disease outcomes associated with HIV-1 by preventing progression to AIDS, it is not a curative strategy as the cessation of ART results in viral rebound[259]. Even with viral loads suppressed through ART treatment, people living with HIV-1 face increased incidence of noncommunicable disease (NCD) and multimorbidity[260]. Cardiovascular disease, hypertension, chronic kidney disease, dyslipidemia, diabetes mellitus, osteoporotic bone disease, chronic lung, disease and psychiatric illnesses are most commonly observed across patient cohorts, while cancers are the leading cause of death in high-income countries[261-268]. Additional hurdles face individuals acquiring HIV-1 perinatally, including fewer approved antiretrovirals (ARV) for children, increased risk of multiclass ARV drug resistance, neurocognitive deficits, and fewer resources for

navigating socio-economic challenges such as orphanhood, stigma, and financial burden[269-277].

ARVs are broken down into classes based on the step of viral replication they target. Entry inhibitors such as Maraviroc block binding of Env to receptors or coreceptors on host cells[278]. Non-nucleoside reverse transcriptase inhibitors (NNRTIs), such as rilpivirine and dapivirine bind to the allosteric site of the RT enzyme, inhibiting reverse transcription[279], while nucleoside reverse transcriptase inhibitors (NRTIs) such as tenofovir disoproxil fumarate and emtricitabine inhibit RT by binding the nucleoside binding site of the enzyme[280]. Integrase inhibitors like cabotegravir (CAB) block the integration of viral DNA into the host genome by acting on the integrase enzyme[281,282]. Protease inhibitors target the latest stage of viral replication out of all VRAs by inhibiting the proteases responsible for the release of HIV-1 from infected cells[280,283]. Capsid inhibitors, the newest class of ARV for HIV-1, inhibit several viral replication processes by binding directly to the interface between HIV-1 viral capsid protein (p24) subunits and have demonstrated significant efficacy at reducing viral load in patients with multi-drug resistant HIV-1[284,285].

In the face of no viable vaccine interventions, ARV's were investigated as a preventative strategy against acquiring HIV-1. In 2012 the US Food and Drug Administration (FDA) approved coformulated tenofovir disoproxil fumarate and emtricitabine (F/TDF) tablets to be taken orally once daily as treatment for HIV-1 pre-exposure prophylaxis (PrEP) for HIV-1 uninfected adults[259,286-288]. Since its approval, PrEP has shown to be effective at preventing both sexual and mother-to-child-transmission (MTCT), with over 3.5 million people worldwide using oral PrEP in 2023[9]. In

2021, the FDA approved injectable cabotegravir, administered at 2 month intervals for PrEP, boasting superior efficacy compared to standard oral PrEP regimens[281,289]. In 2024, a twice-yearly injectable formulation of the capsid inhibitor lenacapavir demonstrated in a clinical trial remarkable efficacy over daily oral F/TDF and F/TAF regimens, reducing HIV-1 incidence comparatively by 100% in adolescent cisgender girls and young women in South Africa and Uganda[285,290]. The superiority of long acting, injectable formulations over daily oral regimens highlights the role adherence plays in HIV-1 prevention. Should this formulation be approved for PrEP, access and cost will play critical roles in determining its impact on HIV-1 prevention.

1.2.6. HIV-1 Vaccine Approaches

Without widespread access and adherence to PrEP, a successful vaccine will prove critical in the fight to eliminate HIV-1 from the human population. This assertion is supported by the studies demonstrating the protective capacity of bNAbs against simian/human immunodeficiency virus (SHIV) when passively transferred to non-human primates[291,292]. However, the only vaccine study to date to elicit protection, RV144 (NCT00223080) trial of the CRFAE_01 canarypox/gp120 vaccine in Thailand, did so with very modest 31% efficacy at 42 months [5], and was not able to be replicated by subsequent trials HIV-1 Vaccine Trials Network (HVTN) 702 (NCT02968849) and HVTN 705 (NCT03060629)[293,294]. Further studies found that passive transfer of the CD4bs targeting bNAb VRC01 was not able to confer protection against heterologous HIV-1 in humans[292].

The discovery of bNAbs fueled a renewed interest in developing an HIV-1 vaccine, providing a construct, on which to base the rational design of a vaccine immunogen. Current efforts focus on a sequential strategy that employ several HIV-1 immunogens to

target known bNAb precursors and facilitate their affinity maturation[295-301]. Germline targeting studies have shown that both precursor prevalence and antigen affinity determine the fitness of B cells within germinal centers, and that reducing off-target antigen binding increases the relative fitness of such precursors[302-304].

1.2.6.1. CD4 Binding Site

2 classes of bNAbs have been found to target the CD4 binding site (CD4bs) that have informed HIV-1 vaccine design: CD4 mimics and HCDR3-binder bNAbs. CD4 mimics are bNAbs that engage the CD4 contact residues within Env primarily with their HCDR2 loops, compared to the long HCDR3 loops that form contact with CD4bs in HCDR3-binder bNAbs[204,205,238,305,306]. VRC01 class bNAbs are designated as CD4 mimics, and due to their high potency and breadth, as well as the higher relative precursor frequency, have informed the design of immunogens that have been tested in clinical trials[307].

Germline-targeting immunogen eOD-GT8 binds inferred VRC01 unmutated common ancestors (UCA) with high affinity and has shown to expand B cells bearing BCRs with characteristics of VRC01 precursors in humans[222,299,307]. However, the Antibody Mediated Protection (AMP) trials in South Africa, showed that passive infusion of VRC01 alone yielded no overall protection from HIV-1 infection[292,308,309]. The AMP study reported that the titer of VRC01 needed for protection from sensitive viruses was 1:200, and that the diversity of clinically relevant HIV-1 strains was greater than anticipated[292]. Together these findings suggested that vaccine eliciting VRC01 class bNAbs would be insufficient without targeting of other neutralizing epitopes and would need to elicit and maintain high titers of bNAbs to confer protection[310,311]. The

8ANC131/CH235 class of CD4bs mimics has been shown to elicit CH235 precursors in RM and select for improbable mutations necessary to achieve heterologous neutralization[312,313], and unlike VRC01 bNAbs, 8ANC131/CH235 class bNAbs do not require highly improbably insertions or deletions[223,314].

Several HIV-1 clade C Env immunogens have been designed based on a transmitted/founder gp120 Env termed CH505 T/F trimer to elicit CH103 class CDRH3-binder bNAb precursors[315,316]. Unlike in preclinical models, however, the CH505 T/F gp120 monomer failed to expand CDRH3-binder bNAb CH103 UCA in HVTN 115 trial (unpublished results)[296]. A follow-up study to assess the effects of affinity on bNAb UCA expansion, HVTN 300, was subsequently initiated, investigating a near-native stabilized CH505 T/F trimer with higher affinity for the CH103 UCA[317].

1.2.6.2. V3

The V3 glycan patch, located at the base of the V3 loop between two N-linked glycans at positions 301 and 332, is targeted by 6 currently known prototypic classes of bNAbs encoded by various VH segments, likely due to increased accessibility compared to other regions like the CD4bs[230,318]. Long HCDR3 segments are observed across classes to extend between surface glycans to reach the polypeptide backbone[230]. V3-glycan bNAbs are the most common type of bNAb and have been observed in up to 38% of subjects with high levels of bNAbs in cohorts of sub-Saharan African descent[229]. Despite this, precursors for these bNAbs are rare, as long HCDR3 regions are selected against by immune tolerance mechanisms and require several improbably mutations to achieve breadth[298,319,320]. Studies on RC1 Env, an immunogen that facilitates the

recognition of the V3-glycan patch, in immunized RM revealed that V3 targeting bNAbs depend on a glycan at position 332[321].

1.2.6.3. V2

The V1-V2 apex is among the most sequence-variable regions of HIV-1[322]. When in the prefusion closed confirmation, 3 sets of V1 and V2 loops shield the conserved apex with a dense configuration of N-linked glycans[323]. The V2-glycan bNAb epitope contains an N-linked glycan at residue 160 and a positively charged, lysine rich, exposed C-strand. There are currently five identified prototypic V2-glycan bNAb B cell lineages (PG9, PGDM1400, VRC26.25, CH01 and PCT64), and are characterized by long (24–36 amino acids), negatively charged HCDR3 loops, sulfated tyrosines, and rare precursors[239,242,248,249]. V2-glycan germline-targeting immunogens have not yet been tested in clinical trials, despite documented bNAb generation in SHIV-infected macaques[324], although a V2-glycan UCA-binding Env called MT145KdV5 is currently in production for phase I clinical testing[325].

1.2.6.4. Membrane Proximal External Region (MPER)

Six prototypic bNAb lineages target two distinct portions of the MPER region, the proximal MPER and the distal MPER. Distal targeting MPER bNAbs exhibit some of the most breadth amongst bNAbs, neutralizing approximately 99% of circulating HIV-1 strains[250,316,326]. In addition to long HCDR3s and large numbers of mutations, MPER targeting bNAbs must also bind lipids in the viral membrane to access their cognate epitopes following conformational changes due to receptor mediated Env activation[210,327,328]. Due to these binding constraints, MPER bNAbs exhibit polyreactivity to host lipids as well as to two known host proteins: kynureninase and SF3B3[329,330].

Studies suggest that tolerance to epitopes contained in these proteins likely limits the bNAb response to MPER epitopes, particularly those contained within the distal MPER[329]. Only proximal MPER targeting bNAb precursors have been successfully expanded in clinical trials. In HVTN 133 (NCT03934541), an MPER peptide liposome engaged bNAb precursors targting the proximal 683-LDKW-686 epitope of gp41 (unpublished results)[331]. In contrast, no clinical or preclinical model system has successfully targeted and expanded the precursors of the more potent distal MPER bNAbs.

1.2.6.5. Fusion Peptide

The fusion peptide (FP) is a 15 to 20 hydrophobic structure at the N terminus of the Env-gp41 subunit responsible for mediating type I viral fusion between the viral and host membranes and is exposed to antibody binding on the surface of Env in its prefusion conformation[332-334]. Membrane fusion is triggered by receptor mediated confirmational changes and subsequent cleavage of the envelope precursor, facilitating FP insertion into the host membrane and the formation of a six helix structure that pulls the two membranes together[335]. FP targeting bNAbs such as VRC34.01 do not exhibit enhanced potency or breadth over other HIV-1 bNAbs, but they do not face any known tolerance mechanisms[233,295,336,337]. Preclinical vaccine studies in RM utilizing an FP-carrier immunogen have not specifically targeted germline precursors but instead rely on epitope focusing strategies and have elicited antibodies that neutralize heterologous HIV-1 strains[222,338,339].

1.2.6.6. Glycans

Some bNAbs have been discovered that bind glycans on the surface of Env. bNAb 2G12 binds high-mannose-type glycans through an unusual domain-exchanged heavy

chain configuration, where the VH domain of one Fab arm swaps places with the VH domain of the other Fab arm[340]. Domain-exchanged antibodies exhibit increased rigidity which prevents Fab arms from moving independently and behave more like a bivalent "clamp." This forms an intertwined, domain-exchanged dimer, creating a rigid, "super-Fab" structure, however, domain- exchange is not required for fab dimerization[341,342]. Several fab-dimerized glycan reactive antibodies have been found both in HIV-1 naive macaques and humans, though these have been phenotypically extra-follicular, and may require unique recruitment strategies for their entry into germinal centers[342-344]. These precursors can be expanded in RM when immunized with a glycosylated V3 peptide immunogen and subsequently boosted with protein scaffolded mannose glycans, producing fab-dimerized glycan reactive antibodies[342].

1.2.6.7. Combined T + B Cell Vaccines

Though the primary focus of HIV-1 vaccine development has been the elicitation of bNAbs, T cell mediated vaccine responses to HIV-1 immunogens can work in concert with current strategies. Strong CD4+ TFH responses support sustained GCs necessary for bNAb induction[213,345]. HIV-1 vaccine studies utilizing new adjuvants such as 3M-052 and ionizable LNPs have yielded stronger GC activity and have entered clinical trials[346,347].

Cytolytic CD8+ T cells comprise the other major T cell subset pursued in HIV-1 vaccine development for their anti-viral activity. While preclinical data demonstrates that neutralizing antibodies can protect 90% of RM against rectal SHIV-1 challenge, the titers required are high (greater than 1:500)[348]. T cell targeting vaccines aim to lower the NAb titer threshold required for protection against neutralization sensitive strains[349]. Although

vaccines solely targeting class Ia restricted $CD8^+$ T cell responses have failed to protect against HIV-1 transmission or reduce viral set points following infection in humans, studies in RM have demonstrated that targeting class Ib MHC-E $CD8^+$ T cells can yield a response capable of eliminating virus-infected cells in 55% of SIV infected animals, with ~20% of the infected animals never exhibiting detectable viremia despite repeated challenges with the highly pathogenic SIVmac239 strain[350,351]. It is hypothesized that RhCMV vectored HIV-1 vaccine elicited protection functions similar to ART treatment during early acute HIV-1 infection by inhibiting viral spread and preventing the establishment of the latent reservoir[352]. The first phase I clinical trial investigating a human CMV (HCMV) vectored HIV-1 vaccine recently completed (NCT04725877) and was found to be well tolerated (unpublished results)[353,354]. A second clinical trial investigating an updated vector HCMV with gene deletions and an *mfuse1* insert to broaden the T cell responses is currently underway (NCT05854381)[355].

Synergy between T and B cell vaccines have shown promise in RM preclinical studies. A sequential regimen of 3 different viral vectored vaccines targeting Gag specific CD8+ T cell responses has been shown to reduce the titer of BG505 SOSIP.664 immunogen elicited neutralizing antibodies required for protection from 10 low-dose vaginal BG505 SHIV-1 challenges[356].

1.2.6.8. BG505 SOSIP

Sequential immunization strategies against HIV-1 typically utilize soluble trimers that mimic the native structure of Env within virions at some point within the vaccination regimen. Several approaches have been developed to stabilize the Env protein into a soluble form that resembles the native conformation in order to deliver it as an

immunogen. The first immunogen employing such strategies was BG505.SOSIP.664 which was based on the env isolated from the clade A transmitter/founder virus, BG505[357]. The BG505 virus was isolated from a 6-week-old infant infected via mother-to-child transmission (MTCT), and contains epitopes targeted by several known bNAbs and with relatively low affinity for non-Nabs[358,359]. The SOSIP modification strategy involves the introduction of a disulfide bond (SOS) to link the gp120 and gp41 subunits, an Isoleucine-to-Proline (IP) substitution at position 559 to prevent helix formation and stabilize to the prefusion state, and the deletion of the deletion of the MPER region at residue 664 to improve homogeneity and solubility[359,360]. SOSIP constructs allowed not only for the first cryo-EM and x-ray crystal structures to be generated, they also allowed for detailed identification of epitopes targeted by bNAbs[360,361]. In its next iteration, substitution T332N was introduced to increase the number of bNAb epitopes contained in the immunogen by introducing a glycan commonly targeted by bNAbs[231,359].

Vaccination of RMs with BG505.SOSIP.664.T332N with novel TLR7/8 signaling adjuvant, 3M-052-AF, provided robust protection against autologous intra-vaginal simian-human immunodeficiency virus (SHIV) challenge, which was predicted by high autologous neutralizing antibody titers[348]. NAb targets were largely dominated by responses to a glycan hole near residue 465 across RM, with varying frequencies of NAb responses elicited to a glycan hole at residues 241/289 in V1[362]. This vaccination strategy also resulted in induction of tier 2 IgA NAbs, becoming the first reported immunization to do so in RM[363].

In 2018, BG505.SOSIP.664 entered clinical trials as an HIV-1 vaccine immunogen, combined with several different adjuvants and vaccination regimens (ClinicalTrails.Gov

2025). In the first trial assessing a BG505 SOSIP.664 trimer formulated with an liposome based adjuvant AS01B, IAVI W001 (NCT03699241), the immunogen primarily induced base-directed serum antibodies without any detectable neutralization of tier 2 viruses[364]. In a subsequent trial, HVTN 137 (NCT04177355), trimeric BG505 SOSIP.664 gp140 was formulated with, 3M-052-AF and/or alum for a first-in-human study[365]. This adjuvant, which has been shown to induce persistent long-lived plasma cells and high autologous tier 2 Nab titers in nonhuman primates by through enhanced germinal center activities[347]. HVTN 137 reported that 3M0-52 was both safe in humans and capable of inducing autologous tier 2 neutralizing antibodies (NAb), suggesting that potent adjuvants may be necessary to engage rarer bNAb precursors and expand the range of epitopes engaged past the non-neutralizing, immunodominant epitopes at the trimer base[365].

A variety of modifications to the BG505.SOSIP.664.T332N have been developed to further stabilize the trimer[366-371]. Introducing the double sulfide bond I201C-A433C (DS), into the BG505.SOSIP.664 reduced conformational triggering by CD4. A clinical trial testing the safety and vaccine-induced antibody responses of BG505.DS-SOSIP.664 adjuvanted with alum (NCT03783130) found that it was well tolerated, and another ongoing trial utilizing BG505.DS-SOSIP.664 is investigating the therapeutic efficacy in adults living with HIV-1 receiving ART (NCT04985760)[364,372,373]. Another modified BG505.SOSIP construct, BG505 SOSIP.v4.1-GT1.1 (GT1.1), includes 18 substitutions and a 7-residue deletion within the V2 loop, resulting in the removal of 5 glycosylation sites. These modifications resulted in enhanced or novel binding of trimer apex and CD4bs bNAb germline precursors to GT1.1 compared to BG505.SOSIP.664.T332N[374,375]. GT1.1 priming followed by BG505.SOSIP.664.T332N boosting has been shown to elicit

antibodies capable of neutralizing subsets of diverse heterologous neutralization-resistant viruses in RM, and has entered phase I clinical trials as an immunogen (NCT04224701, NCT05471076)[376-379]. An additional substitution removing a glycan from GT1.1 resulted in enhanced VRC01 precursor binding and has been shown to prime broadly reactive CD4bs-specific antibody responses in a VRC01-class precursor KI mouse model[378].

1.3. Severe acute respiratory syndrome coronavirus 2 (SARS-CoV-2)

1.3.1. Origin and COVID-19 Pandemic

Four coronaviruses are endemic in humans, alpha coronaviruses HCoV-229E and HCoV-NL63, and beta coronaviruses HCoV-OC43, and HCoV-HKU, infecting the upper respiratory tract and causing symptoms associated with common-cold[380]. Notably the serum of over 90% of all adults contains antibodies specific for each of these viruses[381]. All four are believed to be the result of zoonotic spillover from animal reservoirs, which can occur directly or through an intermediate animal host[382-384]. Three coronaviruses have undergone zoonotic transmission in the last 20 years resulting in epidemics: Middle East respiratory syndrome coronavirus (MERS-CoV), severe acute respiratory syndrome coronavirus (SARS-CoV), and SARS-CoV-2[385-388]. In 2003 an outbreak of SARS-CoV originating from China and lasting from February to June resulted in 8,098 cases and 774 deaths- a case fatality rate of 9.6 percent[389-391]. MERS-CoV was first identified in 2012, and originated from zoonotic transmission from dromedary camels to humans[385,392]. Since April 2012 a total of 2,613 cases have been identified resulting in 943 deaths, with cases declining drastically since the onset of the SARS-CoV-2 pandemic[1]. All three viruses can spread to and replicate within the lower respiratory tract, where they can

cause severe and often fatal acute respiratory distress syndrome, especially in those with comorbidities[393].

SARS-CoV-2 is the causative agent of coronavirus disease 2019 (COVID-19), which was first described in a cohort of patients with pneumonia in late 2019 in the Wuhan region of China[387,394]. The virus is believed to have jumped to humans from an unknown intermediate species infected with a bat coronavirus, as the ancestral SARS-CoV-2 strain shares 96.2% nucleotide homology with RaTG13, a coronavirus isolated from *Rhinolophus affinis* bats, but contains an RBD within the S protein differing significantly at key residues[387]. The virus quickly spread across the globe, causing over 770,000,000 confirmed cases and over 7,000,000 reported deaths worldwide[1]. The fight against the global pandemic included numerous lockdowns, social distancing campaigns, as well as mandatory testing measures, especially prior to the development of effective vaccines against the virus. With an overall fatality rate of around 1%, and anywhere from 3-20% of infected individuals requiring hospitalization, COVID-19 continues to burden global healthcare systems[395]. Through its continued replication in humans, SARS-CoV-2 has accumulated mutations with impacts on transmission rate and pathogenesis. The first notable lineage or “variant” emerged in February of 2020, defined by the D614G mutation within the surface spike protein and a higher transmission rate that propelled it to the dominant circulating variant globally[396]. Numerous variants of concern (VOC) have jeopardized the vaccine efficacy, with emerging Alpha, Beta, Gamma, Delta, and Omicron variants exhibiting increased transmission, escape from neutralizing antibodies generated by prior vaccination or infection[397-402].

In the case of certain SARS-CoV-2 lineages, the number of mutations accumulated rapidly exceeds the expected rate of evolution. The most exemplary case of such divergence is the initial Omicron variant of concern (BA.1) and its lineage offspring[403-405]. The Omicron variant exhibits significant genetic divergence from its probable ancestors, with 50 amino acid alterations—including substitutions, insertions, and deletions—distributed across its genome. Notably, at least 32 of these mutations were located in the spike protein, including functionally important spike mutations observed in other variants[406]. Omicron and its descendent lineages exhibit increased transmissibility due to higher ACE2 affinity, and decreased associated pathology, likely due to lower levels of replication within the lower airway driven by less efficient use of co-receptor TMPRSS2[407]. It has been hypothesized that a majority of the genetic divergence observed in the original Omicron variant occurred within a singular, immunocompromised host[408]. Studies have suggested that chronic SARS-CoV-2 replication within immunocompromised hosts can drive increased rates of evolution, though the exact mechanisms and extent of this differential divergence remains to be elucidated[409-416].

1.3.2. Virology

SARS-CoV-2 is an enveloped virus belonging to the order *Nidovirales,* with a notably large, single stranded, positive sense RNA genome[417]. Viruses within this order all utilize the same coding strategy, with around 2/3 of the genome dedicated to encoding 2 large polyproteins that form the non-structural proteins responsible for viral genome replication and gene transcription[418]. The remaining third of the genome is transcribed through discontinuous transcription into subgenomic RNAs encoding the structural proteins that form the enveloped virion along with a lipid bilayer derived from the host cell

membrane[393,419]. Several non-structural proteins as well the accessory proteins of SARS-CoV-2 have demonstrated immunevasive properties[420,421].

1.3.2.1. Replication Cycle

Respiratory droplets containing SARS-CoV-2 virions mediate the majority of host-to-host transmission, delivering the virus to the respiratory tract of uninfected individuals[422-424]. Once in the respiratory tract, the virus can bind ACE2 on the surface of airway epithelial cells within the nasopharynx or trachea via spike (S) glycoprotein trimers[425,426] (details on the receptor binding and fusion events can be found in section 1.3.2.2). Following release of the viral ribonucleoprotein complex into the host cell, cellular proteases free the viral genome from the nucleoprotein (N) as with other RNA viruses[427,428]. The positive sense genomic RNA (gRNA) is nearly 30 kilobases in length, the largest RNA genome of all RNA viruses and is capped on the 5' end with a m7G-cap structure as well as a polyA tail on the 3' end that prevent degradation by host exoribonucleases[429,430]. The gRNA serves as a direct template for the translation of 2 large polyproteins, ORF1a and ORF1b[431]. These polyproteins are cleaved by intrinsic protease activity to form 16 nonstructural proteins that include the papain-like proteinase protein (NSP3), 3C-like proteinase (NSP5), RNA-dependent RNA polymerase (NSP12, RdRP), helicase (NSP13), endoRNAse (NSP15), 2'-O-Ribose-Methyltransferase (NSP16)[432]. NSP4 and NSP6 aid in the formation of double membrane vesicles (DMVs) that serve as the location for the replication and transcription complex (RTC)[433,434].

The SARS-CoV-2 RTC utilizes a process called discontinuous transcription to express the remaining structural and accessory proteins following expression and cleavage of ORF1a and ORF1b[431]. Discontinuous transcription begins via interactions of

non-structural proteins cleaved from ORF1a and ORF1b, including the RNA dependent RNA polymerase (RdRP), with the gRNA to form the RTC[432]. This complex first generates negative sense gRNA and sgRNA intermediates for the production of positive sense gRNA and sub-genomic RNAs (sgRNAs) respectively[435]. Transcription for all negative sense sgRNAs begins at the poly A tail at the 3' end of the genome[431]. When the RdRP reaches transcription regulatory body sequences (TRS-B), which are located adjacent to each ORF, a conserved 7 nt sequence within the TRS-B causes the RdRP to pause[436]. This pause, accompanied with looping of the gRNA, creates an opportunity for the RdRP to jump to the TRS located at the 5' end of the genome, known as the transcription regulatory leader sequence (TRS-L), each time it reaches a TRS-B. The TRS-L-TRS-B junction created by this process is unique to the sgRNAs, and are used as a marker of active infection when measuring viral loads via PCR in research settings[431,436-438].

Both positive sense gRNA and sgRNAs exit the DMVs, with +sgRNAs serving as mRNA for viral proteins such as nucleoprotein N, which complex with the +gRNA within the cytoplasm following translation[439]. The other structural proteins transcribed at this stage include the membrane bound spike (S), envelope (E), and matrix (M) proteins, all of which are trafficked to the cell surface where they associate with budding virions[434,440]. The process of viral ribonucleoprotein complex (vRNP) packaging, within these budding virions remains largely unknown. Recent research suggests that the N protein–gRNA complex is comprised of 35–40 vRNP complexes, with each vRNP unit containing approximately 12 N protein molecules bound to an estimated 800 nucleotides of gRNA[433,441,442]. The current model proposes that interactions between the N protein and

the cytoplasmic tail of the M protein facilitate incorporation of the vRNP complexes into new virions at the ER-to-Golgi intermediate compartment (ERGIC)[441,443].

1.3.2.2. Spike Glycoprotein (S)

Forming trimers on the surface of SARS-CoV-2 virions, the spike glycoprotein (S) contains 2 major domains: the receptor binding domain (RBD) containing S1, and the membrane fusion mediating S2, separated by a polybasic cleavage site[427,444]. This furin cleavage site is cleaved in the host cell prior to virion release, allowing the trimer to bind to its target receptor angiotensin-converting enzyme 2 (ACE2)[387,427]. S trimers have shown to be very flexible via cryo-EM studies, with each S1 subunit fluctuating between receptor accessible (up) and receptor inaccessible (down) states[444]. Following receptor binding, the S2 subunit is further cleaved by the transmembrane serine protease TMPRSS2 or by lysosomal cysteine proteases cathepsins L and B, which leads to a conformational change that exposes a fusion peptide that anchors the virus into the host cell[428,445-447]. S engagement by other cell surface receptors and proteases has been shown, though their overall contribution to replication and pathogenesis has not been clarified[448]. The membrane fusion event releases the viral ribonucleoprotein complex into the host cell cytoplasm[445]. Neutralizing epitopes and immune responses to S are discussed in section 1.3.3.4.1.

1.3.3. Immune Responses to SARS-CoV-2

1.3.3.1. IFN Responses

Adaptive immune responses and associated clinical outcomes have been found to largely depend on the viral load[449] and type I interferon (IFN I) responses driven by the innate response[450]. Slower declines in viral load as well as early and sustained elevated

levels of IFN alpha have been associated with severe clinical outcomes[451]. Treatment of RM with an interferon signaling modulator that reduced the binding and signaling of all forms of endogenous IFN-I resulted in significantly decreased overall viral loads[452].

1.3.3.2. Macrophage Responses in COVID-19

In COVID-19, macrophages and monocytes produce inflammatory cytokines in response to patter recognition receptor (PRR) stimulation by either damage-associated molecular patterns (DAMPS) released from damaged epithelial cells within the airway or by viral pathogen-associated molecular patterns (PAMPs). Various toll like receptors (TLRS), the retinoic acid-inducible gene I (RIG-I) receptor and the melanoma differentiation associated gene (MDA)-5 receptor in monocytes and macrophages have all shown to contribute to the inflammation following SARS-CoV-2 infection[453-456].

1.3.3.2.1. Tissue Resident Macrophages

The tissue resident macrophages (TRMs) of the lung fulfill a variety of homeostatic niches such as tissue repair, while also serving as patrolling sentinel cells. These cells are ontologically distinct from macrophages originating from bone marrow derived circulating monocytes as they are self-replenishing and originate from the fetal yolk sac[457]. TRMs of the lung can be designated into two distinct populations, based both on location as well as transcriptional profile: alveolar macrophages (AMs) and interstitial macrophages (IMs)[458-460]. During inflammation however, circulating monocytes are recruited to the lung and differentiate into a third transcriptionally distinct set of macrophages[461,462]. While TRMs can be infected by SARS-CoV-2, it has yet to be proven if this infection occurs via viral escape from lysosomes or direct fusion of the cell and viral membranes within the lungs through an ace2 dependent mechanism[463].

1.3.3.2.1.1. Alveolar Macrophages

AMs make up around 95% of the immune cells within the lumen of the alveoli of the lung, where epithelial cells lining the lumen secret a cytokine milieu that results in the unique transcriptional signatures of the AM[464,465]. Four major subsets of AM arise during clustering of their transcriptional signatures, largely based on differential expression of IFI27 and APOC2, with sub clustering driven by expression of interferon (IFN)-inducible genes and chemokines[466]. During SARS-CoV-2 infection, AMs often undergo the "macrophage disappearance reaction"[467,468], possibly due to direct infection or due to loss of survival signals resulting from damaged lung epithelium. Both the cause and purpose of this are still not understood, but it has been speculated that anti-inflammatory AMs may hinder a robust inflammatory response during acute infection[469,470]. Following their loss, AMs are repopulated either from remaining AMs or from CCR2+ Ly6C+++ recruited monocytes responding to GM-CSF[471-473].

AMs are constantly surveying the alveoli, continuously phagocytosing pathogens, cellular debris, and foreign particles without triggering widespread inflammation[474]. Scavenging receptors such as MARCO allow AMs to clear away apoptotic immune and epithelial cells, while producing cytokines that trigger epithelial repair[475]. Subsets of AMs can also trigger inflammation when they are unable to keep up with phagocytic demand during infections, producing type I IFNs, TNF-a, and IL-1b[466,470]. During SARS-CoV-2 infection, macrophages can exhibit both proinflammatory M1 and anti-inflammatory M2 phenotypes, with M1 macrophages possibly contributing to increased viral spread via uptake and replication of SARS-CoV-2 viral particles[476].

1.3.3.2.1.2. Interstitial Macrophages

Lung IMs reside within the bronchovascular bundle, where they patrol the neural, lymphatic and circulatory tissues present within and surrounding the lung interstitial space[477]. Lung IMs exhibit similar transcriptional signatures to the IMs of other organs throughout the body which differ from that of AMs[478,479]. While the functional role of IMs is still not well understood, their gene signatures suggest neuroimmune regulation, leukocyte recruitment, and immunoregulatory roles[473,480]. By day 2 following SARS-CoV-2 infection in RM, C206+ macrophages with transcriptional signatures similar to IM had infiltrated the alveolar space[461]. These macrophages, along with circulating monocyte derived macrophages, were responsible for the majority of inflammatory IL6 and TNF alpha production compared to AM[452].

1.3.3.2.2. Recruited Monocytes and Macrophages

Blood circulating monocytes are an innate myeloid derived immune cell type that can be divided into 3 distinct subsets based on CD14 and CD16 expression: classical monocytes (CD14+, CD16-), intermediate (CD14+, CD16+), and non-classical ($CD14^{low}$, CD16+)[477]. Monocytes are recruited to sites of infection via inflammatory cytokines produced by sentinel cells, and can differentiate to fulfill a wide range of pro- and anti-inflammatory effector function[481]. During COVID-19, proinflammatory chemokines recruit cells to the airway, where they accumulate and differentiate into inflammatory effector cells, producing more inflammatory cytokines and chemokines, facilitating the characteristic “cytokine storm” via positive feedback[452,468,482]. Within patients experiencing severe COVID-19, populations of immature monocytes were found to be elevated, indicating an emergency myelopoiesis[483], with monocyte populations exhibiting dysfunctional phenotypes[484]. In RMs, CCR2+ TREM2+ blood circulating derived

monocytes were found to have infiltrated the alveolar space alongside IM during SARS-CoV-2 infection, where they produced a majority of the inflammatory cytokines TNFa and IL-6[461].

1.3.3.2.3. Antibody Dependent Enhancement

Antibody dependent enhancement (ADE) has been documented in various respiratory viral infections, including SARS-CoV[485-487], but its role in SARS-CoV-2 pathogenesis is still debated. In ADE, complexes of virus and antibodies are internalized via Fc receptor (FcR) binding on immune cells. Because macrophages and certain monocytes express IgG binding Fc gamma receptors (FcγRs)[488] while also producing inflammatory cytokines in response to infection, they can also amplify the virus. Some studies have shown an FcγRII dependent ADE during COVID-19, where convalescent plasma was found to increase the expression of viral N in macrophages[489].

1.3.3.3. Adaptive Immune Responses

1.3.3.3.1. T Cell Responses

T cell responses to endemic HCOV are relatively low in magnitude and longevity compared to other viral infections, especially in elderly and immunocompromised populations[490]. However, SARS-CoV-1 specific T cells are still detectable 17 years following infection despite short lived antibody and B cell responses[491,492]. Despite the relatively recent emergence of SARS-CoV-2, cases of reinfection have been documented, especially with the highly infectious Omicron variant[493]. In cases of reinfection with this variant, a majority of T cell responses are retained, likely contributing to the decrease in clinical severity associated with Omicron[494,495]. Evidence from both SARS-CoV-1 and MERS suggest that T cell mediated immunity plays a critical role in viral control while

greater antibody responses can associate with inflammatory macrophage responses and worse clinical outcomes[496,497].

Cases of mild and moderate COVID-19 correlate with development of robust cytotoxic CD8+ T cell responses within the first 7 days following symptom onset, peaking around day 14[498]. The T cell pool during severe acute infection often undergoes simultaneous loss of up to 80% of peripheral T cells at the same time that around 20% of CD8+ T cells undergoing rapid proliferation[499,500]. Resolution of these dynamics correlates with recovery[501]. In terms of functionality, skewing of CD4+ responses to type I is associated with mild disease while type II phenotypes correlate with more severe outcomes[502]. While early, high levels of effector molecule expression in CD8+ T cells correlates with viral control, excessive sustained activation beyond this threshold is associated with severe clinical outcomes[503,504]. Cytotoxic T cells have been shown to infiltrate tissues, likely driven by high tissue viral loads, where they may be contributing to tissue damage[505,506].

Antigen specific T cell responses have been documented against all SARS-CoV-2 proteins, in most cases proportional in magnitude to the level of expression of the viral proteins[507]. The exception to this trend lies in the enrichment of spike specific responses within the CD4+ T cell pool, likely due to cognate antigen engagement and subsequent help provided by spike specific B cells[508]. Levels of S specific, CD4+ follicular helper T (TFH) cells correlate with convalescent neutralizing antibody titers[509]. CD8+ epitopes of interest include the conserved $NP_{105-113}$ epitope bound by HLA class I molecules in individuals possessing the B*07:02 allele. T cell responses against this epitope were found to correlate with strong viral control and protection from severe disease[510].

Memory T cell responses against SARS-CoV-2 continue to be monitored as we approach the 6th year since the emergence of the virus. Robust memory T cell pools have been documented in recovered individuals; however, their longevity may correlate with the severity of the infection[511-513]. Most CD4+ memory T cells exhibit a central memory phenotype, but there are significant pools of stem central memory cells[514,515]. Long lived CD8+ SARS-CoV-2 specific memory T cells express an interferon gene signature as well as CD45RA[516]. Of the total memory pool, SARS-CoV-2-specific $CD4^+$ and $CD8^+$ memory T cells make up approximately 0.5% and 0.2%, respectively, with CD4+ cells targeting an average 19 epitopes and CD8+'s targeting around 17[517]. The size of tissue resident memory pools within the airway tissues correlates with both age and protection from severe disease[518].

1.3.3.3.2. B cell Responses

A majority of patients with COVID-19 experience a transient increase in plasma cell frequencies, in some cases exceeding 30% of total B cells within the blood, that returns to baseline 3-6 months post infection[503]. These cells arise simultaneously as the patients seroconvert, are highly polyclonal, and show little to no SHM, suggesting early B cell responses to SARS-CoV-2 infection are largely driven by the engagement of naïve B cells[519]. Propagated mostly by extrafollicular B cell proliferation, these peripherally circulating B cells were enriched with CD27- and IgD- populations in patients with severe COVID-19. While some evidence suggests that patients with severe COVID-19 have hindered GC responses during acute infection despite their stronger overall antibody responses, presence of MBCs with high levels of SHM in these patients suggests that the memory phase GC responses may remain in tact[520,521]. Antigen persistence fuels GC

reactions for several months following infection, driving increases of S and N specific memory B cells with accumulating SHM for up to 6 months[521]. Patients with mild disease show vastly heterogenous frequencies of S specific MBCs at 5 months following symptom onset with some exhibiting very high counts, suggesting that severe disease is not necessary to drive strong memory B cell responses[522].

1.3.3.3.3. Antibody Responses

As the sole viral protein exposed on the surface of mature, in-tact virions, S remains the only target for neutralizing antibodies[523]. While over 90% of pre-pandemic serum samples contain HCoV S specific antibodies, only around 1% of samples screened contained antibodies cross reactive with the RBD of SARS-CoV-2[524]. Higher frequencies of cross reactivity were observed against other S epitopes (~4%) and N (16%), consistent with the low to undetectable levels of SARS-CoV-2 neutralizing activity of pre-existing SARS-CoV-2 binding antibody repertoires[524]. Antibody responses to HCoV infections are relatively short lived, similar to corresponding T cell responses[525], while SARS-CoV-1 infection confers neutralizing antibody titers with more substantial half-lives[526].

Approximately 90% of the neutralization activity within the serum stems from antibodies targeting the RBD of SARS-CoV-2 S[527]. IgM, IgA, and IgG responses against SARS-CoV-2 RBD are detectable on average within 11-13 days post symptom onset, with maximum positivity rates occurring around 4-6 weeks[525]. Anti-RBD IgA and IgM titers rapidly decline in weeks 7-10, with a majority of patients negative for both by week 12, while IgG titers exhibit a slower decline. Severity of COVID-19 disease correlates strongly with the magnitude of anti-SARS-CoV-2 antibody responses, with patients who were admitted to the ICU maintaining the highest levels of RBD binding IgM, IgG and IgA[528] as

well a broader binding repertoires[529]. As age correlates with severity of disease, elderly populations exhibit higher likelihood to develop high antibody titers due to the higher likelihood to experience severe disease[530,531], while children largely experience asymptomatic or mild COVID-19, yielding lower antibody titers[532,533]. Neutralizing antibodies are considered the paramount correlate of protection against infection by SARS-CoV-2, but heterogeneity of antibody responses among disease outcomes suggest neutralization plays a smaller role in viral control[525]. Associations of fucosylation states of anti-SARS-CoV-2 antibodies have been made with disease severity, with increased afucosylated antibodies binding FcγRIIIa more strongly and triggering stronger proinflammatory responses[534].

Mucosal antibody responses to SARS-CoV-2 are less characterized than those of the serum. In contrast to the serum, patients with mild disease show elevated neutralizing titers within the airway compared to those with severe disease, and that these correlated with IgA responses[535]. Additionally, the secreted form of IgA, dimeric IgA, was found to neutralize SARS-CoV-2 with greater potency than monomeric IgA[536]. An intranasal vaccine, NanoSTING-SN (NanoSTING-Spike-Nucleocapsid) was found to protect against multiple strains of SARS-CoV-2 and SARS-CoV while preventing transmission to vaccine naïve hamsters[537]. In the NHP model, NanoSTING-SN also elicited cross-reactive IgA responses within the serum and nasal wash, but further challenge studies are needed to determine associations of mucosal antibody repertoires and disease outcomes[538].

The continued emergence of viral variants with significant mutations to the RBD of the S protein have highlighted the need for ongoing characterization of the binding relationships between neutralizing antibodies and the structure of their cognate epitopes

within S. While the majority of neutralizing responses target the RBD of S1, fusion components of S2 exhibit lower levels of mutation and glycosylation, suggesting possible targets for cross variant neutralizing antibodies[527]. Surface plasmon resonance studies have revealed 4 classes of RBD binding antibodies based on epitope targeting or neutralizing function[539-541]. Class 1 and 2 antibodies compete with ACE2 for the ACE2 binding site on receptor accessible RBD-up and receptor inaccessible RBD-down subunits, respectively. Class 3 neutralizing antibodies bind outside the ACE2 interface, in both RBD-up and RBD-down conformations. Class 4 antibodies bind a quaternary epitope only accessible when at least 2 of the RBD subunits are in the up conformation. Other neutralizing antibodies target the NTD, which prevent conformational changes necessary for membrane fusion, rather than prevention of ACE2 binding[542].

Some antibodies have been identified with broad neutralizing capacity against SARS-CoV-2 variants, revealing conserved epitopes within the S protein. Two of such mAbs, derived from memory B cells of SARS-CoV-1 survivors, have been approved for therapeutic and prophylactic use: sotrovimab and pemivibart[543-547]. However, sotrovimab's emergency authorization was revoked by the FDA in December of 2023 due to loss of neutralizing capacity to Omicron variant BA.2 An additional potent neutralizing mAb, VIR-7229, has recently been identified which targets the viral receptor-binding motif (RBM) with even greater cross-reactivity to all sarbecovirus clades, including all SARS-CoV-2 variants[548]. Through molecular mimicry, VIR-7229 binds key residues within the RBM that make contact with ACE2, and therefore functionally and evolutionary constrained. Further preclinical and clinical studies are underway investigating the

therapeutic efficacy of VIR-7229, but its high potency and resistance to epitope diversification could lead to both therapeutic and prophylactic applications[548].

While both sotrovimab and pemivibart bind epitopes within the RBD, additional epitopes are targeted by mAbs that are broadly reactive with all sarbecoviruses, beta-coronaviruses, or multiple coronavirus genera [549-555]. The fusion machinery contained within the S2 domain of the S protein contains several epitopes conserved across beta-coronaviruses. While the fusion peptide itself exhibits high rates of evolution, the two heptad repeats responsible for the formation of helical coiled coils necessary for membrane fusion are highly conserved. Antibodies targeting S2 epitopes are less potent than those targeting RBD, they still have been shown to protect against infection and inflammation in both small animal and RM models[555-557].

1.3.4. SARS-CoV-2 Vaccines

While many public health measures such as social distancing and mandatory testing have been either encouraged or enforced during the pandemic, vaccines remain the most crucial preventative measure to combat the spread and severity of SARS-CoV-2. The current vaccines against SARS-CoV-2 facilitate the generation of neutralizing antibody titers targeting S, the primary correlate of protection, as well as varying antigen specific T cell populations [558]. According to the World Health Organization COVID-19 Dashboard, over 13.6 billion doses of the vaccine have been administered to over 5 billion people around the globe [1]. Unprecedented collaboration and resource allocation has led to the 821 clinical vaccine trials including FDA approved platforms such as the mRNA vaccines developed by Pfizer and Moderna, as well as those yet to be approved such as variant specific boosters [559].

Vaccines against SARS-CoV-2 are available in a variety of conventional and novel platforms. On December 11th 2020, approximately one year following the emergence of SARS-CoV-2, the FDA provided emergency approval for the administration of Pfizer's novel mRNA-based vaccine, BNT162b2[560,561]. It was quickly followed one week later by the approval of Moderna's mRNA-1273, making the two the first mRNA-based vaccines to be approved[3,562]. Both vaccines each conferred around 95% protection against COVID-19 disease at the time, but waning antibody titers and mutations in S acquired by the virus have since necessitated boosters to maintain effective protection[563]. The mRNA vaccines have proven not only to be well tolerated with minimal adverse events, they also have been shown to be effective in heterologous boosting strategies for those that received the now retracted Janssen, Johnson & Johnson human adenovirus type 26 vectored vaccine JNJ-78436735[564,565]. Although the JNJ-78436735 vaccine exhibited mild reactogenicity in early trials, thrombosis with thrombocytopenia syndrome (TTS) was reported at rare frequencies in recipients a few weeks after vaccination, and the FDA limited its application to those unable to receive other authorized vaccines[565,566].

The Pfizer-BioNTech and Moderna COVID-19 vaccines have undergone several iterations to reflect the predominant circulating Omicron variants. In late 2022 to early 2023, both a bivalent ancestral SARS-CoV-2 / BA.1 and a bivalent BA.4/BA.5 based mRNA vaccine were approved[567]. Continued evolution and immune escape of the Omicron lineage necessitated additional updates against the XBB1.5 and JN.1 variants in June 2023 and April 2024, respectively[568-571]. As of March 2025, Omicron subvariants continue to dominate the global circulation of SARS-CoV-2, with 34% of global cases attributed to subvariant XEC and 45% of cases in North America associated with

LP.8.1[572]. While the mRNA platform allows for easy modifications to be made to the immunogen to account for these variants, antigenic sin may pose a substantial challenge to conferring variant specific protection as several studies have shown only slight increases in effectiveness when boosting with omicron S vs ancestral WA1/2020 S[573-575].

In addition to the mRNA vaccines, a recombinant, full-length, prefusion-stabilized, spike nanoparticle vaccine with a saponin-based adjuvant named Matrix-M by Novavax, NVX-CoV2373, was granted authorization for emergency use on July 13, 2022[576-578]. Administered in 2 two 5μg protein, 50μg adjuvant doses spaced 21 days apart, NVX-CoV2373 has shown to be up to 90% effective at preventing symptomatic COVID-19. The FDA has approved two updated, monovalent formulas based on the Omicron subvariants XBB1.5 in 2023 and JN.1. in 2024[579-581]. Compared to homologous boosting with mRNA based SARS-CoV-2 vaccines (3 doses total), heterologous boosting of a primary (2 dose) mRNA vaccine series with NVX-CoV2373 (1 dose) yielded lower NAb titers 28 days post boost[582]. However, NVX-CoV2373 has been associated with significantly lower adverse events and could increase vaccine coverage rates for populations that are hesitant to receive or do not have access to mRNA-based vaccines[578,582,583].

1.3.5. Summary

The literature on SARS-CoV-2 highlights its rapid global spread, driven by high transmissibility and the emergence of new variants. Extensive research has uncovered key mechanisms of viral entry, immune evasion, and host immune responses, with particular attention to the roles of neutralizing antibodies and T cell immunity. Animal models, especially nonhuman primates, have been critical for studying pathogenesis and

evaluating vaccines and therapeutics. Ongoing work continues to explore long-term immunity, variant-specific responses, and strategies to achieve broad, durable protection.

Chapter Two: Passive infusion of an S2-Stem broadly neutralizing antibody protects against SARS-CoV-2 infection and lower airway inflammation in rhesus macaques

AUTHORS

Christopher T. Edwards[1¶], Kirti A. Karunakaran[2¶], Elijah Garcia[3,4¶], Nathan Beutler[3], Matthew Gagne[5], Nadia Golden[6], Hadj Aoued[7], Kathryn L. Pellegrini[7], Matthew R. Burnett[5], Christopher Cole Honeycutt[5], Stacey A. Lapp[1], Thang Ton[1], Mark C. Lin[1], Amanda Metz[1], Andrei Bombin[8], Kelly Goff[6], Sarah E. Scheuermann[6], Amelia Wilkes[9], Jennifer S. Wood[9], Stephanie Ehnert[9], Stacey Weissman[9], Elizabeth H. Curran[10], Melissa Roy[10], Evan Dessasau[11], Mirko Paiardini[1,12,13], Amit A. Upadhyay[1], Ian Moore[10,13], Nicholas J. Maness[6], Daniel C. Douek[5], Anne Piantadosi[8,12,13], Raiees Andrabi[3,14,15*], Thomas R. Rogers[3,16*], Dennis R. Burton[3,14,15,17*], Steven E. Bosinger[1,12,13*]

AFFILIATIONS

[1]Division of Microbiology and Immunology, Emory National Primate Research Center, Emory University, Atlanta, GA 30329, USA.

[2]Department of Pathology, Microbiology & Immunology, Vanderbilt University, Nashville, TN 37235, USA.

[3]Department of Immunology and Microbiology, The Scripps Research Institute, La Jolla, CA 92037, USA.

[4]Mayo Clinic Medical Scientist Training Program, Mayo Clinic College of Medicine and Science, 200 First Street SW, Rochester, Minnesota 55356, USA.

[5]Vaccine Research Center; National Institute of Allergy and Infectious Diseases, National Institutes of Health, Bethesda, MD, USA.

[6]Tulane National Primate Research Center, Covington, LA, USA.

[7]Emory National Primate Research Center Genomics Core, Emory National Primate Research Center, Emory University, Atlanta, GA 30329, USA.

[8]Division of Infectious Diseases, Department of Medicine, Emory University School of Medicine, Atlanta, GA, USA.

[9]Division of Animal Resources, Emory National Primate Research Center, Emory University, Atlanta, GA 30329, USA.

[10]Division of Pathology, Emory National Primate Research Center, Emory University, Atlanta, GA 30329, USA; [11]Division of Histology, Emory National Primate Research Center, Emory University, Atlanta, GA 30329, USA.

[12]Emory Vaccine Center, Emory National Primate Research Center, Atlanta, Georgia, USA.

[13]Department of Pathology and Laboratory Medicine, Emory University School of Medicine, Atlanta, GA, USA.

[14]IAVI Neutralizing Antibody Center, The Scripps Research Institute, La Jolla, CA 92037, USA.

[15]Consortium for HIV/AIDS Vaccine Development (CHAVD), The Scripps Research Institute, La Jolla, CA 92037, USA.

[16]Division of Infectious Diseases, Department of Medicine, University of California, San Diego, La Jolla, CA 92037, USA.

[17]Ragon Institute of Massachusetts General Hospital, Massachusetts Institute of Technology, and Harvard University, Cambridge, MA 02139, USA.

¶These authors contributed equally to this work.

*Corresponding authors. Emails: steven.bosinger@emory.edu (SEB); trogers@scripps.edu (TRR); andrabi@scripps.edu (RA); burton@scripps.edu (DRB)

Published in *PLOS Pathogens* Volume 21, No. 1 e1012456, January 23rd, 2025, PMID: 39847599

ABSTRACT

The continued evolution of SARS-CoV-2 variants capable of subverting vaccine and infection-induced immunity suggests the advantage of a broadly protective vaccine against betacoronaviruses (β-CoVs). Recent studies have isolated monoclonal antibodies (mAbs) from SARS-CoV-2 recovered-vaccinated donors capable of neutralizing a majority of SARS-CoV-2 variants and other β-CoVs. Many of these mAbs target the conserved S2 stem region of the SARS-CoV-2 spike protein, rather than the receptor binding domain contained within S1 primarily targeted by current SARS-CoV-2 vaccines. One of these S2-directed mAbs, CC40.8, has demonstrated protective efficacy in small animal models against SARS-CoV-2 challenge. As the next step in the pre-clinical testing of S2-directed antibodies as a strategy to protect from SARS-CoV-2 infection, we evaluated the *in vivo* efficacy of CC40.8 in a clinically relevant non-human primate model by conducting passive antibody transfer to rhesus macaques (RM) followed by SARS-CoV-2 challenge. CC40.8 mAb was intravenously infused at 10mg/kg, 1mg/kg, or 0.1mg/kg into groups (n=6) of RM, alongside one group that received a control antibody (PGT121). Viral loads in the lower airway were significantly reduced in animals receiving higher doses of CC40.8. We observed a significant reduction in inflammatory cytokines and macrophages within the lower airway of animals infused with 10mg/kg and 1mg/kg doses of CC40.8. Viral genome sequencing demonstrated a lack of escape mutations in the CC40.8 epitope. Collectively, these data demonstrate the protective efficiency of broadly neutralizing S2-targeting antibodies against SARS-CoV-2 infection within the lower airway while providing critical preclinical work necessary for the development of pan–β-CoV vaccines.

MAIN TEXT

INTRODUCTION

Since its emergence in late 2019, severe acute respiratory syndrome coronavirus 2 (SARS-CoV-2) has led to over 700 million cases of coronavirus disease 2019 (COVID-19), resulting in over 6 million deaths[584]. While alphacoronaviruses HCoV-229E and HCoV-NL63, and betacoronaviruses (β-CoVs) HCoV-OC43 and HCoV-HKU1 are endemic to humans, typically causing mild disease, they still pose a serious threat to at-risk populations such as the elderly and immunocompromised[383,585,586]. β-CoVs SARS-CoV-1 (severe acute respiratory syndrome coronavirus 1) and MERS-CoV (Middle East respiratory syndrome CoV) both arose from zoonotic transmission events within the last 20 years and are associated with high morbidity and mortality in humans[586-588]. Together with the COVID-19 pandemic, these transmission events and subsequent public health crises highlight the urgent need for proactive measures to prevent a future coronavirus epidemic.

Today, vaccination remains the most utilized prophylactic strategy against severe COVID-19, with over 13.5 billion doses of SARS-CoV-2 vaccines across various platforms administered worldwide[1]. The majority of approved SARS-CoV-2 vaccines seek to induce neutralizing antibodies against the surface spike (S) glycoprotein, particularly the receptor binding domain (RBD) regardless of platform[2,589-600]. Due to their highly efficient immune responses, rapid development, and ease of scalability, messenger ribonucleic acid (mRNA)-based vaccines developed separately by Moderna (mRNA-1273) and Pfizer/BioNTech (BNT162b2) were the first to be approved by the US Food and Drug Administration and European Medicines Agency, both encoding a prefusion-stabilized,

full-length S protein[2,601-603]. Approval and administration of viral vector and protein subunit-based vaccines also utilizing full-length S proteins have since followed[604,605]. Even though full-length S immunogens do include both the S1 and S2 subunits, the majority of IgG responses target the highly immunogenic S1[606,607].

The majority of human coronavirus (HCoV) infections elicit strain-specific neutralizing antibody responses[608,609]. Only 10-13% of convalescent COVID-19 donors exhibit some degree of neutralizing capacity against multiple β-CoVs[555,610,611]. Several theories have been proposed to explain the rarity of broad neutralizing humoral immunity against β-CoVs, including “antigenic sin” driven by previous coronavirus infection towards non-neutralizing or variant-specific epitopes, steric difficulty in targeting conserved epitopes, and disfavored somatic hypermutation pathways[612]. Broad neutralizing responses have been elicited via heterologous coronavirus (CoV) S subunit vaccinations in human immunoglobulin (Ig) locus transgenic mice. However, much more remains to be investigated on conserved epitope targeting antibody development in more clinically relevant models[613,614].

SARS-CoV-2 has continued to evolve to escape immune pressures applied by B and T cell memory conferred by both infection and vaccination. During the first two years of the pandemic, different lineages designated as “variants of concern” (VOCs) by the World Health Organization (WHO) have repeatedly emerged from distinct temporal and geographic landscapes. These VOCs were defined by up to 16 point mutations and a deletion of 7 nucleotides that conferred an overall fitness advantage over co-circulating variants[615-619]. However, after the Omicron variant emerged in November 2021, its sub-

lineages quickly outcompeted other variants and ushered in what was described as a "fourth-wave" of the pandemic[620]. Harboring a variety of mutations within the S protein, including 30 amino acid substitutions, a deletion of 6 amino acids, and an insertion of 3 new amino acids, the Omicron VOCs represented a phylogenetically distant lineage compared to previous VOCs[615,621]. Omicron and its sub-lineages are characterized by their high transmissibility, less severe disease, and resistance against both previously approved therapeutic antibodies and those from convalescent patients or vaccinated individuals[622-624]. These characteristics are largely attributed to the concentration of over 15 amino acid substitutions within the ACE2 RBD and 9 substitutions within the S1 NTD. The swift rise of a phylogenetically distinct variant able to circumvent existing intervention strategies underscores the prudence of reducing reliance on S1-targeted humoral immunity in favor of a more universal CoV prevention approach.

In terms of S1-targeted immunity, the majority of neutralizing antibodies generated against SARS-CoV-2 target the highly immunogenic RBD contained within the S1 subunit[625,626]. The RBD is responsible for engaging the human angiotensin-converting enzyme 2 (hACE2) on the surface of host cells within the airways[625-629]. While the RBD is the major target of neutralizing antibodies, this region exhibits considerable variation between HCoVs and most RBD-neutralizing epitopes are likely to be susceptible to antigenic drift[402,585,630,631]. The S2 subunit, responsible for mediating membrane fusion, is more conserved among β-CoVs, with both the stem helix region and fusion peptide-containing epitopes targeted by broadly neutralizing antibodies (bNAbs)[614,632,633]. Antibodies targeting this region typically exhibit lower neutralizing potency than those

targeting the RBD, but have been shown to retain similar protective efficacy in vivo, possibly due to Fc-mediated effector mechanisms[555]. Recently, several S2-targeting antibodies with neutralizing breadth against multiple SARS-CoV-2 VOCs or across β-CoVs have been described by us and others[633]. We have shown that these antibodies target a conserved, 25 amino acid long stem-helix region in the S2 domain, use a remarkably restricted set of V genes, and were isolated most frequently in subjects with hybrid immunity (natural infection followed by vaccination) but rarely in individuals exposed to either SARS-CoV-2 by infection or vaccination alone[620].

We have previously shown that CC40.8, a monoclonal antibody (mAb) isolated from a peripheral blood mononuclear cell (PBMC) sample of a 62-year-old convalescent donor, exhibits broad reactivity against β-CoVs by targeting the conserved stem helix (SH) epitope of the S2 region[634]. In addition to neutralizing both SARS-CoV-1 and VOCs of SARS-CoV-2, CC40.8 protects against weight loss and reduces viral burden in SARS-CoV-2 challenge *in vivo* when passively infused into hACE2 mice and Syrian hamsters[555]. However, the efficacy of S2-directed humoral immunity at preventing COVID-19 pathology has yet to be described in non-human primates (NHPs). Owing to the genetic and physiological similarities to humans, NHPs are a highly relevant model for investigating both the pathology of SARS-COV-2 infection, as well as the efficacy of vaccination and therapeutic strategies against the virus[635]. NHPs, including rhesus macaques (RMs), have an ACE2 receptor that is nearly identical to humans, proving valuable when testing vaccine-mediated protection against different variants[452,636-639]. Using β-CoV bNAb CC40.8 in the mild-moderate disease model of SARS-CoV-2–infected

RMs, our data demonstrate the ability of S2-mediated neutralizing antibodies to limit viral load and inflammation within the lower airway.

RESULTS

CC40.8 reduces SARS-CoV-2 replication in the lower airway of rhesus macaques

We have previously shown that β-CoV bNAb CC40.8 consistently neutralizes SARS-CoV-2 VOCs *in vitro* and significantly protects from weight loss and lowers airway viral loads *in vivo* in small animal models[555]. To determine the *in vivo* efficacy of CC40.8 in the non-human primate model, we conducted passive antibody transfer followed by SARS-CoV-2 challenge. CC40.8 mAb was intravenously infused at 10mg/kg, 1mg/kg, 0.1 mg/kg doses into groups of six rhesus macaques (RM) (Fig. 1A, Table S1), and an HIV-specific All animals were screened for pre-existing, SARS-CoV-2 spike specific antibodies prior to enrollment in this study (Table S1). All four groups were challenged with SARS-CoV-2 2019-nCoV/USA-WA1/2020, a strain shown previously to replicate productively and induce inflammatory sequela in the upper and lower airways in the RM model[452,639,640]. Viral challenge was administered intranasally and intratracheally with a combined total of 1.1×10^6 plaque-forming units (PFU) five days following antibody infusion. Three animals per experimental group were euthanized at 7 and 8 days post infection (dpi) each. Animals were scored according to the Coronavirus Vaccine and Treatment Evaluation Network standard clinical assessment at cage-side (Table S2) and during anesthetic (Table S3) accesses. No differences were observed in cage-side, anesthetic, or total clinical scores between treatment groups. All treatment groups experienced similar expected weight loss following transfer to the BSL-3 animal care facility (Fig. S2C), and

vitals including rectal temperature, respiratory rate, heart rate, and SpO2 also did not differ between experimental groups (Fig S2B-E). Levels of CC40.8 and PGT121 in the sera and bronchial alveolar lavages (BALs) accurately reflected experimental dosage across all animals from -4 dpi through 7/8 dpi (Fig 1D-1E).

Viral titers were determined via quantitative polymerase chain reaction (qPCR) for both subgenomic RNA (sgRNA) and genomic RNA (gRNA) to measure replicating virus and to verify inoculation, respectively (Fig. 1B-C, S1A-B). BAL and nasal swab sgRNA levels were reproduced by an independent laboratory and further confirmed by gRNA quantification (Fig. S1E-F). 10mg/kg CC40.8-treated animals exhibited significant reductions ($p = 0.039$) in SARS-CoV-2 subgenomic N (sgN) levels within the BAL at 2 dpi compared to both negative control (PGT121 10mg/kg) and 0.1 mg/kg dose treated animals (Fig. 1B). In addition, BAL subgenomic E (sgE) viral titers at 2 dpi showed significant reduction between the 10 mg/kg treated animals compared to the negative control ($p = 0.042$) and 0.1 mg/kg dose ($p = 0.042$) (Fig. 1B). Levels of replication-competent virus were measured within the BAL at 2dpi using an FRNT assay and trended similarly (Fig S1). At 7/8 dpi, the majority of CC40.8 1 mg/kg and 10 mg/kg treated animals exhibited sgN loads at or below the lower level of quantification, while negative control and 0.1 mg/kg dosed animals retained above 100,000 copies of sgN per mL (Fig. 1B, Fig S1E). Compared to the negative control, 7/8 dpi sgN viral loads within the BAL of 1.0 mg/kg and 10 mg/kg treatment groups were significantly reduced ($p = 0.015$ and $p = 0.011$ respectively), and a significant difference was also observed between 0.1 mg/kg treatment and 1.0 mg/kg treatment ($p=0.045$) (Fig. 1B). Despite these observations within

the BAL and lung tissues, no significant differences in sgN or sgE viral titers were observed within the upper airway in any of the RM groups (Fig. 1C, Figs. S1F, S1H, S1J).

CC40.8 reduces lower airway infiltration of inflammatory monocyte and macrophage populations during SARS-CoV-2 infection

Several studies have reported perturbed macrophage populations within the airways of rhesus macaques during SARS-CoV-2 infection[641-643]. In our prior work in the RM model, we identified the predominant macrophage subsets producing inflammatory cytokines in the lower airway following SARS-CoV-2 infection using single-cell RNA sequencing (scRNA-Seq) as CD163+MRC1+TREM2+ and CD163+MRC1− macrophages[452,461], and that blocking the recruitment of these subsets abrogated associated inflammatory signaling[452,461]. To expand on our characterization of these subsets, we developed a multi-parametric flow cytometry panel to assess changes in frequency within the BAL of alveolar macrophage populations (CD163+ MRC1+) and of non-tissue-resident macrophage populations (CD163+ MRC1-) (Fig. 2A Fig. S3A). Treatment with 1.0 mg/kg and 10 mg/kg of CC40.8 resulted in significant reductions ($p = .008658$ and $p = .030303$, respectively) in infiltrating CD163+ MRC1- macrophage populations within the BAL at 2 dpi (Fig 2B and 2E). Similarly, 1.0 mg/kg and 10 mg/kg groups maintained their CD163+ MRC1+ alveolar macrophage populations across the course of infection, while the 0.1 mg/kg dose and control groups exhibited significant reductions in this population compared to 10 mg/kg treated animals at 2 dpi ($p = .007937$ and $p = .008658$ respectively) (Fig. 2C and 2F).

We also quantified the impact of CC40.8 treatment on airway macrophage populations using droplet based scRNA-Seq. Our previous work delineated the major subsets of lung macrophages driving inflammatory and anti-inflammatory cytokine production within the alveolar space during SARS-CoV-2 infection[452,461]. We employed the same approach in this study, using previously generated scRNA-Seq data from uninfected RMs as a reference to map and annotate 107,830 cells captured from the BAL from all 24 animals (Fig 3A, Fig. S5A-C). Consistent with prior studies, the vast majority of annotated cells were macrophages and monocytes, and transcriptomic analysis identified four major macrophage/monocyte subsets: (i) CD163+MRC1+ resident alveolar macrophages; (ii) macrophages similar to infiltrating monocytes expressing CD163+MRC1+TREM2 (iii) CD163+ MRC1- interstitial-like macrophages; and (iii) CD16+ monocytes (Fig. 3B)[461,644]. scRNA-Seq demonstrated that animals infused with 10 mg/kg of CC40.8 had near complete abrogation of the influx of CD163+MRC1- macrophages to the lower airway at 2 dpi compared to control animals ($p = .030303$) (Fig. 3C 0.1 mg/kg treated animals had significantly higher frequencies of these interstitial-like macrophages at both 2 dpi and 7 / 8 dpi compared to 10 mg/kg treated animals ($p = .031746$ and $p = .015152$ respectively), consistent with our flow cytometry data (Fig. 3C). The frequency of CD163+MRC1- macrophages at 2 dpi within the BAL significantly correlated with BAL viral load (Fig. S6E). While we did not measure significant differences between experimental groups in CD163+MRC1+ alveolar macrophage frequency via scRNA-Seq, there was a trend towards a CC40.8 dose response in maintaining this population in the airway (Fig 3E). We also detected a significant reduction in CD16+ monocyte populations within the BAL of 1.0 mg/kg and 10 mg/kg treatment groups compared to controls ($p = .021645$ and $p =$

.028139 respectively) (Fig. 3F). Interestingly, we did not measure significant differences between treatment conditions in the frequency of CD163+MRC1+TREM2+ macrophages, however, this may be due to timing of sampling, as our prior work has demonstrated that this subset peaks at 4 dpi (Fig. 3D)[461]. Collectively these data demonstrate that S2 targeted neutralization of SARS-CoV-2 by CC40.8 is capable of eliminating the recruitment of inflammatory myeloid cells into the lower airway during infection.

We also observed significant reductions in protein levels of inflammatory cytokines measured within the BAL of 10 mg/kg CC40.8-treated RM following infection (Fig. 3K-M, Fig S4A-J). While both control and 0.1 mg/kg treated animals trended towards higher levels of IFNα at both 2dpi and 7 / 8 dpi, we observed significant differences at 7 / 8 dpi between the 0.1 mg/kg and 10 mg/kg treated groups (p = .021645) (Fig. 3K). IP-10, previously identified as a biomarker for COVID-19 severity, was significantly reduced in 10 mg/kg treated groups at 2 dpi compared to controls (p = .04329), and in both 1.0 mg/kg and 10 mg/kg groups at 7 / 8 dpi compared to 0.1 mg/kg dose (p = .041126 and p = .025947, respectively) (Fig 3M)[645]. G-CSF levels were also significantly elevated in 0.1 mg/kg treated animals at 2 dpi (p = .041126) (Fig.S4A). Many of the measured proinflammatory cytokines and chemokines levels, including TNF-a, IL-1b, and IL-6 correlated highly significantly with BAL SARS-CoV-2 titers (Supplementary Table S4).

CC40.8 abolishes gene expression programs of inflammation driven by infiltrating macrophages following SARS-CoV-2 infection

To further investigate the impact of CC40.8 treatment on pulmonary macrophages within the alveolar space during early SARS-CoV-2 infection, we identified transcriptional changes in the CD163+MRC1+TREM2+, CD163+ MRC1+ and CD163+ MRC1- macrophage populations. Consistent with the reduction in sgRNA in the BAL, 10 mg/kg treatment of CC40.8 abrogated ISG expression in CD163+ MRC1-, CD163+ MRC1+, and CD163+MRC1+TREM2 macrophages at 2 dpi, with 1.0 mg/kg treated animals also showing reduced ISG expression at this time point (Fig 3G, Fig S6C). Also, consistent with previously published data, the CD163+MRC1− population produced the majority of transcripts for the inflammatory cytokines TNF and IL6, and transcripts for the pro-inflammatory chemokines CCL8, CXCL10, and CXCL11 across experimental groups (Fig 3G-H, Fig S6C). The 10 mg/kg CC40.8 treatment group demonstrated a significant reduction of the levels of these transcripts in the CD163+ MRC1- subset. Interestingly, while we observed broad expression of ISGs in the CD163+ MRC1- macrophages, this treatment group exhibited the highest expression levels of the pro-inflammatory cytokine IL1B at 2 dpi.

Acute SARS-CoV-2 infection results in activated monocytes and macrophages, which undergo inflammasome-mediated pyroptosis[646]. This process has been shown to induce secondary inflammation in non-immune cell subsets within the lungs of RM[640]. We observed CC40.8-dependent reductions of several inflammasome-associated genes in CD163+ MRC1− macrophages within the BAL (Fig. 3J). In 10 mg/kg treated animals, we observed reductions in the expression of CASP1, GSDMD, IL1RN, IL27 at 2 dpi and AIM2 and NLRP3 at 7/8 dpi compared to control and 0.1 mg/kg treated animals. 1.0 mg/kg dose

CC40.8 treatment resulted in reductions in AIM2 at 2 dpi, and AIM2, IL1B, and NLRP at 7/8 dpi. Consistent with our previous work, reductions in inflammasome-associated genes were most prominent in CD163+MRC1− cells, with smaller effects observed in the CD163+MRC1+TREM2 and CD163+MRC1+ populations (Fig. 3J, S6C).

CC40.8 treatment reduced inflammation within lung during SARS-CoV-2 infection

To further investigate the effect of CC40.8 mAb treatment within the lower airway, scRNA-seq was conducted on cell suspensions prepared from caudal (lower) lung lobe sections obtained at necropsy (7/8 dpi). Our previous work explored SARS-CoV-2 driven inflammation within lung cell subsets, and we employed a similar approach in this study to annotate 101,766 cells captured from caudal lung tissues from RM treated with PGT121 (n=3), CC40.8 10mg/kg (n=3), and CC40.8 0.1mg/kg (n=3) at 7/8 dpi (Fig 4A, Fig. S7A-D)[461]. Cells were classified into four major groups based on the expression of canonical markers (epithelial, lymphoid, myeloid, and “other”) and then each clustered separately (Fig 4A). Subsets within each major group were defined by the expression of marker genes (Fig. S7 A-D). Pathway analysis at 7/8 dpi revealed stark contrast in IFN-I signaling between PGT121 and CC40.8 10mg/kg treated animals (Fig. 4B), consistent with contrasting BAL and lung tissue viral loads measured at the same time point (Fig 1A, Fig S1D). IFN-I related gene sets were observed to be diminished in CC40.8 10mg/kg animals across several cell subsets in the lung, especially when compared to CD163+ MRC1+ macrophages, non-classical monocytes, pDCs, cDC2’s and adventitial fibroblasts in PGT121 treated animals (Fig. 4B). Additionally, analysis of singular genes revealed at least 9 ISGs that were significantly lower in the adventitial fibroblasts, CD163+

MRC1+ macrophages, CD163+ MRC1- macrophages, and neutrophils of CC40.8 10mg/kg treated animals compared to PGT121 controls (Fig. 4C).

CC40.8 treatment did not select for mutations in the S2 stem-helix epitope

To evaluate within-host SARS-CoV-2 evolution and potential antibody escape, we performed full viral genome sequencing using RNA from BAL fluid. We analyzed consensus mutations and intrahost single-nucleotide variants (iSNVs) compared to the sequence of the infecting viral stock. 11 animals yielded sequence data from both the 2 dpi and 7/8 dpi intervals and 10 animals yielded sequence data at solely the 2 dpi timepoint (Data File S8). Three animals (from the CC40.8 1mg/kg or 10 mg/kg groups) had insufficient SARS-CoV-2 RNA for viral genome sequencing.

Very few consensus-level changes were observed across the genome, but we identified numerous iSNVs (Fig. S9). We compared within-sample SARS-CoV-2 diversity, as measured by the average Shannon entropy across the genome, between 2 dpi and necropsy. While the low number of animals with paired sequences available hindered robust statistical analysis, we observed a trend of increased in entropy in control animals (Fig. 5A), consistent with virus diversification over time, whereas mean entropy trended to decrease in animals treated with 1mg/kg and 10mg/kg of CC40.8 (Fig. 5B). These results suggest that CC40.8 treatment does not enhance within-host SARS-CoV-2 diversification over the course of infection and raise the possibility that it may instead limit it.

To evaluate the stability of the CC40.8 epitope during SARS-CoV-2 infection, we assessed the frequency of consensus changes and iSNVs within a 23-amino acid segment of the conserved stem helix region within the S2 subunit (nt positions 24980-25048; AA positions 1140-1162). We observed two mutations in the CC40.8 epitope: one animal in the control group exhibited a mutation at E1151D, which was determined to be a contact residue for CC40.8, at 3% frequency at necropsy (Fig 5D). One animal in the 0.1 mg/kg treatment group exhibited mutation D1146Y present at 10% frequency at 2 dpi but was not detected within the samples taken at necropsy (Fig. 5C). These results suggest a lack of antibody escape despite selective pressure, underscoring the conserved nature of the epitope.

DISCUSSION

Owing to both the ongoing emergence of SARS-CoV-2 variants that circumvent vaccine-elicited immunity, and the zoonotic potential of new CoVs, the development of pan-CoV therapeutic and preventative strategies remains a biomedical priority[647]. Reverse vaccinology approaches have identified conserved molecular targets on the coronavirus spike protein capable of eliciting antibodies in humans with broad coronavirus neutralizing capacity, including an epitope contained in the S2 subunit of the coronavirus spike protein[614,634,648,649]. Vaccine strategies that elicit neutralizing antibodies by S2 directed binding thus have the potential to reduce the reliance on boosts for novel SARS-CoV-2 VOCs and may provide more protection against novel CoVs. In prior work, we isolated the S2 targeting mAb CC40.8[634], which was capable of neutralizing clade 1b and clade 1a ACE2 receptor-using sarbecoviruses, and had robust *in vivo* protective efficacy against

WA.1 SARS-CoV-2 challenge in small animal models[614]. A key step in the development of S2 targeting antibodies as a viable strategy for vaccines against coronaviruses is to demonstrate their protective efficacy in a clinically relevant animal model.

Here, we demonstrate that infusion of rhesus macaques with the S2 directed antibody CC40.8 was able to provide protection against SARS-CoV-2 replication in the lower airway. Treatment with mAb CC40.8 resulted in reduced viral load within the lower airway, as well as reduced inflammation following SARS-CoV-2 infection. While we did not observe sterilizing immunity in either compartment, it is worthwhile to note that the inoculation dose, 1.1 x 10^6 PFU, administered to both the upper and lower airway, is significantly higher than physiological exposure to SARS-CoV-2, yet CC40.8 monotherapy at 1 mg/kg and 10 mg/kg was able to reduce virus by three orders of magnitude. This level of reduction had a protective effect, as RMs with lower viral load exhibited significantly lower levels of infiltrating macrophage populations, expression of ISGs, inflammasome, and other inflammation-associated genes, as well as lower levels of IFNα and other inflammatory mediators detected within the BAL. These data support the working model that links the magnitude of viral loads within the lower airway to the strength of the resulting SARS-CoV-2 disease pathology[452,461,640]. In this model, higher viral loads within the lower airway result in a more sustained and systemic IFN-I response, which accompanies greater losses of tissue resident alveolar macrophages and greater influxes of macrophage and monocyte subsets that drive the inflammatory milieu[452,453,461,640,650,651].

In our model, animals with high levels of pre-infused neutralizing antibodies harbored lower levels of SARS-CoV-2 within the lower airway, but did not show a reduction in the upper airway. Reduced availability of CC40.8 within the tissues of the upper compared to lower airway may contribute to the observed differences in viral load reductions. RM in our study were infused with IgG1 subclass mAbs, which lack the J-chain contained with polymeric IgA and IgM isotype antibodies, a polypeptide necessary for trans-epithelial secretion[652,653]. Upper airway viral loads have been associated with transmission risk, and studies have shown a dose-dependent, vaccine-mediated reduction in infectiousness of SARS-CoV-2 breakthrough infections, likely due to reductions in upper airway viral loads[654-661]. Recent studies have documented significant increases in neutralizing IgA titers at the mucosae following intramuscular mRNA vaccination against SARS-CoV-2[662-665]. While as a monoclonal therapy CC40.8 did not reduce upper airway viral loads significantly, a S2 directed antibody response including IgA isotype antibodies, such as those elicited by SARS-CoV-2 vaccination or infection, may prove more effective at reducing upper airway viral loads and transmission risk.

Humoral protection in humans against SARS-CoV-2 infection is conferred by combination of vaccinations, boosters, and prior infections, yielding a vast range of immune states across the globe. There are currently two major contributors to SARS-CoV-2 “breakthrough” infections: waning vaccination or infection-induced immunity, and the evolution of new variants of SARS-CoV-2 with greater immune escape[612,615,624,666-670]. Several rounds of boosters have been approved to append the current vaccination series to mitigate the observed waning immunity. Both homologous and heterologous mRNA

platform-based boosters have been shown to recover the neutralizing antibody response temporarily against variants of SARS-CoV-2, including Omicron sub-lineages[669,671-674]. Although these mRNA boosters exhibit lower overall vaccine effectiveness at preventing infection against current circulating strains than the original mRNA vaccine demonstrated during earlier phases of the pandemic, they still exhibit remarkable and durable protection against severe disease outcomes. Our data supports maintaining high enough levels of neutralizing antibody through boosters to limit viral replication within the lower airway, thus limiting the magnitude of subsequent lower airway inflammation.

COVID-19 booster doses have employed both the ancestral spike immunogens utilized by the initial vaccination series as well as variant specific spikes, such as the BA.4/BA.5 bivalent booster[675]. However these variant-specific constructs have shown marginal superiority to ancestral immunogens at eliciting Omicron-specific protection, possibly due to immunogenic bias from existing humoral immunity away from novel, Omicron-specific epitopes on the spike protein[676]. Another concern with designing immunogens to elicit variant-specific responses is, in the time a variant specific immunogen can be tested, produced, and delivered, new variants can displace the dominant circulating strain. A vaccine strategy designed to include a component to elicit neutralizing antibodies directed at the conserved S2 region could circumvent the need for annual updating of COVID-19 boosters to reflect circulating strains[649]. Studies have shown individuals with cross-reactive antibodies to endemic HCoVs have higher survival rates from severe COVID-19 disease and protection from SARS-CoV-2 infection, further supporting development of a bNAb-targeted CoV immunogen[610,611,677].

Our data also provides important preclinical insights surrounding mAb therapies for the treatment and prophylaxis of COVID-19. Based on their loss of neutralization capacity against the Omicron sub-variants, the five previously approved mAb therapies for COVID-19 under emergency use authorizations have all been suspended or revoked by the FDA and no current mAb therapies remain in use[668,678-685]. Our dose-dependent reductions in viral load due to preinfusion with mAb CC40.8, dramatic reductions in inflammation in 10 mg/kg treated animals and the broad reactivity of CC40.8 all suggest that S2-targeting mAb therapies may serve as a preventative strategy in those at high risk of contracting COVID-19 or treatment for those who are infected and at high risk of progressing to severe disease. Additionally, evidence suggests that S1-directed mAb treatment in immunocompromised individuals can promote the emergence of SARS-CoV-2 escape mutations[686]. While this study does not attempt to model immunocompromised humans, the lack of S2 mutations observed, coupled with the decreases in mutational entropy in CC40.8-treated animals, warrants further investigation of S2 targeting as a potential treatment strategy for immunocompromised individuals. In March of 2024, RBD targeting monoclonal antibody therapy Pemgarda (pemivibart) was granted an Emergency Use Authorization as a pre-exposure prophylactic strategy for use in individuals 12 years of age and older unlikely to respond to COVID-19 vaccination due being to moderately to severely immunocompromised, highlighting the niche mAb therapies can occupy when effective against circulating variants[543,687]. While frameworks outlining the difficulty of SARS-CoV-2 to maintain selective fitness in humans when mutating the conserved stem helix epitope are largely supported by the conservation of the epitope across β-CoVs,

some studies have assessed the positional Shannon entropy of each amino acid position within the SARS-CoV-2 spike protein and identified mutation "hot spots"[688]. The CC40.8 epitope lies outside any identified "hotspot," supporting the conserved nature of the CC40.8 epitope within humans[555].

Our assessment of the intra-sample mutational diversity was somewhat limited by the low number of viral genomes recoverable in medium and high CC40.8 treatment groups at the conclusion of the study (7/8 dpi). Moreover, while we observed a lack of S2 escape variants in animals receiving CC40.8 treatment, it should be noted that the short duration of our study likely reduced antibody selective pressure. A prior clinical study of patients with B cell deficiencies receiving bamlanivimab therapy observed mutations arising in the SARS-CoV-2 spike protein in two subjects, however, spike mutations were not detected until days 28 and 51 post first positive test[686]. Within NHP models, consistent mutations in the spike region arose in African green monkeys infected with WA.1 in the absence of any vaccine or antibody therapy, detectable via rectal swabs at 28 dpi[689]. Of note, at least two clinical studies have observed resistance mutations arising shortly after mAb treatment. Jensen et al. described the emergence of escape mutation E484K following treatment with bamlanivimab in five individuals, all of whom developed the mutation within 15 days after treatment, and three of whom developed the mutation within 8 days after treatment[415]. In evaluating more a recent monoclonal antibody therapy, Choudhary et al. identified resistance mutations in 7% of participants treated with single-active mAb, half of whom developed the mutations within 3 days after treatment[690]. Thus, taken in context of these studies, the short duration of our study and low levels of recoverable viral RNA

likely limited the sensitivity of our model to detect escape variants, and the stability of the S2 epitope under selective pressure during longer durations of mAb treatment remains to be investigated in preclinical and clinical settings.

Our study had additional limitations. First, SARS-CoV-2 infection in RMs models mild to moderate COVID-19 disease and the extent of protection this S2 stem helix bNAb treatment provides against severe disease in clinical models must still be investigated[452,635,640,643,650]. A preclinical, model that better mimics the viral kinetics of COVID-19 in individuals experiencing long COVID or in immunocompromised individuals would provide critical insight as these groups may be major recipients of mAb therapies and prophylactics. Second, this study investigated protection against the WA.1 ancestral strain of SARS-CoV-2 and not contemporary strains, (e.g. Omicron) that were circulating at the time of our experiment. Our rationale for the use of the WA.1 strain was due to i) prior work by our group had demonstrated potent neutralization by the CC40.8 mAb against multiple variants of concern *in vitro* and in small animal models[555]; and ii) robust viral replication and induction of immunopathological events by WA.1 in the macaque model, which have not been demonstrated for other strains[691,692]. While the use of WA.1 in RM provided a reproducible model by which to test CC40.8's activity, it leaves the formal possibility that the breadth of CC40.8 against circulating SARS-CoV-2 strains may not be recapitulated in NHPs or humans. Lastly, this study did not address the contribution of antibody effector functions to protection or, conversely, any mechanisms of antibody dependent enhancement of infection, both warranting further preclinical studies.

In conclusion, this study demonstrates the efficacy of a first-generation mAb, CC40.8, targeting a conserved, cross neutralizing β-CoV epitope at reducing *in vivo* viral replication and mitigating the disease pathology of SARS-CoV-2 infection within the lower airway of a clinically relevant animal model. Since the onset of this study, several mAbs targeting the conserved stem helix epitope of CoVs have been identified with considerably greater neutralization potency and breadth than CC40.8[693]. Overall, this study supports furtherance of experimental and clinical development of S2-targeting antibodies as a strategy to protect and treat coronavirus infection.

MATERIALS AND METHODS

Study Overview

An overview of the study design outlined in **Fig. 1a.** 24 RMs were infused intravenously 5 days pre infection with either a 0.1 mg/kg, 1mg/kg, or 10mg/kg concentration of experimental mAb cc40.8 or with control mAb PGT121, with each experimental group consisting of 6 animals (1 female and 5 males). Animals were screened for pre-existing, SARS-CoV-2 spike specific antibodies prior to enrollment in this study (Supplemental Table 1). Preinfection baseline samples were collected at -4 dpi. At 0 dpi, all RM were inoculated with 1mL intranasally and 1mL intratracheally with a combined total of 1.1 x 10^6 plaque forming units (PFU) of SARS-CoV-2 (2019-nCoV/USA-WA1/202). BAL and nasal swabs were collected from inoculated animals at 2dpi and at the time of necropsy (7 or 8dpi), with viral titers peaking in these tissues at 2dpi in the infected animals.

Sex as a Biological Variable: 24 rhesus macaques of Indian origin were sorted by sex, age and weight and then stratified into 4 groups (n=6). Our study examined male and female animals, and similar findings are reported for both sexes.

Animal Models

Animals used in this study were 24 (6 females and 18 males; mean age of 5 years and 11 months old) specific-pathogen free (SPF) Indian-origin rhesus macaques (RM; Macaca mulatta; Table S1). Animals were initially housed in ENPRC's BSL2 facilities. Pre-existing, SARS-CoV-2 spike binding antibodies were below detectable levels in all animals prior to infusion. On Day -5, animals in groups of six were infused intravenously with either the control antibody PGT 121 at 10mg/kg or various doses of CC40.8 (10mg/kg, 1mg/kg, 0.1 mg/kg). All antibodies were supplied in solution and diluted with DPBS. Animals were moved to the ABSL3 facilities on Day -4 following baseline collection for a 4 day acclimatization period before infection. One animal was moved on Day -3 due to vomiting during baseline BAL collections on Day -4. On Day 0, animals were inoculated with 1.1×10^6 plaque forming units (PFU) of SARS-CoV-2 (2019-CoV/USA-WA1/2020) via 1mL intratracheally and 1mL intranasally (0.5mL per nostril). After infection, animals were monitored daily by cageside observations which measured responsiveness, discharge, respiratory rate, respiratory effect, cough, and fecal consistency (Supplementary Table S2). In addition, during each anesthetic access, body weight, body condition score, respiratory rate, pulse oximetry, rectal temperature were recorded along with a clinical assessment of discharge, respiratory character and hydration (Supplementary Table S3). Over the 12/13 day period from baseline to necropsy, the

following tissues were collected from animals: peripheral blood, bronchoalveolar lavage (BAL) and nasal swabs of both nostrils with the addition of right caudal lung, spleen and hilar lymph nodes at necropsy. Additionally, right middle lung, right caudal lung, right cranial lung, left caudal lung, jejunum and ileum were collected for immunohistochemistry.

Viral Stock

SARS-CoV-2 WA1/2020 (10/23/21) stock virus with a titer of 3.2 x 10^6 pfu/mL was provided by the Virus Characterization Isolation Production and Sequencing (VCIPS) Core at Tulane National Primate Research Center. Stock virus was also sequenced to determine the original virus sequence. Using 140uL of the viral stock place in AVL buffer, RNA was extracted using the QiaAmp Mini RNA Viral Kit (#52904). Using 8uL of RNA elution, cDNA is created using the Superscript III First-Strand Synthesis (#18080-051). Next the cDNA is put through NEBNext Ultra II Non directional RNA Second Strand Synthesis Module (NEB Cat #E6111S/L). Finally a PCR clean up is done using the PureLink PCR Purification Kit (#K3100-01/02).

Determination of viral load RNA

SARS-CoV-2 gRNA N, sgRNA N and sgRNA E were quantified in NP swabs and BALs by 2 independent sites as described in the Supplementary Materials.

Tissue SARS-CoV-2 RNA Quantification

Lung tissue was harvested on 7 or 8 dpi and homogenized using Bead Ruptor 12 (Omni International). Modified protocol from Zhou et al. 2022[555].

Expression and purification of monoclonal antibodies CC40.8 and PGT121

mAbs CC40.8 and PGT121 were produced as described in the Supplementary Materials. Modified from Zhou et al. 2023[556].

Anti-Spike Antibody Detection in BAL Supernatant and Serum Samples by ELISA

Anti-spike ELISA's were performed asdescribed in the Supplementary Materials.

Tissue collection and processing

PB, NP swabs, throat swabs, and BAL were collected longitudinally. At necropsy, lower (caudal) lung, upper (cranial) lung, and hilar LNs were also collected. Detailed methods pertaining to the collection and processing of these tissues are included in the Supplementary Materials.

Single-cell RNA-Seq Library and sequencing from NHP BALs and Lung

Single cell suspensions were prepared and loaded onto the 10X Genomics Chromium Controller in the BSL3 facility using the Chromium NextGEM Single Cell 5' Library & Gel Bead kit to capture individual cells and barcoded gel beads within droplets (113). The libraries were prepared according to manufacturer instructions, including the preparation of feature barcode libraries for hashtag detection. They were then sequenced on an Illumina NovaSeq 6000 with a paired-end 26x91 configuration targeting a depth of 50,000

reads per cell. Cell Ranger software was used to perform demultiplexing of cellular transcript data, as well as mapping and annotation of UMIs and transcripts for downstream data analysis.

Single-cell RNA-Seq bioinformatic analysis of BAL and Lung cells

The cellranger v6.1.0 (10X Genomics) pipeline was used for processing the 10X sequencing data and the downstream analysis was performed using the Seurat v4.0.4 R package. A composite reference comprising of Mmul10 from Ensembl release 100 and SARS-CoV2 (strain MT246667.1 - NCBI) was used for alignment with cellranger. The percentage of SARS-CoV-2 reads was determined using the PercentageFeatureSet for SARS-CoV2 genes. For BAL samples, a total of 107,830 cells across all animals passed quality control (QC) and were used for analyses. For lung samples, a total of 101,766 cells passed upstream QC and were used for analysis. The bioinformatic processing of scRNA-Seq data and subsequent analysis was performed as described previously for BAL samples (66) and lung samples(69). Detailed methods pertaining to the bioinformatic analysis are included in the Supplementary Materials.

SARS-CoV-2 ARTIC Library Generation

SARS-CoV-2 ARTIC cDNA libraries were generated from RNA recovered from BAL supernatant at 2 dpi and at NX. Detailed methods pertaining to the generation of these libraries are included in the Supplementary Materials.

SARS-CoV-2 Sequence Analysis

SARS-CoV-2 reference-based assembly was performed with nf-core/viralrecon v2.6, using default parameters with no trim offset (114, 115). First, a consensus sequence was assembled from the reads generated from the infecting virus sample (using reference sequence MN908947.3), and this full-length SARS-CoV-2 sequence ("Input_consensus") was subsequently used at the reference sequence for assembly and variant calling from the reads generated from each experimental sample. Only samples with at least 95% genome coverage in both replicate libraries were included in sequence analysis (Supplemental Table X). These samples had a median depth of coverage across the genome ranging from 25,772X to 119,292X (median 48,563X). Intra-sample single nucleotide variants (iSNVs) were called against the "Input_consensus" sequence with iVar v1.3.1, setting the maximum depth at 29 million bases, minimum quality score at 15 and minimum frequency at 1% (116). Further filtering was used to identify iSNVs present in two replicate libraries, and at positions with at least 100X depth. Using the average frequency of each iSNV from the two replicate libraries, average Shannon entropy for each sample was calculated as the sum of (-ln(frequency)*frequency)/29903, where frequency indicates the allele frequency of each iSNV, and 29903 is the length of the reference genome sequence.

Macrophage Flow Cytometry Immunophenotyping

Macrophage immunophenotyping was performed as described in the supplementary materials.

Statistical analysis

All statistical analyses were performed two-sided with $P \leq 0.05$ deemed significant. Ranges of significance were graphically annotated as follows: *P < 0.05; **P < 0.01; ***P < 0.001; ****P < 0.0001. Analyses for Figs. 1 (B and C), 2 (B to G), 3 (C to F, K to M), and figs. S1 (A to L), S3 (B to E), S4 (A to J), S6 (D to G) were performed with Prism version 10 (GraphPad).

Study Approval

Emory's National Primate Research Center (ENPRC) is certified by the U.S. Department of Agriculture (USDA) and by the Association for Assessment and Accreditation of Laboratory Animal Care (AAALAC). All animal procedures were completed in line with institutional regulations and guidelines set by the NIH's Guide for the Care and Use of Laboratory Animals, 8th edition, and were conducted under anesthesia with appropriate follow-up pain management to ensure minimal animal suffering. All animal experimentation was reviewed and approved by Emory University's Institutional Animal Care and Use Committee (IACUC) under permit PROTO202200025.

Data and Materials Availability: Data tables for expression counts for single-cell RNA-seq for BAL are deposited in NCBI's Gene Expression Omnibus and are accessible through the Gene Expression Omnibus (GEO) under accession number (GSE283190). The processed single-cell lung macrophage reference dataset[461] was originally obtained from GEO under accession no. GSE149758[644]. Custom scripts and supporting documentation on the RNA-seq analyses will be made available at https://github.com/BosingerLab/NHP/COVID_mAb Reagents generated in this study may be requested from michelle.yu-hao.lee@emory.edu with a completed materials

transfer agreement. All data needed to evaluate the conclusions in the paper are present in the paper or the Supplementary Materials.

AUTHOR CONTRIBUTIONS:

CTE, KAK, EG, RA, TR, DRB and SEB conceptualized the study. RA identified and characterized CC40.8. EG produced and validated safety of CC40.8 antibody stocks. SAL wrote the IACUC protocol for the animal studies. SAL, TT, and MCL processed all RM blood samples in an ABSL-2 facility. MP provided critical input in the development of tissues collection protocols and alveolar macrophage flow cytometry methodology. CTE, KAK, and EG processed all SARS-CoV-2–infected samples in an ABSL-3 suite with assistance from HA. CTE performed MSD analysis on BAL fluid from uninfected and SARS-CoV-2–infected RMs with assistance from TT and MCL. MR, SW, JSW, and AW conducted all longitudinal animal collection procedures for SARS-CoV-2–infected RMs in the ABSL-3 and EHC performed necropsy collections. MG, CCH and MRB performed repeat measurements of sgRNA-N and sgRNA-E viral loads in nasopharyngeal swab and BAL. NG performed repeat measurements of sgRNA-E, sgRNA-N, and gRNA-N viral loads in nasopharyngeal swabs and BAL. CTE, KAK, and TT performed multiparameter flow cytometry and CTE analyzed flow data. EG assayed lung tissue viral loads. EG assayed serum-neutralizing antibody titers and NB analyzed BAL antibody titers. H.A. performed 10X Genomics scRNA-seq, and CTE performed preprocessing for single-cell BAL data and conducted and graphed all scRNA-seq analyses with oversight from AA. AM and SAL prepared SARS-CoV-2 ARTIC libraries from BAL supernatant. Mutational entropy analysis was performed by AB and AP. Funding was acquired by DRB

(supplement to UM1AI44462 and by the Bill and Melinda Gates Foundation (INV004923). CTE and SEB wrote the manuscript with KAK, EG, DRB, RA and TFR providing critical input. Order of first authors was determined by amount of contribution towards writing the final manuscript.

ACKNOWLEDGMENTS

We thank the Emory National Primate Research Center (ENPRC) Division of Animal Resources for providing support in animal care. We thank Kalpana Patel from the Environmental Health and Safety Office for BSL-3 training and safety oversight. We thank Dr. Elise Viox and Diane Carnathan for their input in study planning and preparation. We thank Dr. Mehul Suthar for his input on SARS-CoV-2 stock selection. We thank Jianjun Chang at the Emory Multiplexed Immunoassay Core for help with MSD assay. We would like to thank the High Containment Research Performance Core: RRID: SCR_024612; at Tulane National Primate Research Center for technical assistance. We thank Drs. Jessica Raper and Tomas Salinas for their insight into the long COVID-19 model in RM.

Funding: This study was supported by funding from the Bill & Melinda Gates Foundation (INV004923) and by the supplement to UM1AI44462 (all to DRB) and by the National Institutes of Health-(NIH), National Institute of Allergy and Infectious Diseases-(NIAID) award R01AI170928 (to R.A.). This project has been funded in part by the Intramural Program of the NIAID, NIH, Department of Health and Human Services. Next generation sequencing services were provided by the Emory NPRC Genomics Core which is supported in part by NIH P51 OD011132. Sequencing data was acquired on an Illumina

NovaSeq 6000 funded by NIH S10 OD026799. The content of this publication does not necessarily reflect the views or policies of the U.S. Department of Health and Human Services, nor does it imply endorsement of organizations or commercial products. The funders had no role in study design, data collection and analysis, decision to publish, or preparation of the manuscript.

CHAPTER 2 FIGURES

Figure 1

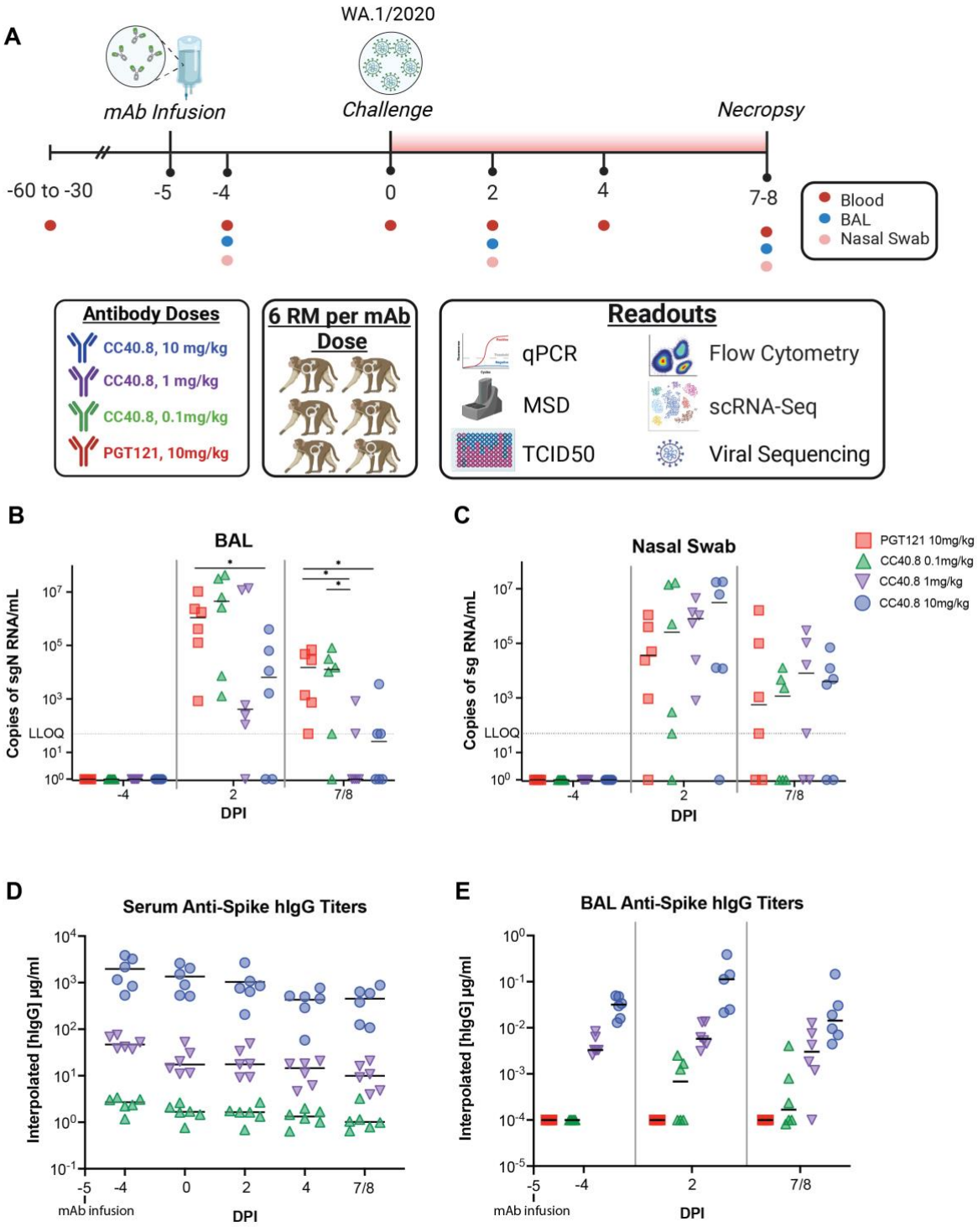

Fig. 1. Preinfusion of S2-targeting bNAb CC40.8 reduced viral loads in RMs on SARS CoV-2 challenge (**A**) 24 RMs (6 females and 18 males; mean age of 5 years and 11 months old; range 5-6 years old) were infused intravenously 5 days pre infection with either a 0.1 mg/kg, 1mg/kg, or 10mg/kg concentration of SARS-CoV-2 bNAb CC40.8 or with control mAb PGT121, with each experimental group consisting of 6 RMs (1 female and 5 males). RMs were screened for pre-existing, SARS-CoV-2 spike specific antibodies prior to CC40.8 administration RMs were euthanized at 7 dpi (n = 3 RMs per treatment arm) or 8 dpi (n = 3 RMs per treatment arm). Levels of SARS-CoV-2 sgRNA N in BAL (**B**) and nasopharyngeal swabs (**C**). Anti-Spike hIgG titers in the serum (**D**) and BAL (**E**) measured via ELISA. Control PGT121-treated RMs are depicted with red squares, CC40.8 0.1mg/kg-treated RMs depicted with green upward pointing triangles, CC40.8 1mg/kg-treated RMs depicted with purple downward pointing triangles, CC40.8 10mg/kg-treated RMs depicted with blue circles. Black lines represent the median viral loads for each treatment group at each time point. Statistical analyses were performed using nonparametric Mann-Whitney tests. *P < 0.05 .

Figure 2

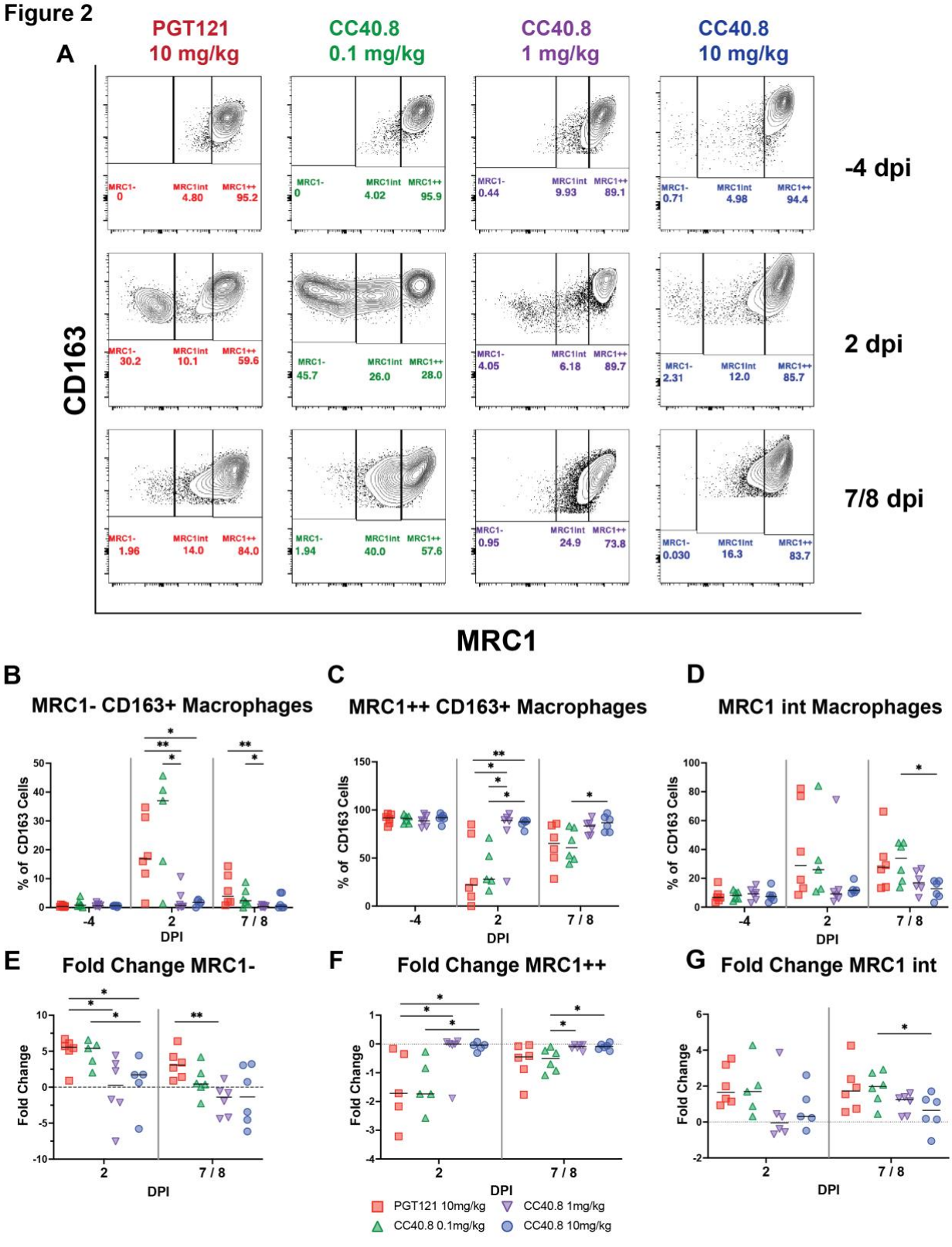
A
PGT121 10 mg/kg
CC40.8 0.1 mg/kg
CC40.8 1 mg/kg
CC40.8 10 mg/kg
-4 dpi
2 dpi
7/8 dpi
CD163
MRC1
MRC1- 0
MRC1int 4.80
MRC1++ 95.2
MRC1- 0
MRC1int 4.02
MRC1++ 95.9
MRC1- 0.44
MRC1int 9.93
MRC1++ 89.1
MRC1- 0.71
MRC1int 4.98
MRC1++ 94.4
MRC1- 30.2
MRC1int 10.1
MRC1++ 59.6
MRC1- 45.7
MRC1int 26.0
MRC1++ 28.0
MRC1- 4.05
MRC1int 6.18
MRC1++ 89.7
MRC1- 2.31
MRC1int 12.0
MRC1++ 85.7
MRC1- 1.96
MRC1int 14.0
MRC1++ 84.0
MRC1- 1.94
MRC1int 40.0
MRC1++ 57.6
MRC1- 0.95
MRC1int 24.9
MRC1++ 73.8
MRC1- 0.030
MRC1int 16.3
MRC1++ 83.7
B
MRC1- CD163+ Macrophages
% of CD163 Cells
DPI
C
MRC1++ CD163+ Macrophages
D
MRC1 int Macrophages
E
Fold Change MRC1-
Fold Change
F
Fold Change MRC1++
G
Fold Change MRC1 int
PGT121 10mg/kg
CC40.8 1mg/kg
CC40.8 0.1mg/kg
CC40.8 10mg/kg

Fig. 2. CC40.8-treated RMs had lower frequencies of inflammatory CD163+ MRC1- macrophages compared with PGT121-treated RMs. (**A**) Representative staining of macrophages for CD163 and MRC1 in the BAL at -4, 2, and 7/8 dpi with frequency as a percentage of total CD163+ cells. Macrophages were gated on singlets, CD45+, FSC and SSC characteristic of granulocytes and alveolar macrophages, live cells, and CD14+ populations. (**B** to **D**) Frequency as a percentage of total CD163+ cells for (**B**) MRC1-, (**C**) MRC1 intermediate and (**D**) MRC1++ cells. (**E** to **F**) Fold change from -4 dpi baseline as a percentage of total CD163+ cells for (**E**) MRC1-, (**F**) MRC1 intermediate, and (**G**) MRC1++ cells. Control PGT121-treated RMs are depicted with red squares, CC40.8 0.1mg/kg-treated RMs depicted with green upward pointing triangles, CC40.8 1mg/kg-treated RMs depicted with purple downward pointing triangles, CC40.8 10mg/kg-treated RMs depicted with blue circles. Black lines represent the median frequency or fold change in RMs from each respective treatment group. Statistical analyses were performed using nonparametric Mann-Whitney tests. *$P < 0.05$, **$P < 0.01$

Figure 3

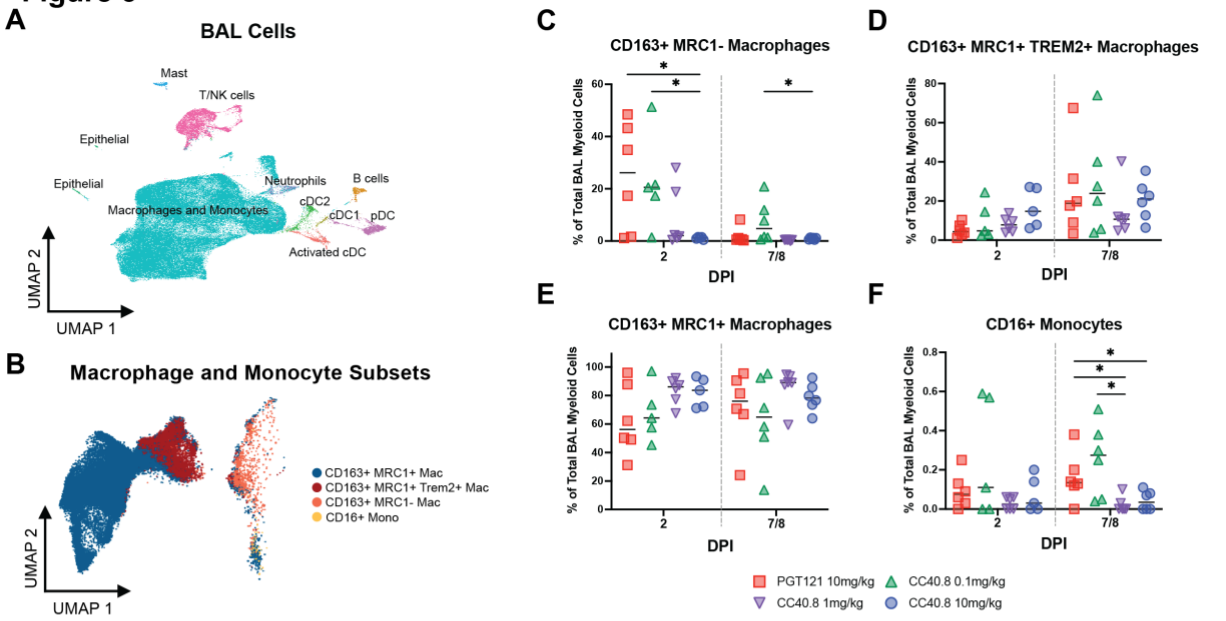
A
BAL Cells
Mast
T/NK cells
Epithelial
Epithelial
Neutrophils
B cells
cDC2
Macrophages and Monocytes
cDC1
pDC
Activated cDC
UMAP 2
UMAP 1
B
Macrophage and Monocyte Subsets
CD163+ MRC1+ Mac
CD163+ MRC1+ Trem2+ Mac
CD163+ MRC1- Mac
CD16+ Mono
UMAP 2
UMAP 1
C
CD163+ MRC1- Macrophages
% of Total BAL Myeloid Cells
DPI
D
CD163+ MRC1+ TREM2+ Macrophages
% of Total BAL Myeloid Cells
DPI
E
CD163+ MRC1+ Macrophages
% of Total BAL Myeloid Cells
DPI
F
CD16+ Monocytes
% of Total BAL Myeloid Cells
DPI
PGT121 10mg/kg
CC40.8 0.1mg/kg
CC40.8 1mg/kg
CC40.8 10mg/kg

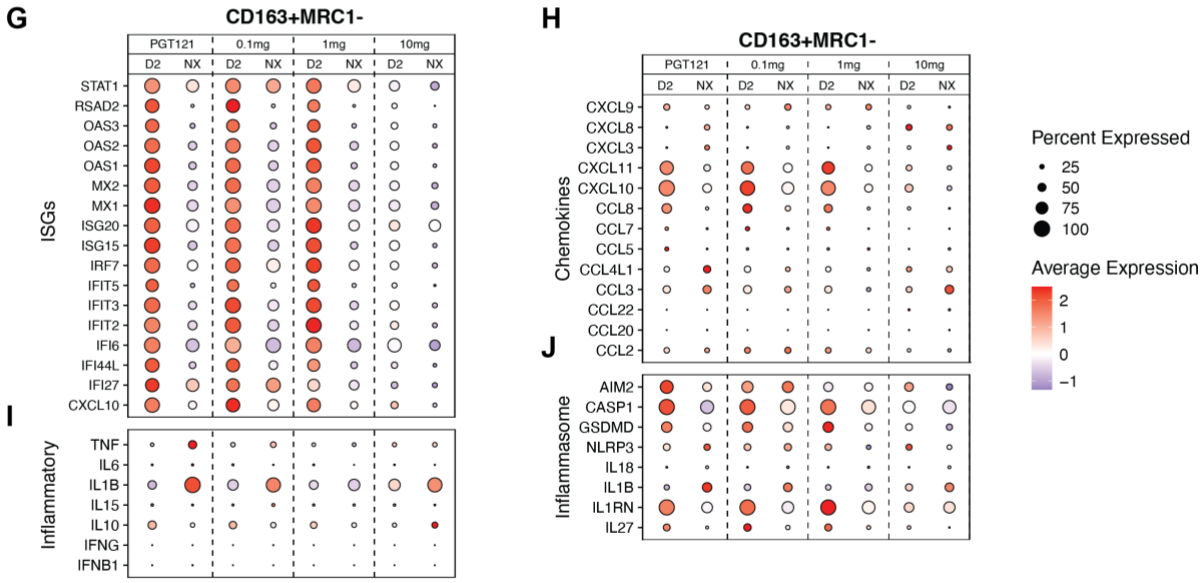
G
CD163+MRC1-
PGT121
0.1mg
1mg
10mg
D2
NX
ISGs
STAT1
RSAD2
OAS3
OAS2
OAS1
MX2
MX1
ISG20
ISG15
IRF7
IFIT5
IFIT3
IFIT2
IFI6
IFI44L
IFI27
CXCL10
I
Inflammatory
TNF
IL6
IL1B
IL15
IL10
IFNG
IFNB1
H
CD163+MRC1-
Chemokines
CXCL9
CXCL8
CXCL3
CXCL11
CXCL10
CCL8
CCL7
CCL5
CCL4L1
CCL3
CCL22
CCL20
CCL2
J
Inflammasome
AIM2
CASP1
GSDMD
NLRP3
IL18
IL1B
IL1RN
IL27
Percent Expressed
25
50
75
100
Average Expression
2
1
0
−1

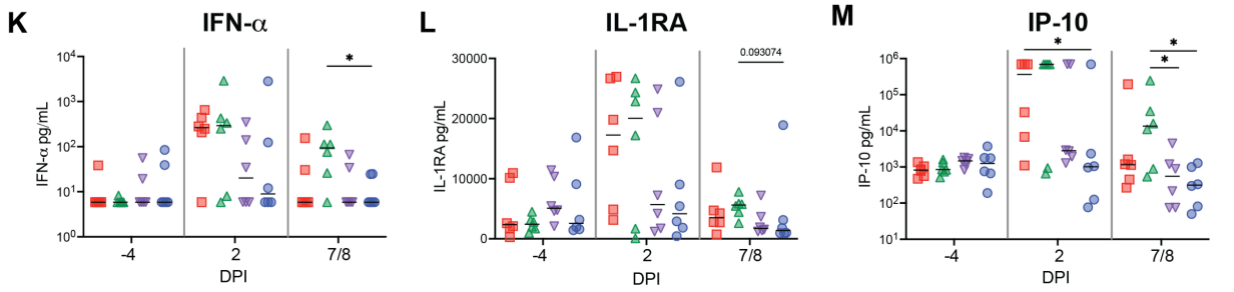
K
IFN-α
IFN-α pg/mL
DPI
L
IL-1RA
0.093074
IL-1RA pg/mL
DPI
M
IP-10
IP-10 pg/mL
DPI

Fig. 3. Effect of CC40.8 treatment on gene expression of BAL single cells during SARS-CoV-2 infection using 10X. A) Uniform Manifold Approximation and Projection (UMAP) of BAL samples (107830 cells) integrated using reciprocal principal components analysis (PCA) showing cell type annotations. Captures were performed on BAL cells from all RMs at 2 and 7/8 dpi. (**B**) Mapping of macrophage/monocyte cells in the BAL of SARS-CoV-2–infected PGT121- and CC40.8-treated RMs to different lung macrophage/monocyte subsets from healthy RMs[644]. (**C** to **F**) Percentage of different macrophage/monocyte subsets of all the macrophage/monocytes in BAL at 2 and 7/8 dpi from PGT121- and CC40.8-treated RMs. Frequency as a percentage of total CD163+ cells for (**C**) MRC1-, (**D**) MRC1+ TREM2+, (**E**) MRC1++, and (**F**) CD16+ monocytes. (**G** to **J**) Dot plots showing the expression of selected (**G**) ISGs, (**I**) inflammatory genes, (**H**) chemokines, and (**J**) inflammasome genes in CD163+ MRC1- macrophages. The size of the dot indicates the percentage of cells that express a given gene, and the color indicates the level of expression. (**K** to **M**) Fold change of cytokines and chemokines in BAL fluid relative to −4 dpi measured by MSD immunoassay. Control PGT121-treated RMs are depicted with red squares, CC40.8 0.1mg/kg-treated RMs depicted with green upward pointing triangles, CC40.8 1mg/kg-treated RMs depicted with purple downward pointing triangles, CC40.8 10mg/kg-treated RMs depicted with blue circles. Black lines represent the median frequency or fold change in RMs from each respective treatment group. Statistical analyses were performed using two-sided nonparametric Mann-Whitney tests. $*P < 0.05$.

Figure 4

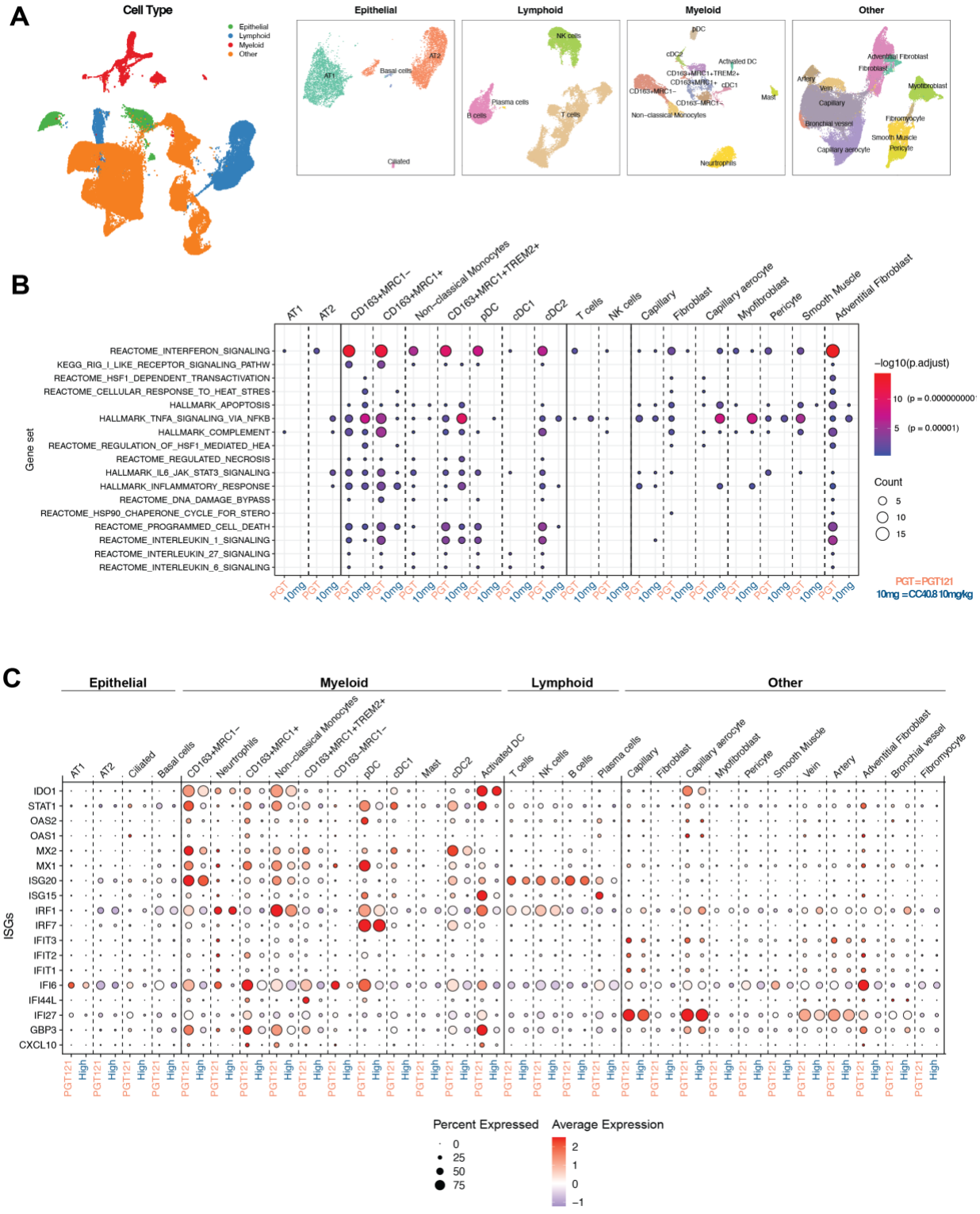
A
Cell Type
Epithelial
Lymphoid
Myeloid
Other
Epithelial
Lymphoid
Myeloid
Other
AT1
AT2
Basal cells
Ciliated
NK cells
Plasma cells
B cells
T cells
pDC
cDC2
Activated DC
CD163+MRC1+TREM2+
CD163+MRC1+
cDC1
CD163+MRC1−
CD163−MRC1−
Non−classical Monocytes
Mast
Neutrophils
Adventitial Fibroblast
Fibroblast
Artery
Vein
Myofibroblast
Capillary
Bronchial vessel
Fibromyocyte
Smooth Muscle
Pericyte
Capillary aerocyte
B
AT1
AT2
CD163+MRC1−
CD163+MRC1+
Non−classical Monocytes
CD163+MRC1+TREM2+
pDC
cDC1
cDC2
T cells
NK cells
Capillary
Fibroblast
Capillary aerocyte
Myofibroblast
Pericyte
Smooth Muscle
Adventitial Fibroblast
Gene set
REACTOME_INTERFERON_SIGNALING
KEGG_RIG_I_LIKE_RECEPTOR_SIGNALING_PATHW
REACTOME_HSF1_DEPENDENT_TRANSACTIVATION
REACTOME_CELLULAR_RESPONSE_TO_HEAT_STRES
HALLMARK_APOPTOSIS
HALLMARK_TNFA_SIGNALING_VIA_NFKB
HALLMARK_COMPLEMENT
REACTOME_REGULATION_OF_HSF1_MEDIATED_HEA
REACTOME_REGULATED_NECROSIS
HALLMARK_IL6_JAK_STAT3_SIGNALING
HALLMARK_INFLAMMATORY_RESPONSE
REACTOME_DNA_DAMAGE_BYPASS
REACTOME_HSP90_CHAPERONE_CYCLE_FOR_STERO
REACTOME_PROGRAMMED_CELL_DEATH
REACTOME_INTERLEUKIN_1_SIGNALING
REACTOME_INTERLEUKIN_27_SIGNALING
REACTOME_INTERLEUKIN_6_SIGNALING
PGT
10mg
−log10(p.adjust)
10 (p = 0.000000000
5 (p = 0.00001)
Count
5
10
15
PGT=PGT121
10mg =CC40.8 10mg/kg
C
Epithelial
Myeloid
Lymphoid
Other
AT1
AT2
Ciliated
Basal cells
CD163+MRC1−
Neutrophils
CD163+MRC1+
Non−classical Monocytes
CD163+MRC1+TREM2+
CD163−MRC1−
pDC
cDC1
Mast
cDC2
Activated DC
T cells
NK cells
B cells
Plasma cells
Capillary
Fibroblast
Capillary aerocyte
Myofibroblast
Pericyte
Smooth Muscle
Vein
Artery
Adventitial Fibroblast
Bronchial vessel
Fibromyocyte
ISGs
IDO1
STAT1
OAS2
OAS1
MX2
MX1
ISG20
ISG15
IRF1
IRF7
IFIT3
IFIT2
IFIT1
IFI6
IFI44L
IFI27
GBP3
CXCL10
PGT121
High
Percent Expressed
0
25
50
75
Average Expression
2
1
0
−1

Fig. 4. Effect of CC40.8 treatment on lung cells during SARS-CoV-2 infection. (**A**) UMAP based on reciprocal PCA of lung single cells (101,766 cells) collected at 7/8 dpi (*n* = 3 PGT121, 3 CC40.8 0.1mg/kg, and 3 CC40.8 10mg/kg). The cells were classified into four broad categories—epithelial, lymphoid, myeloid, and other, followed by subsetting and separate clustering within each category. UMAPs for each category with cell type annotations are also shown. (**B**) Selected gene sets that were found to be enriched (*P*-adjusted value < 0.05) in lung cells from PGT121-treated RMs compared to CC40.8 10mg/kg-treated RMs at 7/8 dpi based on overrepresentation analysis using Hallmark, Reactome, Kyoto Encyclopedia of Genes and Genomes, and BioCarta gene sets from MSigDB. The size of the dots represents the number of genes that were enriched in the gene set, and the color indicates the *P*-adjusted value, with red denoting smaller *P*-adjusted values. The gene set IDs in order are M983, M15913, M27255, M27253, M5902, M5890, M5921, M27250, M41804, M5897, M5932, M27698, M27251, M29666, M27436, M27895, M27897, and M1014. (**C**) Dot plots showing gene expression in lung cells present at higher frequencies from PGT121- and CC40.8-treated macaques at 7/8 dpi. Plot is organized by epithelial, myeloid, lymphoid and other subsets. The size of the dot represents the percentage of cells expressing a given gene, and the color indicates the average expression.

Figure 5

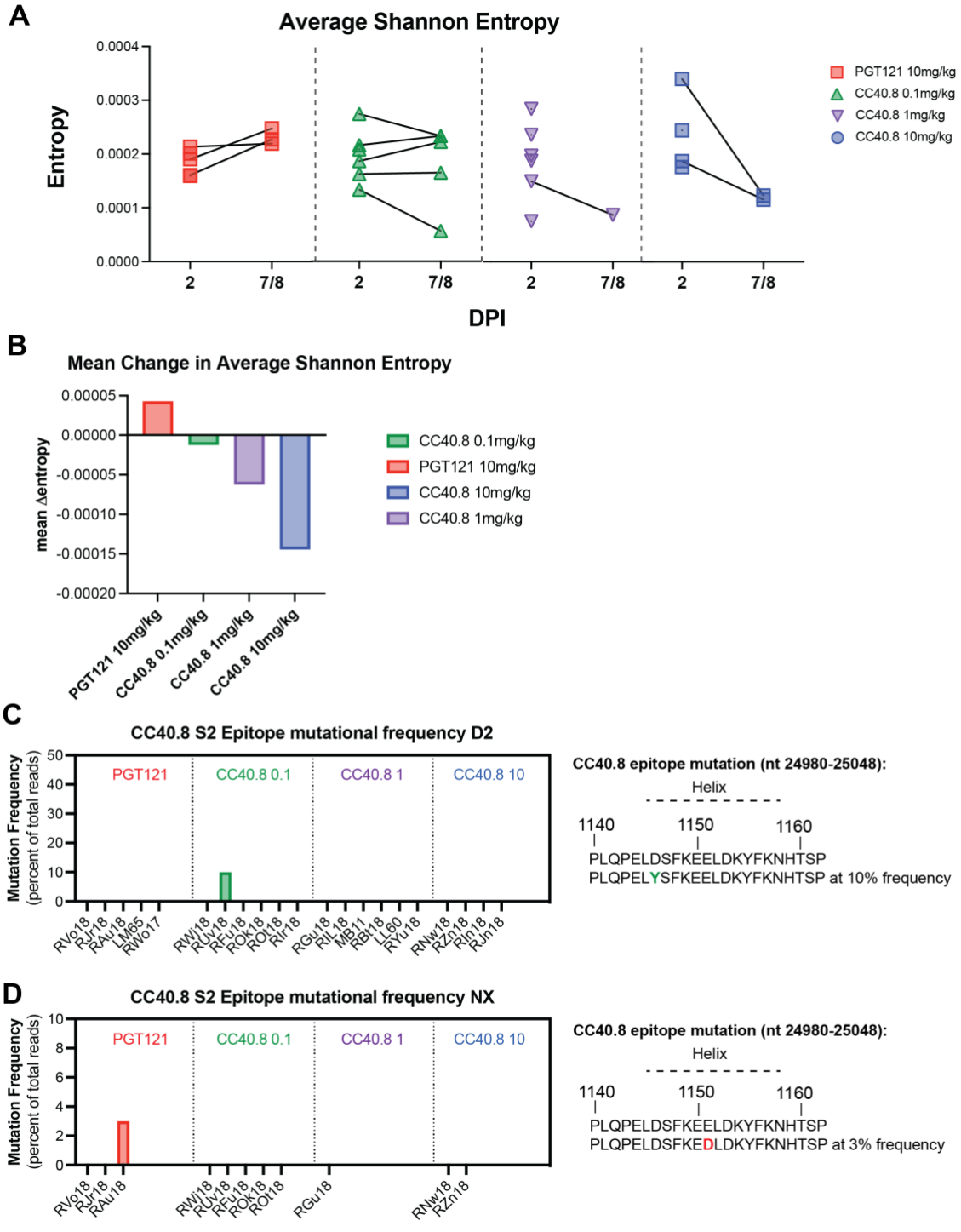
A
Average Shannon Entropy
Entropy
0.0004
0.0003
0.0002
0.0001
0.0000
2
7/8
2
7/8
2
7/8
2
7/8
DPI
PGT121 10mg/kg
CC40.8 0.1mg/kg
CC40.8 1mg/kg
CC40.8 10mg/kg
B
Mean Change in Average Shannon Entropy
mean Δentropy
0.00005
0.00000
-0.00005
-0.00010
-0.00015
-0.00020
PGT121 10mg/kg
CC40.8 0.1mg/kg
CC40.8 1mg/kg
CC40.8 10mg/kg
C
CC40.8 S2 Epitope mutational frequency D2
Mutation Frequency
(percent of total reads)
PGT121
CC40.8 0.1
CC40.8 1
CC40.8 10
RVo18 RJr18 RAu18 LM65 RWo17 RWf18 RUv18 RFu18 ROK18 ROt18 RIr18 RGu18 RIL18 MB11 RBt18 LL60 RVu18 RNw18 RZn18 RIn18 RJn18
CC40.8 epitope mutation (nt 24980-25048):
Helix
1140 1150 1160
PLQPELDSFKEELDKYFKNHTSP
PLQPELYSFKEELDKYFKNHTSP at 10% frequency
D
CC40.8 S2 Epitope mutational frequency NX
Mutation Frequency
(percent of total reads)
PGT121
CC40.8 0.1
CC40.8 1
CC40.8 10
RVo18 RJr18 RAu18 RWf18 RUv18 RFu18 ROK18 ROt18 RGu18 RNw18 RZn18
CC40.8 epitope mutation (nt 24980-25048):
Helix
1140 1150 1160
PLQPELDSFKEELDKYFKNHTSP
PLQPELDSFKEDLDKYFKNHTSP at 3% frequency

Fig. 5. Effect of CC40.8 treatment on SARS-CoV-2 mutant frequency (**A**) The average Shannon entropy calculated from intra-sample single nucleotide variant (iSNV) frequency in replicate SARS-CoV-2 ARTIC libraries generated from BAL supernatant at 2 dpi and NX (7/8 dpi). Black lines connect libraries from same animal at different timepoints (**B**) Mean change in Shannon entropy for each treatment group from 2 dpi to 7/8 dpi. (**C** to **D**) Frequency of intra-sample, single nucleotide variations at the CC40.8 S2 stem helix epitope at (**C**) 2 dpi and (**D**) 7/8 dpi.

Chapter 2 Supplemental Figures

Figure S1

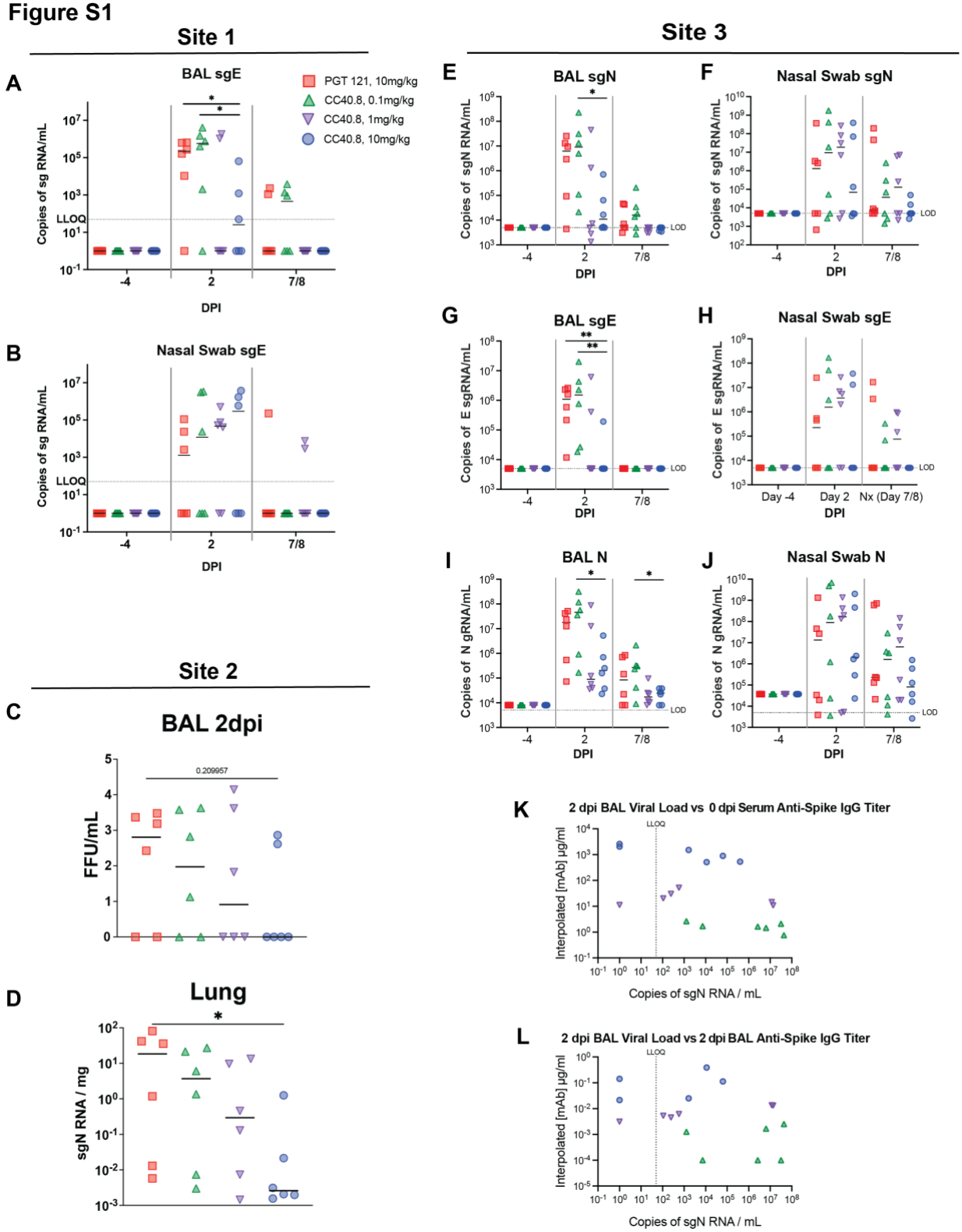

Fig S1. CC40.8 reduced BAL and lung but not nasopharyngeal viral loads in SARS-CoV-2-challenged RMs. Viral sgRNA N and sgRNA E quantification was replicated by two independent laboratories (Site 1 and Site 3). Viral gRNA quantification was performed by site 3. Tissue viral loads and viral plaque assays were performed by site 2. (**A** to **B**) Viral loads based on qPCR analysis generated by site 1. sgRNA-E viral loads for BAL (A) and nasal swab (**B**). (**C** to **D**) Viral loads generated by site 2. **(C**) SARS-CoV-2 infectious virus titers (PFU) as determined by plaque assay from lung tissue at day 5 after infection. (**D**) SARS-CoV-2 viral RNA loads based on the qPCR analysis of lung tissue at day 5 after infection. (**E** to **J**) Viral loads based on qPCR analysis generated by site 3. (**E**) sgRNA-N viral loads for BAL. (**F**) sgRNA-N viral loads for nasopharyngeal swabs. (**G**) sgRNA-E viral loads for BAL. (**H**) sgRNA-E viral loads for nasopharyngeal swabs. (**I**) gRNA-N viral loads for BAL. (**J**) gRNA-N viral loads for nasopharyngeal swabs. (**K**) Correlation of SARS-CoV-2 sgRNA-N levels in the BAL with serum levels of anti-spike IgG titers. (**L**) Correlation of SARS-CoV-2 sgRNA-N levels in the BAL with BAL levels of anti-spike IgG titers. Control PGT121-treated RMs are depicted with red squares, CC40.8 0.1mg/kg-treated RMs depicted with green upward pointing triangles, CC40.8 1mg/kg-treated RMs depicted with purple downward pointing triangles, CC40.8 10mg/kg-treated RMs depicted with blue circles. Black lines represent the median titer in RMs from each respective treatment group. Statistical analyses were performed using two-sided nonparametric Mann-Whitney tests. *$P < 0.05$.

Supplemental Figure 2

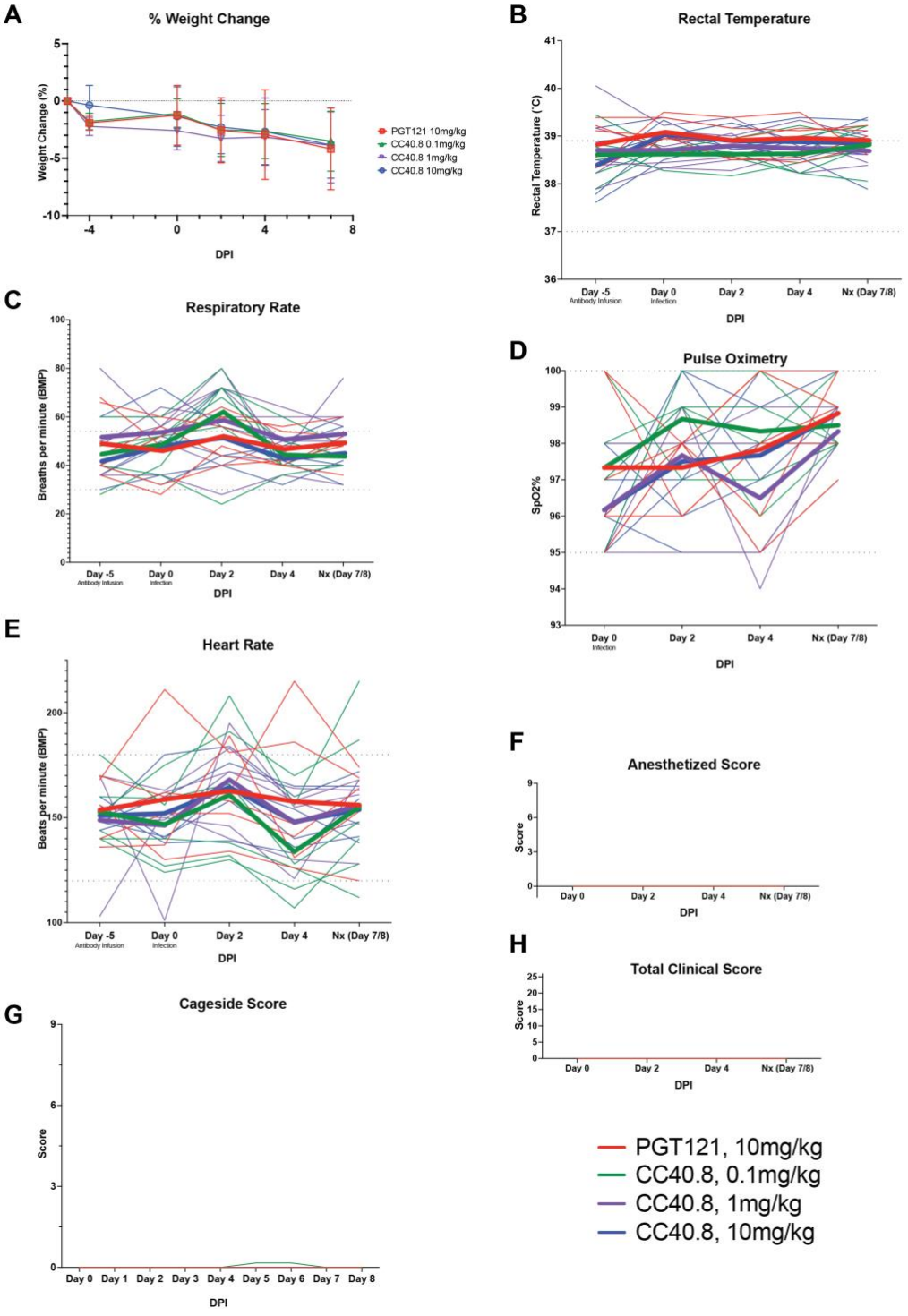

Fig S2. Administration of CC40.8 mAb was safe and well-tolerated in RMs. (**A** to **E**) Longitudinal measurements of (**A**) percent weight change from preinfection baseline, (**B**) rectal temperature, (**C**) respiratory rate, (**D**) pulse oximetry, and (**E**) heart rate in RMs. Statistical analysis between timepoints was performed using two-sided Wilcoxon matched-pairs signed rank tests. * p-value < 0.05. (**F** to **H**) Anesthetized scores, cage-side scores, and total clinical scores of PGT121 and CC40.8-treated SARS-CoV-2-infected RMs. Statistical analyses for panels b-d were performed using non-parametric Mann-Whitney tests. * p-value < 0.05, Black dotted horizontal lines indicate normal ranges for measured parameters for adult indoor RMs. Bolded red, green, purple and blue lines indicate averages for PGT121, CC40.8 0.1mg/kg, CC40.8 1mg/kg, and CC40.8 10mg/kg-treated RMs respectively.

Supplemental Figure 3

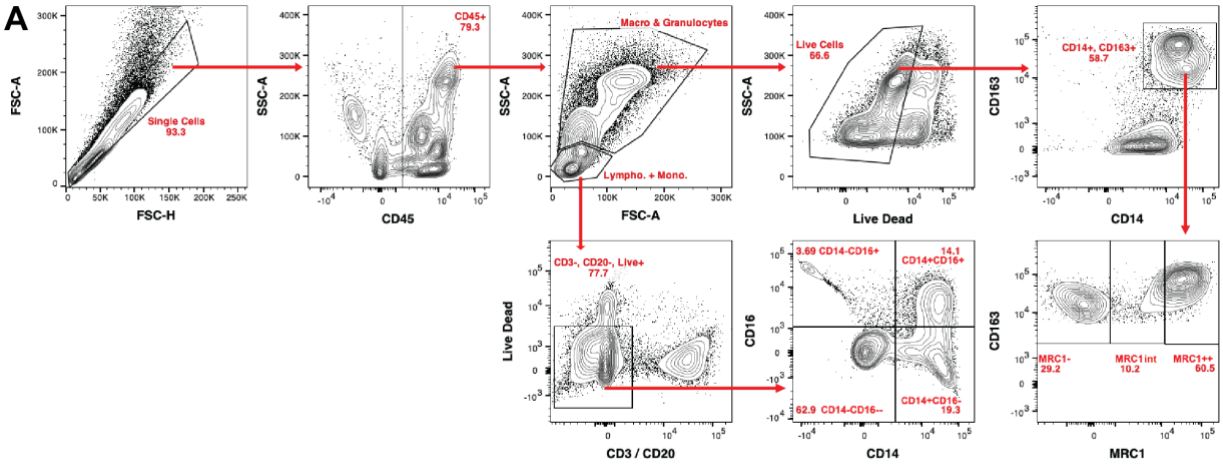

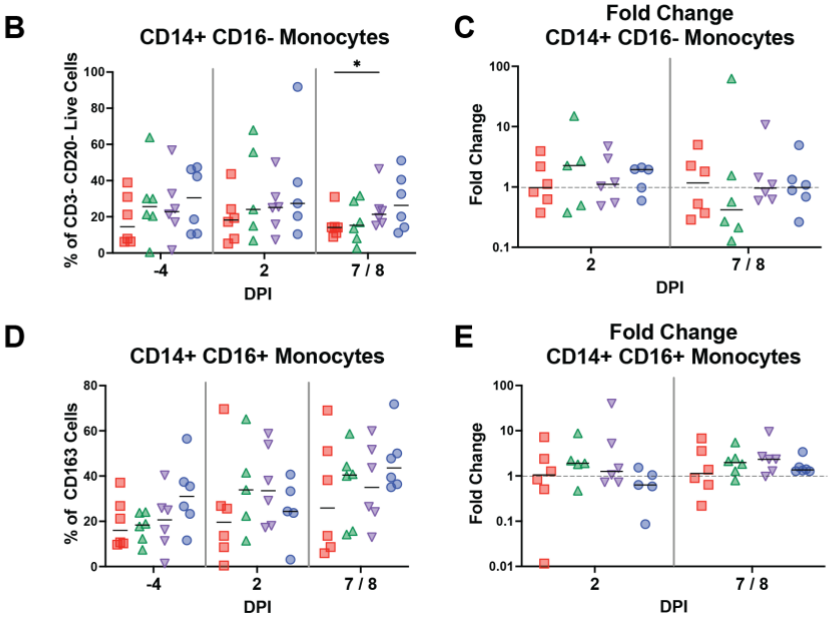

Fig S3. Flow gating strategy for macrophage and monocyte levels in BAL of RMs. (**A**) Gating strategy for innate immune cell phenotyping panel in BAL (shown in Fig. 3). (**B**) Frequency of CD14+CD16- monocytes in BAL mononuclear cells and (**C**) fold change relative to -4 dpi. (**D**) Frequency of CD14+CD16+ monocytes in BAL mononuclear cells and (**E**) fold change relative to -4 dpi. Control PGT121-treated RMs are depicted with red squares, CC40.8 0.1mg/kg-treated RMs depicted with green upward pointing triangles, CC40.8 1mg/kg-treated RMs depicted with purple downward pointing triangles, CC40.8 10mg/kg-treated RMs depicted with blue circles. Statistical analyses were performed using two-sided non-parametric Mann- Whitney tests. * p-value < 0.05

Supplemental Figure 4

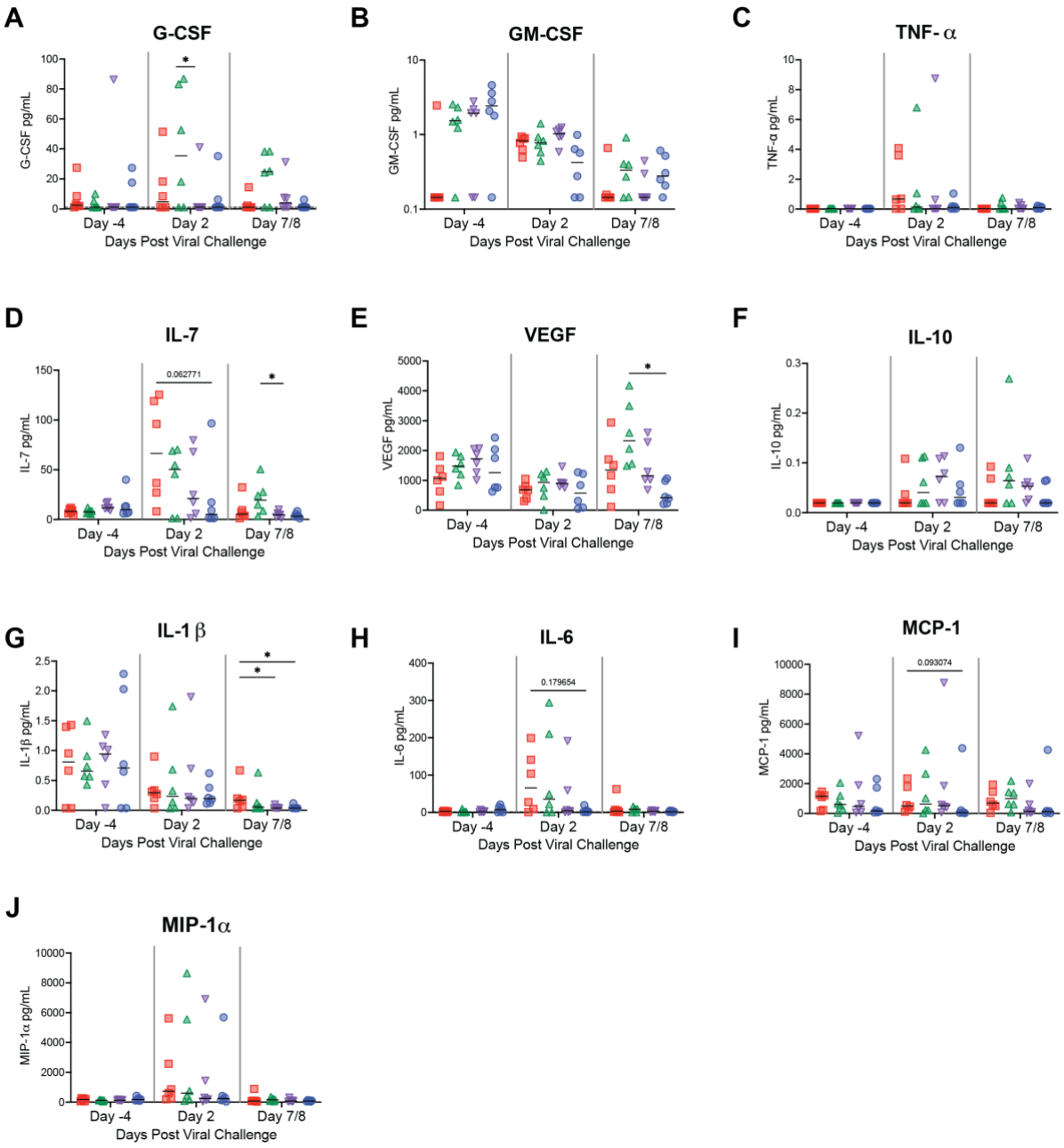

Fig S4. Cytokine and chemokine levels in BAL of RMs. (**A** to **J**) Levels of cytokines and chemokines (pg/mL) in the BAL of RMs at -4, 2 and 7/8 dpi. Control PGT121-treated RMs are depicted with red squares, CC40.8 0.1mg/kg-treated RMs depicted with green upward pointing triangles, CC40.8 1mg/kg-treated RMs depicted with purple downward pointing triangles, CC40.8 10mg/kg-treated RMs depicted with blue circles. Black lines represent the median level in RMs from each respective treatment group. Statistical analyses were performed using two-sided nonparametric Mann-Whitney tests. *$P < 0.05$.

Supplemental Figure 5

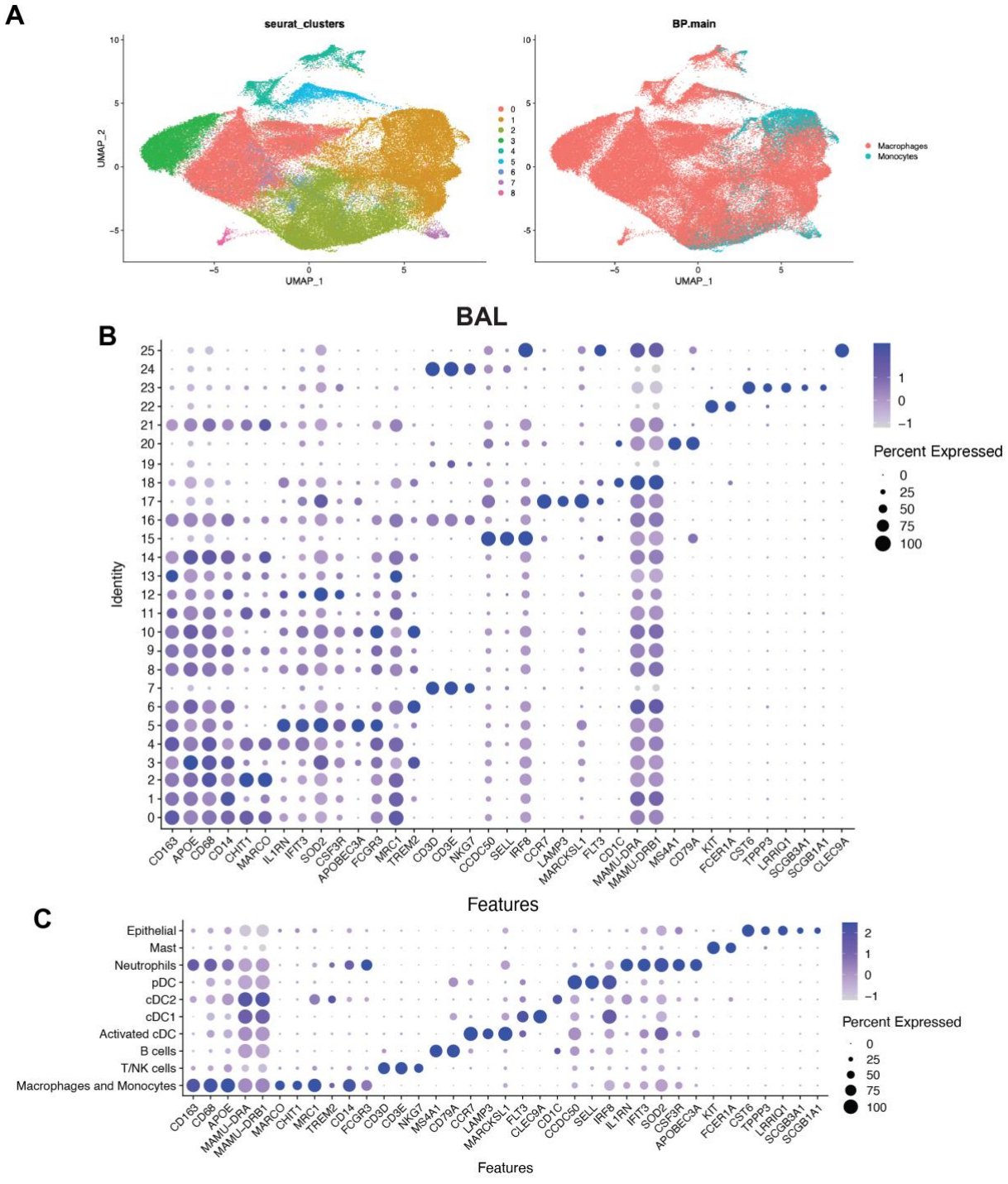

Fig S5. Expression of marker genes in BAL single cells. (**A**) UMAP of BAL samples colored by clusters determined using Seurat and annotated cell types. (**B**) Dot Plot showing expression of canonical marker genes in Seurat clusters. (**C**) Dot Plot showing expression of canonical marker genes in annotated cell types.

Supplemental Figure 6

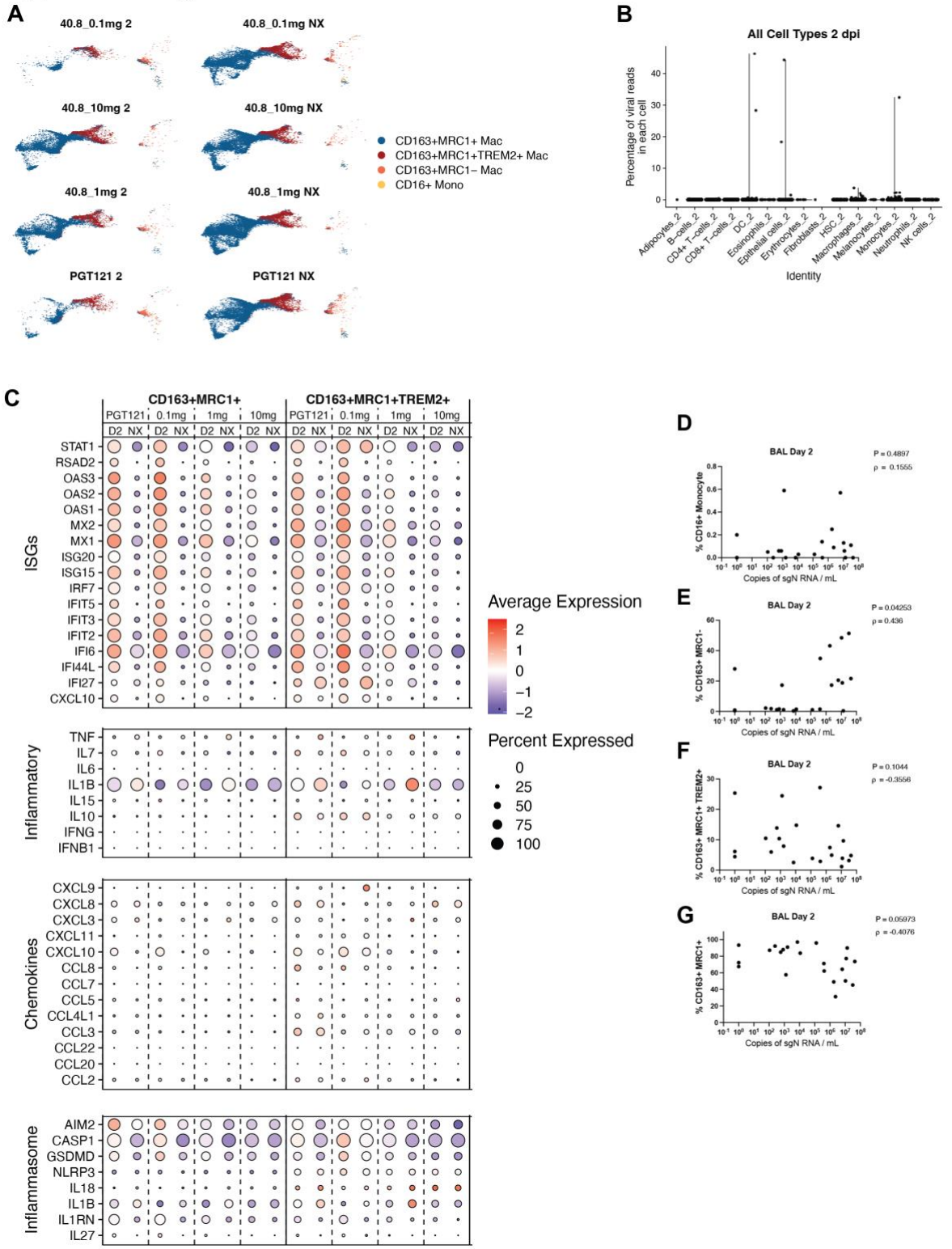

Fig S6. Effect of CC40.8 treatment on BAL single cells following SARS-CoV-2 challenge. (**A**) UMAP split by time point and treatment showing BAL macrophages/monocytes mapped to the reference macrophage/monocytes from lungs of healthy RM. (**B**) Violin plots showing the percentage of viral reads in different BAL cell subsets from all RMs at 2 dpi. Dot plots showing the expression of selected ISGs, inflammatory genes, chemokines, and inflammasome genes in CD163+ MRC1+ and CD163+ MRC1+ TREM2+ macrophages. The size of the dot indicates the percentage of cells that express a given gene, and the color indicates the level of expression. **(D-G)** Correlation of single-cell macrophage and monocyte subsets with SARS-CoV-2 titers (sgRNA-N) within the BAL at 2 dpi for (**D**) CD16+ monocytes, (**E**) CD163+MRC1- macrophages, (**F**) CD163+MRC1+ TREM2+ macrophages, and (**G**) CD163+MRC1- macrophages.

Supplemental Figure 7

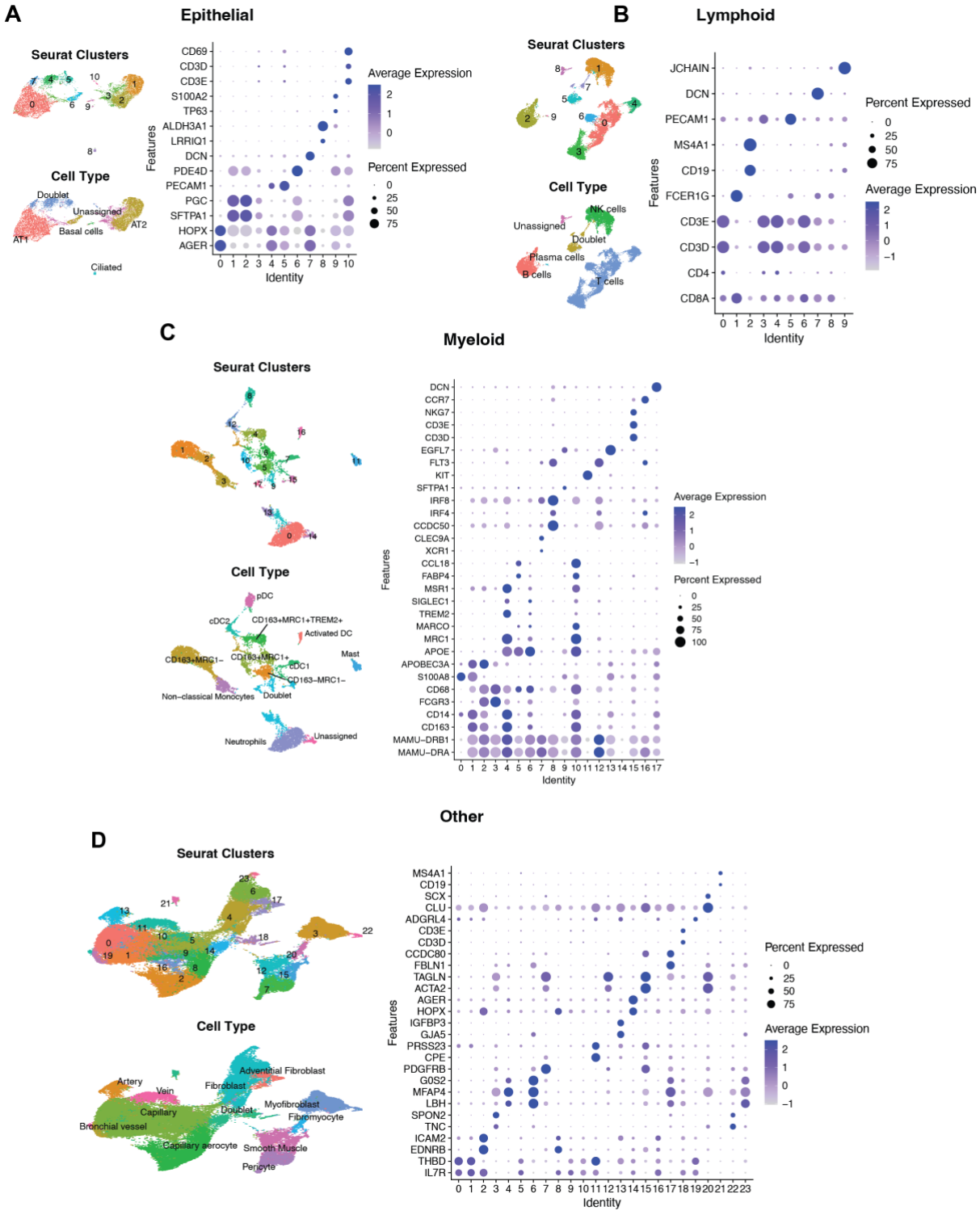

Fig S7 Annotation of lung cells. (**A** to **D**) UMAPs displaying Seurat clustering and cell-type annotations based on the expression of marker genes and dot plots with canonical marker genes for (**A**) epithelial, (**B**) lymphoid, (**C**) myeloid, and (**D**) other (stromal and endothelial) subsets. For each category, cells were clustered separately following preliminary cell-type annotation. The size of the dot in the dotplots indicates the percentage of cells that express a given gene, and the color indicates the level of expression.

Supplemental Figure 8

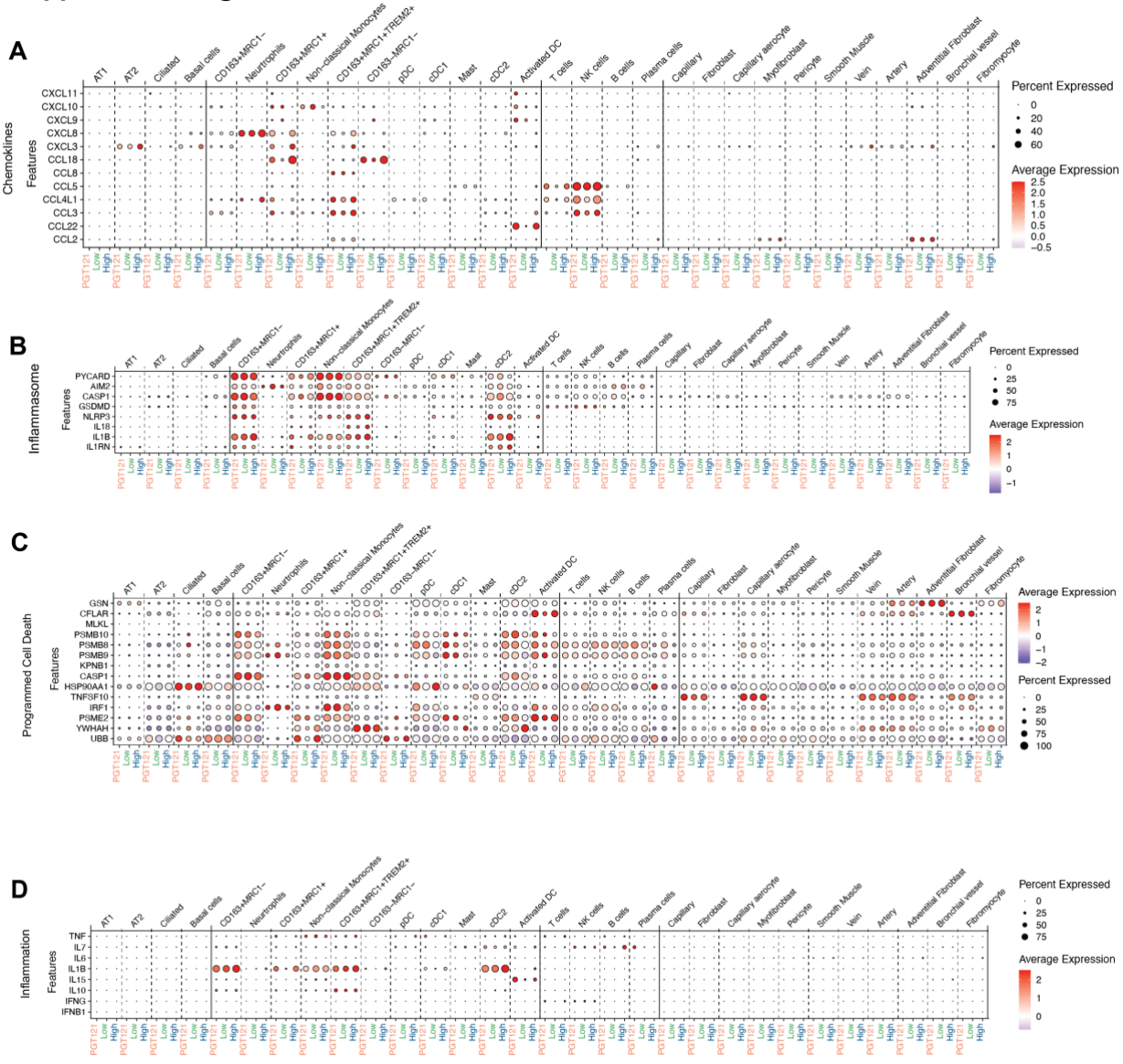

Fig. S8. Effect of CC40.8 treatment on gene expression in lung cells (**A** to **D**) Dot plots showing gene expression in lung cells from PGT121, CC40.8 0.1 mg/kg, and CC40.8 10mg/kg-treated RMs. (**A**) Expression of chemokines in lung cells at 7/8 dpi. (**B**) Expression of inflammasome genes in lung cells at 7/8 dpi. (**C**) Expression of genes related to programmed cell death in lung cells at 7/8 dpi. (**D**) Expression of genes related to inflammation in lung cells at 7/8 dpi. The size of the dot indicates the percentage of cells that express a given gene, and the color indicates the level of expression.

Supplemental Figure 9

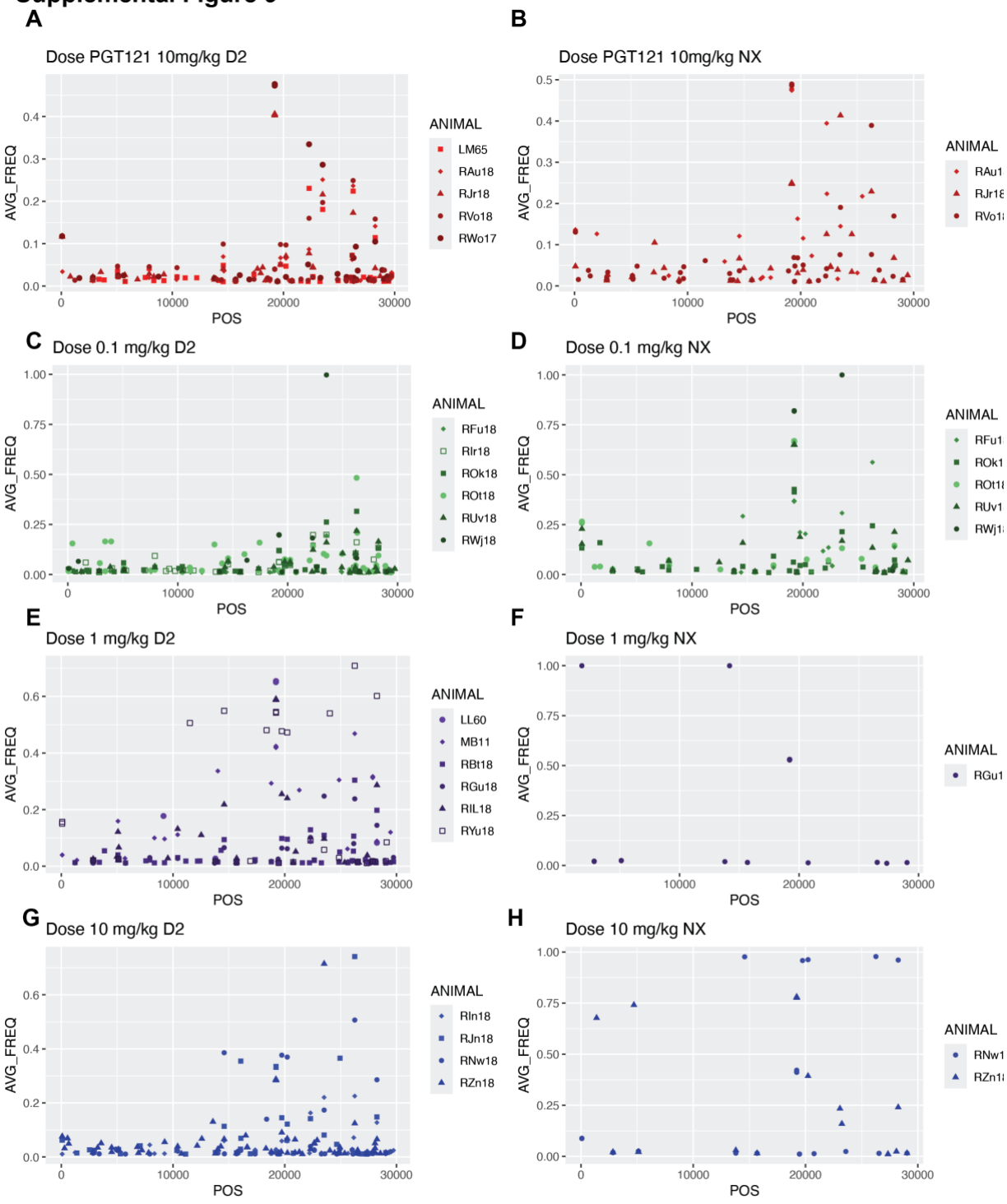

Fig. S9 SARS-CoV-2 iSNV position and frequency (**A** to **H**) Plots of iSNV frequency across the genome for each experimental group at 2 dpi (**A, C, E, G**) and 7/8 dpi **(B, D, F, H**). Control PGT121-treated RMs are depicted in red (**A** to **B**), CC40.8 0.1mg/kg-treated RMs depicted in green (**C** to **D**), CC40.8 1mg/kg-treated RMs depicted in purple (**E** to **F**), CC40.8 10mg/kg-treated RMs depicted in blue (**G** to **H**). SARS-CoV-2 iSNV isolated from BAL supernatant were called against the input consensus sequence with iVar v1.3.1, setting the maximum depth at 29 million bases, minimum quality score at 15 and minimum frequency at 1%, and were only considered if present in both replicate libraries.

Supplemental Figure 10

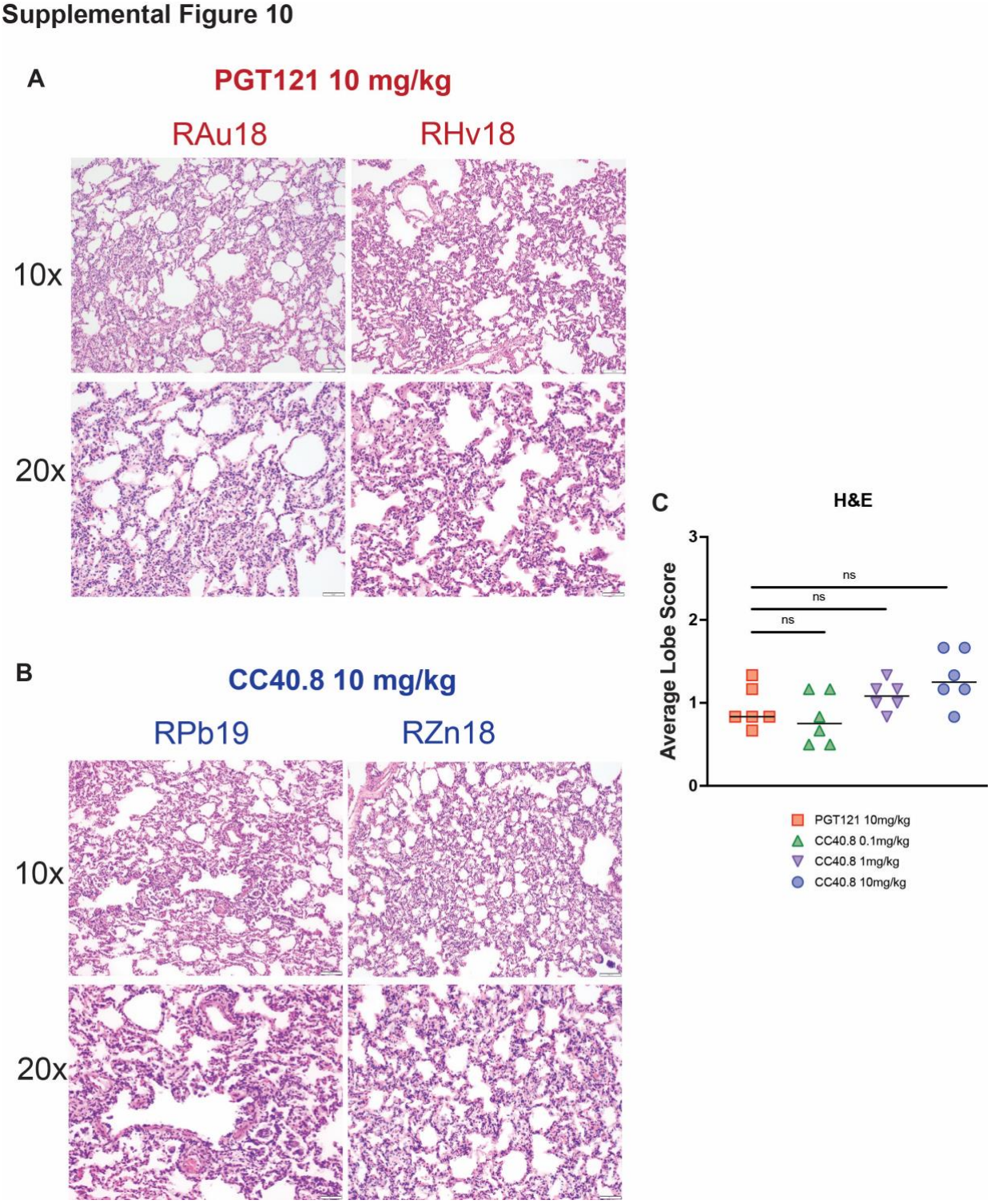

Fig. S10 H&E staining of RM Caudal Lung (**A** to **C**) Photomicrographs of caudal lung tissue sections of control (**A**) and CC40.8 10mg/kg treated (**B**) nonhuman primate groups at 7 or 8 dpi. All photomicrographs taken at either 10x or 20x magnification (scale bars represent 100μm and 50μm, respectively). Average lobe pathology scores for each animal (**C**). Control PGT121-treated RMs are depicted with red squares, CC40.8 0.1mg/kg-treated RMs depicted with green upward pointing triangles, CC40.8 1mg/kg-treated RMs depicted with purple downward pointing triangles, CC40.8 10mg/kg-treated RMs depicted with blue circles. Statistical analyses were performed using two-sided nonparametric Mann-Whitney tests.

.

Supplementary Table 1

Animal Name	Sex	Age (months)	Weight (kgs)	Treatment	Collection Group	Day of Necropsy (dpi)	Baseline Anti-Spike Antibody Titers (AUC)
RWo17	F	77	8.75	PGT121 10mg/kg	1	Day 7	0.08383
RVo18	M	64	9.85	PGT121 10mg/kg	1	Day 7	0.3073
RWj18	M	65	11.69	40.8 0.1mg/kg	1	Day 7	0.1525
LM65	M	75	11.91	PGT121 10mg/kg	1	Day 8	0.1943
RIL18	M	64	7.89	40.8 1mg/kg	1	Day 8	0.2358
RPb19	M	59	14.28	40.8 10mg/kg	1	Day 8	0.07748
RNw18	F	63	6.39	40.8 10mg/kg	2	Day 7	0.02495
RIn18	M	65	9.99	40.8 10mg/kg	2	Day 8	0.1653
MB11	M	65	10.77	40.8 1mg/kg	2	Day 7	0.2652
RBt18	M	64	11.7	40.8 1mg/kg	2	Day 8	0.4202
RJr18	M	64	9.75	PGT121 10mg/kg	2	Day 7	0.07583
RUv18	M	63	9.5	40.8 0.1mg/kg	2	Day 8	0.07367
ROk18	F	65	6.65	40.8 0.1mg/kg	3	Day 8	0.1518
RFu18	M	64	7.48	40.8 0.1mg/kg	3	Day 7	0.3855
LL60	M	76	12.78	40.8 1mg/kg	3	Day 8	0.3133
RYu18	M	64	11.29	40.8 1mg/kg	3	Day 7	0.07517
RHv18	M	64	9.44	PGT121 10mg/kg	3	Day 8	0.1693
RZn18	M	65	11.89	40.8 10mg/kg	3	Day 7	0.3092
RGu18	F	64	7.54	40.8 1mg/kg	4	Day 8	0.1725
ROt18	M	64	10.9	40.8 0.1mg/kg	4	Day 8	0.1643
LM98	M	76	13.37	40.8 10mg/kg	4	Day 8	0.3365
RJn18	M	65	12.35	40.8 10mg/kg	4	Day 7	0.3055
RAu18	M	64	11.15	PGT121 10mg/kg	4	Day 7	0.427
RIr18	M	64	8.8	40.8 0.1mg/kg	4	Day 7	0.3847
RLp17 (SARS-CoV-2+)							1.817
Pre pandemic Serum; RAg5 (SARS-CoV-2-)							0.3012

Supplementary Table S1. Antibody Infused RM characteristics. Animal ID. Sex. Age in months relative to -5 dpi and weight taken from beginning of study in kg. Antibody treatment and collection group. Day post infection that necropsies were performed. Baseline Anti-Spike Antibody titers as measured with SARS-CoV-2 spike binding ELISA, in area under the curve calculations, including positive (RLp17) and negative (RAg5) controls. Curves were generated using absorbance (OD405nm) values plotted against log-transformed serum concentrations. Baselines were corrected based on ELISA absorbance background values. Positive control serum (RLp17) was sampled from a RM infected with WA.1 SARS-CoV-2 at 21 dpi and negative control serum (RAg5) was sampled from a RM prior to the COVID-19 pandemic (5/29/2014).

Supplementary Table 2

Template: Standard Clinical Assessment Version # 1 Effective date mm/dd/yyyy

CORONAVIRUS VACCINE AND TREATMENT EVALUATION NETWORK (COVTEN)
STANDARD CLINICAL ASSESSMENT

Date: _____ Animal ID: _____

Parameter	Rating/Description	Assessment Score
Responsiveness	**0**-Normal - bright, alert, responsive	
	1-Mildly affected - slightly depressed, acts disinterested with personnel in room, lies down in cage but gets up when approached	
	2-Moderately affected/obtunded - non-responsive, very disinterested in personnel, hunched or lying down, will get up when stimulated	
	3-Severely affected/comatose - lying down completely unresponsive to stimuli	
Discharges	**0**-Normal	
	1-Mild nasal/ocular	
	3-Severe nasal/ocular	
Respiratory rate	**0**-Normal	
	1-Mild tachypnea	
	3-Severe tachypnea	
Respiratory effort	**0**-Normal - no apparent changes in breathing	
	1-Mild - slightly increased effort breathing	
	3-Severe - open mouth breathing, abdominal breathing	
Cough	**0**-None	
	1-Mild	
	3-Severe	
Fecal consistency	**0**-Normal	
	1-Soft	
	2-Fluid	
	Total	
Notes		

Supplementary Table S2. Coronavirus Vaccine and Treatment Evaluation Network (CoVTEN) standard clinical assessment for cage-side scores, related to Fig. S2. Cage-side scores were performed at 0, 1, 2, 3, 4, 5, and 7 dpi and added to anesthetized scores to obtain the total clinical score for each dpi. Cageside scores were based on responsiveness, discharges, respiratory rate, respiratory effect, cough, and fecal consistency and were completed prior to anesthesia.

Supplementary Table S3

Template: Standard Clinical Assessment Version #1 Effective date 07/06/21

AMARA ORAL-COV JULY 2021
STANDARD CLINICAL ASSESSMENT

Date: _____ Animal ID: _____

Parameter	Description	Assessment Score
Discharges	**0** – Normal	
	1 – Mild (ocular/nasal)	
	3 – Severe (ocular/nasal)	
Respiratory character	**0** – Normal	
	1 – Mild dyspnea	
	3 – Severe dyspnea	
Hydration	**0** – Normal (normal skin turgor, moist mucous membranes)	
	1 – Mild dehydration (5-10%)	
	3 – Severe dehydration (>10%)	
	Total	

Physical Examination Under Anesthesia – Objective measures

	Body Weight (kg)	Body Condition Score	Respiratory rate (bpm)	SpO2	Rectal Temperature (°F)	
Value						
Notes						

Supplementary Table S3. Coronavirus Vaccine and Treatment Evaluation Network (CoVTEN) standard clinical assessment for anesthetized scores, related to Fig. S2. Anesthetized scores were performed at 0, 1, 2, 3, 4, 5, and 7 dpi and added to cageside scores to obtain the total clinical score for each dpi. Anesthetized scores were based on discharges, respiratory character, and hydration. Body weights (kg), body condition scores, respiratory rates (bpm), SpO2 (%), and rectal temperatures (°F) were also recorded during anesthetic accesses.

Supplementary Table S4

Correlation to BAL SARS-CoV-2 Titers, Day 2	Spearman r	95% Confidence Interval	P (two-tailed)	P value summary
SARS-CoV-2 Nvs.TNFa	0.7688	0.5204 to 0.8972	<0.0001	****
SARS-CoV-2 Nvs.IL-1B	0.7212	0.4381 to 0.8742	<0.0001	****
SARS-CoV-2 N vs. G-CSF	0.7172	0.4312 to 0.8722	<0.0001	****
SARS-CoV-2 Nvs.MIP-1a	0.6999	0.4026 to 0.8636	0.0001	***
SARS-CoV-2 Nvs.IFN-a	0.6504	0.3235 to 0.8386	0.0006	***
SARS-CoV-2 Nvs.IL-6	0.6437	0.3133 to 0.8351	0.0007	***
SARS-CoV-2 Nvs.IL-1RA	0.6345	0.2991 to 0.8303	0.0009	***
SARS-CoV-2 Nvs.IP-10	0.6052	0.2552 to 0.8150	0.0017	**
SARS-CoV-2 Nvs.IL-7	0.5184	0.1330 to 0.7676	0.0095	**
SARS-CoV-2 Nvs.MCP-1	0.3368	-0.08961 to 0.6589	0.1075	ns
SARS-CoV-2 Nvs.IL-9	0.2476	-0.1853 to 0.6000	0.2434	ns
SARS-CoV-2 Nvs.IL-8	0.2301	-0.2031 to 0.5880	0.2793	ns
SARS-CoV-2 Nvs.IL-12p70	0.1983	-0.2349 to 0.5658	0.353	ns
SARS-CoV-2 Nvs.IL-10	0.07348	-0.3511 to 0.4730	0.733	ns
SARS-CoV-2 Nvs.GM-CSF	0.07225	-0.3522 to 0.4721	0.7372	ns
SARS-CoV-2 Nvs.VEGF	0.04526	-0.3757 to 0.4507	0.8337	ns
SARS-CoV-2 Nvs.IL-4	-0.09387	-0.4888 to 0.3330	0.6626	ns
SARS-CoV-2 Nvs.IL-5	-0.1836	-0.5553 to 0.2493	0.3905	ns
SARS-CoV-2 Nvs.IFN-g	-0.2225	-0.5827 to 0.2109	0.2961	ns

Supplementary Table S4. Correlation of cytokine and chemokine levels with SARS-CoV-2 titers within the BAL at 2dpi. Cytokines and chemokines levels (pg/mL) in BAL fluid relative to −4 dpi measured by MSD immunoassay. SARS-CoV-2 titers were measured in BAL via detection of (sgRNA-N) by qPCR. Grey shaded rows indicate significant correlation.

Materials and Methods

Tissue SARS-CoV-2 RNA Quantification

Viral load RNA tested via three different sites.

Site 1 Method

For BAL and nasal swabs media placed in RNazol BD (MRC #RB 192) with acetic acid (Sigma Aldrich #CAS64-19-7, RNA was extracted via the RNazol BD protocol. RNA concentration was obtained using the RNA Broad Range Qubit kit (Q10210). RNA quality was checked via the High Sensitivity RNA Screentape Analysis (Agilent 5067-557) Subgenomic RNA quantification was performed as previously in Corbett et al. 2021[694].

Quantitative real-time polymerase chain reaction (PCR) was conducted using TaqMan Fast Virus 1-Step Master Mix (Applied Biosystems) with 5μL template and primers and probes at concentrations of 500nM and 200nM respectively. Reagents for detection of sgRNA_E include a forward primer in the common leader region: sgLeadSARSCoV2_F: 5'-CGATCTCTTGTAGATCTGTTCTC-3' as well as the following transcript-specific probe and reverse primer: E_Sarbeco_P: 5'-FAM-ACACTAGCCATCCTTACTGCGCTTCG-BHQ1–3' and E_Sarbeco_R: 5'-ATATTGCAGCAGTACGCACACA-3'. Reagents for detection of sgRNA_N include the aforementioned sgLeadSARSCoV2_F and the following transcript-specific probe and reverse primer: wtN_P: 5'-FAM-TAACCAGAATGGAGAACGCAGTGGG-BHQ1–3'and wtN_R: 5'-GGTGAACCAAGACGCAGTAT-3'. PCRs were performed on a QuantStudio 6 Pro Real-Time PCR System (Applied Biosystems) with reverse transcription at 50°C for 5 min and inactivation at 95°C for 20 sec followed by 40 cycles of PCR at 95°C for 3 sec and 60°C for 30 sec. The limit of detection was 50 copies. Design of RNA standards was previously described[695]. Final copy numbers of sgRNA per sample were normalized to total RNA concentration of the indicated sample, which had been determined by Qubit following extraction.

Site 2 Method

For nasal swabs placed in 1x DNA/RNA Shield (Zymo Cat#R1200), samples were frozen and sent to Tulane for extraction and quantification. Samples were heat inactivated prior to processing at 56˚C, 30 minutes per Tulane's Institutional Biosafety stipulations. RNA was extracted from swab samples (nasal, pharyngeal, rectal) using the Zymo Viral RNA Kit (Zymo #R1035) according to the manufacturer's instructions. Viral RNA Buffer (Zymo Catg#R1034) was added at twice the volume of sample in DNA/RNA Shield and swabs were centrifuged in a Zymo IC spin column before removing the swab and adding the remainder of the sample volume. The spin column was washed twice with Wash Buffer before ethanol addition and elution in 50uL DNase/RNase-free water. Samples are stored at -80C until plating and viral load quantification.,
and Bioloanzyer for quality.

For BAL, 200uL of BAL fluid and cells was added to 2X DNA/RNA Shield (Zymo Cat#R1200) and shipped frozen to Tulane. Samples were heat inactivated prior to processing at 65 degrees C for 60 minutes per Tulane's Institutional Biosafety stipulations. RNA is then extracted from bronchoalveolar lavage samples using the Zymo Viral RNA Kit (Zymo #R1035) according to the manufacturer's instructions. Viral RNA Buffer (Zymo Catg#R1034) is added at twice the volume of original sample (200uL sample - 400uL buffer) and sample is then incubated for 30 minutes prior to adding to Zymo IC spin column (Zymo Cat# C1004). Samples are then washed twice with Wash Buffer (Zymo Cat# R1003) before the addition of absolute ethanol. Samples are eluted in 50uL DNase/RNase-free water and stored at -80C until plating and viral load quantification.

Isolated RNA was analyzed in a QuantStudio 6 (Thermo Scientific, USA) using 5uL Sample RNA plated with 1.8uL forward primer, 1.8 reverse primer (Integrated DNA Technologies), 0.5uL probe, 5uL TaqPath 1-Step RT-qPCR (Fisher Cat#A15299), and 5.9uL ddH2O for a total 20uL reaction with the following program: 25°C for 2 minutes, 50°C for 15 minutes, 95°C for 2 minutes followed by 40 cycles of 95°C for 3 seconds and 60°C for 30 seconds. Signals were compared to a standard curve generated using in vitro transcribed RNA of each sequence diluted from 10E8

down to 10 copies. Positive controls consisted of SARS-CoV-2 infected VeroE6 cell lysate. Viral copies per swab were calculated by multiplying mean copies per well by amount in the total swab extract.

Site 3 Methods

Focus Reduction Neutralization Test (FRNT) Assay

HeLa-ACE2 cells were seeded in 50µL of complete DMEM at a density of $6x10^4$ cells per well. In a dilution plate, BAL was serially diluted in a 3 ten-fold series and 50µL of diluted BAL was added to the 96-well cell plate. The plate was incubated for 20 hours after which the plate was fixed for 1 hour with 4% paraformaldehyde. The plate was then washed three times with 300µL of 1xPBS/0.05% Tween-20. 25µL of human polyclonal sera diluted 1:500 in Perm/Wash buffer (BD Biosciences 554723) was added to the plate and incubated at room temperature for 2 hours. The plate was washed three times and 25µL of peroxidase goat anti-human Fab (Jackson Scientific, 109-035-006) were diluted 1:1000 in Perm/Wash buffer then added to the plate and incubated at room temperature for 2 hours. The plate was washed three times and 25µL of Perm/Wash buffer was added to the plate and incubated at room temperature for 5 minutes. The Perm/Wash buffer was flicked off and TrueBlue perodixdase substrate was immediately added (Sera Care 5510-0030). Assay was done in triplicate.Modified FRNT assay from Rogers et al. 2020[696].

Tissue SARS-CoV-2 RNA Quantification

This assay was modified from the methods previously described[556]. Viral RNA was extracted from lung tissue, then amplified and quantified via reserve transcription (RT) qPCR. Lung tissue was collected at day 7 or 8 and placed in 1 mL of TRIzol (Invitrogen Cat#15596018). The samples were homogenized usin a Bead Ruptor 12 (Omni International). The tissue homogenates were centrifuged, and the supernatant was transferred to an RNA purification column (Qiagen). Purified RNA was eluted in 60 µL of DNase-, RNase-, endotoxin-free molecular biology-grade water (Millipore). Purified RNA was then subjected to RT and qPCR with the Centers for Disease Control

and Prevention's N1 (nucleocapside primer sets (forward, 5′-GACCCCAAAATCAGCGAAAT-3′; reverse, 5′-TCTGGTTACTGCCAGTTGAATCTG-3′) and a FAM-labeled probe (5′-FAM-ACCCCGCATTACGTTTGGTGGACC-BHQ1-3′) (Integrated DNA Technologies) on a Bio-Rad CFX96 real-time instrument. For quantification, a standard curve was generated by diluting 2.5 × 10^6 PFU RNA equivalents of SARS-CoV-2. Each run included 11 fivefold serial dilutions of the standard. No-template controls were included for the extraction step as well as the qPCR.

Tissue Collection and Processing

Peripheral blood mononuclear cells (PBMCs) were collected from the femoral vein into EDTA tubes with additional serum collected in serum separator tubes. Serum was then processed by the ENPRC's pathology department for comprehensive blood chemistries. Plasma was collected from the EDTA tubes by spinning at 1,500 x g for 10 minutes at room temperature and then transferring the plasma layer to a 15mL conical and spinning again for another 10 minutes at 600 x g. PBMCs were collected using Sepmate Tubes and the Sepmate protocol with pipetting off the interface instead of pouring (SepMate™-50 Catalog #85450). Following the directed washes, cells were resuspended in ACK lysis buffer (Lonza # 10-548E) and incubated at room temperature for 10 minutes. Samples were then quenched with 2%FBS/DPBS to 50mL and spun again at 300 x g for 10 minutes. Supernatant was removed and samples were resuspended in 2% FBS/DPBS for counting. A 1:1 dilution of 10uL of Trypan blue stain (ThermoFisher # T10282) and 10uL of resuspended cells were added to cell countess slides (Invitrogen # 100078809). Slides were then inserted in the Countess II for determining the percent of live cells and concentration. Cells were then frozen in vials of at least 10 million PBMCs per mL in freezing media containing 10% of DMSO (Millipore Sigma #34869-100mL) in FBS (Gemini # 100-106). 2% FBS/DPBS was created by adding 2% of total volume with FBS (Gemini # 100-106) to DBPS (Corning # 21-031-CM).

Nasopharyngeal swabs were collected under anesthesia using a clean swab (iClean #CYY-96000) that was inserted approximately 2-3 cm deep into the nasal passage. After collection, swabs were placed in either 200uL of DNA/RNA shield (Zymo #R1200-125) or 1mL of DPBS with RNase inhibitor (Invitrogen # AM2694) and then frozen by placing it on dry ice. When processed at a later date, swabs were thawed at room temperature. Once thaw, nasal swabs were vortexed and then squeezed using clean tweezers to remove all media. RNazol (MRC #RB 192) with acetic acid (Sigma Aldrich #CAS64-19-7) was added at a one to one ratio to nasal swab media. Samples were then vigorously vortexed and RNA was extracted using the RNAzol BD protocol.

Swabs placed in 1x DNA/RNA Shield (Zymo Cat#R1200) were frozen and shipped to Tulane for extraction and processing.

To collect non necropsy BAL, a 14Fr, sterile, single-use pediatric suction catheter (Covidien #37424) was inserted into the trachea and directed into a mainstem bronchi. The catheter was advanced until it was secured into a distal subsegmental bronchus. 35-70 mL of physiological saline was instilled into the bronchus and then manually aspirated back into a syringe to obtain a minimum of 20 mL of lavage fluid and placed into a 50mL conical. If less than 20mL was recovered, an additional 10-15mL was administered again and a second attempt was taken and placed into a second 50mL conical. BAL was then filtered through a 70uM strainer (Falcon #352350). 1mL of BAL fluid and cells were taken to perform viral load testing by adding RNazol and Acetic Acid into a 5mL microcentrifuge tube. After vigorous vortexing, samples were frozen for later RNA extraction using the RNAzol BD kit. After viral loads were taken, BAL was spun at 300 x g for 10 minutes to pellet the cells. BAL supernatant was collected for MSD and plaque assay. BAL cells were then lysed with the ACK lysis buffer for 10 minutes at 37˚C and the reaction was quenched using DPBS. Cells were then spun and counted in the same manner as PBMCs. At least 100,000 cells were set aside for 10x sequence and the remaining cells were divided

between the isotype control and stained panel. At necropsy, an additional 100mL of Post Mortem BAL fluid was taken by placing a large sterile irrigation syringe with the plunger removed into the lungs. Approximately 150 mL of sterile 1 x PBS is poured into the lungs via the syringe to infuse both sides. The syringe is then removed and plunger replaced. The syringe goes back into the trachea opening and the lavage fluid is pulled back and dispensed into 50mL conicals. Post mortem BAL sample is processed the same way as non-necropsy through a 70uM filter and lysing. After samples for viral load, supernatant and 10x were taken for pre-mortem samples, the cells for pre and post mortem were combined together for staining. At necropsy, at least 5 million cells were stained for both the isotype and staining panel with any remaining frozen down using the same freezing media as PBMCs.

At necropsy, the tissues above were collected as well as right caudal lung, spleen, and hilar lymph nodes.

Caudal lung is processed by following the steps indicated in Voix et al 2023 with the following changes. During the 1 hour 37˚C incubation, samples were placed on a 50mL tube rotator at 10 rpm (Thermo Scientific # 888810001). Samples were run at least 6 times on the pre-loaded M_Lung_02_01 to ensure proper blending of the tissue. After, the tissue is strained over 100uM filters (Falcon # 352360) and the digestion reaction is quenched with R10. Cells are then centrifuged at 1100 x g for 10 minutes. The supernatant is removed and cells are washed again with R10 and centrifuged at 1100 x g for 10 minutes. The cells are lysed using 10mL of ACK lysis and incubated at 37˚C for 10 minutes. Lysing was then quenched using DPBS and cells were spun down at 1100 x g for 10 minutes. Cells were then counted using the same manner as PBMCs and aliquoted for 10x sequencing, bulk RNA sequencing and freezing.
Cells were used for 10x sequencing and the extra were saved in the same manner as PBMCs.

Spleen was processed in a similar manner to the lung but without the digestion step. Spleen was dissected using blunt scissors and added to C tubes with 5mL of R10. Using the same M_Lung 02_01 protocol run at least 6 times, spleen was blended then passed through a 100uM filter. Due to the nature of the sample, it is then passed through a 70uM filter and then 40uM filter (Falcon #352340) to remove the debris. Cells were then washed using R10 and then spun at 750 x g for 10 minutes to pellet. Supernatant was removed and the cells were washed with DPBS then centrifuged at 750 x g for 10 minutes. Cells were lysed with 20mL of ACK for 10 minutes. The lysing reaction was quenched with DPBS and cells were pelleted following the same speed and time. Cells were counted and frozen for later use.

Lymph nodes were processed by first trimming the fat from the tissue and placing it into a C tube with DBPS. In the gentleMACs dissociator on the preloaded program M-Brain 01_01, lymph nodes were blended. The blended tissue is then strained over a 70uM filter into a 50mL conical and rinsed with DPBS. Cells were centrifuged at 300 x g for 10 minutes at room temperature. After the supernatant is removed, cells are lysed with ACK lysing buffer and incubated at room temperature for 10 minutes. The reaction is stopped by topping off with DPBS and cells are then centrifuged at 300 x g for 10 minutes. Cells are then counted and aliquoted for freezing vials of 10M cells per 1mL of freezing media described above.

In addition to extracting mononuclear cells from lymph nodes, lung and spleen, cassettes of tissues fixed in 4% paraformaldehyde were taken. Following removal, tissues were placed into jars of 4% PFA and fixed for at least 24 hours. Tissues were then cut and placed into cassettes which were then placed in a fresh jar of 4% PFA for additional fixing.

ARTIC Library Generation

Selected RNA samples were converted into cDNA following the manufacturer instructions in the SuperScript™ IV First-Strand Synthesis System kit (Invitrogen, 18091200). The obtained cDNA

was amplified using the ARTIC V4.1 nCOV-2019 Amplicon Panel kit (Integrated DNA Technologies (IDT), 10011442) developed by the ARTIC Network and consisted of 98 primers within two pools to detect presence of mutations within known variants of interest or newly emerging variants[697]. Two separate PCR reactions were performed on small aliquots of cDNA to ensure that each sample was amplified with both ARTIC primer pools required for overlapping size distribution. Both PCR reactions consisted of 5.75 µL of Q5® High-Fidelity DNA Polymerase (New England Biolabs, M0491L) 3.6 µL of the respective ARTIC Primer Pool 1 or 2 (10 µM), 6 µL cDNA and 9.65 µL of Nuclease free water for a total reaction volume of 25 µL and cycling conditions of 1× (98 °C, 30s), 35× (95 °C, 15 s; 63 °C, 5 min). The amplified cDNA products were merged for each sample and submitted to purification of 0.8X SPRISelect size selection bead cleanup (Beckman Coulter, B23318). The xGen™ DNA Library Prep EZ kit (IDT, 10009821) was used to prepare next-generation sequencing (NGS) libraries following the protocol IDT provided with ≤100 ng input of ARTIC amplified cDNA, 14 minutes fragmentation time, 5 indexing PCR cycles, and dual indexing with xGen™ UDI 10nt Primer Plates 1-4 (IDT, 10008052). Sample concentration and quality were measured using FilterMax F3 (Molecular Devices, LLC) with Qubit™ 1X dsDNA High Sensitivity solution (Invitrogen, Q33231) and 4200 Tapestation System (Agilent, G2991BA) with D5000 DNA ScreenTapes and reagents (Agilent, 5067-5588). NGS libraries were sequenced on a NovaSeq6000 SP flow cell system (Illumina, Inc) using 150 paired-end sequencing, targeting 1 million reads per sample.

Expression and purification of monoclonal antibodies CC40.8 and PGT121

Monocloncal antibody expression and purification was conducted as previously described[641]. Plasmids of the variable heavy and light chains of CC40.8 and PGT121 were generated in IgG1 and expressed in Expi293F cells. 228µg heavy chain plasmid and 572µg of light chain plasmid were added into 100µL of Opti-MEM (Thermo Fisher Scientific, catalog #31985070), after filtering with 0.22µM Steriflip (Millipore, catalog #SCGP00525), 800µL of FectoPro (Polyplus, catalog #116-001) reagent was added into the mixture and inverted. After incubating at room temperature

for 10 minutes, the mixture was added to 900mL of Expi293F cells at a cell density of 2.8-3.0e6 cells/mL and incubated in a shaker with 80% humidity and 5% CO_2. After 24hr, 10mL of 0.3M Valproic acid and 9mL of 45% glucose were added to the cell culture. Five days post transfection, Expi293F supernatant was harvested by centrifugation at 1250xg for 15 minutes before filtering with a 0.22μM membrane filter. Protein A Sepharose (GE Healthcare Cat# 17096302) was added to the supernatant and was rotated overnight at 4°C overnight. The solution was then loaded into Econo-Pac columns (BioRad Cat# 7321010), washed with 3 column volume of PBS, and antibodies were eluted with 15mL of 0.2 M citric acid (pH 2.67). The elution was neutralized with 4.5mL of 2M Tris Base solution prior to buffer exchanging into PBS with dialysis cassettes. 30K Amicon centrifugal filters (Millipore Cat# UFC903024) were used to concentrate the antibodies into smaller volumes.

Anti-Spike Antibody Detection in BAL Supernatant and Serum Samples by ELISA

BAL Supernatant and serum samples were obtained on day -60-30, -4, 0, 2, and 7 or 8 to quantify CC40.8 titers. Spike protein diluted to 2μg/mL in 1xPBS was coated on ELISA plates overnight at 4°C and then washed three times with 100μL of 1xPBS/0.05% Tween-20. After blocking the plates with 50μL of 3%BSA/1xPBS for 1 hour at room temperature, 12.5μL the NHP serum dilution series and CC40.8 dilution series for a standard curve were added to the plate and incubated for 1 hour at room temperature. Plates were wash three times with 100μL of 1xPBS/0.05% Tween-20 before adding 12.5μL of alkaline phosphatase (AP)-conjugated goat anti-human IgG Fc secondary antibody (Jackson ImmunoResearch, catalog #109-055-008) diluted in 1%BSA/1xPBS. After washing the plates three times with 100μL of 1xPBS/0.05% Tween-20, 12.5μL of AP substrate was added for detection. Plates were then read at 405 nm, and the data was analyzed with Graphpad Prism 9. Serum samples were ran in triplicate.

Single-cell RNA-Seq bioinformatic analysis of BAL and Lung cells

The cellranger v6.1.0 (10X Genomics) pipeline was used for processing the 10X sequencing data and the downstream analysis was performed using the Seurat v4.0.4 R package. A composite reference comprising of Mmul10 from Ensembl release 100 and SARS-CoV2 (strain MT246667.1 - NCBI) was used for alignment with cellranger. The percentage of SARS-CoV-2 reads was determined using the PercentageFeatureSet for SARS-CoV2 genes. For BAL samples, a total of 107,830 cells across all animals passed quality control (QC) and were used for analyses. For lung samples, a total of 101,766 cells passed upstream QC and were used for analysis. The bioinformatic processing of scRNA-Seq data and subsequent analysis was performed as described previously for BAL samples[461] and lung samples[644]. For single-cell RNA-Seq, approximately 20,000 cells were loaded onto the 10X Genomics Chromium Controller in the BSL3 facility using the Chromium NextGEM Single Cell 5' Library & Gel Bead kit according tomanufacturer instructions[698].

For BAL samples, the samples were demultiplexed using HTODemux function in Seurat, The gene expression matrix was filtered to include protein coding genes and exclude genes encoded on Y chromosome, B and T cell receptor genes, mitochondrial genes, RPS and RPL genes and SARS-CoV2 genes. The cells were further filtered on the following criteria: nFeature_RNA >=500 and <= 3500, ncount_RNA >=250 and log10GenesPerUMI > 0.8. After filtering, the samples were normalized using SCTransform method[698] and integrated using the first 30 dimensions with the default CCA method[699]. Two samples were dropped - two due to low cell numbers (RZn18 2 dpi and ROk18 2 dpi). The integrated object was split into individual samples and after filtering the three samples, the remaining samples were normalized using the SCTransform method[698] and then integrated using the reciprocal PCA method[699]. The first 30 dimensions were used with the FindIntegrationAnchors, FindUMAP and FindNeighbors method. Clustering was carried out using the default Louvain method and the resolution was set to 1. Cell annotations were carried out based on the expression of canonical markers in seurat clusters and SingleR v1.4.0 library

(Blueprint Encode database)[700] annotations were used as a guide. As a distinct cluster could not be determined for neutrophils based on the expression of canonical marker genes, the SingleR annotations were used for neutrophils. Differential gene expression analysis was carried out using the FindMarkers function with "MAST"[701] method. To further classify the macrophages/monocytes in BAL, only cells in the largest cluster comprising the macrophages/monocytes were further processed. The subset function was used to get these cells followed by splitting the object in individual samples. Downstream processing was performed as previously described [461].

For lung samples, we processed sections of lower (caudal) lung obtained from animals necropsied at 7 or 8 dpi (n=3 PGT121, n=3 10mg/kg, n=3 0.1 mg/kg). The cellranger pipeline was used as described above and filtered counts were read into Seurat using the Read10X_h5 function. QC filtering was performed as described above. The first 30 dimensions were used and clustering was carried out with the resolution set to 0.1 using the default Louvain algorithm in seurat. The clusters were annotated based on the expression of canonical markers and roughly divided into four major subsets: epithelial, myeloid, lymphoid and others. Each subset was then clustered separately to fine tune the cell type annotations. The human Lung v1 reference[701] in Azimuth[702] was used to guide the cell annotations. Based on the expression of canonical markers, some clusters were classified as doublets and some remained unassigned. After removing the doublets and unassigned clusters, UMAPs showed some additional cells that coincided with the removed doublets/unassigned clusters, and these were removed as well. Finally, a total of 101,766 cells were used subsequently for downstream analysis. Differential gene expression analysis was carried out using the FindMarkers function with "MAST" method . Over –representation analysis was carried out using clusterProfiler v4.5.0.992[703] with Hallmark, Reactome, KEGG and BioCarta genesets from the msigdb database[500,703-708]. The msigdbr v7.5.1 library (https://igordot.github.io/msigdbr/) was used for retrieving the msigdb databases. Downstream processing was performed as previously described[461].

Macrophage Flow Cytometry Immunophenotyping

Multi–parameter flow cytometric analysis was performed on fresh mononuclear cells isolated from BAL using the following mAbs: anti-CD45 BUV805 (clone D058-1283; 2.5uL; cat # 742055); anti-CD163 BUV395 (clone MAC2-158; 2.5uL; cat # 568191); anti-CD14 BUV786 (clone M5E2; 7.5uL; cat # 563698); and anti-CD206 BV480 (clone 19.2; 7.5uL; cat # 746279) all from BD Bioscience; anti-CD16 PE-Cy5 (clone 3G8; 20uL; cat # 302010) from Biolegend; Fixable Viability Dye eFluor780 4x (Cat. No.: 65-0865-14; 25uL) from eBioscience. After 10x captures and sample banking, all remaining BAL cells were split into 3 aliquots (one for unstained cell control, one for the flow panel, and one for compensation controls). Cells set aside for compensation controls from all animals sampled on the same day were pooled and then split evenly into enough tubes to make cell-based compensation controls for each antibody in the panel. For unstained cells, 2mL of stain buffer, added then spin down at 800 x g at RT for 10 minutes, then resuspend in 100uL of 4% PFA for 10 minutes. Then 300uL of stain buffer were added to bring unstained cells to 1% PFA. Unstained samples were kept at 4˚C until ready to run flow. For the stained samples and compensation controls, 100uL of FC block were added per sample (5uL of stock and 95uL of stain buffer), then incubated in dark at RT for 30 minutes. After samples were washed and spun again, 100uL of staining master mix or singular antibody for compensation control were added and incubated for 30 min in the dark at RT, followed by another wash and spin. Samples were then resuspended in 100uL of 4% PFA for 10 minutes, and then brought to 300uL of stain buffer for a final concentration of 1% PFA. Samples were kept at 4˚C until ready to run. Due to the high autofluorescence of alveolar macrophages, BAL cells were used as the compensation controls instead of beads and fluorophores were selected for channels with minimum autofluorescence, with unstained BAL cells spiked in to each compensation control. Macrophages were gated on singlets, CD45+, FSC and SSC characteristic of granulocytes and alveolar macrophages, live cells, CD14+, and CD163+ populations, and assessed for MRC1 expression. Due to the high variability of the autofluorescence commonly observed in airway macrophage populations, we

found it necessary to gate for CD163 and MRC1 using each animal's pre-infection BAL sample, and to then apply these gates to the later timepoints for that same animal. Samples were run on BD FACSymphony A5 driven by FACS DiVa software and analyzed with FlowJo (Version 10.10).

Lung Histology

Lung samples from nonhuman primates were fixed in 10% neutral buffered formalin, processed, and blocked in paraffin for histological analysis. All samples were sectioned at 5 μm and stained with hematoxylin-eosin (H&E) for routine histopathology. Pathology was scored as described: **(0)**: inflammation minimal to absent; **(.5)**: minimal to mild inflammation (very mild alveolar capillary hypercellularity), areas of perivascular and/or peribronchial (PBr) / peribronchiolar (Pbr) inflammation are rare to absent; **(1)**: Mild to moderate inflammation (alveolar hypercellularity with occasional cells within alveolar spaces), noticeable interstitial capillary expansion, and occasional perivascular (PV) and/or PBr/br infiltrates; **(2)**: Moderate to severe inflammation; alveolar hypercellularity, moderate numbers of cells in alveolar spaces, regular PV and PBr/Pbr infiltrates, occasional areas of diminished airspace in section; *for samples with 25-50% tissue affected, an additional "+/- will be factored in to score*; **(3)** = Severe inflammation; prominent PV/PBr/Pbr inflammation, substantially diminished air spaces (inflammation/consolidation) +/- edema; *for samples with <50% of the tissue affected, an additional "+" will be factored into score.*

Chapter Three: Non-human primate LIBRA-Seq accelerates antibody discovery in RM vaccinated against HIV-1

AUTHORS

Edwards, Christopher[1], Silva-Trenkle, Aaron[2], Sahoo, Anusmita[1,4], Lapp, Stacey[1], Raju, Nagarajan[1], Ton, Thang[1], Metz, Amanda[1], McGhee, Emily[1], Charles, Tysheena[1], Saini, Ankur[1], Pellegrini, Kathryn[4], Rui Kong[1], Derdeyn, Cindy[6,1], Wrammert, Jens[1], Upadhyay, Amit[1], Amara, Rama[1,7], Kwong, Gabriel[2], Bosinger, Steven[1]*

AFFILIATIONS

1Division of Microbiology and Immunology, Emory National Primate Research Center, Emory University, Atlanta, GA 30329, USA; 2Wallace H. Coulter Department of Biomedical Engineering, Georgia Tech College of Engineering and Emory School of Medicine, Atlanta, GA 30332, USA, USA; [3]Department of Biological Sciences and Bioengineering, Indian Institute of Technology, Kanpur, Uttar Pradesh 208016, India; [4]Emory National Primate Research Center Genomics Core, Emory National Primate Research Center, Emory University, Atlanta, GA 30329, USA; [6]Department of Laboratory Medicine and Pathology, University of Washington, Seattle, WA, USA; [7]Department of Microbiology and Immunology, Emory School of Medicine, Emory University, Atlanta, GA, USA

ABSTRACT

Broadly neutralizing antibodies (bNAbs) exhibit protective efficacy against HIV-1 infection making them an ideal archetype for HIV-1 vaccine design. Presently, no vaccine candidate has induced bNAbs or autologous neutralizing antibodies (NAbs) against neutralization-resistant tier 2 viruses. However, the development of stabilized, native-like Env trimers such as BG505.SOSIP.664 has marked a significant advancement in vaccine design, due to their ability to elicit tier 2 NAbs in rhesus macaques (RM). NAb development against tier 2 immunogens in RM remains poorly understood, with hypothesized contributions from genetic variation at the IG loci, naive B cell repertoire, and differential gene expression in B cell lineages. To address these knowledge gaps, we have developed a set of BG505.SOSIP.644.T332N (BG505 SOSIP) probes capable of recovering paired clonotype identity, antigen specificity, and gene expression of B cells in a high throughput fashion. These probes were constructed by conjugating biotinylated BG505 SOSIP to streptavidin covalently linked to both sc-RNA-Seq compatible DNA oligonucleotides and flow cytometry compatible fluorophores. Using these reagents, we isolated and sequenced BG505 SOSIP specific memory B cells from the PBMCs of an RM developing high titers of neutralizing antibodies. To benchmark the accuracy of our technology, we compared our recovered heavy and light chain sequences to those identified from the same animal using conventional methodology, and recovered 100% of previously identified NAbs. We then applied this technology to recover BG505 SOSIP specific memory B cells from 5 additional vaccinated RMs, and cloned 34 antibodies for functional characterization. Our approach will allow for high-throughput analysis of the

evolution of Env specific lineages in both RM and humans in response vaccination with HIV-1 Env immunogens, including BG505.SOSIP.644.

MAIN TEXT

INTRODUCTION

In 2023, approximately 1.3 million people were infected with HIV-1, and over 600,000 people died from AIDS related illnesses[9]. With millions of people living with HIV-1 across the world unable to access antiretroviral therapy and millions of others unaware of their HIV-1 status, developing a protective HIV-1 vaccine remains a central priority in the fight against the HIV-1 pandemic. However, the vast range of genetic variation in circulating strains, rapid establishment of long-lived latent reservoirs, and the prominent glycan shield that protects key neutralizing epitopes, have proven to be formidable hurdles in the pursuit of an efficacious, antibody-based vaccine[5,709]. This is most clearly highlighted by the modest 31.2% vaccine efficacy of the only successful HIV-1 vaccine trial to date[8].

Facing the failure of initial vaccine trials to elicit neutralizing antibody responses, researchers pivoted to a “reverse vaccinology” approach[710-714]. This strategy is based on identifying monoclonal antibodies (mAbs) isolated from people living with HIV-1 with the ability to inhibit infection against a range of neutralization resistant (Tier 2) HIV-1 strains and then designing a vaccine strategy to elicit such antibodies. These antibodies known as “broadly neutralizing antibodies,” or “bNAbs,” are considered a critical correlate of protection against HIV-1 challenge, as they have been shown to both prevent simian – human immunodeficiency virus (SHIV) infection in rhesus macaques (RM) in passive

antibody transfer studies and help maintain the suppression of HIV-1 during chronic infection humans[228,715-722]. However, bNAbs arise in only 20-30% of people living with HIV-1 and have never been elicited in vaccine studies in either humans or non-human primates (NHP)[206,723,724]. Identifying the antigenic determinants of bNAbs and elucidating the critical components of their development is vital for rational design of an HIV-1 vaccine.

A critical leap forward for the study of bNAbs was the development of thermostable, soluble HIV-1 Env trimers such as BG505.SOSIP.644 (BG505 SOSIP) [359,725]. This construct has been used to preferentially capture B cells producing bNAbs and elucidate key bNAb epitopes on Env and has been shown to elicit autologous NAbs against a tier 2 virus in RM[725-727]. We have previously shown that RM immunized with BG505 SOSIP in 3M-052 adjuvant can confer protection against 10 intravaginal challenges with BG505 Simian-Human Immunodeficiency Virus (SHIV)[356]. Though all vaccinated RM developed high levels of BG505 SOSIP binding antibody titers, only one third developed protective NAb titers. Analysis of the NAb responses from RUp16, the animal that developed unusually high NAb titers (ID50 = 6068), revealed the C3/465 glycan hole cluster as the immunodominant epitope among potent NAbs[362]. Additionally, the serum from all but one of the animals protected from infection showed decreased neutralization capacity against a mutant BG505 SHIV-1 with the 465-glycan hole closed.

While RM have proven to be a highly valuable model for testing HIV-1 Env based vaccine constructs, conventional antibody sequencing techniques that rely on plate based single-cell sorting severely limit the throughput of neutralizing antibody discovery. The recent development of LIBRA-Seq (linking B cell receptor to antigen specificity through

sequencing) has been used to dissect humoral immune responses to pathogens and vaccine immunogens at the single cell level via barcoded antigens[10,728-739]. In this study, we adapt the LIBRA-Seq platform to identify BG505.SOSIP.664.T332N specific abs from vaccinated RM *en masse,* identify public clones, and inform the selection of 34 candidate abs for functional characterization.

RESULTS

Probe Design and Construction

To create a flow cytometry and LIBRA-seq compatible cell staining technology (**Fig 1A**), we conjugated streptavidin to alexa fluorophores (AF) and sc-RNA-Seq compatible DNA oligonucleotides, which could be tetramerized with biotinylated proteins for staining of cells. First, we conjugated recombinant streptavidin with C-terminal cysteine to AF-maleimide at a 1 to 10 ratio. After removal of excess AF-meleimide through size exclusion spin filtration, streptavidin-AF were conjugated to DNA oligonucleotides through hydrazone chemistry and purified using size exclusion chromatography (**Fig. 1B**). Size exclusion chromatography results in distinct absorbance profiles between free streptavidin-AF647, free Oligo-1, and the streptavidin-AF647- Oligo-1 conjugate to allow for purification of conjugate with 7 to 12 ml of elution volume (**Fig. 1C**). We validated that the five different constructs constructed (AF647-Oligo-1, AF488-Oligo-2, AF647-Oligo-3, AF488-Oligo-4, and AF546-Oligo-5) have DNA conjugated to streptavidin monomers by protein gel, resulting in an additional band around the molecular weight of streptavidin monomer conjugated to DNA strand in both Coomassie and SYBR DNA gel staining (**Figs. 1D, S1**). To test the conjugation of the Fluorophore, we used a murine tetramer

system we had established previously[121], in which we had prepared streptavidin based Gp100-D^b tetramers. Here we created Gp100-D^b tetramers with streptavidin-AF or streptavidin-AF-DNA constructs to stain P14 splenocytes, resulting in similar staining profiles between DNA free and DNA conjugated streptavidin (**Fig. 1E**). Our streptavidin-AF-DNA conjugates stained P14 splenocytes with similar efficiency to commercially available streptavidin.

NHP LIBRA-seq in vitro Validation

To validate the BCR specificity and 10x single cell RNA-Seq compatibility of our probes, we utilized an engineered Ramos B cell line expressing VRC01, a CD4-binding-site-directed HIV-1 bNAb capable of binding BG505 SOSIP[10,204,740] (**Fig. 2A**). We mixed VRC01 B cells with wild type RA.1 Ramos B cells that do not bind VRC01 at 1:1, 1:100, and 1:1000 VRC01:RA.1 ratios and incubated them with the BG505 SOSIP probe (**Fig. 2B**). Flow cytometry demonstrated that VRC01 expressing cells were recovered at the expected ratios, indicating highly efficient detection of VRC01. In addition to accurate detection of antigen specific VRC01 B cells via flow, we also performed independent 10x captures of RA.1 (9662 cells) and VRC01 (9128 cells) cells stained with the BG505 SOSIP probe. (**Fig. 2C-D**). Following QC filtering, 96.6% percent of VRC01 Ramos cells were found to express the canonical CDRH3, while 94.1% of RA.1 Ramos cells expressed the canonical RA.1 CDRH3 (**Fig. S2C-S3**). Despite the low frequency of BG505 SOSIP probe-positive RA.1 Ramos cells detected by flow cytometry; we observed a high level of background antigen barcode reads in these cells following 10x capture. This discrepancy is likely attributable to ambient barcode contamination and procedural

differences in cell washing and handling between the flow cytometry and single-cell capture workflows.

NHP LIBRA-seq recovers known BG505 Neutralizing Antibodies from Vaccinated NHPs

We next sought to apply our LIBRA-Seq reagents to *ex-vivo* NHP samples. We have previously shown that immunization with BG505 SOSIP in RM provided significant protection against ten intra-vaginal challenges with BG505 SHIV-1[356]. In this previous preclinical efficacy study, two groups of 15 RM received four subcutaneous immunizations with BG505 SOSIP in 3M-052 adjuvant, with one of these groups also receiving SIVmac239 Gag-expressing HVV to boost T cell responses, while a third group of 15 unimmunized RM received only 3M-052 adjuvant (**Fig. 3A**). Significant protection was observed in the SOSIP ($p = 0.0006$) and HVV + SOSIP ($p<0.0001$) vaccination groups compared to the control group[356].

We used NHP LIBRA-Seq to identify the BG505 SOSIP specific antibody repertoire of RUp16, a RM that was protected from ten BG505 SHIV-1 challenges and developed the highest NAb titer (ID50 = 6068). This animal was selected for LIBRA-Seq benchmarking as it had undergone previous high resolution analysis of NAb associated with high titer and protection using conventional methodology[356,362]. PBMCs isolated from RUp16 at weeks 73 and 76 were combined and stained with dual BG505 SOSIP probes and a negative bait probe with unique fluorophores and corresponding DNA oligos (**Fig. 3B, 3C**). To assess congruency between FACS and 10x readouts, we chose to sort dual positive memory B cells regardless of negative bait binding. Over 13,000 dual BG505

SOSIP probe bound memory B cells (defined as FSC and SSC characteristic of lymphocytes, singlets, live cells, CD3-, CD14-, CD16-, CD20+, CD27+, IgM-, IgG+, BG505-AF647+ and BG505-AF488+) were sorted for 10x capture, representing approximately 4.21% of the circulating IgG+ memory B cell population. Of the dual-positive cells sorted for 10x capture, 97.7% were found to be negative for the biotin bound LIBRA-Seq probe by FACS (**Fig. 3C**). In contrast, only 0.12% of memory B cells isolated from an unvaccinated RM were found to bind to BG505 SOSIP probes (**Fig. 3D**). Following 10x capture and subsequent library generation of RUp16's antigen specific memory B cells, we were able to recover both the BCR sequence and antigen barcode libraries from 1706 cells, with 1643 (96.3%) associated with both BG505 SOSIP barcodes and also lacking any biotin bait barcode (**Table 1**). These data highlight the consistency between our FACS generated antigen binding profiles and those generated from the 10x digital readout of antigen associated barcodes.

For each memory B cell with successfully recovered BCR and antigen barcode libraries, the LIBRA-seq scores for each BG505 SOSIP probe and negative bait probe were calculated based on the number of unique molecular identifiers (UMIs) detected for each construct (**Fig. 3E-3F**). Raw counts for each BG505 SOSIP probe were highly correlated with one another (Pearson's r = .98) (**Fig. 3E**), and maintained their high correlation following normalization for total number of reads per cell (Pearson's r = .9) (**Fig. 3F**). Using the original LIBRA-seq analysis pipeline we found that many cells were assigned LIBRA-Seq scores that skewed the ratios of raw antigen barcode counts due to scaling influenced by the cells with higher overall numbers of recovered barcodes. Our dual positive and single negative probe schema necessitated additional oversight when

determining antigen specificity beyond LIBRA-Seq score cutoffs. Thresholds for antigen specificity based on antigen barcode read counts were chosen empirically - 97th percentile for biotin and 3rd percentile for the two BG505 SOSIP barcodes. Using these thresholds, cells were classified as positive if the normalized values were surpassed these thresholds for both BG505 SOSIP antigens and but not for biotin.

To further benchmark our NHP LIBRA-Seq approach, we compared the BCR sequences of the recovered BG505 SOSIP specific memory B cells to the published heavy and light chain sequences of BG505 SOSIP specific abs isolated from RUp16[362]. We recovered 24 of the 48 previously published heavy chains and 40 of the 44 previously published light chains of BG505 SOSIP binding abs within 85% sequence identity (**Fig 4A-4B**). Among the overlapping sequences were the heavy and light chains of all four BG505 SOSIP neutralizing antibodies (NAbs) previously characterized from RUp16. Clonal analysis revealed 302 shared clonotypes of LIRBA-Seq recovered heavy chains, including 22 out of 48 previously described heavy chains, with all four NAb heavy chains represented in the second largest clonal family (**Fig 4C**). The results from vaccinated RM RUp16 suggest that the LIBRA-seq platform can be successfully applied to the NHP model and identify antigen specific mAb characterized using conventional cloning methodology.

NHP LIBRA-seq accelerates discovery of antigen specific mAbs from BG505 Vaccinated RM

We next sought to apply LIBRA-Seq to 5 additional RM vaccinated in the same study as RUp16. Animals were selected based on their protection from NAb challenge

and had ID50 titers ranging from 41 to 529 (**Table 1).** Using the same memory B cell panel and LIBRA-Seq probes as described above, BG505 SOSIP specific memory B cells were sorted from weeks 20 to 27, representing the circulating memory B cell population prior to and following the third boost with BG505 SOSIP. Additionally, only memory B cells negative for the biotin bound bait were sorted for 10x capture from these RM (**Fig. S4A**). Antigen specific cells represented 0.34% to 0.8% of the isolated memory B cells in these RM, lower in comparison to RUp16's 4.21%, likely because these cells were isolated prior to the final boost, as well as the observed differences in ID50. Despite the lower frequencies of antigen specific cells in these samples, we recovered the BCR sequence and associated antigen barcodes for a total of 401 memory B cells from these 5 RM (**Table 1**).

To confirm LIBRA-Seq's accuracy in identifying antigen-specific B cells, we produced five antibodies with high BG505 SOSIP associated LIBRA-Seq Scores per animal (n=30), and an additional four antibodies with high biotin bait associated scores to assess LIBRA-Seq's ability to flag non-specific memory B cells. Antigen specificity as predicted by LIBRA-seq was validated by ELISA. mAbs PGT151 and PGT145, that bind to trimeric epitopes in BG505 SOSIP were run as positive controls and influenza HA specific mAb EM4C04 was run as a negative control (**Fig. 5A**). All 30 antibodies with LIBRA-Seq scores denoting a high specificity for BG505 SOSIP exhibited binding via ELISA, with LIBRA-Seq scores trended with ELISA area under the curve (AUC) values (**Fig. 5B-5C**). Interestingly, of the four antibodies with high LIBRA-Seq scores for the negative bait probe, two were observed to bind BG505 SOSIP, while the remaining two exhibited AUC values below the limit of detection.

We then investigated the properties of the antigen specific memory B cell repertoires recovered with NHP LIBRA-Seq. Clonal analysis revealed an oligoclonal repertoire, with higher clonality correlating with higher ID50 titers (**Fig. 6A, 6D**). Across the cohort, the top 10 clones represented 31% to 50.3% of the of the total antigen specific memory B cell pool. We observed public heavy chain V gene usage across the cohort, with IGHV4-79 representing the most highly shared allele amongst BG505 SOSIP specific memory B cells (**Fig. 6B**). Interestingly, the NAb lineage contributing most significantly to RUp16's high neutralizing titer utilizes IGHV4-79 in its heavy chain. We also observed 6 public clones shared by pairs of vaccinated RM (**Fig 6C**). Frequency of somatic hypermutation (SHM) was analyzed at both the per-cell and per-clone levels for IgH, IgK, and IgL to assess the extent of mutation in memory B cells recovered from BG505 SOSIP-vaccinated macaques (**Fig. 7A-B**). The analysis revealed variation in SHM frequencies across animals, with the highest mutation rates observed in RUp16, consistent with both its sampling at a later timepoint and high NAb titers. SHM was observed at a frequency of 0.045-0.066 in IgH, 0.022-0.039 in IgK, and (0.025 - 0.044). These findings highlight the diverse characteristics of the antigen-specific memory B cell repertoires revealed through LIBRA-Seq and their potential relationship to the generation of potent neutralizing antibody responses in vaccinated rhesus macaques.

DISCUSSION

To date, only one HIV-1 vaccine regimen has been shown to modestly protect humans from HIV-1 infection, an effect that has not been replicated elsewhere[5,7]. Recent

innovations in immunogen design, delivery, and adjuvants have yielded breakthroughs in eliciting autologous, tier 2 NAbs and important bNAb precursors in humans, and protect against challenge with the matched strain in RM[366,727,741-744]. Here, we adapted the recently developed LIBRA-Seq platform to be compatible with the preclinical non-human primate model. We applied LIBRA-Seq to RM vaccine study samples as a proof of concept for studying memory B cell responses to immunogens in a high resolution, high throughput manner. We focused on RM vaccinated with BG505 SOSIP that were protected from infection with high serum NAb ID50 titers[356]. Previous work had shown that clade A BG505 SOSIP immunogens elicit a range of neutralizing titers in the RM model, primarily targeting the C3/465 glycan hole cluster[362].

In this study, we were able to recapitulate many of the previous findings using LIBRA-Seq, and were able to expand on the previous knowledge, recovering the sequences of BG505 SOSIP specific cells across multiple animals in a high throughput manner. In addition to recovering the previously identified neutralizing clones, we were able to identify shared gene usage and clonotypes across animals. LIBRA-Seq scores also served as an additional metric for prioritizing clones for functional validation, with all selected clones exhibiting high BG505 SOSIP binding titers. Though our study only utilized 2 unique probes, we show how LIBRA-Seq can enhance the resolution of the analysis of the vaccine elicited B cell repertoire even with the limited modality. Future studies focusing on a panel of immunogens to probe epitope specificity are necessary to utilize the technology to its full potential.

Recent clinical studies have investigated immunogens specifically designed to elicit responses from bNAb precursors[296,307,331]. Such studies represent the first step in guiding

antibody maturation toward broadly neutralizing lineages, a process referred to as germline shepherding. In such studies, conventional analysis of binding and neutralizing titers lack insight into the gene sequences of elicited B cell lineages. LIBRA-Seq is uniquely poised to support and accelerate *such* studies by enabling high-throughput recovery of antibody specificity and gene usage, which is especially critical for analyzing and tracking precursor lineages over the course of vaccination, as well as identifying shared clonotypes across animals. To date, LIBRA-Seq has successfully recovered NAb from the convalescent plasma of a convalescent COVID-19 donor and subjects living with HIV-1, B cells elicited by the BNT162b2 vaccine in COVID-19 unexperienced and experienced individuals, and has also recovered public clonotypes in a guinea pig model of HIV-1 vaccination, but has yet to be applied to human or RM models of HIV-1 vaccination[10,728,732].

Overall, this study demonstrates the utility of LIBRA-Seq in enhancing the resolution of vaccine elicited B cell repertoire analysis in the RM model. By enabling high-throughput recovery of antigen-specific sequences, LIBRA-Seq provides a powerful approach for investigating the genetic determinants of antibody responses[10,729-739]. As the field advances toward precision immunogen design, applying LIBRA-Seq to larger cohorts and diverse immunogen panels will be essential for optimizing germline-targeting strategies and improving HIV-1 vaccine efficacy.

Chapter 3 Figures

Figure 1

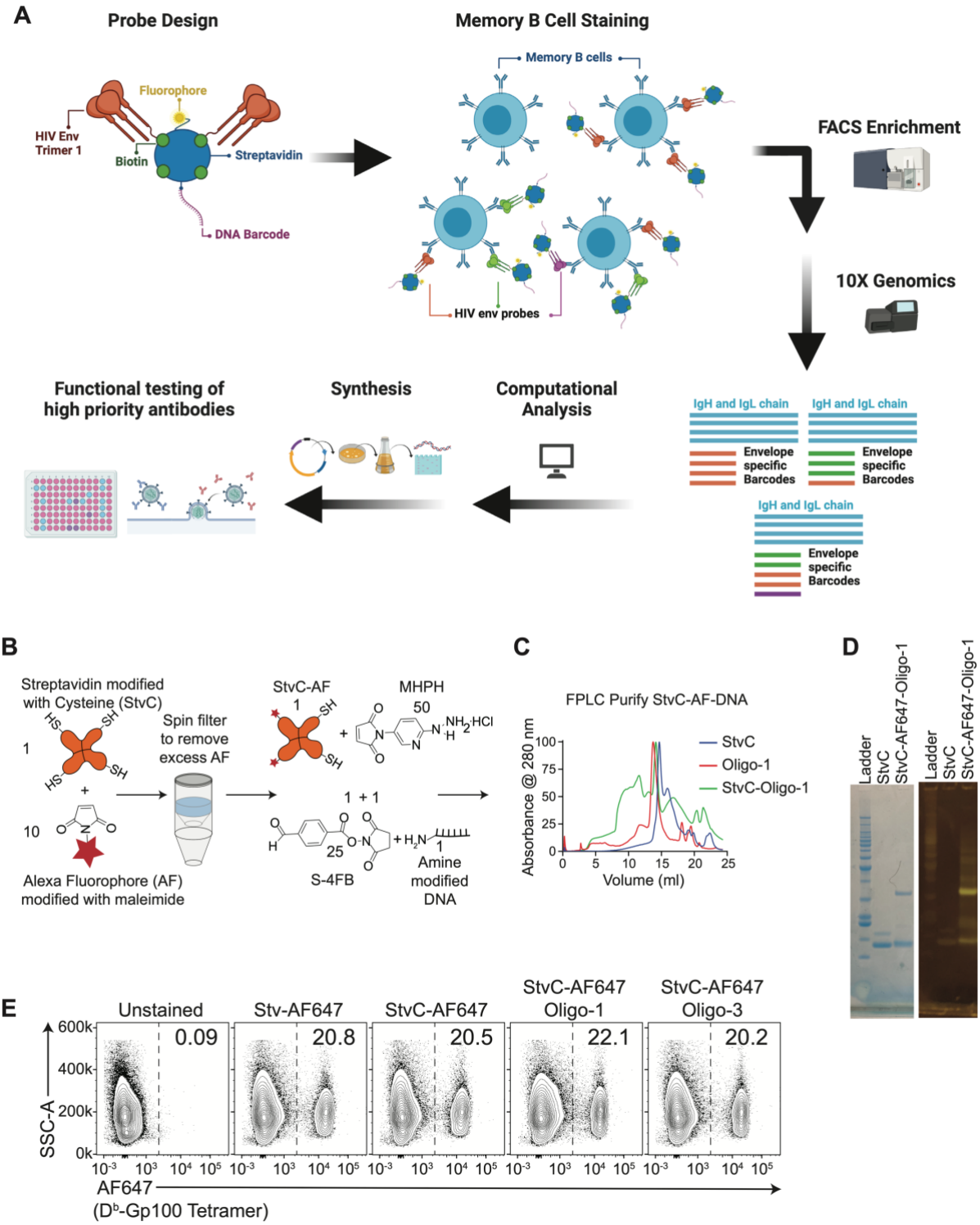

Figure 1. Schematic of the LIBRA-seq assay and probe design. (**A**) Schematic of the LIBRA-seq approach. Fluorophore and DNA oligo conjugated streptavidin are bound to biotinylated HIV-1 Env to create LIBRA-Seq probes. HIV-1 Env specific memory B cells bound to these probes are enriched via FACS prior to 10x capture. DNA libraries are generated from captured RNA and antigen barcodes. Bioinformatic analysis reveals binding profiles of individual memory B cells based on associated antigen barcodes and VDJ sequences. These profiles are used to prioritize clones for downstream functional characterization. (**B**) StvC-AF-Oligo conjugates stain similarly to control Stv-AF. Streptavidin with N-terminal cysteine (StvC) was conjugated to maleimide modified alexa fluorophore (AF) at 10:1 ratio and excess removed by spin column purification before conjugating to amine modified DNA by hydrazone chemistry. (**C**) StvC-AF-Oligo conjugates were purified from free StvC-AF and DNA by size exclusion chromatography. (**D**) Gel electrophoresis of StvC-AF-Oligo conjugates stained with Coommisie Blue (left) and SYBR DNA Gold (right). (**E**) Staining pmel splenocytes for Gp100-specific T cells with Db-Gp100-tetramers made from various streptavidin conjugates.

Figure 2

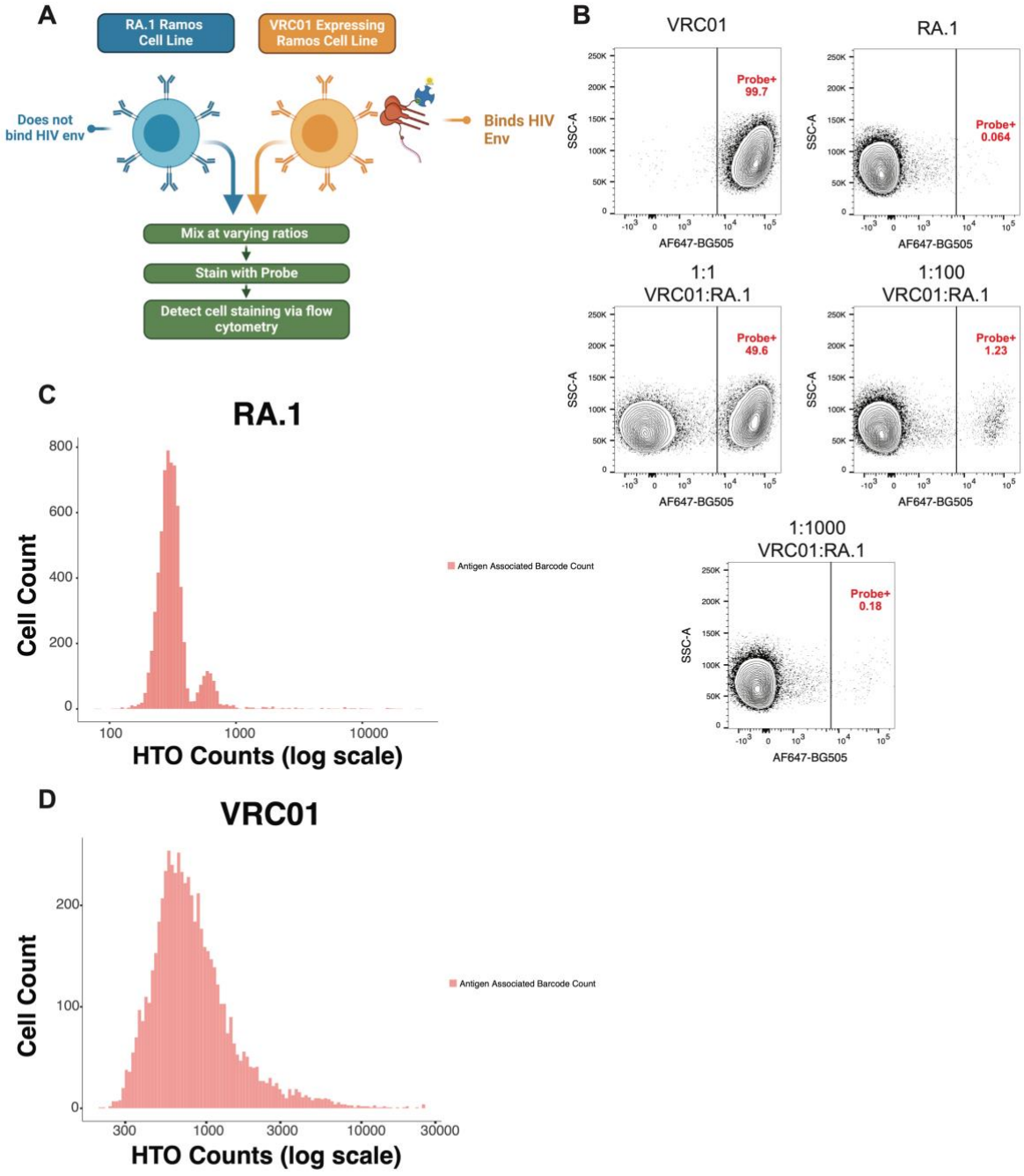
A
RA.1 Ramos Cell Line
VRC01 Expressing Ramos Cell Line
Does not bind HIV env
Binds HIV Env
Mix at varying ratios
Stain with Probe
Detect cell staining via flow cytometry
B
VRC01
RA.1
1:1 VRC01:RA.1
1:100 VRC01:RA.1
1:1000 VRC01:RA.1
Probe+ 99.7
Probe+ 0.064
Probe+ 49.6
Probe+ 1.23
Probe+ 0.18
SSC-A
AF647-BG505
C
RA.1
Cell Count
HTO Counts (log scale)
Antigen Associated Barcode Count
D
VRC01
Cell Count
HTO Counts (log scale)
Antigen Associated Barcode Count

Figure 2. Validation of LIBRA-Seq compatible BG505 SOSIP probes *in vitro*. (**A**) Schematic of BG505 SOSIP based LIBRA-seq probe validation with bNAb expressing B cell lines. (**B**) Binding of VRC01 or RA.1 expressing Ramos B cells to dual DNA-barcoded, fluorescently labeled BG505 SOSIP via flow cytometry. Surface bound VRC01 heavy chain expressing Ramos cells were stained either alone (top) or at 1:1 (third from top), 1:100 (second from bottom), or 1:1000 (bottom) ratios with RA.1 expressing B cells. RA.1 Ramos cells were also stained alone (second from top) to assess nonspecific binding. (**C**) Histogram displaying the number of antigen barcode reads associated with 10x captured VRC01 (top) or Ra.1 (bottom) Ramos B cells.

Figure 3

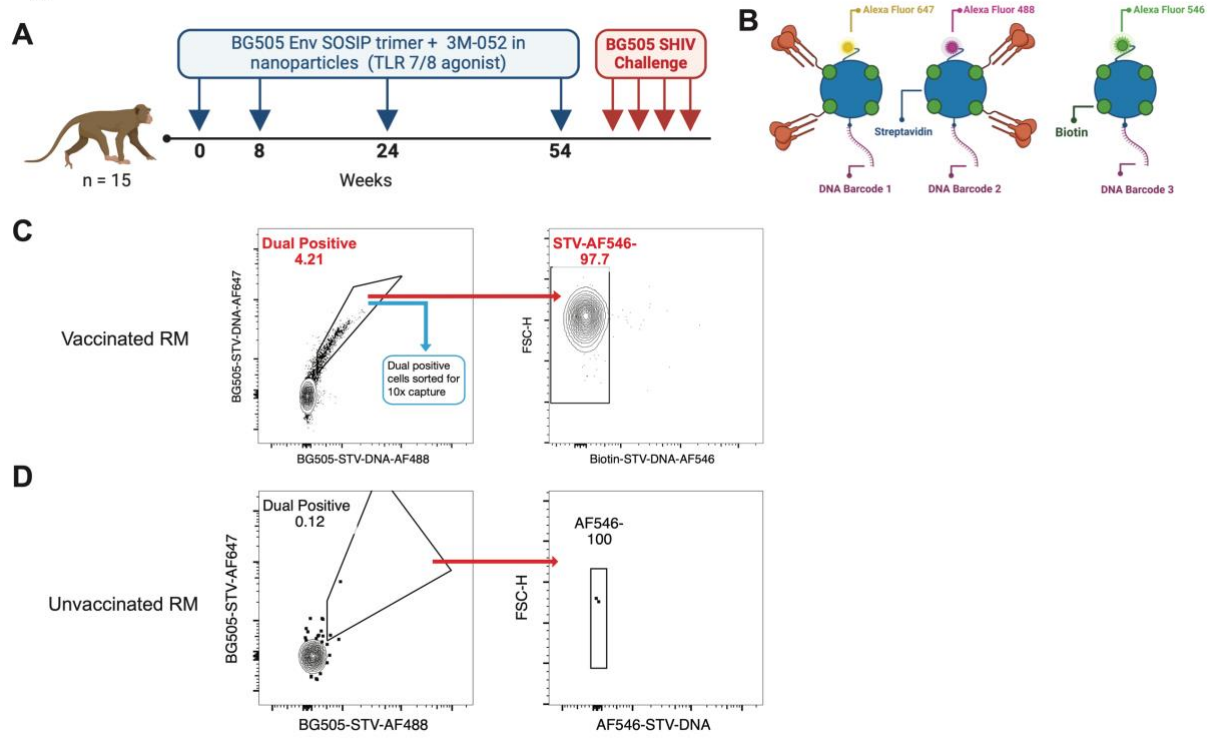
A
BG505 Env SOSIP trimer + 3M-052 in nanoparticles (TLR 7/8 agonist)
BG505 SHIV Challenge
n = 15
0
8
24
54
Weeks
B
Alexa Fluor 647
Alexa Fluor 488
Alexa Fluor 546
Streptavidin
Biotin
DNA Barcode 1
DNA Barcode 2
DNA Barcode 3
C
Vaccinated RM
Dual Positive
4.21
Dual positive cells sorted for 10x capture
BG505-STV-DNA-AF647
BG505-STV-DNA-AF488
STV-AF546-
97.7
FSC-H
Biotin-STV-DNA-AF546
D
Unvaccinated RM
Dual Positive
0.12
BG505-STV-AF647
BG505-STV-AF488
AF546-
100
FSC-H
AF546-STV-DNA

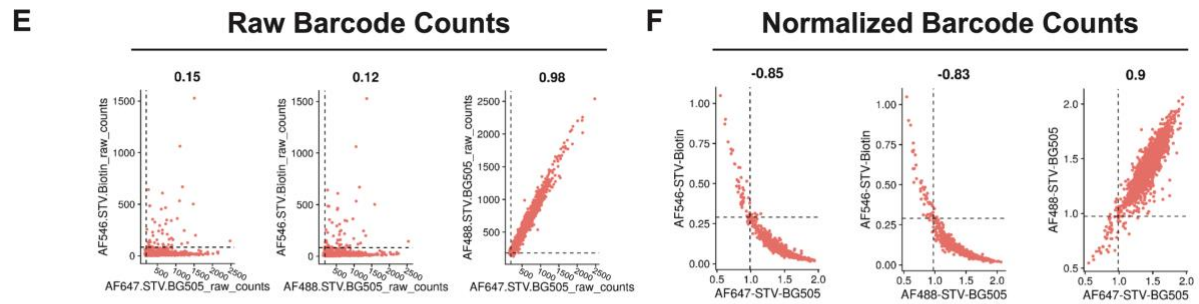
E
Raw Barcode Counts
0.15
0.12
0.98
AF546.STV.Biotin_raw_counts
AF647.STV.BG505_raw_counts
AF488.STV.BG505_raw_counts
F
Normalized Barcode Counts
-0.85
-0.83
0.9
AF546-STV-Biotin
AF647-STV-BG505
AF488-STV-BG505

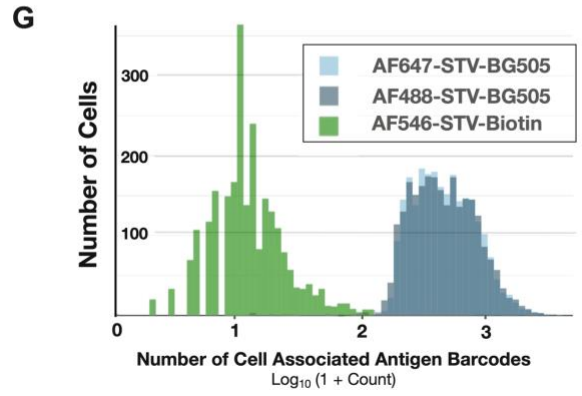
G
AF647-STV-BG505
AF488-STV-BG505
AF546-STV-Biotin
Number of Cells
Number of Cell Associated Antigen Barcodes
Log10 (1 + Count)

Figure 3. Benchmarking of NHP LIBRA-Seq compatible BG505 SOSIP probes *in vivo.* (**A**) Schematic representation of the immunization regimen. (**B**) Design of LIBRA-Seq and flow cytometry compatible, BG505 SOSIP probes for dual antigen staining. Biotinylated BG505 SOSIP was conjugated to barcoded streptavidin linked to either AF647 (left) or AF488 (middle) fluorophores. Barcoded streptavidin bound to biotin only was linked to AF546 (right). (**C**) Fluorescence activated cell sorting gating strategy for the isolation of antigen specific memory B cells from cryopreserved PBMCs from RUp16 collected at weeks 87 and 90. Cells were gated on FSC and SSC characteristic of lymphocytes, singlets, live cells, CD3-, CD14-, CD16-, CD20+, CD27+, IgM-, IgG+, BG505-AF647+ and BG505-AF488+. (**D**) Representative flow cytometry plots showing BG505 SOSIP-specific memory B cells in an unvaccinated RM. Feature scatter plots highlighting the raw (**E**) and normalized (**F**) read counts for LIBRA-Seq barcodes, and show each combination of the biotin control and two BG505 SOSIP baits. The dotted lines represent the thresholds for antigen barcodes that were chosen empirically - 97th percentile for biotin negative control and 3rd percentile for the two BG505 SOSIP barcodes. Each dot represents a unique cell. (**G**) Histogram displaying the number of cell associated antigen barcodes per LIBRA-Seq recovered B cell. Barcodes associated with BG505-AF647 are shown in blue, BG505-AF488 in grey, and Biotin-AF546 in green.

Figure 4

A

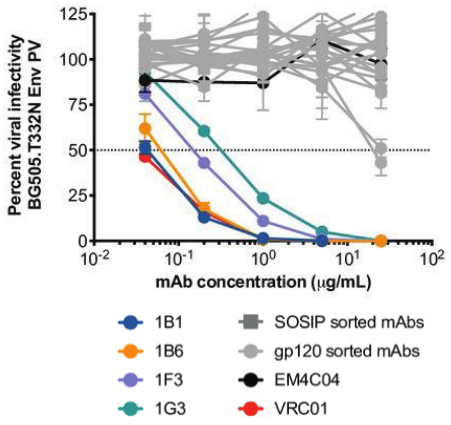

B

	Heavy Chain (HC) (Accession #)	# of Recovered HC	Max % Identity
	MW421835.1_prot_QQX23480.1_1	71	93.96552
	MW421868.1_prot_QQX23513.1_1	37	93.10345
1G3	MW421824.1_prot_QQX23469.1_1	19	88.69565
1F3	MW421830.1_prot_QQX23475.1_1	19	86.15385
	MW421825.1_prot_QQX23470.1_1	16	100
	MW421856.1_prot_QQX23501.1_1	16	95.93496
	MW421842.1_prot_QQX23487.1_1	16	94.16667
	MW421845.1_prot_QQX23490.1_1	12	99.20635
	MW421828.1_prot_QQX23473.1_1	10	99.19355
1B6	MW421862.1_prot_QQX23507.1_1	6	86.95652
1B1	MW421865.1_prot_QQX23510.1_1	1	86.92308

Charles TP, et al. (2021) PLoS Pathog 17(2): e1009257. https://doi.org/10.1371/journal.ppat.1009257

C

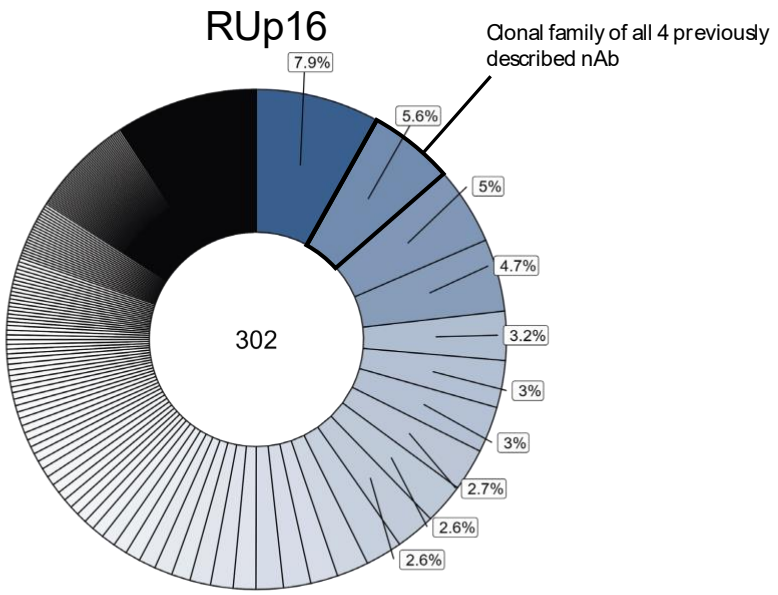

Figure 4. LIBRA-Seq identifies the lineages of BG505 Env neutralizing antibody lineages from animal RUP16. (**A**) Neutralization activities of monoclonal antibodies recovered in the characterization by the original study by Charles et al.[362] (**B**) Heavy chains recovered from RUp16 using LIBRA-Seq. All four neutralizing monoclonal antibodies identified previously by Charles et al. were recovered. (**C**) Clonal diversity of LIBRA-Seq recovered BG505 SOSIP specific B cells from RUp16. The number in the center reflects the total number of B cell clonotypes identified as BG505 SOSIP specific with LIBRA-Seq with clones ranked clockwise from the top center in order of relative frequency. The frequency of the top 10 most abundant clones are indicated, with the most frequent clones noted in dark blue. B cells were considered clones through shared V-genes, J-genes, identical CDR3 length and greater than 70% CDR3 nucleotide sequence identity for both heavy and light chains.

Figure 5

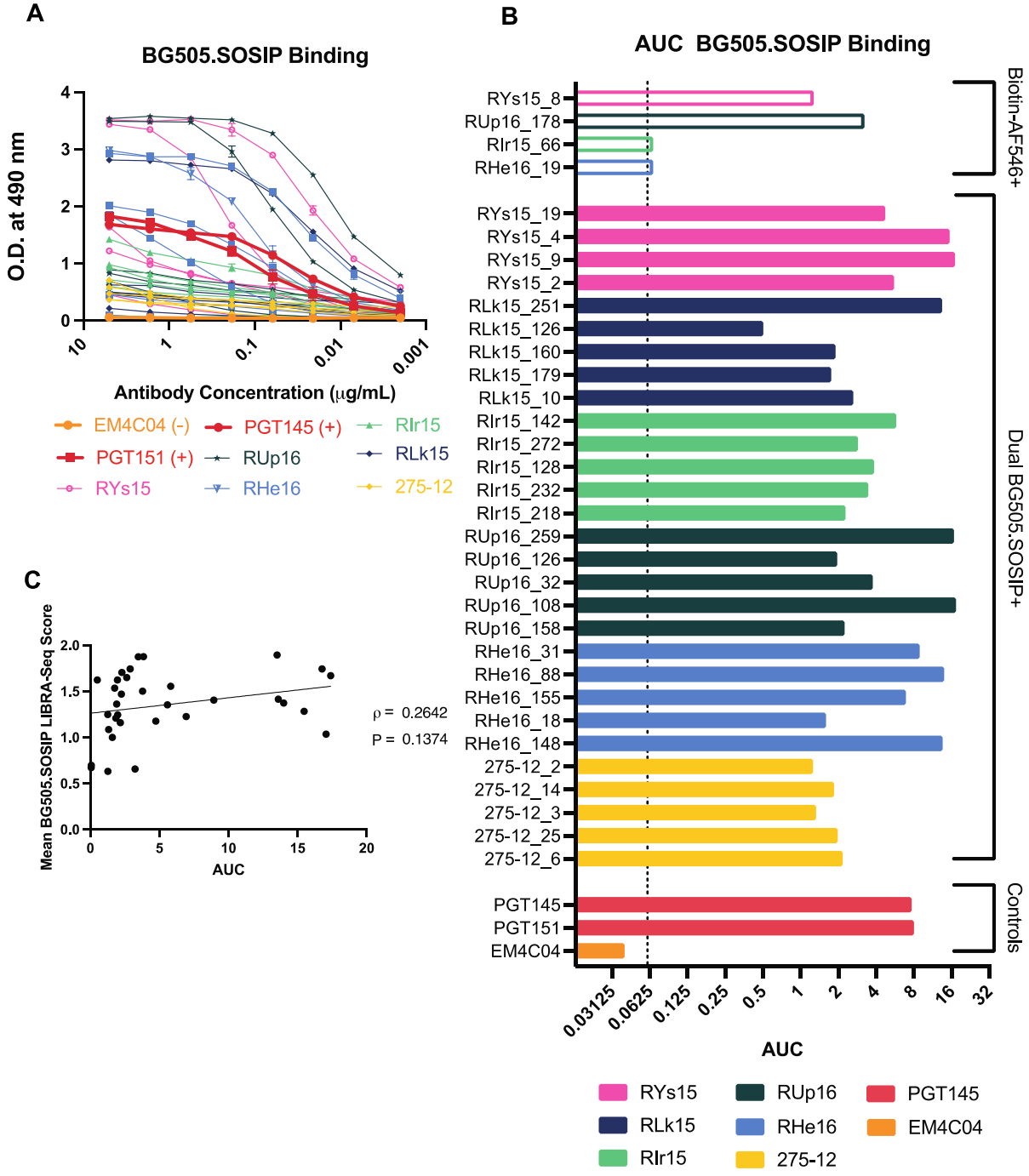
A
BG505.SOSIP Binding
O.D. at 490 nm
Antibody Concentration (μg/mL)
EM4C04 (-)
PGT145 (+)
RIr15
PGT151 (+)
RUp16
RLk15
RYs15
RHe16
275-12
B
AUC BG505.SOSIP Binding
RYs15_8
RUp16_178
RIr15_66
RHe16_19
RYs15_19
RYs15_4
RYs15_9
RYs15_2
RLk15_251
RLk15_126
RLk15_160
RLk15_179
RLk15_10
RIr15_142
RIr15_272
RIr15_128
RIr15_232
RIr15_218
RUp16_259
RUp16_126
RUp16_32
RUp16_108
RUp16_158
RHe16_31
RHe16_88
RHe16_155
RHe16_18
RHe16_148
275-12_2
275-12_14
275-12_3
275-12_25
275-12_6
PGT145
PGT151
EM4C04
Biotin-AF546+
Dual BG505.SOSIP+
Controls
AUC
RYs15
RUp16
PGT145
RLk15
RHe16
EM4C04
RIr15
275-12
C
Mean BG505.SOSIP LIBRA-Seq Score
AUC
ρ = 0.2642
P = 0.1374

Figure 5. LIBRA-Seq successfully identified BG505.SOSIP.664 binding mAbs Quantitative analysis of binding for affinity to BG505 was evaluated and depicted in a binding curve (**A**) or bar graph (**B**). A three-fold dilution of each mAb was done, starting at 5 ug/ml plotted based on the OD at 490nm. Bars represent the area under the curve for each mAb (x axis). The dotted line marks the three times the background signal of samples dilution buffer. Previously characterized HIV-1 specific human IgG1 antibodies (PGT145 and PGT151) were used as a positive control. An influenza HA-specific human IgG1 antibody (EM4C04) was used as a negative control.

Figure 6

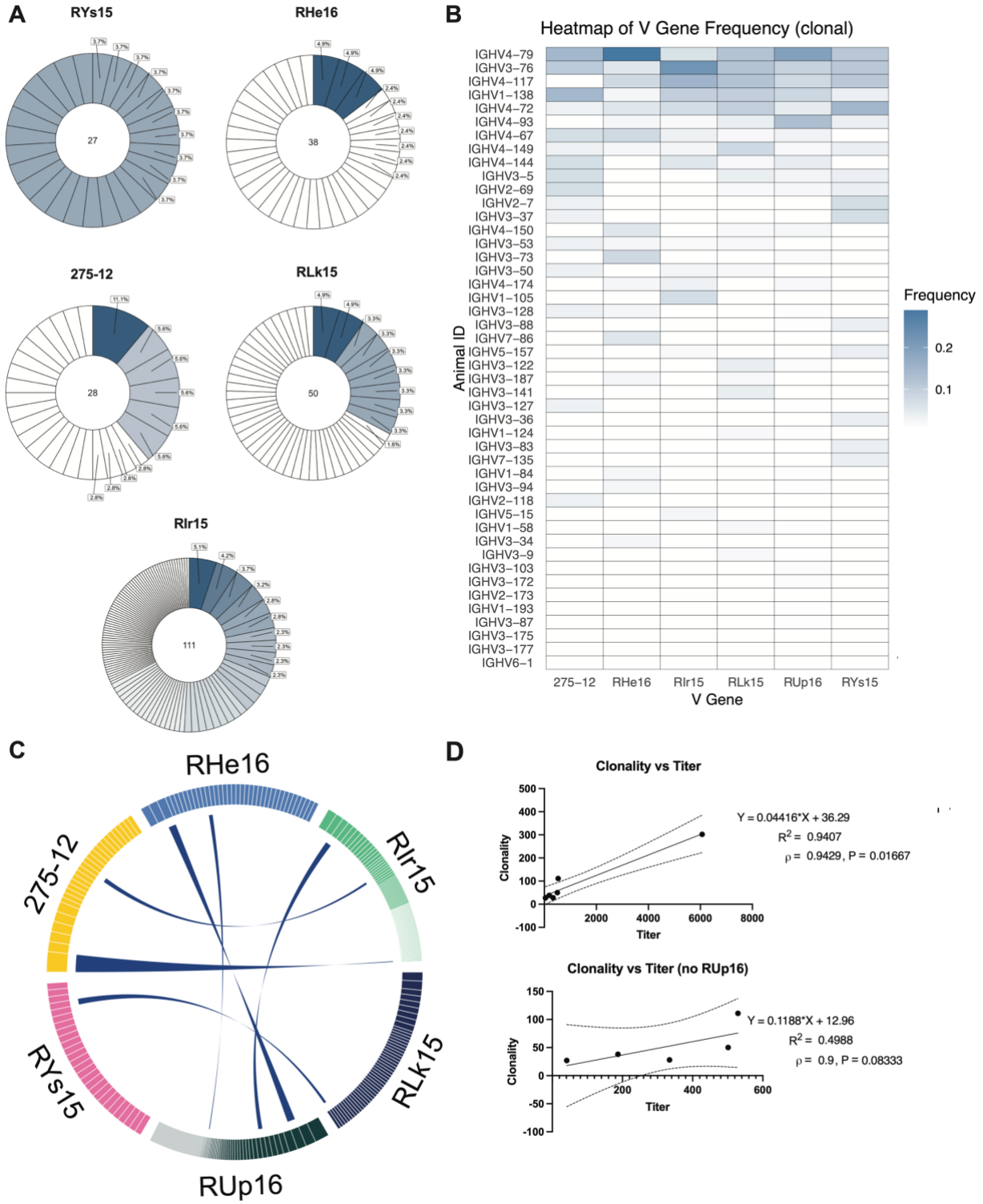
A
RYs15
RHe16
275-12
RLk15
RIr15
27
38
28
50
111
B
Heatmap of V Gene Frequency (clonal)
IGHV4–79
IGHV3–76
IGHV4–117
IGHV1–138
IGHV4–72
IGHV4–93
IGHV4–67
IGHV4–149
IGHV4–144
IGHV3–5
IGHV2–69
IGHV2–7
IGHV3–37
IGHV4–150
IGHV3–53
IGHV3–73
IGHV3–50
IGHV4–174
IGHV1–105
IGHV3–128
IGHV3–88
IGHV7–86
IGHV5–157
IGHV3–122
IGHV3–187
IGHV3–141
IGHV3–127
IGHV3–36
IGHV1–124
IGHV3–83
IGHV7–135
IGHV1–84
IGHV3–94
IGHV2–118
IGHV5–15
IGHV1–58
IGHV3–34
IGHV3–9
IGHV3–103
IGHV3–172
IGHV2–173
IGHV1–193
IGHV3–87
IGHV3–175
IGHV3–177
IGHV6–1
Animal ID
275–12
RHe16
RIr15
RLk15
RUp16
RYs15
V Gene
Frequency
0.2
0.1
C
RHe16
275-12
RIr15
RYs15
RLk15
RUp16
D
Clonality vs Titer
Y = 0.04416*X + 36.29
R2 = 0.9407
ρ = 0.9429, P = 0.01667
Clonality
Titer
Clonality vs Titer (no RUp16)
Y = 0.1188*X + 12.96
R2 = 0.4988
ρ = 0.9, P = 0.08333
Clonality
Titer

Figure 6. LIBRA-Seq identifies shared clonotypes of BG505 SOSIP specific B cells from vaccinated RM. (**A**) Clonal expansion of BG505 SOSIP specific B cells depicted in donut charts. Each donut reflects the total number of B cell clonotypes identified as BG505 SOSIP specific with LIBRA-Seq (center) from each RM and the relative frequency of each individual MBC clonotype. The frequency of the top 10 most abundant clones are indicated, with the most frequent clones noted in dark blue. (**B**) Heatmap of V gene frequency per RM, ranked from most shared V genes at the top to least shared at the bottom. Higher frequency is noted in dark blue. (**C**) Circos plot displaying shared BG505 SOSIP specific memory B cell clonotypes among six RM vaccinated with BG505 SOSIP. Each segment represents an individual animal, with connecting ribbons indicating shared clonotypes between animals. The thickness of each ribbon corresponds to the number of shared clonotypes, with thicker ribbons representing greater overlap. B cells were considered clones through shared V-genes, J-genes, identical CDR3 length and greater than 70% CDR3 nucleotide sequence identity for both heavy and light chains.

Figure 7

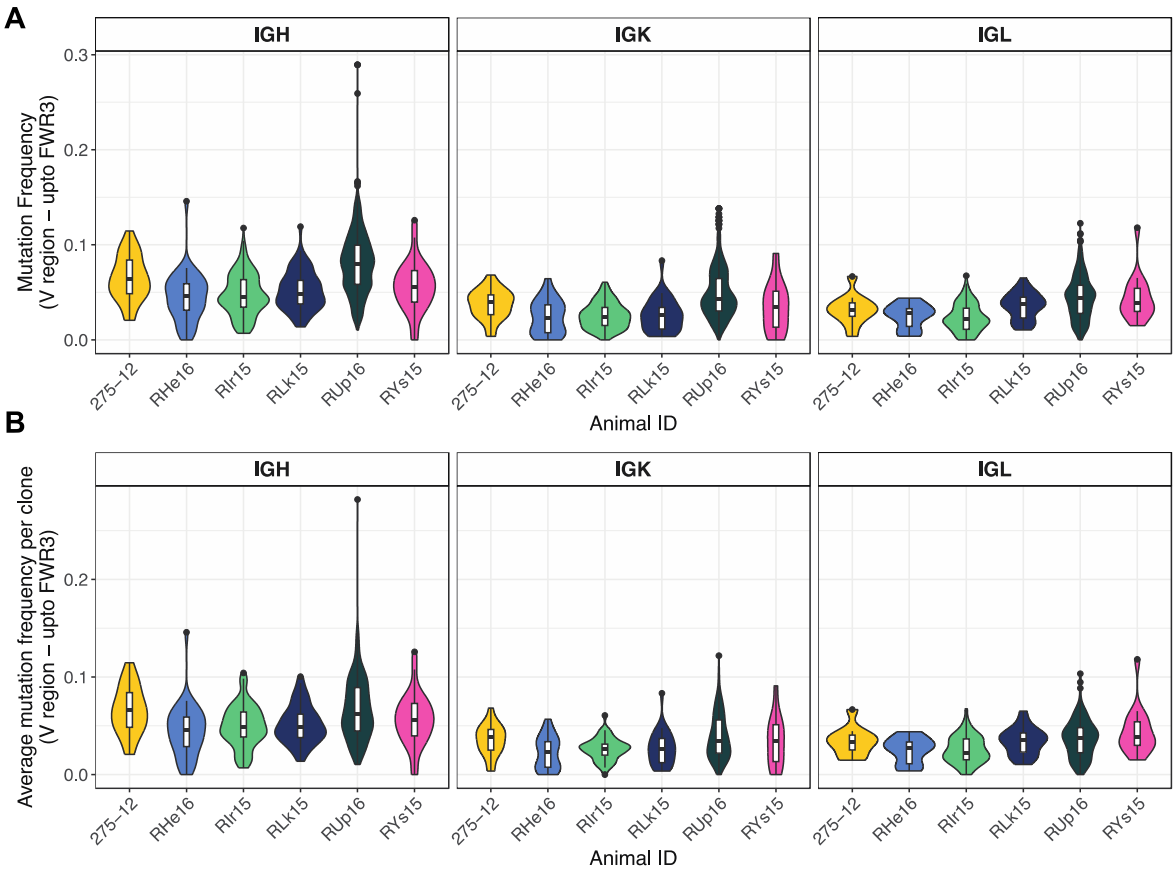
A
IGH
IGK
IGL
Mutation Frequency
(V region – upto FWR3)
0.3
0.2
0.1
0.0
275–12
RHe16
Rlr15
RLk15
RUp16
RYs15
Animal ID
B
IGH
IGK
IGL
Average mutation frequency per clone
(V region – upto FWR3)
0.2
0.1
0.0
275–12
RHe16
Rlr15
RLk15
RUp16
RYs15
Animal ID

Figure 7. LIBRA-Seq recovers somatically hyper mutated BG505 SOSIP specific memory B cells. (**A**) Somatic hyper mutation (SHM) frequencies per LIBRA-Seq recovered BG505 SOSIP specific memory B cell across Ig heavy chain CDR3 (left), and Ig light chain IgK (middle) or IgL (right) . Violin plots show the distribution of mutation frequencies for each animal, with overlaid boxplots indicating medians and interquartile ranges. (**B**) Mean mutational frequency per clone was calculated by averaging the mutation frequencies of all sequences assigned to the same clonal lineage. Violin plots display the distribution of average SHM frequencies per clone for each animal and locus with overlaid boxplots indicating medians and interquartile ranges. B cells were considered clones through shared V-genes, J-genes, identical CDR3 length and greater than 70% CDR3 nucleotide sequence identity for both heavy and light chains.

Figure S1

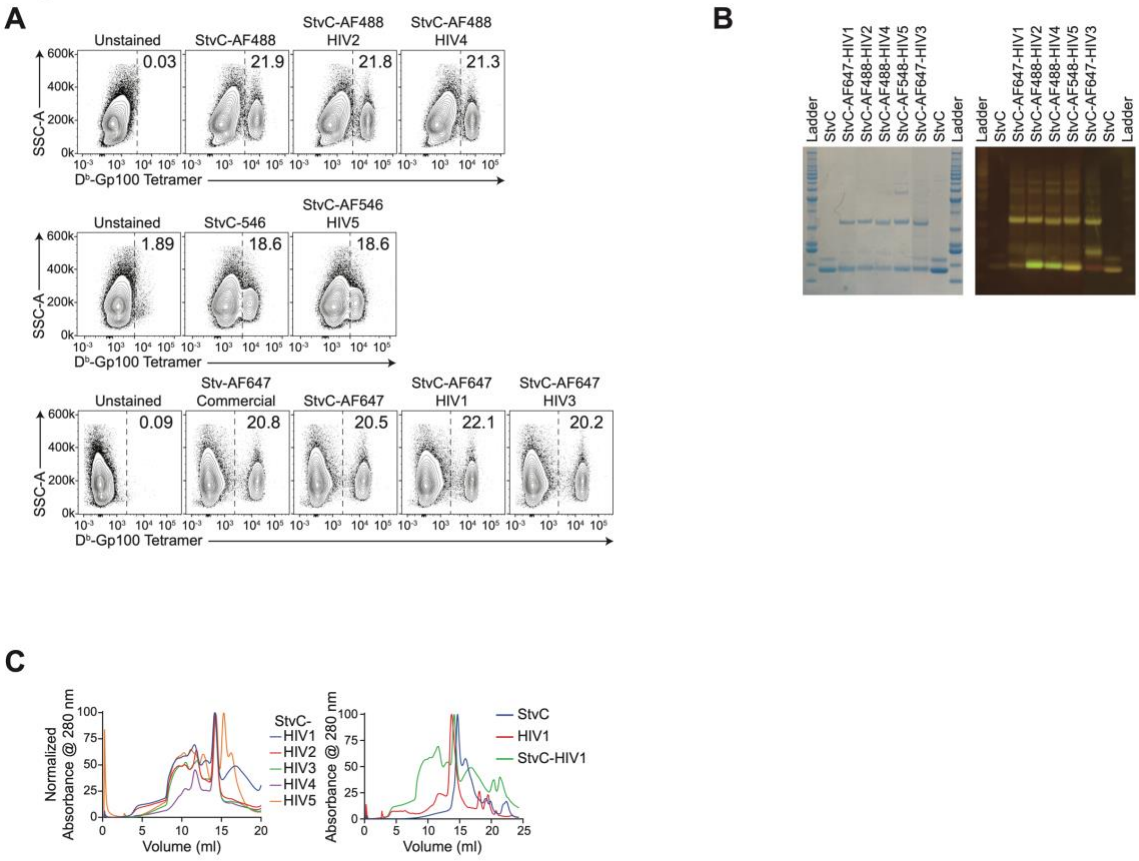
A
Unstained
StvC-AF488
StvC-AF488 HIV2
StvC-AF488 HIV4
0.03
21.9
21.8
21.3
SSC-A
Dᵇ-Gp100 Tetramer
Unstained
StvC-546
StvC-AF546 HIV5
1.89
18.6
18.6
Unstained
Stv-AF647 Commercial
StvC-AF647
StvC-AF647 HIV1
StvC-AF647 HIV3
0.09
20.8
20.5
22.1
20.2
B
Ladder
StvC
StvC-AF647-HIV1
StvC-AF488-HIV2
StvC-AF488-HIV4
StvC-AF548-HIV5
StvC-AF647-HIV3
C
Normalized Absorbance @ 280 nm
Volume (ml)
StvC-HIV1
HIV2
HIV3
HIV4
HIV5
Absorbance @ 280 nm
StvC
HIV1
StvC-HIV1

Figure S1. Construction of LIBRA-Seq compatible BG505 SOSIP probes. (**A**) Staining pmel splenocytes for Gp100-specific T cells with Db-Gp100-tetramers made from various streptavidin. (**B**) Gel electrophoresis of StvC-AF-DNA conjugates stained with Coommisie Blue (left) and SYBR DNA Gold (right). (**C**) StvC-AF-DNA conjugates were purified from free StvC-AF and DNA by size exclusion chromatography.

Figure S2

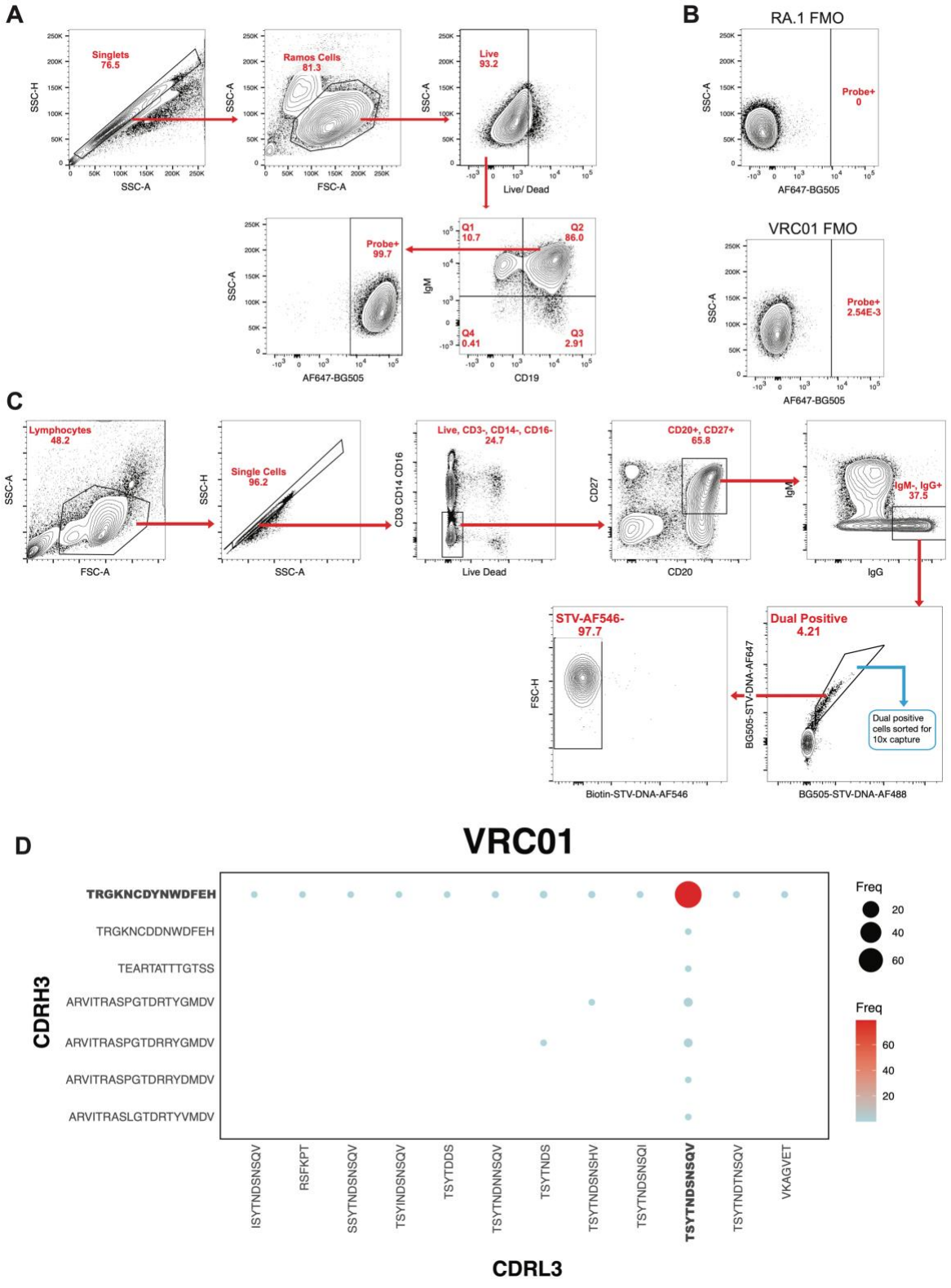
A
Singlets
76.5
SSC-H
SSC-A
Ramos Cells
81.3
FSC-A
Live
93.2
Live/ Dead
Probe+
99.7
AF647-BG505
Q1
10.7
Q2
86.0
Q4
0.41
Q3
2.91
IgM
CD19
B
RA.1 FMO
Probe+
0
AF647-BG505
VRC01 FMO
Probe+
2.54E-3
AF647-BG505
C
Lymphocytes
48.2
FSC-A
Single Cells
96.2
Live, CD3-, CD14-, CD16-
24.7
CD3 CD14 CD16
Live Dead
CD20+, CD27+
65.8
CD27
CD20
IgM-, IgG+
37.5
IgM
IgG
STV-AF546-
97.7
FSC-H
Biotin-STV-DNA-AF546
Dual Positive
4.21
BG505-STV-DNA-AF647
BG505-STV-DNA-AF488
Dual positive cells sorted for 10x capture
D
VRC01
CDRH3
TRGKNCDYNWDFEH
TRGKNCDDNWDFEH
TEARTATTTGTSS
ARVITRASPGTDRTYGMDV
ARVITRASPGTDRRYGMDV
ARVITRASPGTDRRYDMDV
ARVITRASLGTDRTYVMDV
ISYTNDSNSQV
RSFKPT
SSYTNDSNSQV
TSYINDSNSQV
TSYTDDS
TSYTNDNNSQV
TSYTNDS
TSYTNDSNSHV
TSYTNDSNSQI
TSYTNDSNSQV
TSYTNDTNSQV
VKAGVET
CDRL3
Freq
20
40
60
Freq
60
40
20

Figure S2. Validation of LIBRA-Seq compatible BG505 SOSIP probes *in vitro*. (**A**) Flow Cytometry gating strategy for the identification of VRC01 or RA.1 expressing Ramos B cells to DNA-barcoded, fluorescently labeled BG505 SOSIP. Cells were gated on FSC and SSC characteristic of singlets, Ramos cells, live cells, CD19+, IgM+, BG505-AF647+. (**B**) Fluorescence-minus-one plots for RA.1 (top) or VRC01 (bottom) expressing B cells. Cells were stained without BG505-AF647+ to assess background fluorescence in the AF647 channel. (**C**) BG505-AF647 barcode counts associated with VRC01 expressing Ramos B cells (left) or RA.1 expressing Ramos B cells (right). Each dot represents one cell. (**D**) Distribution of heavy and light chain CDR3 usage among 10x captured VRC01 Ramos B cells. Higher percentages denoted in red and lower in light blue. Canonical VRC01 CDRH3 and CDRL3 are bolded.

Figure S3

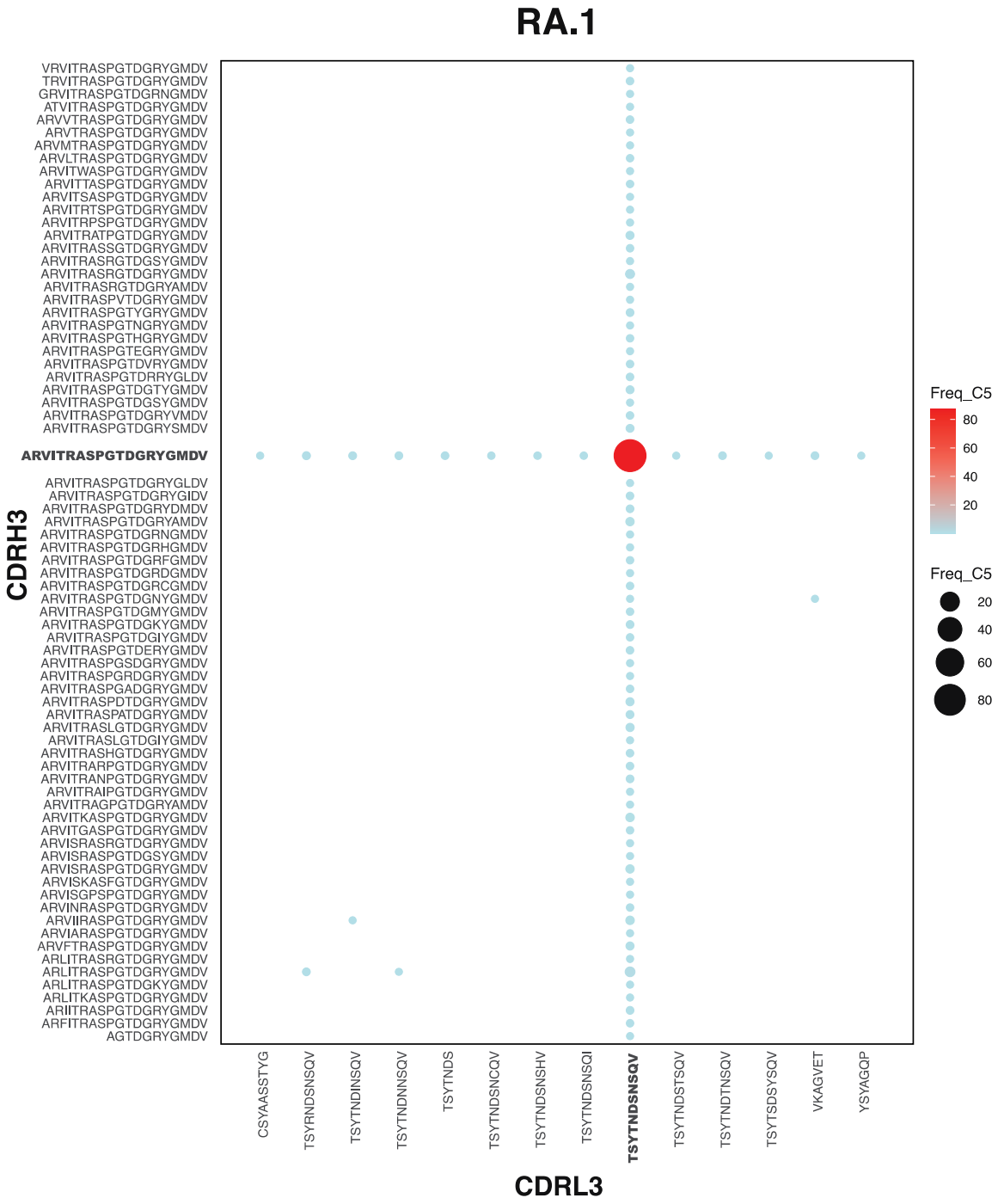
RA.1
CDRH3
VRVITRASPGTDGRYGMDV
TRVITRASPGTDGRYGMDV
GRVITRASPGTDGRNGMDV
ATVITRASPGTDGRYGMDV
ARVVTRASPGTDGRYGMDV
ARVTRASPGTDGRYGMDV
ARVMTRASPGTDGRYGMDV
ARVLTRASPGTDGRYGMDV
ARVITWASPGTDGRYGMDV
ARVITTASPGTDGRYGMDV
ARVITSASPGTDGRYGMDV
ARVITRTSPGTDGRYGMDV
ARVITRPSPGTDGRYGMDV
ARVITRATPGTDGRYGMDV
ARVITRASSGTDGRYGMDV
ARVITRASRGTDGSYGMDV
ARVITRASRGTDGRYGMDV
ARVITRASRGTDGRYAMDV
ARVITRASPVTDGRYGMDV
ARVITRASPGTYGRYGMDV
ARVITRASPGTNGRYGMDV
ARVITRASPGTHGRYGMDV
ARVITRASPGTEGRYGMDV
ARVITRASPGTDVRYGMDV
ARVITRASPGTDRRYGLDV
ARVITRASPGTDGTYGMDV
ARVITRASPGTDGSYGMDV
ARVITRASPGTDGRYVMDV
ARVITRASPGTDGRYSMDV
ARVITRASPGTDGRYGMDV
ARVITRASPGTDGRYGLDV
ARVITRASPGTDGRYGIDV
ARVITRASPGTDGRYDMDV
ARVITRASPGTDGRYAMDV
ARVITRASPGTDGRNGMDV
ARVITRASPGTDGRHGMDV
ARVITRASPGTDGRFGMDV
ARVITRASPGTDGRDGMDV
ARVITRASPGTDGRCGMDV
ARVITRASPGTDGNYGMDV
ARVITRASPGTDGMYGMDV
ARVITRASPGTDGKYGMDV
ARVITRASPGTDGIYGMDV
ARVITRASPGTDERYGMDV
ARVITRASPGSDGRYGMDV
ARVITRASPGRDGRYGMDV
ARVITRASPGADGRYGMDV
ARVITRASPDTDGRYGMDV
ARVITRASPATDGRYGMDV
ARVITRASLGTDGRYGMDV
ARVITRASLGTDGIYGMDV
ARVITRASHGTDGRYGMDV
ARVITRARPGTDGRYGMDV
ARVITRANPGTDGRYGMDV
ARVITRAIPGTDGRYGMDV
ARVITRAGPGTDGRYAMDV
ARVITKASPGTDGRYGMDV
ARVITGASPGTDGRYGMDV
ARVISRASRGTDGRYGMDV
ARVISRASPGTDGSYGMDV
ARVISRASPGTDGRYGMDV
ARVISKASFGTDGRYGMDV
ARVISGPSPGTDGRYGMDV
ARVINRASPGTDGRYGMDV
ARVIIRASPGTDGRYGMDV
ARVIARASPGTDGRYGMDV
ARVFTRASPGTDGRYGMDV
ARLITRASRGTDGRYGMDV
ARLITRASPGTDGRYGMDV
ARLITRASPGTDGKYGMDV
ARLITKASPGTDGRYGMDV
ARIITRASPGTDGRYGMDV
ARFITRASPGTDGRYGMDV
AGTDGRYGMDV
CSYAASSTYG
TSYRNDSNSQV
TSYTNDINSQV
TSYTNDNNSQV
TSYTNDS
TSYTNDSNCQV
TSYTNDSNSHV
TSYTNDSNSQI
TSYTNDSNSQV
TSYTNDSTSQV
TSYTNDTNSQV
TSYTSDSYSQV
VKAGVET
YSYAGQP
CDRL3
Freq_C5
80
60
40
20
Freq_C5
20
40
60
80

Figure S3. Validation of RA.1 Ramos Cell line CDR3 usage. Distribution of heavy and light chain CDR3 usage among 10x captured Ra.1 Ramos B cells. Higher percentages denoted in red and lower in light blue. Canonical Ra.1 CDRH3 and CDRL3 are bolded.

Figure S4

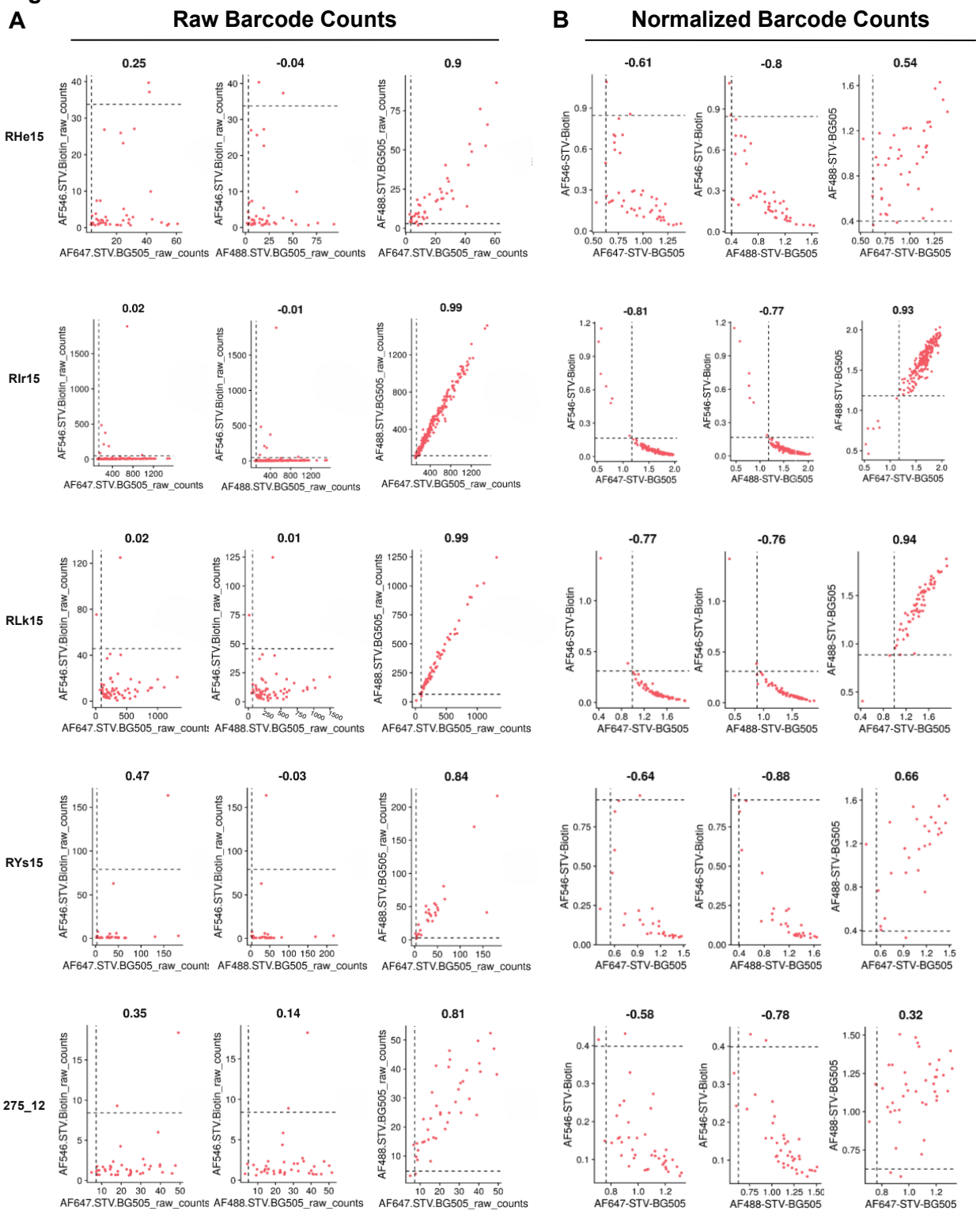
A
Raw Barcode Counts
B
Normalized Barcode Counts
RHe15
RIr15
RLk15
RYs15
275_12
0.25
-0.04
0.9
-0.61
-0.8
0.54
0.02
-0.01
0.99
-0.81
-0.77
0.93
0.02
0.01
0.99
-0.77
-0.76
0.94
0.47
-0.03
0.84
-0.64
-0.88
0.66
0.35
0.14
0.81
-0.58
-0.78
0.32
AF546.STV.Biotin_raw_counts
AF488.STV.BG505_raw_counts
AF647.STV.BG505_raw_counts
AF488.STV.BG505_raw_counts
AF546-STV-Biotin
AF488-STV-BG505
AF647-STV-BG505
AF488-STV-BG505

Figure S4. Validation of LIBRA-Seq compatible BG505 SOSIP probes *in vivo*. Feature scatter plots highlighting the raw (**A**) and normalized (**B**) read counts for LIBRA-Seq barcodes and show each combination of the biotin control and two BG505 SOSIP baits. The dotted lines represent the thresholds for antigen barcodes that were chosen empirically - 97th percentile for biotin negative control and 3rd percentile for the two BG505 SOSIP barcodes. Each dot represents a unique cell.

Figure S5

A

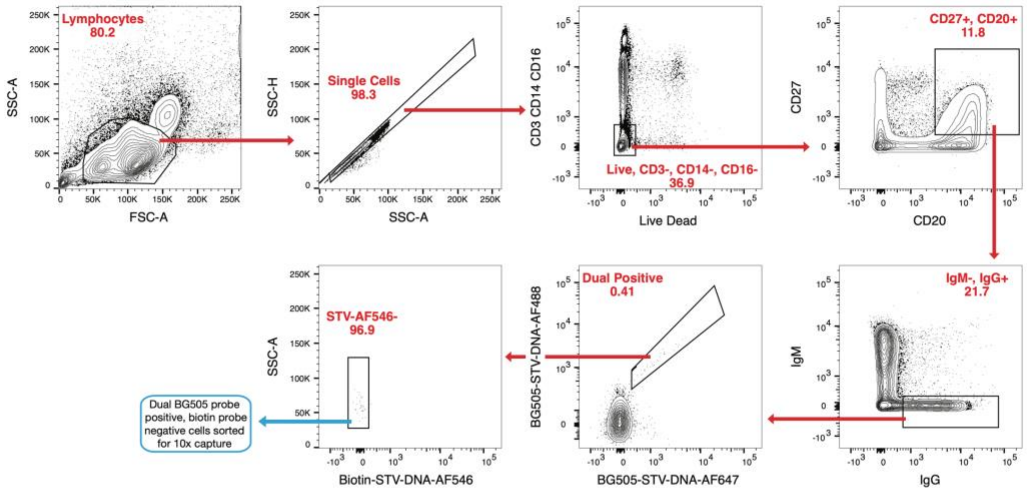
Lymphocytes
80.2
SSC-A
FSC-A
Single Cells
98.3
SSC-H
SSC-A
CD3 CD14 CD16
Live, CD3-, CD14-, CD16-
36.9
Live Dead
CD27
CD27+, CD20+
11.8
CD20
IgM
IgM-, IgG+
21.7
IgG
BG505-STV-DNA-AF488
Dual Positive
0.41
BG505-STV-DNA-AF647
STV-AF546-
96.9
SSC-A
Biotin-STV-DNA-AF546
Dual BG505 probe positive, biotin probe negative cells sorted for 10x capture

B

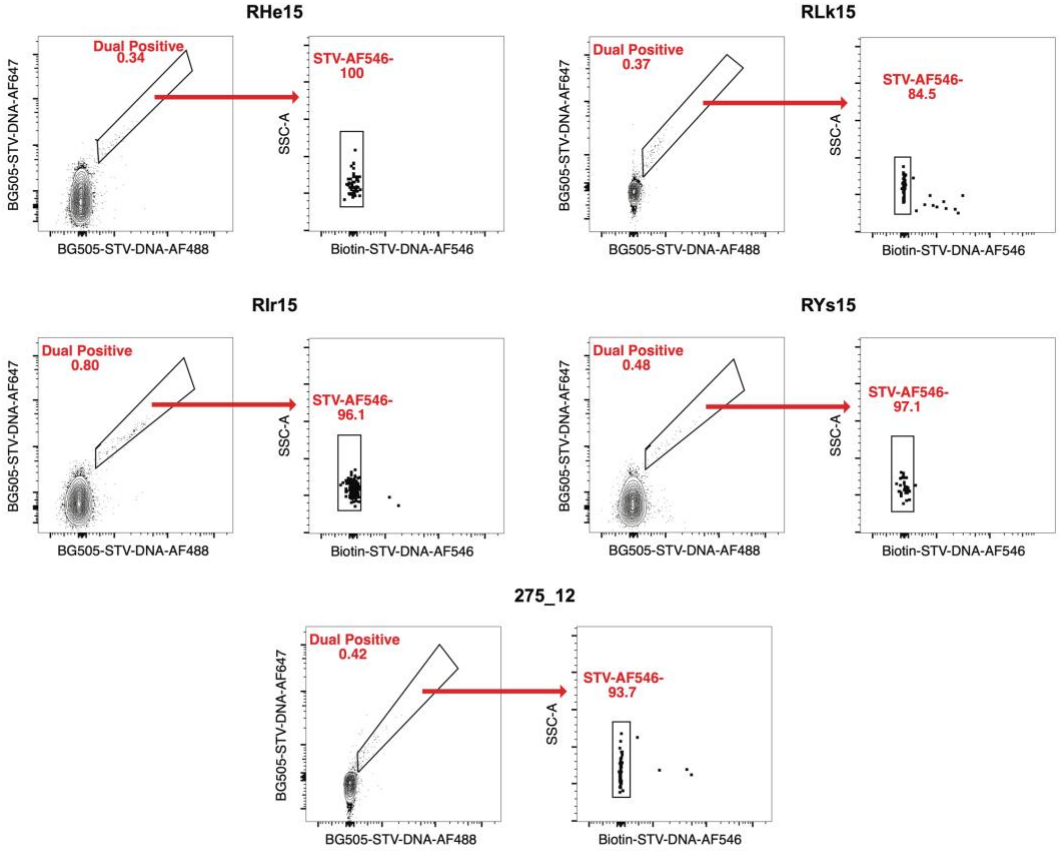
RHe15
Dual Positive
0.34
BG505-STV-DNA-AF647
BG505-STV-DNA-AF488
STV-AF546-
100
SSC-A
Biotin-STV-DNA-AF546
RLk15
Dual Positive
0.37
STV-AF546-
84.5
RIr15
Dual Positive
0.80
STV-AF546-
96.1
RYs15
Dual Positive
0.48
STV-AF546-
97.1
275_12
Dual Positive
0.42
STV-AF546-
93.7

Figure S5. Isolation of BG505 SOSIP specific memory B cells from vaccinated RM. (**A**) Fluorescence activated cell sorting gating strategy for the isolation of antigen specific memory B cells from cryopreserved PBMCs from vaccinated RM collected at timepoints noted in Table 1. Cells were gated on FSC and SSC characteristic of lymphocytes, singlets, live cells, CD3-, CD14-, CD16-, CD20+, CD27+, IgM-, IgG+, BG505-AF647+ and BG505-AF488+ and Biotin-AF546-. (**B**) Fluorescence activated cell sorting plots showing BG505 SOSIP-specific memory B cells isolated from cryopreserved PBMCs from vaccinated RM collected at timepoints noted in Table 1. Cells were gated on FSC and SSC characteristic of lymphocytes, singlets, live cells, CD3-, CD14-, CD16-, CD20+, CD27+, IgM-, IgG+, BG505-AF647+ and BG505-AF488+ and Biotin-AF546-.

EXPERIMENTAL MODEL AND SUBJECT DETAILS

Ethics Statement

The RM immunization experiment from which the serum samples were derived have been described previously[356]. The study was approved by the Institutional Animal Care and Use Committee (IACUC) at Emory University and was in compliance with NIH guidelines. Animal research was also in compliance with the Animal Welfare Act and other Federal statutes and regulations relating to experiments involving animals. All animal research adhered to the principles stated in the 2011 Guide for the Care and Use of Laboratory Animals prepared by the National Research Council. Yerkes National Primate Research Center (YNPRC) is fully accredited by the Association for Assessment and Accreditation of Laboratory Animal Care (AAALAC). Methods of euthanasia were consistent with the American Veterinary Medical Association with Guidelines.

Cell Lines

Surface VRC01 expressing Ramos B cells were provided by Dr. Daniel Lingwood at the Ragon Institute of MGH, MIT and Harvard. This cell line was generated and cultured as previously described[740], and validated for binding to our antigen probes by FACS (Figure S1B). RA.1 ramos cells were obtained from ATCC and cultured according to manufacturer instructions.

Animal Models

PBMC samples were obtained from a total of 6 Indian rhesus macaques (*Macaca mulatta*) immunized during a vaccine efficacy study carried out previously at the Yerkes National

Primate Research Center[356]. The study utilized female RM that were 3–15 years of age and confirmed negative for SIV infection. The immunization regimen has been previously described[356].

MATERIALS AND METHODS

Expression and purification of trimeric BG505.SOSIP.664 T332N-avi-biotinylated protein

The BG505 SOSIP Env insert (Genebank id ANG65466.1, res. 31-664, A501C/T605C/T332N, 508RRRRRR511) was synthesized by Genescript with (a) GMCSF leader sequence (MWLQGLLLLGTVACSIS) at its N-terminus end; (b) GTGS linker sequence and Avi tag (GLNDIFEAQKIEWHE) at its C-terminus. The insert was sub-cloned between ClaI and NheI sites of pGA1vector (KanR). NEB® 5-alpha E. coli cells (NEB, catalog no C2987H) and Sanger sequencing were used to transform, screen and confirm the positive clones respectively. The envelope protein cloned in pGA1 plasmid was expressed along with furin (expressed from an AmpR plasmid provided by Prof. John P. Moore), by transient transfection of Expi293F cells, in the ratio 4:1[359] using the ExpifectamineTM 293 transfection kit (ThermoScientific) as per manufacture's protocol and grown at 37oC, 8% CO2 at 130rpm. The purification process used here has been previously described[745]. Briefly, the supernatant was harvested 72hrs after transfection in presence of EDTA free protease inhibitor (Millipore Sigma, catalog no 11836170001) and affinity purified by lectin agarose (Vector Labs, catalog no AL-1243-5, pre-equilibrated with PBS). Bound protein was eluted in presence of 1M methyl a-D-

mannopyranoside (Sigma). The protein was dialyzed against PBS and subjected to size-exclusion chromatography using a Superdex 200 Increase 10/300 GL (Sigma, GE Healthcare product) column on an AktaTM Pure (GE) system. The trimeric peak was collected, concentrated using Amicon Ultra-4, MWCO 100kDa, and quantified by BCA assay (PierceTM, ThermoScientific). The trimeric status and purity of the protein was confirmed by BN-PAGE (NuPAGETM,4-12%BisTris Protein Gels, ThermoScientific). The protein was concentrated to ~9mg/ml. Reaction mixture containing BG505.SOSIP.664-avi protein, BirA (25µg for 10nmole of avi tagged protein), BiomixA (10X), BiomixB(10X) was incubated at 30oC for 45min, as per manufacture's protocol (BirA500, Avidity). Free biotin was removed by passing the reaction mixture through a Amicon Ultra-4, MWCO either 100kDa. The protein was found to be ~90% biotinylated, as estimated by ELISA using standards (MBP, MBP-avi-biotinylated) provided with the kit. The trimeric status of the biotinylated protein was confirmed by BN-PAGE. The protein was stored at 1mg/ml concentration.

Memory B cell Immunophenotyping

(AMQAX1000). Appropriate volume for 1 million cells and 5 million cells were added to FACS tubes for control and flow panel respectively. Samples were centrifuged at 180g for 5 minutes then decanted. Control samples were immediately fixed and resuspended in 300µL of 1% PFA then stored in 4˚C until ready for flow acquisition. Samples were incubated with 100µL of Fixable Viability Dye eFluor506 mix (65-0866-14) from eBioscience (1:1000 dilution) for 20 minutes at room temperature (RT) in the dark. Followed by a wash step with 2mLs of BSA Stain Buffer (554657), centrifuged at 300g for

5 minutes then decant. Samples were then incubated with 100µL of FC Block mix (14-9165-42) from Invitrogen (1:50 dilution) for 30 minutes at RT in the dark and followed by a wash step. Samples were then incubated with 100µL of biotin-quenched conjugated BG505 AF647/AF488 probe mix (1:1 dilution) for 30 minutes at RT in the dark and followed by a wash step. Samples were then incubated with 100µL of biotin-quenched unconjugated probe mix for 30 minutes at RT in the dark and followed by a wash step. Samples were then incubated with 100µL of the stain mix for 30 minutes at RT in the dark using the following mAbs: IgG BV650 (clone G18-145; 1.0µL; cat # 740596); IgM PerCP-Cy5.5 (clone G20-127; 3.0µL; cat # 561285); CD3 PE-CF594 (clone SP34-2; 2.0µL; cat # 562406); CD14 PE-CF594 (clone MφP9; 1.0µL; cat # 562334); CD16 PE-CF594 (clone 3G8; 1.0µL; cat # 562320) from BD Bioscience; CD27 BV421 (clone O323; 2.5µL; cat # 302824); CD20 APC-Cy7 (clone 2H7; 2.0µL; cat # 302314); BSA Stain Buffer (87.5µL; cat # 554657) from Biolegend; followed by a wash step. Samples were fixed and resuspended in 500µL of 1% PFA for cytometry acquisition. RAMOS cells were gated based on their FSC and SSC characteristics, singlets, live cells, CD3/CD14/CD16 (-) and CD20 (+), CD27 (+) and CD20 (+), IgM (-) and IgG (+). These cells were then assessed for their affinity to BG505 probes. Samples were run on BD FACSymphony A5 driven by FACS DiVa software and analyzed with FlowJo (Version 10.10).

The same protocol was performed on PBMCs extracted from Rhesus Macaques with the exception of the centrifuge speed at 300g for 10 minutes. Additionally, PBMCs were resuspended and strained through 70µM cell strainers in pre-chilled R10 media for sorting on BD FACSDiva.

BD CompBeads Anti-Mouse Ig, κ/Negative Control Compensation Particles Set (cat # 552843) were used for single fluorophore stains to select for the brightest peak. Compensations were prepared fresh and acquired for each assay.

Oligonucleotide barcodes

69 base pair (bp) in length oligonucleotide barcodes were designed with the following structure: 5'-5AmMC12-Read 2N-N10-Feature Barcode-N9-Capture Sequence-3', where the 5AmMC12 represents a 5' amino modification and 12 carbon linker for conjugation to streptavidin, the Read 2N is the Truseq read 2 sequence, 5'-CGGAGATGTGTATAAGAGACAG-3', N10 and N9 denote random nucleotide sequences of 10 and 9 bp in length respectively and are used as universal molecular identifiers (UMIs), the Feature Barcode is a known 15 bp sequence selected from the 10x feature barcode whitelist, and the capture sequence, 5'-CCCATATAAGA*A*A-3' is required for annealing to Chromium Next GEM Single Cell 5' Gel Beads (V2). For ramos cell line experiments feature barcode 5'-TTGTCACGGTAATAA-3' was used. For RM experiments feature barcodes 5'-TTGTCACGGTAATAA-3' (AF647 bound probes), 5'ATCGCATTCTAAGAA3' (AF488 bound probes), and 5'ATCTGCGCACATCTA3' (AF546 negative bait) was used. Oligos were ordered from IDT and HPLC purified.

Expression of recombinant streptavidin

One Shot^{TM} BL21(DE3) pLysE Chemically Competent E. coli (Invitrogen C656503) were transformed with plasmid of streptavidin modified with C-terminal cysteine with ampicillin

resistance. Shortly, plasmid was added to a stock of bacteria. After 30 minutes on ice, bacteria were heat shocked for 30 seconds at 42° C. Afterward, bacteria were placed on ice for 5 minutes before culturing at 37° C for 60 min. A portion of the bacteria was plated onto an agar plate with 1:1000 ampicillin overnight at 37° C. A colony of bacteria was grown in lysogeny broth (LB) with 1:1000 ampicillin overnight at 37° C. Bacteria were diluted 1:1000 in Erlenmeyer flask and once an OD600 of 0.6 was reached, 0.4 mM IPTG was added for 4 hours before collecting bacteria at 4k x g for 15 min at 23° C.

To isolate and refold streptavidin, bacteria pellet was lysed with lysis buffer (30 mM Tris-HCl, 0.1% Triton X-100, 2 mM EDTA, pH 8) for 30 minutes on ice. Afterward, 12 mM MgSO4, 10 ug/ml DNAse 1, and 10 ug/ml RNAse A was added for 30 minutes on ice. Lysate was centrifuged at 14k x g for 20 minutes at 4° C, after which the pellet was washed three times with lysis buffer. Isolated streptavidin inclusion body was dissolved in denaturing buffer (6 M Guanidine Hydrochloride, pH 6.5). The dissolved streptavidin inclusion bodies were added to 3.5 kDa dialysis tubing and dialyzed overnight at 4° C in 6 M Guanidine Hydrochloride with 10 mM β-mercaptoethanol pH 1.5. Streptavidin monomers were refolded into tetramers by dialysis in refolding buffer (0.2 M sodium acetate, 10 mM β-mercaptoethanol, pH 6) over 8 hours at 4 C; this process was repeated 3 times with fresh refolding buffer. Refolded streptavidin was collected by 10 kDa size exclusion filtration.

Conjugation of fluorophores to streptavidin

Recombinant streptavidin with C-terminal cysteine was buffer exchanged into cysteine buffer (100 mM Sodium Phosphate, 150 mM NaCl pH 7.2). Streptavidin was reduced with

50 molar excess tris(2-carboxyethyl)phosphine (TCEP) for 30 min at 23° C. Alexa fluorophores (AF) 488, 546, and 647 with maleimide group (Thermo Fisher) were dissolved in dimethyl sulfoxide (DMSO) and added at 10 molar excess to streptavidin for 2 hours at 23° C. Excess AF was removed through size exclusion spin columns (BIORAD 7326227) into spin buffer (150 mM NaCl, 100 mM Sodium Phosphate pH 6.5) according to manufacturer instructions. Concentration of streptavidin-AF was measured using Rapid Gold BCA Protein Assay (Thermo Fisher A55861) according to manufacture instructions.

Conjugation of oligonucleotide barcodes to streptavidin

Streptavidin-AF was reduced with 50 molar excess TCEP for 30 min at 23° C. Afterwhich, 50 molar excess maleimide 6-hydrazinonicotinate acetone hydrazone (MHPH) (VectorLabs S-1009) dissolved in dimethylformamide (DMF) was added for 4 hours at 23° C. Excess MHPH was removed by 10 kD size exclusion filtration and buffer exchanged into conjugation buffer (150 mM Sodium Chloride, 50 mM Sodium Citrate pH 6). Additionally, oligonucleotide with 5’ amine modification was buffered exchanged into oligo buffer (100 mM Sodium Phosphate, 150 mM NaCl pH 8) and reacted to 25 molar excess sulfo succinimidyl 4-formylbenzoate (S-4FB) (VectorLabs S-1008) for 4 hours at 23° C. Excess S-4FB was removed by 3 kD size exclusion filtration and buffer exchanged into conjugation buffer. Streptavidin-AF and oligonucleotide were combined at 1 to 1 overnight at 23° C. Streptavidin-AF-oligonucleotide conjugate was purified from unconjugated streptavidin-AF and oligonucleotide using size exclusion chromatography Superdex 200 Increase 10/300 GL (Cytiva 28990944) on Akta pure chromatography system. Concentration of Streptavidin-AF-oligonucleotide conjugate was measured using

Rapid Gold BCA Protein Assay (Thermo Fisher A55861) according to manufacturer instructions. Conjugate was visualized using NuPAGE Bis-Tris Mini Protein Gels, 4-12% (Thermo Fisher NP0321BOX) and stained with SYBR Gold Nucleic Acid Gel Stain (Thermo Fisher S11494) and Coomassie Brilliant Blue R-250 (Bio Rad 1610436) according to manufacturer instructions.

Isolation of splenocytes from transgenic mouse spleen

Spleen was isolated from P14 transgenic mouse and placed in RPMI media (VWR 16750-070). Spleen was mashed using frosted glass slides and strained through 40 μm cell strainer. Red blood cells lysis (VWR 420301-BL) was added for 5 minutes at 4° C then diluted 5x with PBS. Splenocytes were suspended in RPMI media and strained through 40 μm cell strainer before use.

Staining of splenocytes with pMHC tetramers

Recombinant Gp100-Db biotinylated monomers were tetramirized by adding streptavidin in 4 additions with 5 minute wait steps. Splenocytes were washed 3x with FACS buffer (1X PBS, 0.1% BSA, 2mM EDTA pH 7.4). Splenocytes were stained with Live/Dead aqua (Thermo Fisher L34957), PerCP/Cy5.5 anti-mouse CD8 (Biolegend Clone 53-6.7), and Gp100 tetramers (streptavidin-AF, streptavidin-AF-oligonucleotide, and Streptavidin-AF647 Thermo Fisher S21374) for 30 min at 4° C. Splenocytes were washed 3x with FACS buffer before running on Cytek Northern Light Flow Cytometer.

Conjugation of streptavidin to biotinylated antigen

Biotinylated Env proteins and oligonucleotide bound streptavidin (DNA-STV) were centrifuged at 14,000 rcf for 10 min at 4C to spin down aggregates. Samples for conjugation were then pipetted from the top of each solution. 2.5ug of biotinylated Env (1ug/μL) were combined with 1ug of DNA-STV, and brought up to 10μL PBS (2:1 mass ratio of Env to DNA-STV), then mixed by pipetting up and down slowly 5x without introducing bubbles. Conjugation reactions were then incubated at 4 degrees for 1 hour away from light.

Isolation of PBMCs

Peripheral blood lymphocytes were isolated from whole blood as described previously[746].

Enrichment of antigen-specific B cells (FACS)

Up to 28 million PBMCs isolated from RM were sorted for 10x capture. Antigen specific memory B cells were classified through the following gates for sorting: lymphocytes and monocytes, singlet, live cells, CD3-CD14-CD16-, HLA-DR+, CD20+CD27+, IgM-IgG+, and BG505-STV-DNA-AF647+BG505-STV-DNA-AF488+ and Biotin-STV-DNA-AF546-. Cells were sorted using a BD FACSAria II instrument (BD Biosciences) at the Emory Vaccine Center Flow Cytometry Core at the ENPRC.

Single-cell RNA-Sequencing

Single cell suspensions of FACS enriched memory B cells were prepared and loaded onto the 10X Genomics Chromium Controller using the Chromium NextGEM Single Cell 5' Library & Gel Bead kit to capture individual cells and barcoded gel beads within

droplets[698]. For RM experiments, counting steps were skipped due to low number of antigen specific B cells isolated via FACS. VDJ and feature barcode libraries were prepared according to manufacturer instructions. They were then sequenced on an Illumina NovaSeq 6000 with a paired-end 26x91 configuration targeting a depth of 5,000 reads for both surface barcode libraries and VDJ libraires. Cell Ranger software was used to perform demultiplexing of cellular transcript data, as well as mapping and annotation of UMIs and transcripts for downstream data analysis.

Single-cell RNA-Seq bioinformatic analysis of Memory B cells and Determination of LIBRA-seq Score

Cellranger v6.1.2 multi was used to obtain antigen barcode counts using the antigen barcode library and VDJ library. The VDJ reference that was used with multi was created using the fetch-imgt utility of cell ranger 6.0.2 for Macaca mulatta on 17th March 2023. The constant region sequences from Ramesh et al.[747] were added to the IMGT sequences [748]. Since the multi option is only available with newer versions of cellranger which have specific requirements for VDJ reference, we used another VDJ reference comprised of heavy chain V gene sequences from Cirelli et al.[749], KimDB v1.1[750], IMPre[751] in addition to IMGT sequences to start with a comprehensive database for assembly with cellranger v3.1.0. The assembled sequences were once again annotated with the Cirelli et al database[749] using IgBLAST v1.21.0[752]. The sequences were filtered to keep only those that were productive and with a predicted CDR3 region. After filtering Ig sequences, cells with only a single heavy and a single light chain were used downstream.

The antigen barcode data was processed using Seurat package v4.4.0[753]. A seurat object was created after adding a pseudocount of 1 to the raw count data. The CLR normalization method was used with margin 2. Considering these were sorted to be antigen-specific cells, the thresholds for antigen barcodes were chosen empirically - 97th percentile for biotin and 3rd percentile for the two BG505-SOSIP barcodes. Using these thresholds, cells were classified as positive if the normalized values were higher for both BG505-SOSIP antigens and lower for biotin. Cells that were classified as double positive for BG505 and negative for biotin were considered as antigen-specific and subsequently used for downstream analysis. Clonal assignment was performed using a custom script with the family defined as cells having the same V genes, same J gene, same CDR3 length and CDR3 nucleotide identity >=70%. The V gene usage was calculated for clonal lineages using the countGenes function in the alakazam package[754].

The public clonotypes were defined using the same definition of clonal families as described above. The visualization for public clonotypes was generated using the Circos package[755].

To determine the neutralizing antibody lineage in the current dataset, the sequences for monoclonal antibodies of the neutralizing lineage[362] were downloaded from GenBank. These sequences were annotated using IgBLAST with the Cirelli et al database. The clonal lineage was determined using the definition described above.

For calculating SHM, we used the MUSA database (2025-02-05)[756]. Only alleles that were found in both genomic and AIRR-Seq libraries of a given sample were used to create the IgBLAST v1.21.0 databases. The receptor_utils (http://pypi.org/project/receptor-utils/) package was used to create the J aux file. The MakeDB module from Immcantation

v4.4.0[754] was used to create ChangeO tables from IgBLAST output. The observedMutations function was used from the shazam package[754] with the regionDefinition set to IMGT_V_BY_SEGMENTS and both frequency and combine set to TRUE to obtain SHM.

Cellranger v6.1.2 multi was used to obtain antigen barcode counts using the antigen barcode library and VDJ library. The reference that was used with multi was created using the fetch-imgt utility of cell ranger 6.0.2 for Macaca mulatta on 17th March 2023. The constant region sequences from Ramesh et al[747] were added to the IMGT sequences. Since the multi-option is only available with newer versions of Cellranger which have specific requirements for VDJ reference, we used another VDJ reference comprised of heavy chain V gene sequences from Cirelli et al.[749], KimDB v1.1[750], IMPre[751] in addition to IMGT sequences to start with a comprehensive database for assembly. To enable comparisons with the single-cell and bulk plasmablasts, the assembled sequences were once again annotated with the Cirelli et al.[749] database. The sequences were filtered to keep only productive sequences and cells with only a single heavy and a single light chain.

LIBRA-Seq Scoring

The antigen barcode data was processed using Seurat package. A Seurat object was created after adding 1 to the counts. Only cells that had a single productive heavy and light chain were retained. The CLR normalization method was used with margin 2. Considering these were sorted to be antigen-specific cells, the thresholds for antigen barcodes were chosen empirically - 97th percentile for biotin and 3rd percentile for the two BG505 SOSIP barcodes. Using these thresholds, cells were classified as positive if

the normalized values were higher for both BG505 SOSIP antigens and lower for biotin. Cells that were classified as double positive for BG505 SOSIP and negative for biotin were subsequently used for downstream analysis.

IgBLAST v1.21.0 was used to annotate sequences and obtain AIRR-formatted outputs. The clones were defined as follows: (i) same V gene, (ii) same J gene, (iii) same CDR3 length and (iv) CDR3 nucleotide identity >= 70% for both heavy and light chains for determining clonal lineages.

Monoclonal antibody generation: Variable domains were synthesized using Twist Bioscience. Next, they were directionally cloned into human mAb heavy chain (IgG1) and light chain (kappa/lambda) expression vectors (Genbank accession numbers FJ475055, FJ475056, and FJ517647). Following vector construction and sequence confirmation, heavy and light chain vectors were transiently co-transfected into Expi293F cells according to manufacturer's instructions (Life Technologies). Antibodies were purified from cell culture supernatants using protein-A conjugated agarose beads (Pierce).

ELISA Assay: MaxiSorp plates were coated with BG505$_{[MOU1]}$ .SOSIP.664 at 1µg/mL diluted in 50 mM carbonate buffer overnight at 4^{o}C overnight at 4^{o}C. The following day plates were washed with PBS Tween 0.05% then blocked with PBS 1% BSA for 90 minutes. Next, plates were incubated with mAbs diluted in PBS Tween 0.05% 1% BSA for 90 minutes. Plates were then washed and incubated with peroxidase conjugated goat anti human IgG (109-036-098) diluted in PBS Tween 0.5% 1% BSA for 90 minutes. Wells

were developed with OPD substrate solution: 0.4 mg/ml of O-phenylenediamine (Sigma #P8787) dissolved into 50 mM citrate buffer (Sigma #P4560) with 30% H_2O_2. Plates were incubated with OPD substrate solution for 5 minutes. 100 ul of 1M HCl was added to stop the reaction and O.D. was recorded at 490 nm using the Bio-Rad IMark microplate reader.

ACKNOWLEDGMENTS

We thank the Emory National Primate Research Center (ENPRC) Division of Animal Resources for providing support in animal care. We thank Kalpana Patel from the Environmental Health and Safety Office for BSL-3 training and safety oversight. We thank Dr. Daniel Lingwood and his group at the Ragon Institute for providing the engineered Ramos B cell lines. We thank Dr. Ivelin Georgiev and his group at Vanderbilt University for conceptualizing and developing the LIBRA-Seq approach and associated code.

Funding

This study was supported primarily by the grant U24AI120134-10 from the National Institutes of Health (NIH), National Institute of Allergy and Infectious Diseases (NIAID) and by the supplement (to SEB). This project has been funded in part by the Intramural Program of the NIAID, NIH, Department of Health and Human Services. Next generation sequencing services were provided by the Emory NPRC Genomics Core which is supported in part by NIH P51 OD011132 (to Jonathan Lewin). Sequencing data was acquired on an Illumina NovaSeq 6000 funded by NIH S10 OD026799 (to SEB). The content of this publication does not necessarily reflect the views or policies of the U.S. Department of Health and Human Services, nor does it imply endorsement of organizations or commercial products. This work was supported by the NIAID P30

AI050409 awarded to Carlos Del Rio and the Center for AIDS Research (CFAR) and Emory University Emory National Primate Research Center Flow Cytometry Core.

Author Contributions

CTE, GK, RA, and SEB conceptualized the study. AST produced and validated barcoded streptavidin probes with oversight from GK. A. Sahoo produced avi-tagged BG505.SOSIP.664 trimers with oversight from RA. CTE conjugated barcoded streptavidin to biotinylated antigen. CTE and TT performed ramos cell assays and memory B cell staining. A. Saini at the Emory Primate/Vaccine/CFAR-Flow Cytometry Core performed sorting of antigen specific cells. AM and SAL performed 10x captures and library preparation. KP at the Emory Primate Center Genomics Core performed sequencing on 10x libraries. NR and AA performed bioinformatic scRNA-seq analyses. TCP performed BG505 binding ELISAs with oversight from JW. CTE analyzed flow cytometry, ELISA, and pseudovirus neutralization assay data and assembled figures. Funding was acquired by SEB (U24). CTE, AST, and SEB wrote the manuscript with input from TT.

Chapter 4: Discussion

The COVID-19 pandemic has caused widespread illness and death, with more than 777 million confirmed SARS-CoV-2 infections and 7 million deaths attributed to the disease[1]. While vaccines have proven effective at preventing severe outcomes, the ongoing emergence of variants of concern capable of escaping both vaccine-induced and natural immunity continues to pose a major challenge to global health. At the time of writing, SARS-CoV-2 variants under monitoring Omicron sub-lineage XEC is the most prevalent variant worldwide[572]. XEC, a recombinant of variants KS.1.1 and KP.3.3, contains T22N and F59S mutations in the spike protein's N-terminal domain (NTD) which impact antigenicity, neutralization, and spike protein stability[757]. The genetic shift associated with recombination can result in substantial changes to viral fitness and immune evasion capacity similar to the emergence of the original Omicron lineage, which represented a large genetic leap that enabled widespread escape from preexisting immunity and rapidly altered the pandemic trajectory[403-405]. The continued emergence of variants capable of evading infection- or vaccine-induced immunity underscores the urgent need for broadly protective β-coronavirus vaccines[397-402]. Although current COVID-19 vaccines have significantly reduced severe disease and mortality, their effectiveness against rapidly evolving variants has waned over time, necessitating ongoing updates and booster programs[676,758]. Recent mRNA vaccine formulations targeting new variants represent important progress, yet the limited durability of protection highlights the value of developing next-generation vaccine platforms[568-571,573-575]. With the threat of future genetic shifts in SARS-CoV-2 subverting existing immunity from recombination or from other coronaviruses undergoing zoonotic transmission, we are limited in our responses

by the technical and logistical obstacles presented by developing, testing, and distributing an effective vaccine.

Broadly neutralizing antibodies (bNAbs) targeting conserved viral regions, such as the S2 stem of the SARS-CoV-2 spike protein, offer a promising path forward. Our work demonstrates that prophylactic treatment with an S2-targeted bNAb in rhesus macaques significantly reduces viral loads and airway inflammation, supporting an S2 targeting therapeutic strategy and a foundation for pan-β-CoV vaccine design. Because COVID-19 is generally an acute, self-limiting infection, and because severe disease is associated with high viral loads and inflammatory responses in the lower respiratory tract, the primary goal of vaccination has remained mitigating disease severity rather than achieving complete sterilizing immunity[449]. In contrast, HIV-1 presents a fundamentally different challenge, as successful prevention must occur prior to or immediately at the point of transmission to block the irreversible establishment of latent viral reservoirs. This distinction means that HIV-1 vaccines must generate extremely potent and durable immune responses capable of preventing even low-level infection[348].

For SARS-CoV-2 and other β-coronaviruses, however, a vaccine does not necessarily need to prevent infection entirely to be clinically valuable. Instead, reducing viral replication and dampening inflammation may be sufficient to prevent hospitalization and long-term sequelae such as long COVID. This opens the door for a unique niche in which pan-β-CoV vaccines can operate. Rather than focusing on narrowly tailored immune responses to specific variants, which are subverted by immune escape, pan-β-CoV vaccines can instead promote immune recognition of conserved viral elements, such as the S2 subunit of the spike protein. By biasing immune responses away from highly

mutable, variant-specific regions and toward functionally constrained, conserved domains, it may be possible to achieve broader and longer-lasting protection, even at sub-sterilizing levels of neutralizing antibodies. This approach is practical and widely applicable for pandemic preparedness, especially in vulnerable and diverse populations, and highlights the potential of bNAbs as valuable tools for both emergency response and vaccine design[555,693].

Equitable access to vaccines, prophylactics, and antiviral therapies remains critical, particularly for immunocompromised populations who are disproportionately at risk for severe disease and prolonged infection. Global pandemic preparedness efforts must prioritize protection of the most vulnerable populations, as doing so provides both direct and indirect protection for broader society. For example efforts to prevent HIV-1 infection not only address the global HIV-1 burden but may also have far-reaching implications for controlling other pathogens like SARS-CoV-2. Immunocompromised individuals, including those with living with untreated HIV-1, are at increased risk for prolonged SARS-CoV-2 infection, which is associated with more severe disease outcomes, including long COVID. These prolonged infections provide fertile ground for viral evolution within a single host, increasing the likelihood of immune escape mutations and potentially contributing to the emergence of novel variants[409-416]. By reducing the number of immunocompromised individuals through effective HIV-1 prevention and treatment strategies, we may also reduce the overall reservoir for SARS-CoV-2 (or other pathogen) evolution, thereby mitigating both individual and population-level risk. Broadly acting therapies, such as pan-β-coronaviruses vaccines or broadly neutralizing antibodies, further enhance this effect by offering protection against a wide range of

SARS-CoV-2 variants, even in the face of antigenic drift. These interventions target conserved regions of the virus that are functionally constrained, limiting the virus's ability to evolve without compromising its fitness. As such, they not only help contain ongoing infections but also serve as a proactive barrier against the emergence and spread of highly divergent or immune-evasive strains. Together, comprehensive HIV-1 prevention and broad SARS-CoV-2 countermeasures represent a synergistic strategy to reduce both disease burden and the risk of future viral evolution. Expanding access to broader prophylactic and therapeutic antivirals for mild-to-moderate disease may also help reduce transmission and minimize the long-term consequences of SARS-CoV-2 infection, including the development of post-acute sequelae of SARS-CoV-2 infection (PASC), also known as long COVID[759,760].

Due to their physiological and genetical similarity to humans, non-human primate models such as rhesus macaques (RM) remain essential for evaluating immune responses and therapeutic interventions against SARS-CoV-2[761]. The use of the RM model of SARS-CoV-2 infection further allowed us to control key variables that influence clinical outcomes in humans, such as strain, dose, and route of exposure. This controlled setting enabled repeated sampling of BAL fluid- a critical sample for the analysis of immune cells within the lower airway, including multiple macrophage subsets instrumental in mitigating inflammatory signals related to SARS-CoV-2 infection. Importantly, the RM model allowed for characterization of hyperacute (2 dpi) responses to infection. We profiled viral load, myeloid cell dynamics, and inflammatory signaling at such timepoints, which would prove difficult to obtain in human studies without the use of currently unethical controlled challenge trials. Therefore, the rhesus macaque (RM) model of

SARS-CoV-2 remains uniquely appropriate to investigate protective and therapeutic strategies against SARS-CoV-2 pathogenesis.

While the RM model has proven effective in recapitulating key features of mild-to-moderate COVID-19, the absence of a robust model for severe disease remains a significant limitation in preclinical research[761]. A model that better mimics the full spectrum of clinical severity observed in humans, particularly among high-risk individuals is urgently needed to advance the development of next-generation therapeutics and vaccines. Currently, severe disease phenotypes have been primarily achieved in small animal models such as K18-hACE2 transgenic mice, which constitutively express the human ACE2 under the cytokeratin-18 promoter and develop severe pulmonary pathology upon SARS-CoV-2 infection[762]. However, K18-hACE2 mice rapidly succumb to infection within 5 to 7 days, often due to neuroinvasion and exaggerated lung pathology[763]. These features, while useful for modeling acute, severe disease, limit their utility for studying the longer-term consequences of infection, such as post-acute sequelae or immune recovery.

Establishing a model of severe or prolonged SARS-CoV-2 disease in RM would bridge this gap and offer a platform for studying critical mechanisms of COVID-19 pathogenesis. Such a model could enable in-depth investigation of persistent viral reservoirs, chronic inflammation, tissue remodeling, and immune dysregulation- all hallmarks of long COVID[759,760]. Moreover, the ability to monitor immune responses over time in a genetically tractable and immunologically relevant system would facilitate rigorous testing of mutation-resistant treatments, such as broadly neutralizing antibodies (bNAbs), as well as next-generation vaccines and antivirals. A non-human primate model

that mirrors both acute and chronic phases of severe COVID-19 would significantly enhance translational research and inform clinical strategies for vulnerable populations.

In parallel, the RM model continues to be foundational to HIV-1 vaccine development, particularly for studying infection and immune responses in a genetically tractable, immunologically relevant system. The recent development of high-throughput technologies such as LIBRA-Seq enable the recovery of large numbers of antigen-specific B cell receptor sequences, greatly enhancing our ability to evaluate allelic variation and representation within the antigen-specific B cell repertoire in RM[10]. Prior studies have demonstrated that polymorphisms in immunoglobulin heavy chain variable (IGHV) genes can significantly influence neutralizing antibody responses. For instance, alleles encoding a phenylalanine (F) at position 54 of IGHV1-69 are associated with increased frequencies of broadly neutralizing antibodies (bNAbs) against influenza[764,765], while alleles encoding a leucine (L) at the same position have been implicated in the immunodominance of non-neutralizing anti-gp41 responses to HIV-1 envelope vaccination, even in individuals heterozygous for F/L at IGHV1-69[764]. Similar patterns have been observed in the context of SARS-CoV-2, where IGHV1-69 polymorphisms have been shown to influence the potency and epitope targeting of neutralizing antibodies[766]. Furthermore, a phase 1 clinical trial of the germline-targeting HIV-1 Env immunogen eOD-GT8 revealed that the induction of VRC01-class precursors was restricted by IGHV1-2 allele usage[767]. However, the impact of allelic polymorphisms at the IGH locus on neutralizing antibody responses in RM remains poorly defined. A study recently published on Biorxv has greatly expanded on the breadth of previously used datasets describing the RM Ig loci with the Macaque Unified Set of Alleles (MUSA)[756] and

highlights the complexity of immunoglobulin gene variation in this model, with critical implications for B cell responses to vaccination. These insights are especially relevant as we continue to evaluate why only a subset of BG505 SOSIP vaccinated animals develop robust neutralizing antibody responses capable of protecting against autologous SHIV challenge.

To address these questions, we developed a high-throughput LIBRA-seq pipeline capable of linking B cell receptor identity, antigen specificity, and transcriptomic profiles at single-cell resolution. Using this approach, we simultaneously recovered and profiled the antigen specificity, BCR sequences, clonal lineages, public clones, and somatic hypermutation patterns in BG505 SOSIP-vaccinated RMs. While our initial efforts focused on identifying BG505 SOSIP B cells in RM that developed neutralizing antibody responses, expanding LIBRA-seq to include animals with non-neutralizing or discordant outcomes, potentially using epitope-modified probe panels, could reveal critical determinants of response heterogeneity. This strategy is especially well-suited to explore how Ig locus variation, naive repertoire bias, and transcriptional programs shape effective B cell immunity. Broadening LIBRA-seq panels to encompass a diverse set of HIV-1 Env probes would enable comprehensive analysis of Env-specific repertoires across large RM cohorts, supporting the detection of allele-associated differences in antibody responses and informing immunogen design that accounts for host genetic diversity. Such work could have wide reaching impacts for antibody based vaccine design, allowing for experimental group assignment for both non-human primates and humans based on Ig haplotype.

In 2023, an estimated 1 to 1.7 million people were newly infected with HIV, underscoring the urgent need for a prophylactic vaccine to address this ongoing global health crisis[9]. Despite progress in treatment, millions of individuals remain unaware of their status or lack access to antiretroviral therapy, making vaccine development a critical component of the long-term HIV-1 response. While long-acting injectable antivirals like lenacapavir show promise, their effectiveness still hinges on consistent, lifelong adherence—an ongoing challenge, especially in resource-limited settings. Gilead, the pharmaceutical company behind lenacapavir (Sunlenca), has set the price at $42,250 USD for the first year of therapy and $39,000 annually thereafter[284,285,290,768]. At this cost, and without substantial financial support from assistance programs, insurance coverage, or significant price reductions, this highly effective, first-in-class capsid inhibitor remains out of reach for much of the global population. Given that protection rapidly diminishes once treatment is interrupted, these barriers further underscore the urgent need for a durable, broadly accessible, and preventive HIV-1 vaccine.

Taken together, these findings underscore the growing necessity of precision-guided, equitable, and evolution-resilient approaches to pandemic preparedness. As the biomedical research community confronts viral pathogens with high mutation rates, immune evasion capabilities, and global transmission potential, traditional vaccinology falls short. The convergence of high throughput immunoprofiling tools with robust preclinical models enables a more nuanced understanding of how host genetics, B cell ontogeny, and antigen design can better elicit protective immunity. This precision framework not only helps optimize immunogen strategies for current public health crises but also equips us with the tools to rapidly respond to emerging threats. Through

leveraging conserved targets and tailoring vaccines to human and NHP repertoires, we can develop platforms that are both durable and adaptable in the face of disruptive and emerging pathogens.

REFERENCES

1. Organization, W.H. (2020). WHO Coronavirus (COVID-19) Dashboard. https://data.who.int/dashboards/covid19/cases?n=c.
2. Polack, F.P., Thomas, S.J., Kitchin, N., Absalon, J., Gurtman, A., Lockhart, S., Perez, J.L., Marc, G.P., Moreira, E.D., Zerbini, C., et al. (2020). Safety and Efficacy of the BNT162b2 mRNA Covid-19 Vaccine. N. Engl. J. Med. *383*, 2603-2615. 10.1056/nejmoa2034577.
3. Baden, L.R., El Sahly, H.M., Essink, B., Kotloff, K., Frey, S., Novak, R., Diemert, D., Spector, S.A., Rouphael, N., Creech, C.B., et al. (2021). Efficacy and Safety of the mRNA-1273 SARS-CoV-2 Vaccine. N Engl J Med *384*, 403-416. 10.1056/NEJMoa2035389.
4. Carabelli, A.M., Peacock, T.P., Thorne, L.G., Harvey, W.T., Hughes, J., Silva, T.I.d., Peacock, S.J., Barclay, W.S., Silva, T.I.d., Towers, G.J., and Robertson, D.L. (2023). SARS-CoV-2 variant biology: immune escape, transmission and fitness. Nat Rev Microbiol *21*, 162-177. 10.1038/s41579-022-00841-7.
5. Rerks-Ngarm, S., Pitisuttithum, P., Nitayaphan, S., Kaewkungwal, J., Chiu, J., Paris, R., Premsri, N., Namwat, C., Souza, M.d., Adams, E., et al. (2009). Vaccination with ALVAC and AIDSVAX to Prevent HIV-1 Infection in Thailand. N. Engl. J. Med. 0.1056/NEJMoa0908492.
6. Gray, G.E., Andersen-Nissen, E., Grunenberg, N., Huang, Y., Roux, S., Laher, F., Innes, C., Gu, N., DiazGranados, C., Phogat, S., et al. (2014). HVTN 097: Evaluation of the RV144 Vaccine Regimen in HIV Uninfected South African

Adults. AIDS Res. Hum. Retroviruses *30*, A33-A34. 10.1089/aid.2014.5052a.abstract.

7. Lazarus, E.M., Otwombe, K., Adonis, T., Sebastian, E., Gray, G., Grunenberg, N., Roux, S., Churchyard, G., Innes, C., and Laher, F. (2014). Uptake of Genital Mucosal Sampling in HVTN 097, a Phase 1b HIV Vaccine Trial in South Africa. Plos One *9*, e112303. 10.1371/journal.pone.0112303.
8. Ng'uni, T., Chasara, C., and Ndhlovu, Z.M. (2020). Major Scientific Hurdles in HIV Vaccine Development: Historical Perspective and Future Directions. Front Immunol *11*, 590780. 10.3389/fimmu.2020.590780.
9. Unaids (2023). UNAIDS GLOBAL AIDS UPDATE.
10. Setliff, I., Shiakolas, A.R., Pilewski, K.A., Murji, A.A., Mapengo, R.E., Janowska, K., Richardson, S., Oosthuysen, C., Raju, N., Ronsard, L., et al. (2019). High-Throughput Mapping of B Cell Receptor Sequences to Antigen Specificity. Cell *179*, 1636-1646.e1615. 10.1016/j.cell.2019.11.003.
11. Vogt, M., Craven, D., Crawford, D., Witt, D., Byington, R., Schooley, R., and Hirsch, M. (1986). ISOLATION OF HTLV-III/LAV FROM CERVICAL SECRETIONS OF WOMEN AT RISK FOR AIDS. Lancet *327*, 525-527. 10.1016/s0140-6736(86)90884-6.
12. Poon, D.T., Wu, J., and Aldovini, A. (1996). Charged amino acid residues of human immunodeficiency virus type 1 nucleocapsid p7 protein involved in RNA packaging and infectivity. J Virol *70*, 6607-6616. 10.1128/jvi.70.10.6607-6616.1996.

13. Bowzard, J.B., Bennett, R.P., Krishna, N.K., Ernst, S.M., Rein, A., and Wills, J.W. (1998). Importance of Basic Residues in the Nucleocapsid Sequence for Retrovirus Gag Assembly and Complementation Rescue. J Virol *72*, 9034-9044. 10.1128/jvi.72.11.9034-9044.1998.

14. Zhu, K., Dobard, C., and Chow, S.A. (2004). Requirement for Integrase during Reverse Transcription of Human Immunodeficiency Virus Type 1 and the Effect of Cysteine Mutations of Integrase on Its Interactions with Reverse Transcriptase. J Virol *78*, 5045-5055. 10.1128/jvi.78.10.5045-5055.2004.

15. Warrilow, D., Stenzel, D., and Harrich, D. (2007). Isolated HIV-1 core is active for reverse transcription. Retrovirology *4*, 77. 10.1186/1742-4690-4-77.

16. Briggs, J.A.G., Grünewald, K., Glass, B., Förster, F., Kräusslich, H.-G., and Fuller, S.D. (2006). The Mechanism of HIV-1 Core Assembly: Insights from Three-Dimensional Reconstructions of Authentic Virions. Structure *14*, 15-20. 10.1016/j.str.2005.09.010.

17. Chertova, E., Bess, J.W., Crise, B.J., Sowder, R.C., Schaden, T.M., Hilburn, J.M., Hoxie, J.A., Benveniste, R.E., Lifson, J.D., Henderson, L.E., and Arthur, L.O. (2002). Envelope Glycoprotein Incorporation, Not Shedding of Surface Envelope Glycoprotein (gp120/SU), Is the Primary Determinant of SU Content of Purified Human Immunodeficiency Virus Type 1 and Simian Immunodeficiency Virus. J Virol *76*, 5315-5325. 10.1128/jvi.76.11.5315-5325.2002.

18. Zhu, P., Chertova, E., Bess, J., Lifson, J.D., Arthur, L.O., Liu, J., Taylor, K.A., and Roux, K.H. (2003). Electron tomography analysis of envelope glycoprotein

trimers on HIV and simian immunodeficiency virus virions. Proc National Acad Sci *100*, 15812-15817. 10.1073/pnas.2634931100.

19. Zhu, P., Liu, J., Bess, J., Chertova, E., Lifson, J.D., Grisé, H., Ofek, G.A., Taylor, K.A., and Roux, K.H. (2006). Distribution and three-dimensional structure of AIDS virus envelope spikes. Nature *441*, 847-852. 10.1038/nature04817.

20. Checroune, F., Yao, X.-J., Göttlinger, H.G., Bergeron, D., and Cohen, E.A. (1995). Incorporation of Vpr into Human Immunodeficiency Virus Type 1. J. Acquir. Immune Defic. Syndr. Hum. Retrovirology *10*, 1-7. 10.1097/00042560-199509000-00001.

21. Müller, B., Patschinsky, T., and Kräusslich, H.-G. (2002). The Late-Domain-Containing Protein p6 Is the Predominant Phosphoprotein of Human Immunodeficiency Virus Type 1 Particles. J Virol *76*, 1015-1024. 10.1128/jvi.76.3.1015-1024.2002.

22. Pandori, M.W., Fitch, N.J., Craig, H.M., Richman, D.D., Spina, C.A., and Guatelli, J.C. (1996). Producer-cell modification of human immunodeficiency virus type 1: Nef is a virion protein. J Virol *70*, 4283-4290. 10.1128/jvi.70.7.4283-4290.1996.

23. Welker, R., Kottler, H., Kalbitzer, H.R., and KrÄUsslich, H.-G. (1996). Human Immunodeficiency Virus Type 1 Nef Protein Is Incorporated into Virus Particles and Specifically Cleaved by the Viral Proteinase. Virology *219*, 228-236. 10.1006/viro.1996.0240.

24. Dalgleish, A.G., Beverley, P.C.L., Clapham, P.R., Crawford, D.H., Greaves, M.F., and Weiss, R.A. (1984). The CD4 (T4) antigen is an essential component of the receptor for the AIDS retrovirus. Nature *312*, 763-767. 10.1038/312763a0.

25. Hong, P.W.P., Nguyen, S., Young, S., Su, S.V., and Lee, B. (2007). Identification of the Optimal DC-SIGN Binding Site on Human Immunodeficiency Virus Type 1 gp120. J Virol *81*, 8325-8336. 10.1128/jvi.01765-06.

26. Witte, L.d., Nabatov, A., and Geijtenbeek, T.B.H. (2008). Distinct roles for DC-SIGN+-dendritic cells and Langerhans cells in HIV-1 transmission. Trends Mol Med *14*, 12-19. 10.1016/j.molmed.2007.11.001.

27. Hoffman, T.L., and Doms, R.W. (2009). HIV-1 envelope determinants for cell tropism and chemokine receptor use. Mol. Membr. Biol. *16*, 57-65. 10.1080/096876899294760.

28. Zhang, W., Canziani, G., Plugariu, C., Wyatt, R., Sodroski, J., Sweet, R., Kwong, P., Hendrickson, W., and Chaiken, I. (1999). Conformational Changes of gp120 in Epitopes near the CCR5 Binding Site Are Induced by CD4 and a CD4 Miniprotein Mimetic †. Biochemistry *38*, 9405-9416. 10.1021/bi990654o.

29. Alkhatib, G., Combadiere, C., Broder, C.C., Feng, Y., Kennedy, P.E., Murphy, P.M., and Berger, E.A. (1996). CC CKR5: A RANTES, MIP-1α, MIP-1β Receptor as a Fusion Cofactor for Macrophage-Tropic HIV-1. Science *272*, 1955-1958. 10.1126/science.272.5270.1955.

30. Deng, H., Liu, R., Ellmeier, W., Choe, S., Unutmaz, D., Burkhart, M., Marzio, P.D., Marmon, S., Sutton, R.E., Hill, C.M., et al. (1996). Identification of a major co-receptor for primary isolates of HIV-1. Nature *381*, 661-666. 10.1038/381661a0.

31. Feng, Y., Broder, C.C., Kennedy, P.E., and Berger, E.A. (1996). HIV-1 Entry Cofactor: Functional cDNA Cloning of a Seven-Transmembrane, G Protein-Coupled Receptor. Science *272*, 872-877. 10.1126/science.272.5263.872.

32. Shimizu, N., Tanaka, A., Oue, A., Mori, T., Ohtsuki, T., Apichartpiyakul, C., Uchiumi, H., Nojima, Y., and Hoshino, H. (2009). Broad usage spectrum of G protein-coupled receptors as coreceptors by primary isolates of HIV. AIDS *23*, 761. 10.1097/qad.0b013e328326cc0d.

33. Han, X., and Tamm, L.K. (2000). A host–guest system to study structure–function relationships of membrane fusion peptides. Proc National Acad Sci *97*, 13097-13102. 10.1073/pnas.230212097.

34. Braaten, D., Franke, E.K., and Luban, J. (1996). Cyclophilin A is required for an early step in the life cycle of human immunodeficiency virus type 1 before the initiation of reverse transcription. J Virol *70*, 3551-3560. 10.1128/jvi.70.6.3551-3560.1996.

35. Chan, D.C., Fass, D., Berger, J.M., and Kim, P.S. (1997). Core Structure of gp41 from the HIV Envelope Glycoprotein. Cell *89*, 263-273. 10.1016/s0092-8674(00)80205-6.

36. Weissenhorn, W., Dessen, A., Harrison, S.C., Skehel, J.J., and Wiley, D.C. (1997). Atomic structure of the ectodomain from HIV-1 gp41. Nature *387*, 426-430. 10.1038/387426a0.

37. Selyutina, A., Persaud, M., Lee, K., KewalRamani, V., and Diaz-Griffero, F. (2020). Nuclear Import of the HIV-1 Core Precedes Reverse Transcription and Uncoating. Cell Reports *32*, 108201. 10.1016/j.celrep.2020.108201.

38. Abram, M.E., Ferris, A.L., Shao, W., Alvord, W.G., and Hughes, S.H. (2010). Nature, Position, and Frequency of Mutations Made in a Single Cycle of HIV-1 Replication. J Virol *84*, 9864-9878. 10.1128/jvi.00915-10.

39. Farnet, C.M., and Haseltine, W.A. (1991). Determination of viral proteins present in the human immunodeficiency virus type 1 preintegration complex. J Virol *65*, 1910-1915. 10.1128/jvi.65.4.1910-1915.1991.

40. Bukrinsky, M.I., Haggerty, S., Dempsey, M.P., Sharova, N., Adzhubei, A., Spitz, L., Lewis, P., Goldfarb, D., Emerman, M., and Stevenson, M. (1993). A nuclear localization signal within HIV-1 matrix protein that governs infection of non-dividing cells. Nature *365*, 666-669. 10.1038/365666a0.

41. Gallay, P., Swingler, S., Song, J., Bushman, F., and Trono, D. (1995). HIV nuclear import is governed by the phosphotyrosine-mediated binding of matrix to the core domain of integrase. Cell *83*, 569-576. 10.1016/0092-8674(95)90097-7.

42. Miller, M.D., Farnet, C.M., and Bushman, F.D. (1997). Human immunodeficiency virus type 1 preintegration complexes: studies of organization and composition. J Virol *71*, 5382-5390. 10.1128/jvi.71.7.5382-5390.1997.

43. Bouyac-Bertoia, M., Dvorin, J.D., Fouchier, R.A.M., Jenkins, Y., Meyer, B.E., Wu, L.I., Emerman, M., and Malim, M.H. (2001). HIV-1 Infection Requires a Functional Integrase NLS. Mol. Cell *7*, 1025-1035. 10.1016/s1097-2765(01)00240-4.

44. Noronha, C.M.C.d., Sherman, M.P., Lin, H.W., Cavrois, M.V., Moir, R.D., Goldman, R.D., and Greene, W.C. (2001). Dynamic Disruptions in Nuclear Envelope Architecture and Integrity Induced by HIV-1 Vpr. Science *294*, 1105-1108. 10.1126/science.1063957.

45. Ellison, V., Abrams, H., Roe, T., Lifson, J., and Brown, P. (1990). Human immunodeficiency virus integration in a cell-free system. J Virol *64*, 2711-2715. 10.1128/jvi.64.6.2711-2715.1990.

46. Pruss, D., Reeves, R., Bushman, F.D., and Wolffe, A.P. (1994). The influence of DNA and nucleosome structure on integration events directed by HIV integrase. J. Biol. Chem. *269*, 25031-25041.

47. Siliciano, R.F., and Greene, W.C. (2011). HIV Latency. Cold Spring Harb. Perspect. Med. *1*, a007096. 10.1101/cshperspect.a007096.

48. Isegawa, Y., Katahira, J., Yamanishi, K., and Sugimoto, N. (2007). Reactivation of latent human immunodeficiency virus 1 by human herpesvirus 6 infection. Acta Virol. *51*, 13-20.

49. Berkhout, B., and Jeang, K.T. (1992). Functional roles for the TATA promoter and enhancers in basal and Tat-induced expression of the human immunodeficiency virus type 1 long terminal repeat. J Virol *66*, 139-149. 10.1128/jvi.66.1.139-149.1992.

50. Robert-Guroff, M., Popovic, M., Gartner, S., Markham, P., Gallo, R.C., and Reitz, M.S. (1990). Structure and expression of tat-, rev-, and nef-specific transcripts of human immunodeficiency virus type 1 in infected lymphocytes and macrophages. J Virol *64*, 3391-3398. 10.1128/jvi.64.7.3391-3398.1990.

51. Cullen, B.R. (1986). Trans-activation of human immunodeficiency virus occurs via a bimodal mechanism. Cell *46*, 973-982. 10.1016/0092-8674(86)90696-3.

52. Rosorius, O., Reichart, B., Krätzer, F., Heger, P., Dabauvalle, M.-C., and Hauber, J. (1999). Nuclear pore localization and nucleocytoplasmic transport of eIF-5A:

evidence for direct interaction with the export receptor CRM1. J. Cell Sci. *112*, 2369-2380. 10.1242/jcs.112.14.2369.

53. Stein, B.S., and Engleman, E.G. (1990). Intracellular processing of the gp160 HIV-1 envelope precursor. Endoproteolytic cleavage occurs in a cis or medial compartment of the Golgi complex. J. Biol. Chem. *265*, 2640-2649.

54. Earl, P.L., Moss, B., and Doms, R.W. (1991). Folding, interaction with GRP78-BiP, assembly, and transport of the human immunodeficiency virus type 1 envelope protein. J Virol *65*, 2047-2055. 10.1128/jvi.65.4.2047-2055.1991.

55. Otteken, A., Earl, P.L., and Moss, B. (1996). Folding, assembly, and intracellular trafficking of the human immunodeficiency virus type 1 envelope glycoprotein analyzed with monoclonal antibodies recognizing maturational intermediates. J Virol *70*, 3407-3415. 10.1128/jvi.70.6.3407-3415.1996.

56. Fuller, S.D., Wilk, T., Gowen, B.E., Kräusslich, H.-G., and Vogt, V.M. (1997). Cryo-electron microscopy reveals ordered domains in the immature HIV-1 particle. Curr. Biol. *7*, 729-738. 10.1016/s0960-9822(06)00331-9.

57. Wright, E.R., Schooler, J.B., Ding, H.J., Kieffer, C., Fillmore, C., Sundquist, W.I., and Jensen, G.J. (2007). Electron cryotomography of immature HIV-1 virions reveals the structure of the CA and SP1 Gag shells. EMBO J. *26*, 2218-2226. 10.1038/sj.emboj.7601664.

58. Briggs, J.A.G., Riches, J.D., Glass, B., Bartonova, V., Zanetti, G., and Kräusslich, H.G. (2009). Structure and assembly of immature HIV. Proc National Acad Sci *106*, 11090-11095. 10.1073/pnas.0903535106.

59. Bukovsky, A.A., Dorfman, T., Weimann, A., and Göttlinger, H.G. (1997). Nef association with human immunodeficiency virus type 1 virions and cleavage by the viral protease. J Virol *71*, 1013-1018. 10.1128/jvi.71.2.1013-1018.1997.

60. Pettit, S.C., Moody, M.D., Wehbie, R.S., Kaplan, A.H., Nantermet, P.V., Klein, C.A., and Swanstrom, R. (1994). The p2 domain of human immunodeficiency virus type 1 Gag regulates sequential proteolytic processing and is required to produce fully infectious virions. J Virol *68*, 8017-8027. 10.1128/jvi.68.12.8017-8027.1994.

61. Kaplan, A.H., Zack, J.A., Knigge, M., Paul, D.A., Kempf, D.J., Norbeck, D.W., and Swanstrom, R. (1993). Partial inhibition of the human immunodeficiency virus type 1 protease results in aberrant virus assembly and the formation of noninfectious particles. J Virol *67*, 4050-4055. 10.1128/jvi.67.7.4050-4055.1993.

62. Zagury, D., Bernard, J., Leibowitch, J., Safai, B., Groopman, J.E., Feldman, M., Sarngadharan, M.G., and Gallo, R.C. (1984). HTLV-III in Cells Cultured from Semen of Two Patients with AIDS. Science *226*, 449-451. 10.1126/science.6208607.

63. Ho, D.D., Rota, T.R., Schooley, R.T., Kaplan, J.C., Allan, J.D., Groopman, J.E., Resnick, L., Felsenstein, D., Andrews, C.A., and Hirsch, M.S. (1985). Isolation of HTLV-III from Cerebrospinal Fluid and Neural Tissues of Patients with Neurologic Syndromes Related to the Acquired Immunodeficiency Syndrome. The New England Journal of Medicine *313*, 1493-1497. 10.1056/nejm198512123132401.

64. Thiry, L., Sprecher-Goldberger, S., Jonckheer, T., Levy, J., Perre, P.V.D., Henrivaux, P., Cogniaux-Leclerc, J., and Clumeck, N. (1985). ISOLATION OF

AIDS VIRUS FROM CELL-FREE BREAST MILK OF THREE HEALTHY VIRUS CARRIERS. Lancet *326*, 891-892. 10.1016/s0140-6736(85)90156-4.

65. Royce, R.A., Seña, A., Cates, W., and Cohen, M.S. (1997). Sexual Transmission of HIV. The New England Journal of Medicine *336*, 1072-1078. 10.1056/nejm199704103361507.

66. Boily, M.-C., Baggaley, R.F., Wang, L., Masse, B., White, R.G., Hayes, R.J., and Alary, M. (2009). Heterosexual risk of HIV-1 infection per sexual act: systematic review and meta-analysis of observational studies. Lancet Infect. Dis. *9*, 118-129. 10.1016/s1473-3099(09)70021-0.

67. Gray, R.H., Wawer, M.J., Brookmeyer, R., Sewankambo, N.K., Serwadda, D., Wabwire-Mangen, F., Lutalo, T., Li, X., vanCott, T., Quinn, T.C., and Team, t.R.P. (2001). Probability of HIV-1 transmission per coital act in monogamous, heterosexual, HIV-1-discordant couples in Rakai, Uganda. Lancet *357*, 1149-1153. 10.1016/s0140-6736(00)04331-2.

68. Gianella, S., Strain, M.C., Rought, S.E., Vargas, M.V., Little, S.J., Richman, D.D., Spina, C.A., and Smith, D.M. (2011). Associations between Virologic and Immunologic Dynamics in Blood and in the Male Genital Tract. J Virol *86*, 1307-1315. 10.1128/jvi.06077-11.

69. Quinn, T.C., Wawer, M.J., Sewankambo, N., Serwadda, D., Li, C., Wabwire-Mangen, F., Meehan, M.O., Lutalo, T., and Gray, R.H. (2000). Viral Load and Heterosexual Transmission of Human Immunodeficiency Virus Type 1. The New England Journal of Medicine *342*, 921-929. 10.1056/nejm200003303421303.

70. Wolfs, T.F.W., Zwart, G., Bakker, M., and Goudsmit, J. (1992). HIV-1 genomic rna diversification following sexual and parenteral virus transmission. Virology *189*, 103-110. 10.1016/0042-6822(92)90685-i.

71. Zhang, L.Q., MacKenzie, P., Cleland, A., Holmes, E.C., Brown, A.J., and Simmonds, P. (1993). Selection for specific sequences in the external envelope protein of human immunodeficiency virus type 1 upon primary infection. J Virol *67*, 3345-3356. 10.1128/jvi.67.6.3345-3356.1993.

72. Zhu, T., Wang, N., Carr, A., Nam, D.S., Moor-Jankowski, R., Cooper, D.A., and Ho, D.D. (1996). Genetic characterization of human immunodeficiency virus type 1 in blood and genital secretions: evidence for viral compartmentalization and selection during sexual transmission. J Virol *70*, 3098-3107. 10.1128/jvi.70.5.3098-3107.1996.

73. Isaacman-Beck, J., Hermann, E.A., Yi, Y., Ratcliffe, S.J., Mulenga, J., Allen, S., Hunter, E., Derdeyn, C.A., and Collman, R.G. (2009). Heterosexual Transmission of Human Immunodeficiency Virus Type 1 Subtype C: Macrophage Tropism, Alternative Coreceptor Use, and the Molecular Anatomy of CCR5 Utilization. J Virol *83*, 8208-8220. 10.1128/jvi.00296-09.

74. Salazar-Gonzalez, J.F., Salazar, M.G., Keele, B.F., Learn, G.H., Giorgi, E.E., Li, H., Decker, J.M., Wang, S., Baalwa, J., Kraus, M.H., et al. (2009). Genetic identity, biological phenotype, and evolutionary pathways of transmitted/founder viruses in acute and early HIV-1 infection. J. Exp. Med. *206*, 1273-1289. 10.1084/jem.20090378.

75. Ping, L.-H., Jabara, C.B., Rodrigo, A.G., Hudelson, S.E., Piwowar-Manning, E., Wang, L., Eshleman, S.H., Cohen, M.S., and Swanstrom, R. (2013). HIV-1 Transmission during Early Antiretroviral Therapy: Evaluation of Two HIV-1 Transmission Events in the HPTN 052 Prevention Study. Plos One *8*, e71557. 10.1371/journal.pone.0071557.

76. Hladik, F., Sakchalathorn, P., Ballweber, L., Lentz, G., Fialkow, M., Eschenbach, D., and McElrath, M.J. (2007). Initial Events in Establishing Vaginal Entry and Infection by Human Immunodeficiency Virus Type-1. Immunity *26*, 257-270. 10.1016/j.immuni.2007.01.007.

77. Parrish, N.F., Gao, F., Li, H., Giorgi, E.E., Barbian, H.J., Parrish, E.H., Zajic, L., Iyer, S.S., Decker, J.M., Kumar, A., et al. (2013). Phenotypic properties of transmitted founder HIV-1. Proc National Acad Sci *110*, 6626-6633. 10.1073/pnas.1304288110.

78. Zhang, R., Li, M., Chen, C., and Yao, Q. (2004). SHIV virus-like particles bind and activate human dendritic cells. Vaccine *23*, 139-147. 10.1016/j.vaccine.2004.05.036.

79. Miller, C.J., Li, Q., Abel, K., Kim, E.-Y., Ma, Z.-M., Wietgrefe, S., Franco-Scheuch, L.L., Compton, L., Duan, L., Shore, M.D., et al. (2005). Propagation and Dissemination of Infection after Vaginal Transmission of Simian Immunodeficiency Virus. J Virol *79*, 9217-9227. 10.1128/jvi.79.14.9217-9227.2005.

80. Guadalupe, M., Reay, E., Sankaran, S., Prindiville, T., Flamm, J., McNeil, A., and Dandekar, S. (2003). Severe CD4+ T-Cell Depletion in Gut Lymphoid Tissue

during Primary Human Immunodeficiency Virus Type 1 Infection and Substantial Delay in Restoration following Highly Active Antiretroviral Therapy. J Virol *77*, 11708-11717. 10.1128/jvi.77.21.11708-11717.2003.

81. Mehandru, S., Poles, M.A., Tenner-Racz, K., Horowitz, A., Hurley, A., Hogan, C., Boden, D., Racz, P., and Markowitz, M. (2004). Primary HIV-1 Infection Is Associated with Preferential Depletion of CD4+ T Lymphocytes from Effector Sites in the Gastrointestinal Tract. J Exp Medicine *200*, 761-770. 10.1084/jem.20041196.

82. Chun, T.-W., Engel, D., Berrey, M.M., Shea, T., Corey, L., and Fauci, A.S. (1998). Early establishment of a pool of latently infected, resting CD4+ T cells during primary HIV-1 infection. Proc National Acad Sci *95*, 8869-8873. 10.1073/pnas.95.15.8869.

83. Clark, S.J., Saag, M.S., Decker, W.D., Campbell-Hill, S., Roberson, J.L., Veldkamp, P.J., Kappes, J.C., Hahn, B.H., and Shaw, G.M. (1991). High Titers of Cytopathic Virus in Plasma of Patients with Symptomatic Primary HIV-1 Infection. The New England Journal of Medicine *324*, 954-960. 10.1056/nejm199104043241404.

84. Schacker, T., Collier, A.C., Hughes, J., Shea, T., and Corey, L. (1996). Clinical and Epidemiologic Features of Primary HIV Infection. Ann. Intern. Med. *125*, 257-264. 10.7326/0003-4819-125-4-199608150-00001.

85. Little, S.J., McLean, A.R., Spina, C.A., Richman, D.D., and Havlir, D.V. (1999). Viral Dynamics of Acute HIV-1 Infection. J Exp Medicine *190*, 841-850. 10.1084/jem.190.6.841.

86. Li, J.Z., and Blankson, J.N. (2021). How elite controllers and posttreatment controllers inform our search for an HIV-1 cure. J Clin Invest *131*, e149414. 10.1172/jci149414.

87. Begtrup, K., Melbye, M., Biggar, R.J., Goedert, J.J., Knudsen, K., and Anderson, P.K. (1997). Progression to Acquired Immunodeficiency Syndrome Is Influenced by CD4 T-Lymphocyte Count and Time Since Seroconversion. Am. J. Epidemiology *145*, 629-635. 10.1093/oxfordjournals.aje.a009160.

88. Mellors, J.W., Jr, C.R.R., Gupta, P., White, R.M., Todd, J.A., and Kingsley, L.A. (1996). Prognosis in HIV-1 Infection Predicted by the Quantity of Virus in Plasma. Science *272*, 1167-1170. 10.1126/science.272.5265.1167.

89. Carrington, M., Dean, M., Martin, M.P., and O'Brien, S.J. (1999). Genetics of HIV-1 Infection: Chemokine Receptor Ccr5 Polymorphism and Its Consequences. Hum. Mol. Genet. *8*, 1939-1945. 10.1093/hmg/8.10.1939.

90. Sorrentino, A.H.d., Marinic, K., Motta, P., Sorrentino, A., López, R., and Illiovich, E. (2000). HLA Class I Alleles Associated with Susceptibility or Resistance to Human Immunodeficiency Virus Type 1 Infection among a Population in Chaco Province, Argentina. J. Infect. Dis. *182*, 1523-1526. 10.1086/315854.

91. Organisation, U.K.H.C.D., Darby, I., Ewart, D.W., Giangrande, I.P.L.F., Spooner, R.J.D., and Rizza, C.R. (1996). Importance of age at infection with HIV-1 for survival and development of AIDS in UK haemophilia population. Lancet *347*, 1573-1579. 10.1016/s0140-6736(96)91073-9.

92. Corti, M., and Palmero, D. (2008). Mycobacterium avium complex infection in HIV/AIDS patients. Expert Rev. Anti-Infect. Ther. *6*, 351-363. 10.1586/14787210.6.3.351.

93. Morris, A., Wei, K., Afshar, K., and Huang, L. (2008). Epidemiology and Clinical Significance of Pneumocystis Colonization. J. Infect. Dis. *197*, 10-17. 10.1086/523814.

94. Ribeiro, R.M., Hazenberg, M.D., Perelson, A.S., and Davenport, M.P. (2006). Naïve and Memory Cell Turnover as Drivers of CCR5-to-CXCR4 Tropism Switch in Human Immunodeficiency Virus Type 1: Implications for Therapy. J Virol *80*, 802-809. 10.1128/jvi.80.2.802-809.2006.

95. Albarillo, F., and O'Keefe, P. (2016). Opportunistic Neurologic Infections in Patients with Acquired Immunodeficiency Syndrome (AIDS). Curr. Neurol. Neurosci. Rep. *16*, 10. 10.1007/s11910-015-0603-8.

96. Farram, E., and Smithyman, A.M. (1991). Opportunistic infections in AIDS and their diagnosis. Aust. J. Biotechnol. *5*, 37-40, 43.

97. Limper, A.H., Adenis, A., Le, T., and Harrison, T.S. (2017). Fungal infections in HIV/AIDS. Lancet Infect. Dis. *17*, e334-e343. 10.1016/s1473-3099(17)30303-1.

98. McNally, G.A. (2019). HIV and Cancer: An Overview of AIDS-Defining and Non–AIDS-Defining Cancers in Patients With HIV. Clin. J. Oncol. Nurs. *23*, 327-331. 10.1188/19.cjon.327-331.

99. Berman, P.W., Nunes, W.M., and Haffar, O.K. (1988). Expression of membrane-associated and secreted variants of gp160 of human immunodeficiency virus

type 1 in vitro and in continuous cell lines. J Virol *62*, 3135-3142. 10.1128/jvi.62.9.3135-3142.1988.

100. Haffar, O.K., Dowbenko, D.J., and Berman, P.W. (1988). Topogenic analysis of the human immunodeficiency virus type 1 envelope glycoprotein, gp160, in microsomal membranes. J. cell Biol. *107*, 1677-1687. 10.1083/jcb.107.5.1677.

101. Wyatt, R., and Sodroski, J. (1998). The HIV-1 Envelope Glycoproteins: Fusogens, Antigens, and Immunogens. Science *280*, 1884-1888. 10.1126/science.280.5371.1884.

102. Ellerbrok, H., D'Auriol, L., Vaquero, C., and Sitbon, M. (1992). Functional tolerance of the human immunodeficiency virus type 1 envelope signal peptide to mutations in the amino-terminal and hydrophobic regions. J Virol *66*, 5114-5118. 10.1128/jvi.66.8.5114-5118.1992.

103. Hallenberger, S., Bosch, V., Angliker, H., Shaw, E., Klenk, H.-D., and Garten, W. (1992). Inhibition of furin-mediated cleavage activation of HIV-1 glycoprotein gpl60. Nature *360*, 358-361. 10.1038/360358a0.

104. Decroly, E., Vandenbranden, M., Ruysschaert, J.M., Cogniaux, J., Jacob, G.S., Howard, S.C., Marshall, G., Kompelli, A., Basak, A., and Jean, F. (1994). The convertases furin and PC1 can both cleave the human immunodeficiency virus (HIV)-1 envelope glycoprotein gp160 into gp120 (HIV-1 SU) and gp41 (HIV-I TM). J. Biol. Chem. *269*, 12240-12247.

105. Gu, M., Rappapor, J., and Leppla, S.H. (1995). Furin is important but not essential for the proteolytic maturation of gp160 of HIV-1. FEBS Lett. *365*, 95-97. 10.1016/0014-5793(95)00447-h.

106. Allan, J.S., Coligan, J.E., Barin, F., McLane, M.F., Sodroski, J.G., Rosen, C.A., Haseltine, W.A., Lee, T.H., and Essex, M. (1985). Major Glycoprotein Antigens That Induce Antibodies in AIDS Patients Are Encoded by HTLV-III. Science *228*, 1091-1094. 10.1126/science.2986290.

107. Lasky, L.A., Groopman, J.E., Fennie, C.W., Benz, P.M., Capon, D.J., Dowbenko, D.J., Nakamura, G.R., Nunes, W.M., Renz, M.E., and Berman, P.W. (1986). Neutralization of the AIDS Retrovirus by Antibodies to a Recombinant Envelope Glycoprotein. Science *233*, 209-212. 10.1126/science.3014647.

108. Ott, D.E. (2008). Cellular proteins detected in HIV-1. Rev. Méd. Virol. *18*, 159-175. 10.1002/rmv.570.

109. Lusso, P., Veronese, F.d.M., Ensoli, B., Franchini, G., Jemma, C., DeRocco, S.E., Kalyanaraman, V.S., and Gallo, R.C. (1990). Expanded HIV-1 Cellular Tropism by Phenotypic Mixing with Murine Endogenous Retroviruses. Science *247*, 848-852. 10.1126/science.2305256.

110. Arthur, L.O., Jr, J.W.B., Ii, R.C.S., Benveniste, R.E., Mann, D.L., Chermann, J.-C., and Henderson, L.E. (1992). Cellular Proteins Bound to Immunodeficiency Viruses: Implications for Pathogenesis and Vaccines. Science *258*, 1935-1938. 10.1126/science.1470916.

111. Tedbury, P.R., and Freed, E.O. (2014). The role of matrix in HIV-1 envelope glycoprotein incorporation. Trends Microbiol. *22*, 372-378. 10.1016/j.tim.2014.04.012.

112. Checkley, M.A., Luttge, B.G., and Freed, E.O. (2011). HIV-1 Envelope Glycoprotein Biosynthesis, Trafficking, and Incorporation. J. Mol. Biol. *410*, 582-608. 10.1016/j.jmb.2011.04.042.

113. Fortin, J.F., Cantin, R., Lamontagne, G., and Tremblay, M. (1997). Host-derived ICAM-1 glycoproteins incorporated on human immunodeficiency virus type 1 are biologically active and enhance viral infectivity. J Virol *71*, 3588-3596. 10.1128/jvi.71.5.3588-3596.1997.

114. Imbeault, M.l., Ouellet, M., Giguère, K., Bertin, J., Bélanger, D., Martin, G.v., and Tremblay, M.J. (2010). Acquisition of Host-Derived CD40L by HIV-1 In Vivo and Its Functional Consequences in the B-Cell Compartment. J Virol *85*, 2189-2200. 10.1128/jvi.01993-10.

115. Munoz, O., Banga, R., and Perreau, M. (2022). Host Molecule Incorporation into HIV Virions, Potential Influences in HIV Pathogenesis. Viruses *14*, 2523. 10.3390/v14112523.

116. Munoz, O., Banga, R., Schelling, R., Procopio, F.A., Mastrangelo, A., Nortier, P., Ohmiti, K., Daraspe, J., Cavassini, M., Fenwick, C., et al. (2022). Active PD-L1 incorporation within HIV virions functionally impairs T follicular helper cells. PLoS Pathog. *18*, e1010673. 10.1371/journal.ppat.1010673.

117. Center, R.J., Leapman, R.D., Lebowitz, J., Arthur, L.O., Earl, P.L., and Moss, B. (2002). Oligomeric Structure of the Human Immunodeficiency Virus Type 1 Envelope Protein on the Virion Surface. J Virol *76*, 7863-7867. 10.1128/jvi.76.15.7863-7867.2002.

118. Willey, R.L., Rutledge, R.A., Dias, S., Folks, T., Theodore, T., Buckler, C.E., and Martin, M.A. (1986). Identification of conserved and divergent domains within the envelope gene of the acquired immunodeficiency syndrome retrovirus. Proc National Acad Sci *83*, 5038-5042. 10.1073/pnas.83.14.5038.

119. Modrow, S., Hahn, B.H., Shaw, G.M., Gallo, R.C., Wong-Staal, F., and Wolf, H. (1987). Computer-assisted analysis of envelope protein sequences of seven human immunodeficiency virus isolates: prediction of antigenic epitopes in conserved and variable regions. J Virol *61*, 570-578. 10.1128/jvi.61.2.570-578.1987.

120. Leonard, C.K., Spellman, M.W., Riddle, L., Harris, R.J., Thomas, J.N., and Gregory, T.J. (1990). Assignment of intrachain disulfide bonds and characterization of potential glycosylation sites of the type 1 recombinant human immunodeficiency virus envelope glycoprotein (gp120) expressed in Chinese hamster ovary cells. J. Biol. Chem. *265*, 10373-10382.

121. Kwong, P.D., Wyatt, R., Robinson, J., Sweet, R.W., Sodroski, J., and Hendrickson, W.A. (1998). Structure of an HIV gp120 envelope glycoprotein in complex with the CD4 receptor and a neutralizing human antibody. Nature *393*, 648-659. 10.1038/31405.

122. Pancera, M., Majeed, S., Ban, Y.-E.A., Chen, L., Huang, C.-c., Kong, L., Kwon, Y.D., Stuckey, J., Zhou, T., Robinson, J.E., et al. (2010). Structure of HIV-1 gp120 with gp41-interactive region reveals layered envelope architecture and basis of conformational mobility. Proc National Acad Sci *107*, 1166-1171. 10.1073/pnas.0911004107.

123. Lyumkis, D., Julien, J.-P., Val, N.d., Cupo, A., Potter, C.S., Klasse, P.-J., Burton, D.R., Sanders, R.W., Moore, J.P., Carragher, B., et al. (2013). Cryo-EM Structure of a Fully Glycosylated Soluble Cleaved HIV-1 Envelope Trimer. Science *342*, 1484-1490. 10.1126/science.1245627.

124. Pollard, S.R., Meier, W., Chow, P., Rosa, J.J., and Wiley, D.C. (1991). CD4-binding regions of human immunodeficiency virus envelope glycoprotein gp120 defined by proteolytic digestion. Proc National Acad Sci *88*, 11320-11324. 10.1073/pnas.88.24.11320.

125. Pollard, S.R., Rosa, M.D., Rosa, J.J., and Wiley, D.C. (1992). Truncated variants of gp120 bind CD4 with high affinity and suggest a minimum CD4 binding region. EMBO J. *11*, 585-591. 10.1002/j.1460-2075.1992.tb05090.x.

126. Liu, J., Bartesaghi, A., Borgnia, M.J., Sapiro, G., and Subramaniam, S. (2008). Molecular architecture of native HIV-1 gp120 trimers. Nature *455*, 109-113. 10.1038/nature07159.

127. White, T.A., Bartesaghi, A., Borgnia, M.J., Meyerson, J.R., Cruz, M.J.V.d.l., Bess, J.W., Nandwani, R., Hoxie, J.A., Lifson, J.D., Milne, J.L.S., and Subramaniam, S. (2010). Molecular Architectures of Trimeric SIV and HIV-1 Envelope Glycoproteins on Intact Viruses: Strain-Dependent Variation in Quaternary Structure. PLoS Pathog. *6*, e1001249. 10.1371/journal.ppat.1001249.

128. Harris, A., Borgnia, M.J., Shi, D., Bartesaghi, A., He, H., Pejchal, R., Kang, Y., Depetris, R., Marozsan, A.J., Sanders, R.W., et al. (2011). Trimeric HIV-1 glycoprotein gp140 immunogens and native HIV-1 envelope glycoproteins

display the same closed and open quaternary molecular architectures. Proc National Acad Sci *108*, 11440-11445. 10.1073/pnas.1101414108.

129. Munro, J.B., Gorman, J., Ma, X., Zhou, Z., Arthos, J., Burton, D.R., Koff, W.C., Courter, J.R., Iii, A.B.S., Kwong, P.D., et al. (2014). Conformational dynamics of single HIV-1 envelope trimers on the surface of native virions. Science *346*, 759-763. 10.1126/science.1254426.

130. Bosch, M.L., Earl, P.L., Fargnoli, K., Picciafuoco, S., Giombini, F., Wong-Staal, F., and Franchini, G. (1989). Identification of the Fusion Peptide of Primate Immunodeficiency Viruses. Science *244*, 694-697. 10.1126/science.2541505.

131. Poumbourios, P., Wilson, K.A., Center, R.J., Ahmar, W.E., and Kemp, B.E. (1997). Human immunodeficiency virus type 1 envelope glycoprotein oligomerization requires the gp41 amphipathic alpha-helical/leucine zipper-like sequence. J Virol *71*, 2041-2049. 10.1128/jvi.71.3.2041-2049.1997.

132. Jacobs, A., Quraishi, O., Huang, X., Bousquet-Gagnon, N., Nault, G., Francella, N., Alvord, W.G., Pham, N., Soucy, C., Robitaille, M., et al. (2007). A Covalent Inhibitor Targeting an Intermediate Conformation of the Fusogenic Subunit of the HIV-1 Envelope Complex*. J. Biol. Chem. *282*, 32406-32413. 10.1074/jbc.m705577200.

133. Baribaud, F., Pöhlmann, S., and Doms, R.W. (2001). The Role of DC-SIGN and DC-SIGNR in HIV and SIV Attachment, Infection, and Transmission. Virology *286*, 1-6. 10.1006/viro.2001.0975.

134. Montfort, T.v., Eggink, D., Boot, M., Tuen, M., Hioe, C.E., Berkhout, B., and Sanders, R.W. (2011). HIV-1 N-Glycan Composition Governs a Balance between

Dendritic Cell-Mediated Viral Transmission and Antigen Presentation. J Immunol *187*, 4676-4685. 10.4049/jimmunol.1101876.

135. Chen, B., Vogan, E.M., Gong, H., Skehel, J.J., Wiley, D.C., and Harrison, S.C. (2005). Structure of an unliganded simian immunodeficiency virus gp120 core. Nature *433*, 834-841. 10.1038/nature03327.

136. Tamm, L.K., and Han, X. (2000). Viral Fusion Peptides: A Tool Set to Disrupt and Connect Biological Membranes. Bioscience Rep *20*, 501-518. 10.1023/a:1010406920417.

137. Gifford, L.B., and Melikyan, G.B. (2024). HIV-1 Capsid Uncoating Is a Multistep Process That Proceeds through Defect Formation Followed by Disassembly of the Capsid Lattice. ACS Nano *18*, 2928-2947. 10.1021/acsnano.3c07678.

138. Crozat, K., and Beutler, B. (2004). TLR7: A new sensor of viral infection. Proc National Acad Sci *101*, 6835-6836. 10.1073/pnas.0401347101.

139. Kramer, H.B., Lavender, K.J., Qin, L., Stacey, A.R., Liu, M.K.P., Gleria, K.d., Simmons, A., Gasper-Smith, N., Haynes, B.F., McMichael, A.J., et al. (2010). Elevation of Intact and Proteolytic Fragments of Acute Phase Proteins Constitutes the Earliest Systemic Antiviral Response in HIV-1 Infection. PLoS Pathog. *6*, e1000893. 10.1371/journal.ppat.1000893.

140. Alter, G., Suscovich, T.J., Teigen, N., Meier, A., Streeck, H., Brander, C., and Altfeld, M. (2007). Single-Stranded RNA Derived from HIV-1 Serves as a Potent Activator of NK Cells. J Immunol *178*, 7658-7666. 10.4049/jimmunol.178.12.7658.

141. Lambotte, O., Ferrari, G., Moog, C., Yates, N.L., Liao, H.-X., Parks, R.J., Hicks, C.B., Owzar, K., Tomaras, G.D., Montefiori, D.C., et al. (2009). Heterogeneous neutralizing antibody and antibody-dependent cell cytotoxicity responses in HIV-1 elite controllers. AIDS *23*, 897-906. 10.1097/qad.0b013e328329f97d.

142. Scully, E., and Alter, G. (2016). NK Cells in HIV Disease. Curr. HIVAIDS Rep. *13*, 85-94. 10.1007/s11904-016-0310-3.

143. Alter, G., Rihn, S., Walter, K., Nolting, A., Martin, M., Rosenberg, E.S., Miller, J.S., Carrington, M., and Altfeld, M. (2009). HLA Class I Subtype-Dependent Expansion of KIR3DS1+ and KIR3DL1+ NK Cells during Acute Human Immunodeficiency Virus Type 1 Infection. J Virol *83*, 6798-6805. 10.1128/jvi.00256-09.

144. Koppensteiner, H., Banning, C., Schneider, C., Hohenberg, H., and Schindler, M. (2011). Macrophage Internal HIV-1 Is Protected from Neutralizing Antibodies. J Virol *86*, 2826-2836. 10.1128/jvi.05915-11.

145. Clayton, K.L., Collins, D.R., Lengieza, J., Ghebremichael, M., Dotiwala, F., Lieberman, J., and Walker, B.D. (2018). Resistance of HIV-infected macrophages to CD8+ T lymphocyte–mediated killing drives activation of the immune system. Nat Immunol *19*, 475-486. 10.1038/s41590-018-0085-3.

146. Honeycutt, J.B., Thayer, W.O., Baker, C.E., Ribeiro, R.M., Lada, S.M., Cao, Y., Cleary, R.A., Hudgens, M.G., Richman, D.D., and Garcia, J.V. (2017). HIV persistence in tissue macrophages of humanized myeloid-only mice during antiretroviral therapy. Nat Med *23*, 638-643. 10.1038/nm.4319.

147. Ganor, Y., Real, F., Sennepin, A., Dutertre, C.-A., Prevedel, L., Xu, L., Tudor, D., Charmeteau, B., Couedel-Courteille, A., Marion, S., et al. (2019). HIV-1 reservoirs in urethral macrophages of patients under suppressive antiretroviral therapy. Nat. Microbiol. *4*, 633-644. 10.1038/s41564-018-0335-z.

148. Cribbs, S.K., Lennox, J., Caliendo, A.M., Brown, L.A., and Guidot, D.M. (2015). Healthy HIV-1-Infected Individuals on Highly Active Antiretroviral Therapy Harbor HIV-1 in Their Alveolar Macrophages. AIDS Res. Hum. Retroviruses *31*, 64-70. 10.1089/aid.2014.0133.

149. Ko, A., Kang, G., Hattler, J.B., Galadima, H.I., Zhang, J., Li, Q., and Kim, W.-K. (2019). Macrophages but not Astrocytes Harbor HIV DNA in the Brains of HIV-1-Infected Aviremic Individuals on Suppressive Antiretroviral Therapy. J. Neuroimmune Pharmacol. *14*, 110-119. 10.1007/s11481-018-9809-2.

150. Lamers, S.L., Salemi, M., Galligan, D.C., Morris, A., Gray, R., Fogel, G., Zhao, L., and McGrath, M.S. (2010). Human immunodeficiency virus-1 evolutionary patterns associated with pathogenic processes in the brain. J. NeuroVirology *16*, 230-241. 10.3109/13550281003735709.

151. Tso, F.Y., Kang, G., Kwon, E.H., Julius, P., Li, Q., West, J.T., and Wood, C. (2018). Brain is a potential sanctuary for subtype C HIV-1 irrespective of ART treatment outcome. Plos One *13*, e0201325. 10.1371/journal.pone.0201325.

152. Mattiola, I., Pesant, M., Tentorio, P.F., Molgora, M., Marcenaro, E., Lugli, E., Locati, M., and Mavilio, D. (2015). Priming of Human Resting NK Cells by Autologous M1 Macrophages via the Engagement of IL-1β, IFN-β, and IL-15 Pathways. J Immunol *195*, 2818-2828. 10.4049/jimmunol.1500325.

153. Demers, K.R., Makedonas, G., Buggert, M., Eller, M.A., Ratcliffe, S.J., Goonetilleke, N., Li, C.K., Eller, L.A., Rono, K., Maganga, L., et al. (2016). Temporal Dynamics of CD8+ T Cell Effector Responses during Primary HIV Infection. PLoS Pathog. *12*, e1005805. 10.1371/journal.ppat.1005805.

154. Ndhlovu, Zaza M., Kamya, P., Mewalal, N., Kløverpris, Henrik N., Nkosi, T., Pretorius, K., Laher, F., Ogunshola, F., Chopera, D., Shekhar, K., et al. (2015). Magnitude and Kinetics of CD8+ T Cell Activation during Hyperacute HIV Infection Impact Viral Set Point. Immunity *43*, 591-604. 10.1016/j.immuni.2015.08.012.

155. Takata, H., Buranapraditkun, S., Kessing, C., Fletcher, J.L.K., Muir, R., Tardif, V., Cartwright, P., Vandergeeten, C., Bakeman, W., Nichols, C.N., et al. (2017). Delayed differentiation of potent effector CD8+ T cells reducing viremia and reservoir seeding in acute HIV infection. Sci Transl Med *9*. 10.1126/scitranslmed.aag1809.

156. Bernardin, F., Kong, D., Peddada, L., Baxter-Lowe, L.A., and Delwart, E. (2005). Human Immunodeficiency Virus Mutations during the First Month of Infection Are Preferentially Found in Known Cytotoxic T-Lymphocyte Epitopes. J Virol *79*, 11523-11528. 10.1128/jvi.79.17.11523-11528.2005.

157. Goonetilleke, N., Liu, M.K.P., Salazar-Gonzalez, J.F., Ferrari, G., Giorgi, E., Ganusov, V.V., Keele, B.F., Learn, G.H., Turnbull, E.L., Salazar, M.G., et al. (2009). The first T cell response to transmitted/founder virus contributes to the control of acute viremia in HIV-1 infection. J. Exp. Med. *206*, 1253-1272. 10.1084/jem.20090365.

158. Turnbull, E.L., Wong, M., Wang, S., Wei, X., Jones, N.A., Conrod, K.E., Aldam, D., Turner, J., Pellegrino, P., Keele, B.F., et al. (2009). Kinetics of Expansion of Epitope-Specific T Cell Responses during Primary HIV-1 Infection. J Immunol *182*, 7131-7145. 10.4049/jimmunol.0803658.

159. Wang, Y.E., Li, B., Carlson, J.M., Streeck, H., Gladden, A.D., Goodman, R., Schneidewind, A., Power, K.A., Toth, I., Frahm, N., et al. (2008). Protective HLA Class I Alleles That Restrict Acute-Phase CD8+ T-Cell Responses Are Associated with Viral Escape Mutations Located in Highly Conserved Regions of Human Immunodeficiency Virus Type 1. J Virol *83*, 1845-1855. 10.1128/jvi.01061-08.

160. Addo, M.M., Yu, X.G., Rathod, A., Cohen, D., Eldridge, R.L., Strick, D., Johnston, M.N., Corcoran, C., Wurcel, A.G., Fitzpatrick, C.A., et al. (2003). Comprehensive Epitope Analysis of Human Immunodeficiency Virus Type 1 (HIV-1)-Specific T-Cell Responses Directed against the Entire Expressed HIV-1 Genome Demonstrate Broadly Directed Responses, but No Correlation to Viral Load. J Virol *77*, 2081-2092. 10.1128/jvi.77.3.2081-2092.2003.

161. Brumme, Z.L., Tao, I., Szeto, S., Brumme, C.J., Carlson, J.M., Chan, D., Kadie, C., Frahm, N., Brander, C., Walker, B., et al. (2008). Human leukocyte antigen-specific polymorphisms in HIV-1 Gag and their association with viral load in chronic untreated infection. AIDS *22*, 1277-1286. 10.1097/qad.0b013e3283021a8c.

162. Cao, W., Mehraj, V., Kaufmann, D.E., Li, T., and Routy, J.P. (2016). Elevation and persistence of CD8 T-cells in HIV infection: the Achilles heel in the ART era. J. Int. AIDS Soc. *19*, 20697. 10.7448/ias.19.1.20697.

163. Betts, M.R., Gray, C.M., Cox, J.H., and Ferrari, G. (2006). Antigen-specific T-cell-mediated immunity after HIV-1 infection: implications for vaccine control of HIV development. Expert Rev. Vaccines *5*, 505-516. 10.1586/14760584.5.4.505.

164. Day, C.L., Kaufmann, D.E., Kiepiela, P., Brown, J.A., Moodley, E.S., Reddy, S., Mackey, E.W., Miller, J.D., Leslie, A.J., DePierres, C., et al. (2006). PD-1 expression on HIV-specific T cells is associated with T-cell exhaustion and disease progression. Nature *443*, 350-354. 10.1038/nature05115.

165. Chen, H., Piechocka-Trocha, A., Miura, T., Brockman, M.A., Julg, B.D., Baker, B.M., Rothchild, A.C., Block, B.L., Schneidewind, A., Koibuchi, T., et al. (2009). Differential Neutralization of Human Immunodeficiency Virus (HIV) Replication in Autologous CD4 T Cells by HIV-Specific Cytotoxic T Lymphocytes. J Virol *83*, 3138-3149. 10.1128/jvi.02073-08.

166. Sáez-Cirión, A., Lacabaratz, C., Lambotte, O., Versmisse, P., Urrutia, A., Boufassa, F., Barré-Sinoussi, F., Delfraissy, J.-F., Sinet, M., Pancino, G., et al. (2007). HIV controllers exhibit potent CD8 T cell capacity to suppress HIV infection ex vivo and peculiar cytotoxic T lymphocyte activation phenotype. Proc National Acad Sci *104*, 6776-6781. 10.1073/pnas.0611244104.

167. Freel, S.A., Picking, R.A., Ferrari, G., Ding, H., Ochsenbauer, C., Kappes, J.C., Kirchherr, J.L., Soderberg, K.A., Weinhold, K.J., Cunningham, C.K., et al. (2012). Initial HIV-1 Antigen-Specific CD8+ T Cells in Acute HIV-1 Infection Inhibit

Transmitted/Founder Virus Replication. J Virol *86*, 6835-6846. 10.1128/jvi.00437-12.

168. Cocchi, F., DeVico, A.L., Yarchoan, R., Redfield, R., Cleghorn, F., Blattner, W.A., Garzino-Demo, A., Colombini-Hatch, S., Margolis, D., and Gallo, R.C. (2000). Higher macrophage inflammatory protein (MIP)-1α and MIP-1β levels from CD8+ T cells are associated with asymptomatic HIV-1 infection. Proc National Acad Sci *97*, 13812-13817. 10.1073/pnas.240469997.

169. Mackewicz, C.E., Blackbourn, D.J., and Levy, J.A. (1995). CD8+ T cells suppress human immunodeficiency virus replication by inhibiting viral transcription. Proc National Acad Sci *92*, 2308-2312. 10.1073/pnas.92.6.2308.

170. Kiepiela, P., Ngumbela, K., Thobakgale, C., Ramduth, D., Honeyborne, I., Moodley, E., Reddy, S., Pierres, C.d., Mncube, Z., Mkhwanazi, N., et al. (2007). CD8+ T-cell responses to different HIV proteins have discordant associations with viral load. Nat Med *13*, 46-53. 10.1038/nm1520.

171. Borrow, P., and Bhardwaj, N. (2008). Innate immune responses in primary HIV-1 infection. Curr. Opin. HIV AIDS *3*, 36-44. 10.1097/coh.0b013e3282f2bce7.

172. Brenchley, J.M., Schacker, T.W., Ruff, L.E., Price, D.A., Taylor, J.H., Beilman, G.J., Nguyen, P.L., Khoruts, A., Larson, M., Haase, A.T., and Douek, D.C. (2004). CD4+ T Cell Depletion during all Stages of HIV Disease Occurs Predominantly in the Gastrointestinal Tract. J Exp Medicine *200*, 749-759. 10.1084/jem.20040874.

173. Brenchley, J.M., and Douek, D.C. (2008). The mucosal barrier and immune activation in HIV pathogenesis. Curr. Opin. HIV AIDS *3*, 356-361. 10.1097/coh.0b013e3282f9ae9c.

174. Pantaleo, G., Graziosi, C., Demarest, J.F., Butini, L., Montroni, M., Fox, C.H., Orenstein, J.M., Kotler, D.P., and Fauci, A.S. (1993). HIV infection is active and progressive in lymphoid tissue during the clinically latent stage of disease. Nature *362*, 355-358. 10.1038/362355a0.

175. Zeng, M., Smith, A.J., Wietgrefe, S.W., Southern, P.J., Schacker, T.W., Reilly, C.S., Estes, J.D., Burton, G.F., Silvestri, G., Lifson, J.D., et al. (2011). Cumulative mechanisms of lymphoid tissue fibrosis and T cell depletion in HIV-1 and SIV infections. J Clin Invest *121*, 998-1008. 10.1172/jci45157.

176. Zeng, M., Paiardini, M., Engram, J.C., Beilman, G.J., Chipman, J.G., Schacker, T.W., Silvestri, G., and Haase, A.T. (2012). Critical role of CD4 T cells in maintaining lymphoid tissue structure for immune cell homeostasis and reconstitution. Blood *120*, 1856-1867. 10.1182/blood-2012-03-418624.

177. Connick, E., Folkvord, J.M., Lind, K.T., Rakasz, E.G., Miles, B., Wilson, N.A., Santiago, M.L., Schmitt, K., Stephens, E.B., Kim, H.O., et al. (2014). Compartmentalization of Simian Immunodeficiency Virus Replication within Secondary Lymphoid Tissues of Rhesus Macaques Is Linked to Disease Stage and Inversely Related to Localization of Virus-Specific CTL. J Immunol *193*, 5613-5625. 10.4049/jimmunol.1401161.

178. Perreau, M., Savoye, A.-L., Crignis, E.D., Corpataux, J.-M., Cubas, R., Haddad, E.K., Leval, L.D., Graziosi, C., and Pantaleo, G. (2013). Follicular helper T cells serve as the major CD4 T cell compartment for HIV-1 infection, replication, and production. J. Exp. Med. *210*, 143-156. 10.1084/jem.20121932.

179. Petrovas, C., Yamamoto, T., Gerner, M.Y., Boswell, K.L., Wloka, K., Smith, E.C., Ambrozak, D.R., Sandler, N.G., Timmer, K.J., Sun, X., et al. (2012). CD4 T follicular helper cell dynamics during SIV infection. J Clin Invest *122*, 3281-3294. 10.1172/jci63039.

180. Fukazawa, Y., Lum, R., Okoye, A.A., Park, H., Matsuda, K., Bae, J.Y., Hagen, S.I., Shoemaker, R., Deleage, C., Lucero, C., et al. (2015). B cell follicle sanctuary permits persistent productive simian immunodeficiency virus infection in elite controllers. Nat Med *21*, 132-139. 10.1038/nm.3781.

181. Yamamoto, T., Lynch, R.M., Gautam, R., Matus-Nicodemos, R., Schmidt, S.D., Boswell, K.L., Darko, S., Wong, P., Sheng, Z., Petrovas, C., et al. (2015). Quality and quantity of TFH cells are critical for broad antibody development in SHIVAD8 infection. Sci Transl Med *7*, 298ra120. 10.1126/scitranslmed.aab3964.

182. Petrovas, C., and Koup, R.A. (2014). T follicular helper cells and HIV/SIV-specific antibody responses. Curr. Opin. HIV AIDS *9*, 235-241. 10.1097/coh.0000000000000053.

183. Buckner, C.M., Moir, S., Ho, J., Wang, W., Posada, J.G., Kardava, L., Funk, E.K., Nelson, A.K., Li, Y., Chun, T.-W., and Fauci, A.S. (2013). Characterization of Plasmablasts in the Blood of HIV-Infected Viremic Individuals: Evidence for Nonspecific Immune Activation. J Virol *87*, 5800-5811. 10.1128/jvi.00094-13.

184. Cagigi, A., Nilsson, A., Pensieroso, S., and Chiodi, F. (2010). Dysfunctional B-cell responses during HIV-1 infection: implication for influenza vaccination and highly active antiretroviral therapy. Lancet Infect. Dis. *10*, 499-503. 10.1016/s1473-3099(10)70117-1.

185. Tomaras, G.D., Yates, N.L., Liu, P., Qin, L., Fouda, G.G., Chavez, L.L., Decamp, A.C., Parks, R.J., Ashley, V.C., Lucas, J.T., et al. (2008). Initial B-Cell Responses to Transmitted Human Immunodeficiency Virus Type 1: Virion-Binding Immunoglobulin M (IgM) and IgG Antibodies Followed by Plasma Anti-gp41 Antibodies with Ineffective Control of Initial Viremia. J Virol *82*, 12449-12463. 10.1128/jvi.01708-08.

186. Fecteau, J.F., Côté, G., and Néron, S. (2006). A New Memory CD27−IgG+ B Cell Population in Peripheral Blood Expressing VH Genes with Low Frequency of Somatic Mutation. J Immunol *177*, 3728-3736. 10.4049/jimmunol.177.6.3728.

187. Budeus, B., Reynoso, S.S.d., Przekopowitz, M., Hoffmann, D., Seifert, M., and Küppers, R. (2015). Complexity of the human memory B-cell compartment is determined by the versatility of clonal diversification in germinal centers. Proc National Acad Sci *112*, E5281-E5289. 10.1073/pnas.1511270112.

188. Wirths, S., and Lanzavecchia, A. (2005). ABCB1 transporter discriminates human resting naive B cells from cycling transitional and memory B cells. Eur. J. Immunol. *35*, 3433-3441. 10.1002/eji.200535364.

189. Levesque, M.C., Moody, M.A., Hwang, K.-K., Marshall, D.J., Whitesides, J.F., Amos, J.D., Gurley, T.C., Allgood, S., Haynes, B.B., Vandergrift, N.A., et al. (2009). Polyclonal B Cell Differentiation and Loss of Gastrointestinal Tract Germinal Centers in the Earliest Stages of HIV-1 Infection. PLoS Med. *6*, e1000107. 10.1371/journal.pmed.1000107.

190. Liao, H.-X., Chen, X., Munshaw, S., Zhang, R., Marshall, D.J., Vandergrift, N., Whitesides, J.F., Lu, X., Yu, J.-S., Hwang, K.-K., et al. (2011). Initial antibodies

binding to HIV-1 gp41 in acutely infected subjects are polyreactive and highly mutated. J. Exp. Med. *208*, 2237-2249. 10.1084/jem.20110363.

191. Trama, Ashley M., Moody, M.A., Alam, S.M., Jaeger, Frederick H., Lockwood, B., Parks, R., Lloyd, Krissey E., Stolarchuk, C., Scearce, R., Foulger, A., et al. (2014). HIV-1 Envelope gp41 Antibodies Can Originate from Terminal Ileum B Cells that Share Cross-Reactivity with Commensal Bacteria. Cell Host Microbe *16*, 215-226. 10.1016/j.chom.2014.07.003.

192. Williams, W.B., Liao, H.X., Moody, M.A., Kepler, T.B., Alam, S.M., Gao, F., Wiehe, K., Trama, A.M., Jones, K., Zhang, R.J., et al. (2015). Diversion of HIV-1 vaccine-induced immunity by gp41-microbiota cross-reactive antibodies. Science *349*. ARTN aab1253

10.1126/science.aab1253.

193. Hraber, P., Seaman, M.S., Bailer, R.T., Mascola, J.R., Montefiori, D.C., and Korber, B.T. (2014). Prevalence of broadly neutralizing antibody responses during chronic HIV-1 infection. AIDS *28*, 163-169. 10.1097/qad.0000000000000106.

194. Mansky, L.M., Rouzic, E.L., Benichou, S., and Gajary, L.C. (2003). Influence of Reverse Transcriptase Variants, Drugs, and Vpr on Human Immunodeficiency Virus Type 1 Mutant Frequencies. J Virol *77*, 2071-2080. 10.1128/jvi.77.3.2071-2080.2003.

195. Mansky, L.M. (2000). In Vivo Analysis of Human T-Cell Leukemia Virus Type 1 Reverse Transcription Accuracy. J Virol *74*, 9525-9531. 10.1128/jvi.74.20.9525-9531.2000.

196. Yeo, J.Y., Goh, G.-R., Su, C.T.-T., and Gan, S.K.-E. (2020). The Determination of HIV-1 RT Mutation Rate, Its Possible Allosteric Effects, and Its Implications on Drug Resistance. Viruses *12*, 297. 10.3390/v12030297.

197. Richman, D.D., Wrin, T., Little, S.J., and Petropoulos, C.J. (2003). Rapid evolution of the neutralizing antibody response to HIV type 1 infection. Proc National Acad Sci *100*, 4144-4149. 10.1073/pnas.0630530100.

198. Bricault, C.A., Yusim, K., Seaman, M.S., Yoon, H., Theiler, J., Giorgi, E.E., Wagh, K., Theiler, M., Hraber, P., Macke, J.P., et al. (2019). HIV-1 Neutralizing Antibody Signatures and Application to Epitope-Targeted Vaccine Design. Cell Host Microbe *26*, 296. 10.1016/j.chom.2019.07.016.

199. Nduati, E.W., Gorman, M.J., Sein, Y., Hermanus, T., Yuan, D., Oyaro, I., Muema, D.M., Ndung'u, T., Alter, G., and Moore, P.L. (2021). Coordinated Fc-effector and neutralization functions in HIV-infected children define a window of opportunity for HIV vaccination. AIDS *35*, 1895-1905. 10.1097/qad.0000000000002976.

200. Simonich, Cassandra A., Williams, Katherine L., Verkerke, Hans P., Williams, James A., Nduati, R., Lee, Kelly K., and Overbaugh, J. (2016). HIV-1 Neutralizing Antibodies with Limited Hypermutation from an Infant. Cell *166*, 77-87. 10.1016/j.cell.2016.05.055.

201. Bonsignori, M., Montefiori, D.C., Wu, X., Chen, X., Hwang, K.-K., Tsao, C.-Y., Kozink, D.M., Parks, R.J., Tomaras, G.D., Crump, J.A., et al. (2012). Two Distinct Broadly Neutralizing Antibody Specificities of Different Clonal Lineages in a Single HIV-1-Infected Donor: Implications for Vaccine Design. J Virol *86*, 4688-4692. 10.1128/jvi.07163-11.

202. Li, M., Gao, F., Mascola, J.R., Stamatatos, L., Polonis, V.R., Koutsoukos, M., Voss, G., Goepfert, P., Gilbert, P., Greene, K.M., et al. (2005). Human Immunodeficiency Virus Type 1 env Clones from Acute and Early Subtype B Infections for Standardized Assessments of Vaccine-Elicited Neutralizing Antibodies. J Virol *79*, 10108-10125. 10.1128/jvi.79.16.10108-10125.2005.

203. Seaman, M.S., Janes, H., Hawkins, N., Grandpre, L.E., Devoy, C., Giri, A., Coffey, R.T., Harris, L., Wood, B., Daniels, M.G., et al. (2009). Tiered Categorization of a Diverse Panel of HIV-1 Env Pseudoviruses for Assessment of Neutralizing Antibodies. J Virol *84*, 1439-1452. 10.1128/jvi.02108-09.

204. Wu, X., Yang, Z.-Y., Li, Y., Hogerkorp, C.-M., Schief, W.R., Seaman, M.S., Zhou, T., Schmidt, S.D., Wu, L., Xu, L., et al. (2010). Rational design of envelope identifies broadly neutralizing human monoclonal antibodies to HIV-1. Science *329*, 856-861. 10.1126/science.1187659.

205. Zhou, T., Georgiev, I., Wu, X., Yang, Z.-Y., Dai, K., Finzi, A., Kwon, Y.D., Scheid, J.F., Shi, W., Xu, L., et al. (2010). Structural Basis for Broad and Potent Neutralization of HIV-1 by Antibody VRC01. Science *329*, 811-817. 10.1126/science.1192819.

206. Doria-Rose, N.A., Klein, R.M., Daniels, M.G., O'Dell, S., Nason, M., Lapedes, A., Bhattacharya, T., Migueles, S.A., Wyatt, R.T., Korber, B.T., et al. (2009). Breadth of Human Immunodeficiency Virus-Specific Neutralizing Activity in Sera: Clustering Analysis and Association with Clinical Variables. J Virol *84*, 1631-1636. 10.1128/jvi.01482-09.

207. Gray, E.S., Madiga, M.C., Hermanus, T., Moore, P.L., Wibmer, C.K., Tumba, N.L., Werner, L., Mlisana, K., Sibeko, S., Williamson, C., et al. (2011). The Neutralization Breadth of HIV-1 Develops Incrementally over Four Years and Is Associated with CD4+ T Cell Decline and High Viral Load during Acute Infection. J Virol *85*, 4828-4840. 10.1128/jvi.00198-11.

208. Piantadosi, A., Chohan, B., Panteleeff, D., Baeten, J.M., Mandaliya, K., Ndinya-Achola, J.O., and Overbaugh, J. (2009). HIV-1 evolution in gag and env is highly correlated but exhibits different relationships with viral load and the immune response. AIDS *23*, 579-587. 10.1097/qad.0b013e328328f76e.

209. Liu, M., Yang, G., Wiehe, K., Nicely, N.I., Vandergrift, N.A., Rountree, W., Bonsignori, M., Alam, S.M., Gao, J., Haynes, B.F., and Kelsoe, G. (2014). Polyreactivity and Autoreactivity among HIV-1 Antibodies. J Virol *89*, 784-798. 10.1128/jvi.02378-14.

210. Haynes, B.F., Fleming, J., Clair, E.W.S., Katinger, H., Stiegler, G., Kunert, R., Robinson, J., Scearce, R.M., Plonk, K., Staats, H.F., et al. (2005). Cardiolipin Polyspecific Autoreactivity in Two Broadly Neutralizing HIV-1 Antibodies. Science *308*, 1906-1908. 10.1126/science.1111781.

211. Mouquet, H., Scheid, J.F., Zoller, M.J., Krogsgaard, M., Ott, R.G., Shukair, S., Artyomov, M.N., Pietzsch, J., Connors, M., Pereyra, F., et al. (2010). Polyreactivity increases the apparent affinity of anti-HIV antibodies by heteroligation. Nature *467*, 591-595. 10.1038/nature09385.

212. Mouquet, H., Warncke, M., Scheid, J.F., Seaman, M.S., and Nussenzweig, M.C. (2012). Enhanced HIV-1 neutralization by antibody heteroligation. Proc National Acad Sci *109*, 875-880. 10.1073/pnas.1120059109.

213. Moody, M.A., Pedroza-Pacheco, I., Vandergrift, N.A., Chui, C., Lloyd, K.E., Parks, R., Soderberg, K.A., Ogbe, A.T., Cohen, M.S., Liao, H.-X., et al. (2016). Immune perturbations in HIV-1–infected individuals who make broadly neutralizing antibodies. Sci Immunol *1*, aag0851. 10.1126/sciimmunol.aag0851.

214. Roskin, K.M., Jackson, K.J.L., Lee, J.-Y., Hoh, R.A., Joshi, S.A., Hwang, K.-K., Bonsignori, M., Pedroza-Pacheco, I., Liao, H.-X., Moody, M.A., et al. (2020). Aberrant B cell repertoire selection associated with HIV neutralizing antibody breadth. Nat Immunol *21*, 199-209. 10.1038/s41590-019-0581-0.

215. Jacob, J., Kassir, R., and Kelsoe, G. (1991). In situ studies of the primary immune response to (4-hydroxy-3-nitrophenyl)acetyl. I. The architecture and dynamics of responding cell populations. J Exp Medicine *173*, 1165-1175. 10.1084/jem.173.5.1165.

216. Jacob, J., Przylepa, J., Miller, C., and Kelsoe, G. (1993). In situ studies of the primary immune response to (4-hydroxy-3-nitrophenyl)acetyl. III. The kinetics of V region mutation and selection in germinal center B cells. J Exp Medicine *178*, 1293-1307. 10.1084/jem.178.4.1293.

217. Liu, Y.J., Joshua, D.E., Williams, G.T., Smith, C.A., Gordon, J., and MacLennan, I.C.M. (1989). Mechanism of antigen-driven selection in germinal centres. Nature *342*, 929-931. 10.1038/342929a0.

218. Zhang, J., MacLennan, I.C.M., Liu, Y.-J., and Lane, P.J.L. (1988). Is rapid proliferation in B centroblasts linked to somatic mutation in memory B cell clones? Immunol. Lett. *18*, 297-299. 10.1016/0165-2478(88)90178-2.

219. Allen, C.D.C., Okada, T., Tang, H.L., and Cyster, J.G. (2007). Imaging of Germinal Center Selection Events During Affinity Maturation. Science *315*, 528-531. 10.1126/science.1136736.

220. Elsner, R.A., and Shlomchik, M.J. (2020). Germinal Center and Extrafollicular B Cell Responses in Vaccination, Immunity, and Autoimmunity. Immunity *53*, 1136-1150. 10.1016/j.immuni.2020.11.006.

221. Muramatsu, M., Kinoshita, K., Fagarasan, S., Yamada, S., Shinkai, Y., and Honjo, T. (2018). Pillars Article: Class Switch Recombination and Hypermutation Require Activation-Induced Cytidine Deaminase (AID), a Potential RNA Editing Enzyme. Cell. 2000. 102: 553-563. J Immunol *201*, 2530-2540.

222. Wiehe, K., Bradley, T., Meyerhoff, R.R., Hart, C., Williams, W.B., Easterhoff, D., Faison, W.J., Kepler, T.B., Saunders, K.O., Alam, S.M., et al. (2018). Functional Relevance of Improbable Antibody Mutations for HIV Broadly Neutralizing Antibody Development. Cell Host Microbe *23*, 759-765.e756. 10.1016/j.chom.2018.04.018.

223. Bonsignori, M., Zhou, T., Sheng, Z., Chen, L., Gao, F., Joyce, M.G., Ozorowski, G., Chuang, G.-Y., Schramm, C.A., Wiehe, K., et al. (2016). Maturation Pathway from Germline to Broad HIV-1 Neutralizer of a CD4-Mimic Antibody. Cell *165*, 449-463. 10.1016/j.cell.2016.02.022.

224. Hwang, J.K., Wang, C., Du, Z., Meyers, R.M., Kepler, T.B., Neuberg, D., Kwong, P.D., Mascola, J.R., Joyce, M.G., Bonsignori, M., et al. (2017). Sequence intrinsic somatic mutation mechanisms contribute to affinity maturation of VRC01-class HIV-1 broadly neutralizing antibodies. Proc National Acad Sci *114*, 8614-8619. 10.1073/pnas.1709203114.

225. Yeap, L.-S., Hwang, J.K., Du, Z., Meyers, R.M., Meng, F.-L., Jakubauskaitė, A., Liu, M., Mani, V., Neuberg, D., Kepler, T.B., et al. (2015). Sequence-Intrinsic Mechanisms that Target AID Mutational Outcomes on Antibody Genes. Cell *163*, 1124-1137. 10.1016/j.cell.2015.10.042.

226. Bonsignori, M., Kreider, E.F., Fera, D., Meyerhoff, R.R., Bradley, T., Wiehe, K., Alam, S.M., Aussedat, B., Walkowicz, W.E., Hwang, K.-K., et al. (2017). Staged induction of HIV-1 glycan–dependent broadly neutralizing antibodies. Sci Transl Med *9*. 10.1126/scitranslmed.aai7514.

227. Bonsignori, M., Liao, H.X., Gao, F., Williams, W.B., Alam, S.M., Montefiori, D.C., and Haynes, B.F. (2017). Antibody-virus co-evolution in HIV infection: paths for HIV vaccine development. Immunol Rev *275*, 145-160. 10.1111/imr.12509.

228. McCoy, L.E., and Burton, D.R. (2017). Identification and specificity of broadly neutralizing antibodies against HIV. Immunol Rev *275*, 11-20. 10.1111/imr.12484.

229. Landais, E., Huang, X., Havenar-Daughton, C., Murrell, B., Price, M.A., Wickramasinghe, L., Ramos, A., Bian, C.B., Simek, M., Allen, S., et al. (2016). Broadly Neutralizing Antibody Responses in a Large Longitudinal Sub-Saharan HIV Primary Infection Cohort. PLoS Pathog. *12*, e1005369. 10.1371/journal.ppat.1005369.

230. Doores, K.J., Kong, L., Krumm, S.A., Le, K.M., Sok, D., Laserson, U., Garces, F., Poignard, P., Wilson, I.A., and Burton, D.R. (2014). Two Classes of Broadly Neutralizing Antibodies within a Single Lineage Directed to the High-Mannose Patch of HIV Envelope. J Virol *89*, 1105-1118. 10.1128/jvi.02905-14.

231. Walker, L.M., Sok, D., Nishimura, Y., Donau, O., Sadjadpour, R., Gautam, R., Shingai, M., Pejchal, R., Ramos, A., Simek, M.D., et al. (2011). Rapid development of glycan-specific, broad, and potent anti–HIV-1 gp120 neutralizing antibodies in an R5 SIV/HIV chimeric virus infected macaque. Proc National Acad Sci *108*, 20125-20129. 10.1073/pnas.1117531108.

232. Garces, F., Sok, D., Kong, L., McBride, R., Kim, Helen J., Saye-Francisco, Karen F., Julien, J.-P., Hua, Y., Cupo, A., Moore, John P., et al. (2014). Structural Evolution of Glycan Recognition by a Family of Potent HIV Antibodies. Cell *159*, 69-79. 10.1016/j.cell.2014.09.009.

233. Kong, R., Xu, K., Zhou, T., Acharya, P., Lemmin, T., Liu, K., Ozorowski, G., Soto, C., Taft, J.D., Bailer, R.T., et al. (2016). Fusion peptide of HIV-1 as a site of vulnerability to neutralizing antibody. Science *352*, 828-833. 10.1126/science.aae0474.

234. Blattner, C., Lee, Jeong H., Sliepen, K., Derking, R., Falkowska, E., de la Peña, Alba T., Cupo, A., Julien, J.-P., van Gils, M., Lee, Peter S., et al. (2014). Structural Delineation of a Quaternary, Cleavage-Dependent Epitope at the gp41-gp120 Interface on Intact HIV-1 Env Trimers. Immunity *40*, 669-680. 10.1016/j.immuni.2014.04.008.

235. Huang, J., Kang, B.H., Pancera, M., Lee, J.H., Tong, T., Feng, Y., Imamichi, H., Georgiev, I.S., Chuang, G.-Y., Druz, A., et al. (2014). Broad and potent HIV-1 neutralization by a human antibody that binds the gp41–gp120 interface. Nature *515*, 138-142. 10.1038/nature13601.

236. Wu, X., Zhou, T., Zhu, J., Zhang, B., Georgiev, I., Wang, C., Chen, X., Longo, N.S., Louder, M., McKee, K., et al. (2011). Focused Evolution of HIV-1 Neutralizing Antibodies Revealed by Structures and Deep Sequencing. Science *333*, 1593-1602. 10.1126/science.1207532.

237. Scheid, J.F., Mouquet, H., Ueberheide, B., Diskin, R., Klein, F., Oliveira, T.Y.K., Pietzsch, J., Fenyo, D., Abadir, A., Velinzon, K., et al. (2011). Sequence and Structural Convergence of Broad and Potent HIV Antibodies That Mimic CD4 Binding. Science *333*, 1633-1637. 10.1126/science.1207227.

238. Zhou, T., Zhu, J., Wu, X., Moquin, S., Zhang, B., Acharya, P., Georgiev, I.S., Altae-Tran, H.R., Chuang, G.-Y., Joyce, M.G., et al. (2013). Multidonor Analysis Reveals Structural Elements, Genetic Determinants, and Maturation Pathway for HIV-1 Neutralization by VRC01-Class Antibodies. Immunity *39*, 245-258. 10.1016/j.immuni.2013.04.012.

239. Walker, L.M., Phogat, S.K., Chan-Hui, P.-Y., Wagner, D., Phung, P., Goss, J.L., Wrin, T., Simek, M.D., Fling, S., Mitcham, J.L., et al. (2009). Broad and Potent Neutralizing Antibodies from an African Donor Reveal a New HIV-1 Vaccine Target. Science *326*, 285-289. 10.1126/science.1178746.

240. Muster, T., Steindl, F., Purtscher, M., Trkola, A., Klima, A., Himmler, G., Rüker, F., and Katinger, H. (1993). A conserved neutralizing epitope on gp41 of human

immunodeficiency virus type 1. J Virol *67*, 6642-6647. 10.1128/jvi.67.11.6642-6647.1993.

241. Zwick, M.B., Jensen, R., Church, S., Wang, M., Stiegler, G., Kunert, R., Katinger, H., and Burton, D.R. (2005). Anti-Human Immunodeficiency Virus Type 1 (HIV-1) Antibodies 2F5 and 4E10 Require Surprisingly Few Crucial Residues in the Membrane-Proximal External Region of Glycoprotein gp41 To Neutralize HIV-1. J Virol *79*, 1252-1261. 10.1128/jvi.79.2.1252-1261.2005.

242. Bonsignori, M., Hwang, K.-K., Chen, X., Tsao, C.-Y., Morris, L., Gray, E., Marshall, D.J., Crump, J.A., Kapiga, S.H., Sam, N.E., et al. (2011). Analysis of a Clonal Lineage of HIV-1 Envelope V2/V3 Conformational Epitope-Specific Broadly Neutralizing Antibodies and Their Inferred Unmutated Common Ancestors. J Virol *85*, 9998-10009. 10.1128/jvi.05045-11.

243. Doria-Rose, N.A., Bhiman, J.N., Roark, R.S., Schramm, C.A., Gorman, J., Chuang, G.-Y., Pancera, M., Cale, E.M., Ernandes, M.J., Louder, M.K., et al. (2015). New Member of the V1V2-Directed CAP256-VRC26 Lineage That Shows Increased Breadth and Exceptional Potency. J Virol *90*, 76-91. 10.1128/jvi.01791-15.

244. Sok, D., Doores, K.J., Briney, B., Le, K.M., Saye-Francisco, K.L., Ramos, A., Kulp, D.W., Julien, J.-P., Menis, S., Wickramasinghe, L., et al. (2014). Promiscuous Glycan Site Recognition by Antibodies to the High-Mannose Patch of gp120 Broadens Neutralization of HIV. Sci Transl Med *6*, 236ra263. 10.1126/scitranslmed.3008104.

245. Briney, B.S., Willis, J.R., and Crowe, J.E. (2012). Human Peripheral Blood Antibodies with Long HCDR3s Are Established Primarily at Original Recombination Using a Limited Subset of Germline Genes. Plos One *7*, e36750. 10.1371/journal.pone.0036750.

246. Briney, B.S., Willis, J.R., and Crowe, J.E. (2012). Location and length distribution of somatic hypermutation-associated DNA insertions and deletions reveals regions of antibody structural plasticity. Genes Immun *13*, 523-529. 10.1038/gene.2012.28.

247. Doyle-Cooper, C., Hudson, K.E., Cooper, A.B., Ota, T., Skog, P., Dawson, P.E., Zwick, M.B., Schief, W.R., Burton, D.R., and Nemazee, D. (2013). Immune Tolerance Negatively Regulates B Cells in Knock-In Mice Expressing Broadly Neutralizing HIV Antibody 4E10. J Immunol *191*, 3186-3191. 10.4049/jimmunol.1301285.

248. Andrabi, R., Voss, James E., Liang, C.-H., Briney, B., McCoy, Laura E., Wu, C.-Y., Wong, C.-H., Poignard, P., and Burton, Dennis R. (2015). Identification of Common Features in Prototype Broadly Neutralizing Antibodies to HIV Envelope V2 Apex to Facilitate Vaccine Design. Immunity *43*, 959-973. 10.1016/j.immuni.2015.10.014.

249. Gorman, J., Soto, C., Yang, M.M., Davenport, T.M., Guttman, M., Bailer, R.T., Chambers, M., Chuang, G.-Y., DeKosky, B.J., Doria-Rose, N.A., et al. (2016). Structures of HIV-1 Env V1V2 with broadly neutralizing antibodies reveal commonalities that enable vaccine design. Nat. Struct. Mol. Biol. *23*, 81-90. 10.1038/nsmb.3144.

250. Huang, J., Ofek, G., Laub, L., Louder, M.K., Doria-Rose, N.A., Longo, N.S., Imamichi, H., Bailer, R.T., Chakrabarti, B., Sharma, S.K., et al. (2012). Broad and potent neutralization of HIV-1 by a gp41-specific human antibody. Nature *491*, 406-412. 10.1038/nature11544.

251. Scheid, J.F., Mouquet, H., Feldhahn, N., Seaman, M.S., Velinzon, K., Pietzsch, J., Ott, R.G., Anthony, R.M., Zebroski, H., Hurley, A., et al. (2009). Broad diversity of neutralizing antibodies isolated from memory B cells in HIV-infected individuals. Nature *458*, 636-640. 10.1038/nature07930.

252. Wu, X., Zhang, Z., Schramm, C.A., Joyce, M.G., Kwon, Y.D., Zhou, T., Sheng, Z., Zhang, B., O'Dell, S., McKee, K., et al. (2015). Maturation and Diversity of the VRC01-Antibody Lineage over 15 Years of Chronic HIV-1 Infection. Cell *161*, 470-485. 10.1016/j.cell.2015.03.004.

253. Moir, S., Buckner, C.M., Ho, J., Wang, W., Chen, J., Waldner, A.J., Posada, J.G., Kardava, L., O'Shea, M.A., Kottilil, S., et al. (2010). B cells in early and chronic HIV infection: evidence for preservation of immune function associated with early initiation of antiretroviral therapy. Blood *116*, 5571-5579. 10.1182/blood-2010-05-285528.

254. Moir, S., Ho, J., Malaspina, A., Wang, W., DiPoto, A.C., O'Shea, M.A., Roby, G., Kottilil, S., Arthos, J., Proschan, M.A., et al. (2008). Evidence for HIV-associated B cell exhaustion in a dysfunctional memory B cell compartment in HIV-infected viremic individuals. J Exp Medicine *205*, 1797-1805. 10.1084/jem.20072683.

255. Meffre, E., Louie, A., Bannock, J., Kim, L.J.Y., Ho, J., Frear, C.C., Kardava, L., Wang, W., Buckner, C.M., Wang, Y., et al. (2016). Maturational characteristics of

HIV-specific antibodies in viremic individuals. JCI Insight *1*, e84610. 10.1172/jci.insight.84610.

256. Zhou, T., Lynch, R.M., Chen, L., Acharya, P., Wu, X., Doria-Rose, N.A., Joyce, M.G., Lingwood, D., Soto, C., Bailer, R.T., et al. (2015). Structural Repertoire of HIV-1-Neutralizing Antibodies Targeting the CD4 Supersite in 14 Donors. Cell *161*, 1280-1292. 10.1016/j.cell.2015.05.007.

257. Housny, A.E.D.M.S., Azab, M.M., Bahnasawy, M.M.M.E., Hassan, A., and Mohamed, A.R. (2016). MONITORING THE VIRAL LOAD IN HIV PATIENTS UNDER ANTI-RETROVIRAL THERAPY (ART). J. Egypt. Soc. Parasitol. *46*, 347-352.

258. Gandhi, R.T., Landovitz, R.J., Sax, P.E., Smith, D.M., Springer, S.A., Günthard, H.F., Thompson, M.A., Bedimo, R.J., Benson, C.A., Buchbinder, S.P., et al. (2025). Antiretroviral Drugs for Treatment and Prevention of HIV in Adults: 2024 Recommendations of the International Antiviral Society–USA Panel. JAMA *333*, 609-628. 10.1001/jama.2024.24543.

259. Mayer, K.H., and Venkatesh, K.K. (2010). Chemoprophylaxis for HIV Prevention: New Opportunities and New Questions. JAIDS J. Acquir. Immune Defic. Syndr. *55*, S122-S127. 10.1097/qai.0b013e3181fbcb4c.

260. Collini, P., and Mawson, R.L. (2023). A new era of HIV care for age-associated multimorbidity. Curr. Opin. Infect. Dis. *36*, 9-14. 10.1097/qco.0000000000000890.

261. Collins, L.F., Palella, F.J., Mehta, C.C., Holloway, J., Stosor, V., Lake, J.E., Brown, T.T., Topper, E.F., Naggie, S., Anastos, K., et al. (2023). Aging-Related Comorbidity Burden Among Women and Men With or At-Risk for HIV in the US,

2008-2019. JAMA Netw. Open *6*, e2327584. 10.1001/jamanetworkopen.2023.27584.

262. Gooden, T.E., Gardner, M., Wang, J., Jolly, K., Lane, D.A., Benjamin, L.A., Mwandumba, H.C., Kandoole, V., Lwanga, I.B., Taylor, S., et al. (2021). Incidence of Cardiometabolic Diseases in People With and Without Human Immunodeficiency Virus in the United Kingdom: A Population-Based Matched Cohort Study. J. Infect. Dis. *225*, 1348-1356. 10.1093/infdis/jiab420.

263. Jespersen, N.A., Axelsen, F., Dollerup, J., Nørgaard, M., and Larsen, C.S. (2021). The burden of non-communicable diseases and mortality in people living with HIV (PLHIV) in the pre-, early- and late-HAART era. HIV Med. *22*, 478-490. 10.1111/hiv.13077.

264. Pourcher, V., Gourmelen, J., Bureau, I., and Bouee, S. (2020). Comorbidities in people living with HIV: An epidemiologic and economic analysis using a claims database in France. Plos One *15*, e0243529. 10.1371/journal.pone.0243529.

265. Camps-Vilaró, A., Pérez-Fernández, S., Subirana, I., Teira, R., Estrada, V., Domingo, P., Dégano, I.R., and Marrugat, J. (2021). Standardized Comparison of Cardiovascular Risk Factors Prevalence in Spanish Women and Men Living with HIV and in the General Population. J. Pers. Med. *11*, 1085. 10.3390/jpm11111085.

266. Slama, S., Hammerich, A., Mandil, A., Sibai, A.M., Tuomilehto, J., Wickramasinghe, K., and McGee, T. (2018). The integration and management of noncommunicable diseases in primary health care. East. Mediterr. Heal. J. Rev. sante Mediterr. Orient. al-Majallah al-sihhiyah li-sharq al-mutawassit *24*, 5-6.

267. Noy, A. (2019). Optimizing treatment of HIV-associated lymphoma. Blood *134*, 1385-1394. 10.1182/blood-2018-01-791400.

268. Smith, R., and Wilkins, M. (2015). Perinatally acquired HIV infection: Long-term neuropsychological consequences and challenges ahead. Child Neuropsychol. *21*, 234-268. 10.1080/09297049.2014.898744.

269. Fogel, J.M., Mwatha, A., Richardson, P., Brown, E.R., Chipato, T., Alexandre, M., Moodley, D., Elbireer, A., Mirochnick, M., George, K., et al. (2013). Impact of Maternal and Infant Antiretroviral Drug Regimens on Drug Resistance in HIV-infected Breastfeeding Infants. Pediatr. Infect. Dis. J. *32*, e164-e169. 10.1097/inf.0b013e31827f44ee.

270. Hunt, G.M., Ledwaba, J., Salimo, A., Kalimashe, M., Dinh, T.-H., Jackson, D., Sherman, G., Puren, A., Ngandu, N.K., Lombard, C., et al. (2019). Prevalence of HIV-1 drug resistance amongst newly diagnosed HIV-infected infants age 4–8 weeks, enrolled in three nationally representative PMTCT effectiveness surveys, South Africa: 2010, 2011–12 and 2012–13. BMC Infect. Dis. *19*, 787. 10.1186/s12879-019-4339-y.

271. Atalell, K.A., Tebeje, N.B., and Ekubagewargies, D.T. (2018). Survival and predictors of mortality among children co-infected with tuberculosis and human immunodeficiency virus at University of Gondar Comprehensive Specialized Hospital, Northwest Ethiopia. A retrospective follow-up study. Plos One *13*, e0197145. 10.1371/journal.pone.0197145.

272. Malee, K.M., Tassiopoulos, K., Huo, Y., Siberry, G., Williams, P.L., Hazra, R., Smith, R.A., Allison, S.M., Garvie, P.A., Kammerer, B., et al. (2011). Mental health

functioning among children and adolescents with perinatal HIV infection and perinatal HIV exposure. AIDS Care *23*, 1533-1544. 10.1080/09540121.2011.575120.

273. Sohn, A.H., and Hazra, R. (2013). The changing epidemiology of the global paediatric HIV epidemic: keeping track of perinatally HIV-infected adolescents. J. Int. AIDS Soc. *16*, 18555. 10.7448/ias.16.1.18555.

274. Mulder, M.d., Yebra, G., Navas, A., Martin, L., Jose, M.I.d., Navarro, M.L., Ory, S.J.d., Gonzalez-Granado, I., Mellado, M.J., Ramos, J.T., and Holguin, A. (2012). Trends in Drug Resistance Prevalence in HIV-1–infected Children in Madrid. Pediatr. Infect. Dis. J. *31*, e213-e221. 10.1097/inf.0b013e3182678c7c.

275. Hansudewechakul, R., Sirisanthana, V., Kurniati, N., Puthanakit, T., Lumbiganon, P., Saphonn, V., Yusoff, N.K.N., Kumarasamy, N., Fong, S.M., Nallusamy, R., et al. (2010). Antiretroviral Therapy Outcomes of HIV-Infected Children in the TREAT Asia Pediatric HIV Observational Database. JAIDS J. Acquir. Immune Defic. Syndr. *55*, 503-509. 10.1097/qai.0b013e3181f5379a.

276. Anderson, K., Muloiwa, R., and Davies, M.-A. (2020). Long-term outcomes in perinatally HIV-infected adolescents and young adults on antiretroviral therapy: a review of South African and global literature. Afr. J. AIDS Res. *19*, 1-12. 10.2989/16085906.2019.1676802.

277. McHenry, M.S., Apondi, E., Ayaya, S.O., Yang, Z., Li, W., Tu, W., Bi, G., Sang, E., and Vreeman, R.C. (2019). Growth of young HIV-infected and HIV-exposed children in western Kenya: A retrospective chart review. Plos One *14*, e0224295. 10.1371/journal.pone.0224295.

278. Lieberman-Blum, S.S., Fung, H.B., and Bandres, J.C. (2008). Maraviroc: A CCR5-receptor antagonist for the treatment of HIV-1 infection. Clin. Ther. *30*, 1228-1250. 10.1016/s0149-2918(08)80048-3.

279. Taki, E., Soleimani, F., Asadi, A., Ghahramanpour, H., Namvar, A., and Heidary, M. (2022). Cabotegravir/Rilpivirine: the last FDA-approved drug to treat HIV. Expert Rev. Anti-Infect. Ther. *20*, 1135-1147. 10.1080/14787210.2022.2081153.

280. Simon, V., Ho, D.D., and Karim, Q.A. (2006). HIV/AIDS epidemiology, pathogenesis, prevention, and treatment. Lancet *368*, 489-504. 10.1016/s0140-6736(06)69157-5.

281. Landovitz, R.J., Donnell, D., Clement, M.E., Hanscom, B., Cottle, L., Coelho, L., Cabello, R., Chariyalertsak, S., Dunne, E.F., Frank, I., et al. (2021). Cabotegravir for HIV Prevention in Cisgender Men and Transgender Women. N. Engl. J. Med. *385*, 595-608. 10.1056/nejmoa2101016.

282. Delany-Moretlwe, S., Hughes, J.P., Bock, P., Ouma, S.G., Hunidzarira, P., Kalonji, D., Kayange, N., Makhema, J., Mandima, P., Mathew, C., et al. (2022). Cabotegravir for the prevention of HIV-1 in women: results from HPTN 084, a phase 3, randomised clinical trial. Lancet *399*, 1779-1789. 10.1016/s0140-6736(22)00538-4.

283. Yap, P.K., Xin, G.L.L., Tan, Y.Y., Chellian, J., Gupta, G., Liew, Y.K., Collet, T., Dua, K., and Chellappan, D.K. (2019). Antiretroviral agents in pre-exposure prophylaxis: emerging and advanced trends in HIV prevention. J. Pharm. Pharmacol. *71*, 1339-1352. 10.1111/jphp.13107.

284. Dvory-Sobol, H., Shaik, N., Callebaut, C., and Rhee, M.S. (2022). Lenacapavir: a first-in-class HIV-1 capsid inhibitor. Curr. Opin. HIV AIDS *17*, 15-21. 10.1097/coh.0000000000000713.

285. Segal-Maurer, S., DeJesus, E., Stellbrink, H.J., Castagna, A., Richmond, G.J., Sinclair, G.I., Siripassorn, K., Ruane, P.J., Berhe, M., Wang, H., et al. (2022). Capsid Inhibition with Lenacapavir in Multidrug-Resistant HIV-1 Infection. N Engl J Med *386*, 1793-1803. 10.1056/NEJMoa2115542.

286. Administration, F., and Drug (2012). Truvada for PrEP Fact Sheet: Enduring Safe and Proper Use - Truvada-for-PrEP-Fact-Sheet--Ensuring-Safe-and-Proper-Use.pdf.

287. Mutua, G., Sanders, E., Mugo, P., Anzala, O., Haberer, J.E., Bangsberg, D., Barin, B., Rooney, J.F., Mark, D., Chetty, P., et al. (2012). Safety and Adherence to Intermittent Pre-Exposure Prophylaxis (PrEP) for HIV-1 in African Men Who Have Sex with Men and Female Sex Workers. Plos One *7*, e33103. 10.1371/journal.pone.0033103.

288. Rivera, C.G., Zeuli, J.D., Smith, B.L., Johnson, T.M., Bhatia, R., Otto, A.O., and Temesgen, Z. (2023). HIV Pre-Exposure Prophylaxis: New and Upcoming Drugs to Address the HIV Epidemic. Drugs *83*, 1677-1698. 10.1007/s40265-023-01963-9.

289. Administration, F., and Drug (2021). FDA Approves First Injectable Treatment for HIV Pre-Exposure Prevention | FDA.

290. Bekker, L.G., Das, M., Abdool Karim, Q., Ahmed, K., Batting, J., Brumskine, W., Gill, K., Harkoo, I., Jaggernath, M., Kigozi, G., et al. (2024). Twice-Yearly

Lenacapavir or Daily F/TAF for HIV Prevention in Cisgender Women. N Engl J Med. 10.1056/NEJMoa2407001.

291. Escolano, A., Dosenovic, P., and Nussenzweig, M.C. (2017). Progress toward active or passive HIV-1 vaccination. J. Exp. Med. *214*, 3-16. 10.1084/jem.20161765.

292. Corey, L., Gilbert, P.B., Juraska, M., Montefiori, D.C., Morris, L., Karuna, S.T., Edupuganti, S., Mgodi, N.M., deCamp, A.C., Rudnicki, E., et al. (2021). Two Randomized Trials of Neutralizing Antibodies to Prevent HIV-1 Acquisition. N. Engl. J. Med. *384*, 1003-1014. 10.1056/nejmoa2031738.

293. Gray, G.E., Bekker, L.-G., Laher, F., Malahleha, M., Allen, M., Moodie, Z., Grunenberg, N., Huang, Y., Grove, D., Prigmore, B., et al. (2021). Vaccine Efficacy of ALVAC-HIV and Bivalent Subtype C gp120–MF59 in Adults. N. Engl. J. Med. *384*, 1089-1100. 10.1056/nejmoa2031499.

294. Johnson, J.P.C.o.J. (2021). Johnson & Johnson and Global Partners Announce Results from Phase 2b Imbokodo HIV Vaccine Clinical Trial in Young Women in Sub-Saharan Africa.

295. Xu, K., Acharya, P., Kong, R., Cheng, C., Chuang, G.-Y., Liu, K., Louder, M.K., O'Dell, S., Rawi, R., Sastry, M., et al. (2018). Epitope-based vaccine design yields fusion peptide-directed antibodies that neutralize diverse strains of HIV-1. Nat Med *24*, 857-867. 10.1038/s41591-018-0042-6.

296. Haynes, B.F., Wiehe, K., Borrow, P., Saunders, K.O., Korber, B., Wagh, K., McMichael, A.J., Kelsoe, G., Hahn, B.H., Alt, F., and Shaw, G.M. (2023).

Strategies for HIV-1 vaccines that induce broadly neutralizing antibodies. Nat Rev Immunol *23*, 142-158. 10.1038/s41577-022-00753-w.

297. Haynes, B.F., Kelsoe, G., Harrison, S.C., and Kepler, T.B. (2012). B-cell–lineage immunogen design in vaccine development with HIV-1 as a case study. Nat Biotechnol *30*, 423-433. 10.1038/nbt.2197.

298. Steichen, J.M., Lin, Y.C., Havenar-Daughton, C., Pecetta, S., Ozorowski, G., Willis, J.R., Toy, L., Sok, D., Liguori, A., Kratochvil, S., et al. (2019). A generalized HIV vaccine design strategy for priming of broadly neutralizing antibody responses. Science *366*. 10.1126/science.aax4380.

299. Jardine, J.G., Kulp, D.W., Havenar-Daughton, C., Sarkar, A., Briney, B., Sok, D., Sesterhenn, F., Ereno-Orbea, J., Kalyuzhniy, O., Deresa, I., et al. (2016). HIV-1 broadly neutralizing antibody precursor B cells revealed by germline-targeting immunogen. Science *351*, 1458-1463. 10.1126/science.aad9195.

300. Stamatatos, L., Pancera, M., and McGuire, A.T. (2017). Germline-targeting immunogens. Immunol Rev *275*, 203-216. 10.1111/imr.12483.

301. McGuire, A.T., Hoot, S., Dreyer, A.M., Lippy, A., Stuart, A., Cohen, K.W., Jardine, J., Menis, S., Scheid, J.F., West, A.P., et al. (2013). Engineering HIV envelope protein to activate germline B cell receptors of broadly neutralizing anti-CD4 binding site antibodies. J Exp Med *210*, 655-663. 10.1084/jem.20122824.

302. Abbott, R.K., Lee, J.H., Menis, S., Skog, P., Rossi, M., Ota, T., Kulp, D.W., Bhullar, D., Kalyuzhniy, O., Havenar-Daughton, C., et al. (2018). Precursor Frequency and Affinity Determine B Cell Competitive Fitness in Germinal

Centers, Tested with Germline-Targeting HIV Vaccine Immunogens. Immunity *48*, 133-146.e136. 10.1016/j.immuni.2017.11.023.

303. Dosenovic, P., Kara, E.E., Pettersson, A.-K., McGuire, A.T., Gray, M., Hartweger, H., Thientosapol, E.S., Stamatatos, L., and Nussenzweig, M.C. (2018). Anti–HIV-1 B cell responses are dependent on B cell precursor frequency and antigen-binding affinity. Proc National Acad Sci *115*, 4743-4748. 10.1073/pnas.1803457115.

304. Duan, H., Chen, X., Boyington, J.C., Cheng, C., Zhang, Y., Jafari, A.J., Stephens, T., Tsybovsky, Y., Kalyuzhniy, O., Zhao, P., et al. (2018). Glycan Masking Focuses Immune Responses to the HIV-1 CD4-Binding Site and Enhances Elicitation of VRC01-Class Precursor Antibodies. Immunity *49*, 301-311.e305. 10.1016/j.immuni.2018.07.005.

305. Umotoy, J., Bagaya, B.S., Joyce, C., Schiffner, T., Menis, S., Saye-Francisco, K.L., Biddle, T., Mohan, S., Vollbrecht, T., Kalyuzhniy, O., et al. (2019). Rapid and Focused Maturation of a VRC01-Class HIV Broadly Neutralizing Antibody Lineage Involves Both Binding and Accommodation of the N276-Glycan. Immunity *51*, 141-154.e146. 10.1016/j.immuni.2019.06.004.

306. Lee, J.H., Toy, L., Kos, J.T., Safonova, Y., Schief, W.R., Havenar-Daughton, C., Watson, C.T., and Crotty, S. (2021). Vaccine genetics of IGHV1-2 VRC01-class broadly neutralizing antibody precursor naïve human B cells. npj Vaccines *6*, 113. 10.1038/s41541-021-00376-7.

307. Initiative, I.A.V. (2021). First-in-human clinical trial confirms novel HIV vaccine approach developed by IAVI and Scripps Research - IAVI.

308. Gilbert, P.B., Juraska, M., deCamp, A.C., Karuna, S., Edupuganti, S., Mgodi, N., Donnell, D.J., Bentley, C., Sista, N., Andrew, P., et al. (2017). Basis and Statistical Design of the Passive HIV-1 Antibody Mediated Prevention (AMP) Test-of-Concept Efficacy Trials. Stat. Commun. Infect. Dis. *9*, 20160001. 10.1515/scid-2016-0001.

309. Magaret, C.A., Benkeser, D.C., Williamson, B.D., Borate, B.R., Carpp, L.N., Georgiev, I.S., Setliff, I., Dingens, A.S., Simon, N., Carone, M., et al. (2019). Prediction of VRC01 neutralization sensitivity by HIV-1 gp160 sequence features. PLoS Comput. Biol. *15*, e1006952. 10.1371/journal.pcbi.1006952.

310. Kong, R., Louder, M.K., Wagh, K., Bailer, R.T., deCamp, A., Greene, K., Gao, H., Taft, J.D., Gazumyan, A., Liu, C., et al. (2014). Improving Neutralization Potency and Breadth by Combining Broadly Reactive HIV-1 Antibodies Targeting Major Neutralization Epitopes. J Virol *89*, 2659-2671. 10.1128/jvi.03136-14.

311. Wagh, K., Bhattacharya, T., Williamson, C., Robles, A., Bayne, M., Garrity, J., Rist, M., Rademeyer, C., Yoon, H., Lapedes, A., et al. (2016). Optimal Combinations of Broadly Neutralizing Antibodies for Prevention and Treatment of HIV-1 Clade C Infection. PLoS Pathog. *12*, e1005520. 10.1371/journal.ppat.1005520.

312. Saunders, K.O., Wiehe, K., Tian, M., Acharya, P., Bradley, T., Alam, S.M., Go, E.P., Scearce, R., Sutherland, L., Henderson, R., et al. (2019). Targeted selection of HIV-specific antibody mutations by engineering B cell maturation. Science *366*, eaay7199. 10.1126/science.aay7199.

313. LaBranche, C.C., Henderson, R., Hsu, A., Behrens, S., Chen, X., Zhou, T., Wiehe, K., Saunders, K.O., Alam, S.M., Bonsignori, M., et al. (2019). Neutralization-guided design of HIV-1 envelope trimers with high affinity for the unmutated common ancestor of CH235 lineage CD4bs broadly neutralizing antibodies. PLoS Pathog. *15*, e1008026. 10.1371/journal.ppat.1008026.

314. Gristick, H.B., Boehmer, L.v., Jr, A.P.W., Schamber, M., Gazumyan, A., Golijanin, J., Seaman, M.S., Fätkenheuer, G., Klein, F., Nussenzweig, M.C., and Bjorkman, P.J. (2016). Natively glycosylated HIV-1 Env structure reveals new mode for antibody recognition of the CD4-binding site. Nat. Struct. Mol. Biol. *23*, 906-915. 10.1038/nsmb.3291.

315. Liao, H.-X., Lynch, R., Zhou, T., Gao, F., Alam, S.M., Boyd, S.D., Fire, A.Z., Roskin, K.M., Schramm, C.A., Zhang, Z., et al. (2013). Co-evolution of a broadly neutralizing HIV-1 antibody and founder virus. Nature *496*, 469-476. 10.1038/nature12053.

316. Williams, L.D., Ofek, G., Schätzle, S., McDaniel, J.R., Lu, X., Nicely, N.I., Wu, L., Lougheed, C.S., Bradley, T., Louder, M.K., et al. (2017). Potent and broad HIV-neutralizing antibodies in memory B cells and plasma. Sci Immunol *2*. 10.1126/sciimmunol.aal2200.

317. Study Details | Evaluating the Safety and Immunogenicity of Stabilized CH505 TF chTrimer in Healthy, HIV-uninfected Adult Participants. | ClinicalTrials.gov. (2021).

318. Daniels, C.N., and Saunders, K.O. (2019). Antibody responses to the HIV-1 envelope high mannose patch. Adv. Immunol. *143*, 11-73. 10.1016/bs.ai.2019.08.002.

319. Meffre, E., Milili, M., Blanco-Betancourt, C., Antunes, H., Nussenzweig, M.C., and Schiff, C. (2001). Immunoglobulin heavy chain expression shapes the B cell receptor repertoire in human B cell development. J Clin Invest *108*, 879-886. 10.1172/jci13051.

320. Verkoczy, L. (2017). Chapter Five Humanized Immunoglobulin Mice Models for HIV Vaccine Testing and Studying the Broadly Neutralizing Antibody Problem. Adv. Immunol. *134*, 235-352. 10.1016/bs.ai.2017.01.004.

321. Escolano, A., Gristick, H.B., Abernathy, M.E., Merkenschlager, J., Gautam, R., Oliveira, T.Y., Pai, J., West, A.P., Barnes, C.O., Cohen, A.A., et al. (2019). Immunization expands B cells specific to HIV-1 V3 glycan in mice and macaques. Nature *570*, 468-473. 10.1038/s41586-019-1250-z.

322. Ratner, L.E.E., Fisher, A., Jagodzinski, L.L., Mitsuya, H., Liou, R.-S., Gallo, R.C., and Wong-Staal, F. (1987). Complete Nucleotide Sequences of Functional Clones of the AIDS Virus. AIDS Res. Hum. Retroviruses *3*, 57-69. 10.1089/aid.1987.3.57.

323. Pan, R., Gorny, M.K., Zolla-Pazner, S., and Kong, X.-P. (2015). The V1V2 Region of HIV-1 gp120 Forms a Five-Stranded Beta Barrel. J Virol *89*, 8003-8010. 10.1128/jvi.00754-15.

324. Roark, R.S., Li, H., Williams, W.B., Chug, H., Mason, R.D., Gorman, J., Wang, S., Lee, F.-H., Rando, J., Bonsignori, M., et al. (2021). Recapitulation of HIV-1

Env-antibody coevolution in macaques leading to neutralization breadth. Science *371*. 10.1126/science.abd2638.

325. Andrabi, R., Pallesen, J., Allen, J.D., Song, G., Zhang, J., Val, N.d., Gegg, G., Porter, K., Su, C.-Y., Pauthner, M., et al. (2019). The Chimpanzee SIV Envelope Trimer: Structure and Deployment as an HIV Vaccine Template. Cell Reports *27*, 2426-2441.e2426. 10.1016/j.celrep.2019.04.082.

326. Zhang, L., Irimia, A., He, L., Landais, E., Rantalainen, K., Leaman, D.P., Vollbrecht, T., Stano, A., Sands, D.I., Kim, A.S., et al. (2019). An MPER antibody neutralizes HIV-1 using germline features shared among donors. Nat. Commun. *10*, 5389. 10.1038/s41467-019-12973-1.

327. Haynes, B.F., Nicely, N.I., and Alam, S.M. (2010). HIV-1 autoreactive antibodies: are they good or bad for HIV-1 prevention? Nat. Struct. Mol. Biol. *17*, 543-545. 10.1038/nsmb0510-543.

328. Dennison, S.M., Sutherland, L.L., Jaeger, F.H., Anasti, K.M., Parks, R., Stewart, S., Bowman, C., Xia, S.-M., Zhang, R., Shen, X., et al. (2011). Induction of Antibodies in Rhesus Macaques That Recognize a Fusion-Intermediate Conformation of HIV-1 gp41. Plos One *6*, e27824. 10.1371/journal.pone.0027824.

329. Yang, G., Holl, T.M., Liu, Y., Li, Y., Lu, X., Nicely, N.I., Kepler, T.B., Alam, S.M., Liao, H.-X., Cain, D.W., et al. (2013). Identification of autoantigens recognized by the 2F5 and 4E10 broadly neutralizing HIV-1 antibodies. J. Exp. Med. *210*, 241-256. 10.1084/jem.20121977.

330. Finney, J., Yang, G., Kuraoka, M., Song, S., Nojima, T., Verkoczy, L., Kitamura, D., Haynes, B.F., and Kelsoe, G. (2019). Cross-Reactivity to Kynureninase Tolerizes B Cells That Express the HIV-1 Broadly Neutralizing Antibody 2F5. J Immunol *203*, 3268-3281. 10.4049/jimmunol.1900069.

331. Haynes, B.F., Wiehe, K., Alam, S.M., Weissman, D., and Saunders, K.O. (2023). Progress with induction of HIV broadly neutralizing antibodies in the Duke Consortia for HIV/AIDS Vaccine Development. Curr. Opin. HIV AIDS *18*, 300-308. 10.1097/coh.0000000000000820.

332. Harrison, S.C. (2008). Viral membrane fusion. Nat. Struct. Mol. Biol. *15*, 690-698. 10.1038/nsmb.1456.

333. Julien, J.-P., Cupo, A., Sok, D., Stanfield, R.L., Lyumkis, D., Deller, M.C., Klasse, P.-J., Burton, D.R., Sanders, R.W., Moore, J.P., et al. (2013). Crystal Structure of a Soluble Cleaved HIV-1 Envelope Trimer. Science *342*, 1477-1483. 10.1126/science.1245625.

334. Pancera, M., Zhou, T., Druz, A., Georgiev, I.S., Soto, C., Gorman, J., Huang, J., Acharya, P., Chuang, G.-Y., Ofek, G., et al. (2014). Structure and immune recognition of trimeric pre-fusion HIV-1 Env. Nature *514*, 455-461. 10.1038/nature13808.

335. Kwon, Y.D., Pancera, M., Acharya, P., Georgiev, I.S., Crooks, E.T., Gorman, J., Joyce, M.G., Guttman, M., Ma, X., Narpala, S., et al. (2015). Crystal structure, conformational fixation and entry-related interactions of mature ligand-free HIV-1 Env. Nat. Struct. Mol. Biol. *22*, 522-531. 10.1038/nsmb.3051.

336. Ou, L., Kong, W.-P., Chuang, G.-Y., Ghosh, M., Gulla, K., O'Dell, S., Varriale, J., Barefoot, N., Changela, A., Chao, C.W., et al. (2020). Preclinical Development of a Fusion Peptide Conjugate as an HIV Vaccine Immunogen. Sci Rep-uk *10*, 3032. 10.1038/s41598-020-59711-y.

337. Shen, C.-H., DeKosky, B.J., Guo, Y., Xu, K., Gu, Y., Kilam, D., Ko, S.H., Kong, R., Liu, K., Louder, M.K., et al. (2020). VRC34-Antibody Lineage Development Reveals How a Required Rare Mutation Shapes the Maturation of a Broad HIV-Neutralizing Lineage. Cell Host Microbe *27*, 531-543.e536. 10.1016/j.chom.2020.01.027.

338. Brouwer, P.J.M., Antanasijevic, A., Gast, M.d., Allen, J.D., Bijl, T.P.L., Yasmeen, A., Ravichandran, R., Burger, J.A., Ozorowski, G., Torres, J.L., et al. (2021). Immunofocusing and enhancing autologous Tier-2 HIV-1 neutralization by displaying Env trimers on two-component protein nanoparticles. npj Vaccines *6*, 24. 10.1038/s41541-021-00285-9.

339. Pantophlet, R., and Burton, D.R. (2003). Immunofocusing: antigen engineering to promote the induction of HIV-neutralizing antibodies. Trends Mol Med *9*, 468-473. 10.1016/j.molmed.2003.09.001.

340. Trkola, A., Purtscher, M., Muster, T., Ballaun, C., Buchacher, A., Sullivan, N., Srinivasan, K., Sodroski, J., Moore, J.P., and Katinger, H. (1996). Human monoclonal antibody 2G12 defines a distinctive neutralization epitope on the gp120 glycoprotein of human immunodeficiency virus type 1. J Virol *70*, 1100-1108. 10.1128/jvi.70.2.1100-1108.1996.

341. Calarese, D.A., Scanlan, C.N., Zwick, M.B., Deechongkit, S., Mimura, Y., Kunert, R., Zhu, P., Wormald, M.R., Stanfield, R.L., Roux, K.H., et al. (2003). Antibody Domain Exchange Is an Immunological Solution to Carbohydrate Cluster Recognition. Science *300*, 2065-2071. 10.1126/science.1083182.

342. Williams, W.B., Meyerhoff, R.R., Edwards, R.J., Li, H., Manne, K., Nicely, N.I., Henderson, R., Zhou, Y., Janowska, K., Mansouri, K., et al. (2021). Fab-dimerized glycan-reactive antibodies are a structural category of natural antibodies. Cell *184*, 2955-2972.e2925. 10.1016/j.cell.2021.04.042.

343. Weill, J.-C., Weller, S., and Reynaud, C.-A. (2009). Human Marginal Zone B Cells. Annu Rev Immunol *27*, 267-285. 10.1146/annurev.immunol.021908.132607.

344. Holodick, N.E., Rodríguez-Zhurbenko, N., and Hernández, A.M. (2017). Defining Natural Antibodies. Front Immunol *8*, 872. 10.3389/fimmu.2017.00872.

345. Locci, M., Havenar-Daughton, C., Landais, E., Wu, J., Kroenke, M.A., Arlehamn, C.L., Su, L.F., Cubas, R., Davis, M.M., Sette, A., et al. (2013). Human Circulating PD-1+CXCR3−CXCR5+ Memory Tfh Cells Are Highly Functional and Correlate with Broadly Neutralizing HIV Antibody Responses. Immunity *39*, 758-769. 10.1016/j.immuni.2013.08.031.

346. Pardi, N., and Weissman, D. (2016). RNA Vaccines, Methods and Protocols. Methods Mol Biology *1499*, 109-121. 10.1007/978-1-4939-6481-9_6.

347. Kasturi, S.P., Rasheed, M.A.U., Havenar-Daughton, C., Pham, M., Legere, T., Sher, Z.J., Kovalenkov, Y., Gumber, S., Huang, J.Y., Gottardo, R., et al. (2020). 3M-052, a synthetic TLR-7/8 agonist, induces durable HIV-1 envelope–specific

plasma cells and humoral immunity in nonhuman primates. Sci Immunol *5*. 10.1126/sciimmunol.abb1025.

348. Pauthner, M.G., Nkolola, J.P., Havenar-Daughton, C., Murrell, B., Reiss, S.M., Bastidas, R., Prévost, J., Nedellec, R., Bredow, B.v., Abbink, P., et al. (2019). Vaccine-Induced Protection from Homologous Tier 2 SHIV Challenge in Nonhuman Primates Depends on Serum-Neutralizing Antibody Titers. Immunity *50*, 241-+. 10.1016/j.immuni.2018.11.011.

349. Collins, D.R., Gaiha, G.D., and Walker, B.D. (2020). CD8+ T cells in HIV control, cure and prevention. Nat Rev Immunol *20*, 471-482. 10.1038/s41577-020-0274-9.

350. Picker, L.J., Hansen, S.G., and Lifson, J.D. (2012). New Paradigms for HIV/AIDS Vaccine Development. Medicine *63*, 95-111. 10.1146/annurev-med-042010-085643.

351. Verweij, M.C., Hansen, S.G., Iyer, R., John, N., Malouli, D., Morrow, D., Scholz, I., Womack, J., Abdulhaqq, S., Gilbride, R.M., et al. (2021). Modulation of MHC-E transport by viral decoy ligands is required for RhCMV/SIV vaccine efficacy. Science *372*. 10.1126/science.abe9233.

352. Malouli, D., Hansen, S.G., Hancock, M.H., Hughes, C.M., Ford, J.C., Gilbride, R.M., Ventura, A.B., Morrow, D., Randall, K.T., Taher, H., et al. (2021). Cytomegaloviral determinants of CD8+ T cell programming and RhCMV/SIV vaccine efficacy. Sci Immunol *6*. 10.1126/sciimmunol.abg5413.

353. Maciel, M., Amara, R.R., Bar, K.J., Crotty, S., Deeks, S.G., Duplessis, C., Gaiha, G., McElrath, M.J., McMichael, A., Palin, A., et al. (2024). Exploring synergies

between B- and T-cell vaccine approaches to optimize immune responses against HIV—workshop report. npj Vaccines *9*, 39. 10.1038/s41541-024-00818-y.

354. Study Details | VIR-1111: A Prototype Human CMV-based Vaccine for Human Immunodeficiency Virus (HIV) in Healthy Volunteers | ClinicalTrials.gov.

355. Study Details | To Investigate Safety, Reactogenicity and Immunogenicity of VIR-1388 Compared With Placebo in Participants Without HIV | ClinicalTrials.gov.

356. Arunachalam, P.S., Charles, T.P., Joag, V., Bollimpelli, V.S., Scott, M.K.D., Wimmers, F., Burton, S.L., Labranche, C.C., Petitdemange, C., Gangadhara, S., et al. (2020). T cell-inducing vaccine durably prevents mucosal SHIV infection even with lower neutralizing antibody titers. Nat Med *26*, 932-940. 10.1038/s41591-020-0858-8.

357. Hoffenberg, S., Powell, R., Carpov, A., Wagner, D., Wilson, A., Pond, S.K., Lindsay, R., Arendt, H., DeStefano, J., Phogat, S., et al. (2013). Identification of an HIV-1 Clade A Envelope That Exhibits Broad Antigenicity and Neutralization Sensitivity and Elicits Antibodies Targeting Three Distinct Epitopes. J Virol *87*, 5372-5383. 10.1128/jvi.02827-12.

358. Wu, L., Yang, Z.-Y., Xu, L., Welcher, B., Winfrey, S., Shao, Y., Mascola, J.R., and Nabel, G.J. (2006). Cross-clade recognition and neutralization by the V3 region from clade C human immunodeficiency virus-1 envelope. Vaccine *24*, 4995-5002. 10.1016/j.vaccine.2006.03.083.

359. Sanders, R.W., Derking, R., Cupo, A., Julien, J.-P., Yasmeen, A., Val, N.d., Kim, H.J., Blattner, C., Peña, A.T.d.l., Korzun, J., et al. (2013). A Next-Generation Cleaved, Soluble HIV-1 Env Trimer, BG505 SOSIP.664 gp140, Expresses

Multiple Epitopes for Broadly Neutralizing but Not Non-Neutralizing Antibodies. PLoS Pathog. *9*, e1003618. 10.1371/journal.ppat.1003618.

360. Sanders, R.W., Venturi, M., Schiffner, L., Kalyanaraman, R., Katinger, H., Lloyd, K.O., Kwong, P.D., and Moore, J.P. (2002). The Mannose-Dependent Epitope for Neutralizing Antibody 2G12 on Human Immunodeficiency Virus Type 1 Glycoprotein gp120. J Virol *76*, 7293-7305. 10.1128/jvi.76.14.7293-7305.2002.

361. Binley, J.M., Sanders, R.W., Clas, B., Schuelke, N., Master, A., Guo, Y., Kajumo, F., Anselma, D.J., Maddon, P.J., Olson, W.C., and Moore, J.P. (2000). A Recombinant Human Immunodeficiency Virus Type 1 Envelope Glycoprotein Complex Stabilized by an Intermolecular Disulfide Bond between the gp120 and gp41 Subunits Is an Antigenic Mimic of the Trimeric Virion-Associated Structure. J Virol *74*, 627-643. 10.1128/jvi.74.2.627-643.2000.

362. Charles, T.P., Burton, S.L., Arunachalam, P.S., Cottrell, C.A., Sewall, L.M., Bollimpelli, V.S., Gangadhara, S., Dey, A.K., Ward, A.B., Shaw, G.M., et al. (2021). The C3/465 glycan hole cluster in BG505 HIV-1 envelope is the major neutralizing target involved in preventing mucosal SHIV infection. PLoS Pathog. *17*, e1009257. 10.1371/journal.ppat.1009257.

363. Smith, J.C., Arunachalam, P.S., Legere, T.H., Cavacini, L.A., Hunter, E., Pulendran, B., Amara, R.R., and Kozlowski, P.A. (2024). Induction of Tier 2 HIV-Neutralizing IgA Antibodies in Rhesus Macaques Vaccinated with BG505.664 SOSIP. Nato Adv Sci Inst Se *12*, 1386. 10.3390/vaccines12121386.

364. Houser, K.V., Gaudinski, M.R., Happe, M., Narpala, S., Verardi, R., Sarfo, E.K., Corrigan, A.R., Wu, R., Rothwell, R.S., Novik, L., et al. (2022). Safety and

immunogenicity of an HIV-1 prefusion-stabilized envelope trimer (Trimer 4571) vaccine in healthy adults: A first-in-human open-label, randomized, dose-escalation, phase 1 clinical trial. eClinicalMedicine *48*, 101477. 10.1016/j.eclinm.2022.101477.

365. Hahn, W.O., Parks, K.R., Shen, M., Ozorowski, G., Janes, H., Ballweber-Fleming, L., Davis, A.S.W., Duplessis, C., Tomai, M., Dey, A.K., et al. (2024). Use of 3M-052-AF with Alum adjuvant in HIV trimer vaccine induces human autologous neutralizing antibodies. J. Exp. Med. *221*, e20240604. 10.1084/jem.20240604.

366. de Taeye, Steven W., Ozorowski, G., Torrents de la Peña, A., Guttman, M., Julien, J.-P., van den Kerkhof, Tom L.G.M., Burger, Judith A., Pritchard, Laura K., Pugach, P., Yasmeen, A., et al. (2015). Immunogenicity of Stabilized HIV-1 Envelope Trimers with Reduced Exposure of Non-neutralizing Epitopes. Cell *163*, 1702-1715. 10.1016/j.cell.2015.11.056.

367. Peña, A.T.d.l., Julien, J.-P., Taeye, S.W.d., Garces, F., Guttman, M., Ozorowski, G., Pritchard, L.K., Behrens, A.-J., Go, E.P., Burger, J.A., et al. (2017). Improving the Immunogenicity of Native-like HIV-1 Envelope Trimers by Hyperstabilization. Cell Reports *20*, 1805-1817. 10.1016/j.celrep.2017.07.077.

368. Sliepen, K., Han, B.W., Bontjer, I., Mooij, P., Garces, F., Behrens, A.-J., Rantalainen, K., Kumar, S., Sarkar, A., Brouwer, P.J.M., et al. (2019). Structure and immunogenicity of a stabilized HIV-1 envelope trimer based on a group-M consensus sequence. Nat. Commun. *10*, 2355. 10.1038/s41467-019-10262-5.

369. Taeye, S.W.d., Go, E.P., Sliepen, K., Peña, A.T.d.l., Badal, K., Medina-Ramírez, M., Lee, W.-H., Desaire, H., Wilson, I.A., Moore, J.P., et al. (2019). Stabilization of the V2 loop improves the presentation of V2 loop–associated broadly neutralizing antibody epitopes on HIV-1 envelope trimers. J. Biol. Chem. *294*, 5616-5631. 10.1074/jbc.ra118.005396.

370. Chuang, G.-Y., Lai, Y.-T., Boyington, J.C., Cheng, C., Geng, H., Narpala, S., Rawi, R., Schmidt, S.D., Tsybovsky, Y., Verardi, R., et al. (2020). Development of a 3Mut-Apex-Stabilized Envelope Trimer That Expands HIV-1 Neutralization Breadth When Used To Boost Fusion Peptide-Directed Vaccine-Elicited Responses. J Virol *94*, 10.1128/jvi.00074-00020. 10.1128/jvi.00074-20.

371. Brouwer, P.J.M., Antanasijevic, A., Berndsen, Z., Yasmeen, A., Fiala, B., Bijl, T.P.L., Bontjer, I., Bale, J.B., Sheffler, W., Allen, J.D., et al. (2019). Enhancing and shaping the immunogenicity of native-like HIV-1 envelope trimers with a two-component protein nanoparticle. Nat. Commun. *10*, 4272. 10.1038/s41467-019-12080-1.

372. Study Details | Dose, Safety, Tolerability, and Immunogenicity of an HIV-1 Vaccine, VRC-HIVRGP096-00-VP, With Alum in Healthy Adults | ClinicalTrials.gov.

373. Study Details | Evaluation of Trimer 4571 Therapeutic Vaccination in Adults Living with HIV on Suppressive Antiretroviral Therapy | ClinicalTrials.gov.

374. Medina-Ramírez, M., Garces, F., Escolano, A., Skog, P., Taeye, S.W.d., Moral-Sanchez, I.D., McGuire, A.T., Yasmeen, A., Behrens, A.-J., Ozorowski, G., et al. (2017). Design and crystal structure of a native-like HIV-1 envelope trimer that

engages multiple broadly neutralizing antibody precursors in vivo. J. Exp. Med. *214*, 2573-2590. 10.1084/jem.20161160.

375. Whitaker, N., Hickey, J.M., Kaur, K., Xiong, J., Sawant, N., Cupo, A., Lee, W.-H., Ozorowski, G., Medina-Ramírez, M., Ward, A.B., et al. (2019). Developability Assessment of Physicochemical Properties and Stability Profiles of HIV-1 BG505 SOSIP.664 and BG505 SOSIP.v4.1-GT1.1 gp140 Envelope Glycoprotein Trimers as Candidate Vaccine Antigens. J. Pharm. Sci. *108*, 2264-2277. 10.1016/j.xphs.2019.01.033.

376. Study Details | A Clinical Trial to Evaluate the Safety and Immunogenicity of Recombinant HIV-1 Envelope Protein BG505 SOSIP.GT1.1 Gp140 Vaccine, Adjuvanted in Healthy, HIV-uninfected Adults | ClinicalTrials.gov.

377. Study Details | Trial to Evaluate the Safety and Immunogenicity of Priming Regimens of 426c.Mod.Core-C4b and Optional Boost Regimen With HIV Trimer BG505 SOSIP.GT1.1 gp140, Both Adjuvanted With 3M-052-AF + Alum in Healthy, Adult Participants Without HIV | ClinicalTrials.gov.

378. Caniels, T.G., Medina-Ramìrez, M., Zhang, S., Kratochvil, S., Xian, Y., Koo, J.-H., Derking, R., Samsel, J., Schooten, J.v., Pecetta, S., et al. (2024). Germline-targeting HIV vaccination induces neutralizing antibodies to the CD4 binding site. Sci Immunol *9*, eadk9550-eadk9550. 10.1126/sciimmunol.adk9550.

379. Nelson, A.N., Shen, X., Vekatayogi, S., Zhang, S., Ozorowski, G., Dennis, M., Sewall, L.M., Milligan, E., Davis, D., Cross, K.A., et al. (2024). Immunization with germ line–targeting SOSIP trimers elicits broadly neutralizing antibody precursors in infant macaques. Sci Immunol *9*, eadm7097. 10.1126/sciimmunol.adm7097.

380. Liu, D.X., Liang, J.Q., and Fung, T.S. (2021). Encyclopedia of Virology. Encycl. Virol., 428-440. 10.1016/b978-0-12-809633-8.21501-x.

381. Gorse, G.J., Patel, G.B., Vitale, J.N., and O'Connor, T.Z. (2010). Prevalence of Antibodies to Four Human Coronaviruses Is Lower in Nasal Secretions than in Serum. Clin. Vaccine Immunol. *17*, 1875-1880. 10.1128/cvi.00278-10.

382. Rodriguez-Morales, A.J., Balbin-Ramon, G.J., Rabaan, A.A., Sah, R., Dhama, K., Paniz-Mondolfi, A., Pagliano, P., and Esposito, S. (2020). Genomic Epidemiology and its importance in the study of the COVID-19 pandemic. Le Infez. Med. *28*, 139-142.

383. Su, S., Wong, G., Shi, W., Liu, J., Lai, A.C.K., Zhou, J., Liu, W., Bi, Y., and Gao, G.F. (2016). Epidemiology, Genetic Recombination, and Pathogenesis of Coronaviruses. Trends Microbiol. *24*, 490-502. 10.1016/j.tim.2016.03.003.

384. Li, X., Song, Y., Wong, G., and Cui, J. (2020). Bat origin of a new human coronavirus: there and back again. Sci. China Life Sci. *63*, 461-462. 10.1007/s11427-020-1645-7.

385. M, Z.A., Sander, v.B., M, B.T., D.M.E, O.A., and A.M, F.R. (2012). Isolation of a Novel Coronavirus from a Man with Pneumonia in Saudi Arabia. N. Engl. J. Med. *367*, 1814-1820. 10.1056/nejmoa1211721.

386. Zumla, A., Hui, D.S., and Perlman, S. (2015). Middle East respiratory syndrome. Lancet *386*, 995-1007. 10.1016/s0140-6736(15)60454-8.

387. Zhou, P., Yang, X.-L., Wang, X.-G., Hu, B., Zhang, L., Zhang, W., Si, H.-R., Zhu, Y., Li, B., Huang, C.-L., et al. (2020). A pneumonia outbreak associated with a

new coronavirus of probable bat origin. Nature *579*, 270-273. 10.1038/s41586-020-2012-7.

388. Viruses, C.S.G.o.t.I.C.o.T.o., Gorbalenya, A.E., Baker, S.C., Baric, R.S., Groot, R.J.d., Drosten, C., Gulyaeva, A.A., Haagmans, B.L., Lauber, C., Leontovich, A.M., et al. (2020). The species Severe acute respiratory syndrome-related coronavirus: classifying 2019-nCoV and naming it SARS-CoV-2. Nat. Microbiol. *5*, 536-544. 10.1038/s41564-020-0695-z.

389. Drosten, C., Günther, S., Preiser, W., Werf, S.v.d., Brodt, H.-R., Becker, S., Rabenau, H., Panning, M., Kolesnikova, L., Fouchier, R.A.M., et al. (2003). Identification of a Novel Coronavirus in Patients with Severe Acute Respiratory Syndrome. The New England Journal of Medicine *348*, 1967-1976. 10.1056/nejmoa030747.

390. Rota, P.A., Oberste, M.S., Monroe, S.S., Nix, W.A., Campagnoli, R., Icenogle, J.P., Peñaranda, S., Bankamp, B., Maher, K., Chen, M.-h., et al. (2003). Characterization of a Novel Coronavirus Associated with Severe Acute Respiratory Syndrome. Science *300*, 1394-1399. 10.1126/science.1085952.

391. Gao, H., Yao, H., Yang, S., and Li, L. (2016). From SARS to MERS: evidence and speculation. Frontiers of Medicine *10*, 377-382. 10.1007/s11684-016-0466-7.

392. House, N.N.C., Palissery, S., and Sebastian, H. (2021). Corona Viruses: A Review on SARS, MERS and COVID-19. Microbiol. Insights *14*, 11786361211002481. 10.1177/11786361211002481.

393. Lamers, M.M., and Haagmans, B.L. (2022). SARS-CoV-2 pathogenesis. Nat Rev Microbiol *20*, 270-284. 10.1038/s41579-022-00713-0.

394. Zhu, N., Zhang, D., Wang, W., Li, X., Yang, B., Song, J., Zhao, X., Huang, B., Shi, W., Lu, R., et al. (2020). A Novel Coronavirus from Patients with Pneumonia in China, 2019. N. Engl. J. Med. *382*, 727-733. 10.1056/nejmoa2001017.

395. Mahajan, S., Caraballo, C., Li, S.-X., Dong, Y., Chen, L., Huston, S.K., Srinivasan, R., Redlich, C.A., Ko, A.I., Faust, J.S., et al. (2021). SARS-CoV-2 Infection Hospitalization Rate and Infection Fatality Rate Among the Non-Congregate Population in Connecticut. Am. J. Med. *134*, 812-816.e812. 10.1016/j.amjmed.2021.01.020.

396. Baric, R.S. (2020). Emergence of a Highly Fit SARS-CoV-2 Variant. N. Engl. J. Med. *383*, 2684-2686. 10.1056/nejmcibr2032888.

397. Hoffman, S.A., Costales, C., Sahoo, M.K., Palanisamy, S., Yamamoto, F., Huang, C., Verghese, M., Solis, D.A., Sibai, M., Subramanian, A., et al. (2021). SARS-CoV-2 Neutralization Resistance Mutations in Patient with HIV/AIDS, California, USA - Volume 27, Number 10—October 2021 - Emerging Infectious Diseases journal - CDC. Emerg. Infect. Dis. *27*, 2720-2723. 10.3201/eid2710.211461.

398. Garcia-Beltran, W.F., Lam, E.C., Denis, K.S., Nitido, A.D., Garcia, Z.H., Hauser, B.M., Feldman, J., Pavlovic, M.N., Gregory, D.J., Poznansky, M.C., et al. (2021). Multiple SARS-CoV-2 variants escape neutralization by vaccine-induced humoral immunity. Cell *184*, 2372-2383.e2379. 10.1016/j.cell.2021.03.013.

399. Planas, D., Saunders, N., Maes, P., Guivel-Benhassine, F., Planchais, C., Buchrieser, J., Bolland, W.-H., Porrot, F., Staropoli, I., Lemoine, F., et al. (2022). Considerable escape of SARS-CoV-2 Omicron to antibody neutralization. Nature *602*, 671-675. 10.1038/s41586-021-04389-z.

400. Challen, R., Brooks-Pollock, E., Read, J.M., Dyson, L., Tsaneva-Atanasova, K., and Danon, L. (2021). Risk of mortality in patients infected with SARS-CoV-2 variant of concern 202012/1: matched cohort study. BMJ *372*, n579. 10.1136/bmj.n579.

401. Walensky, R.P., Walke, H.T., and Fauci, A.S. (2021). SARS-CoV-2 Variants of Concern in the United States—Challenges and Opportunities. JAMA *325*, 1037-1038. 10.1001/jama.2021.2294.

402. Harvey, W.T., Carabelli, A.M., Jackson, B., Gupta, R.K., Thomson, E.C., Harrison, E.M., Ludden, C., Reeve, R., Rambaut, A., Consortium, C.-G.U.K., et al. (2021). SARS-CoV-2 variants, spike mutations and immune escape. Nat Rev Microbiol *19*, 409-424. 10.1038/s41579-021-00573-0.

403. Viana, R., Moyo, S., Amoako, D.G., Tegally, H., Scheepers, C., Althaus, C.L., Anyaneji, U.J., Bester, P.A., Boni, M.F., Chand, M., et al. (2022). Rapid epidemic expansion of the SARS-CoV-2 Omicron variant in southern Africa. Nature *603*, 679-686. 10.1038/s41586-022-04411-y.

404. Tegally, H., Wilkinson, E., Giovanetti, M., Iranzadeh, A., Fonseca, V., Giandhari, J., Doolabh, D., Pillay, S., San, E.J., Msomi, N., et al. (2021). Detection of a SARS-CoV-2 variant of concern in South Africa. Nature *592*, 438-443. 10.1038/s41586-021-03402-9.

405. Tegally, H., Wilkinson, E., Lessells, R.J., Giandhari, J., Pillay, S., Msomi, N., Mlisana, K., Bhiman, J.N., Gottberg, A.v., Walaza, S., et al. (2021). Sixteen novel lineages of SARS-CoV-2 in South Africa. Nat Med *27*, 440-446. 10.1038/s41591-021-01255-3.

406. Martin, D.P., Lytras, S., Lucaci, A.G., Maier, W., Grüning, B., Shank, S.D., Weaver, S., MacLean, O.A., Orton, R.J., Lemey, P., et al. (2022). Selection Analysis Identifies Clusters of Unusual Mutational Changes in Omicron Lineage BA.1 That Likely Impact Spike Function. Mol. Biol. Evol. *39*, msac061. 10.1093/molbev/msac061.

407. Meng, B., Datir, R., Choi, J., Bradley, J.R., Smith, K.G.C., Lee, J.H., Gupta, R.K., Baker, S., Dougan, G., Hess, C., et al. (2022). SARS-CoV-2 spike N-terminal domain modulates TMPRSS2-dependent viral entry and fusogenicity. Cell Reports *40*, 111220. 10.1016/j.celrep.2022.111220.

408. Sun, Y., Lin, W., Dong, W., and Xu, J. (2022). Origin and evolutionary analysis of the SARS-CoV-2 Omicron variant. J. Biosaf. Biosecurity *4*, 33-37. 10.1016/j.jobb.2021.12.001.

409. Choi, B., Choudhary, M.C., Regan, J., Sparks, J.A., Padera, R.F., Qiu, X., Solomon, I.H., Kuo, H.-H., Boucau, J., Bowman, K., et al. (2020). Persistence and Evolution of SARS-CoV-2 in an Immunocompromised Host. N. Engl. J. Med. *383*, 2291-2293. 10.1056/nejmc2031364.

410. Kemp, S.A., Collier, D.A., Datir, R.P., Ferreira, I.A.T.M., Gayed, S., Jahun, A., Hosmillo, M., Rees-Spear, C., Mlcochova, P., Lumb, I.U., et al. (2021). SARS-CoV-2 evolution during treatment of chronic infection. Nature *592*, 277-282. 10.1038/s41586-021-03291-y.

411. Weigang, S., Fuchs, J., Zimmer, G., Schnepf, D., Kern, L., Beer, J., Luxenburger, H., Ankerhold, J., Falcone, V., Kemming, J., et al. (2021). Within-host evolution of

SARS-CoV-2 in an immunosuppressed COVID-19 patient as a source of immune escape variants. Nat. Commun. *12*, 6405. 10.1038/s41467-021-26602-3.

412. Chen, P.Z., Bobrovitz, N., Premji, Z.A., Koopmans, M., Fisman, D.N., and Gu, F.X. (2021). SARS-CoV-2 shedding dynamics across the respiratory tract, sex, and disease severity for adult and pediatric COVID-19. eLife *10*. 10.7554/eLife.70458.

413. Borges, V., Isidro, J., Cunha, M., Cochicho, D., Martins, L., Banha, L., Figueiredo, M., Rebelo, L., Trindade, M.C., Duarte, S., et al. (2021). Long-Term Evolution of SARS-CoV-2 in an Immunocompromised Patient with Non-Hodgkin Lymphoma. mSphere *6*, 10.1128/msphere.00244-00221. 10.1128/msphere.00244-21.

414. Avanzato, V.A., Matson, M.J., Seifert, S.N., Pryce, R., Williamson, B.N., Anzick, S.L., Barbian, K., Judson, S.D., Fischer, E.R., Martens, C., et al. (2020). Case Study: Prolonged Infectious SARS-CoV-2 Shedding from an Asymptomatic Immunocompromised Individual with Cancer. Cell *183*, 1901-1912.e1909. 10.1016/j.cell.2020.10.049.

415. Jensen, B., Luebke, N., Feldt, T., Keitel, V., Brandenburger, T., Kindgen-Milles, D., Lutterbeck, M., Freise, N.F., Schoeler, D., Haas, R., et al. (2021). Emergence of the E484K mutation in SARS-COV-2-infected immunocompromised patients treated with bamlanivimab in Germany. Lancet Reg. Heal. - Eur. *8*, 100164. 10.1016/j.lanepe.2021.100164.

416. Clark, S.A., Clark, L.E., Pan, J., Coscia, A., McKay, L.G.A., Shankar, S., Johnson, R.I., Brusic, V., Choudhary, M.C., Regan, J., et al. (2021). SARS-CoV-2 evolution

in an immunocompromised host reveals shared neutralization escape mechanisms. Cell *184*, 2605-2617.e2618. 10.1016/j.cell.2021.03.027.

417. V'kovski, P., Kratzel, A., Steiner, S., Stalder, H., and Thiel, V. (2021). Coronavirus biology and replication: implications for SARS-CoV-2. Nat Rev Microbiol *19*, 155-170. 10.1038/s41579-020-00468-6.

418. Gorbalenya, A.E., Enjuanes, L., Ziebuhr, J., and Snijder, E.J. (2006). Nidovirales: Evolving the largest RNA virus genome. Virus Res *117*, 17-37. 10.1016/j.virusres.2006.01.017.

419. Wit, E.d., Doremalen, N.v., Falzarano, D., and Munster, V.J. (2016). SARS and MERS: recent insights into emerging coronaviruses. Nat Rev Microbiol *14*, 523-534. 10.1038/nrmicro.2016.81.

420. Wong, L.-Y.R., and Perlman, S. (2022). Immune dysregulation and immunopathology induced by SARS-CoV-2 and related coronaviruses — are we our own worst enemy? Nat Rev Immunol *22*, 47-56. 10.1038/s41577-021-00656-2.

421. Redondo, N., Zaldívar-López, S., Garrido, J.J., and Montoya, M. (2021). SARS-CoV-2 Accessory Proteins in Viral Pathogenesis: Knowns and Unknowns. Front Immunol *12*, 708264. 10.3389/fimmu.2021.708264.

422. Harrison, A.G., Lin, T., and Wang, P. (2020). Mechanisms of SARS-CoV-2 Transmission and Pathogenesis. Trends Immunol *41*, 1100-1115. 10.1016/j.it.2020.10.004.

423. Doremalen, N.v., Bushmaker, T., Morris, D.H., Holbrook, M.G., Gamble, A., Williamson, B.N., Tamin, A., Harcourt, J.L., Thornburg, N.J., Gerber, S.I., et al.

(2020). Aerosol and Surface Stability of SARS-CoV-2 as Compared with SARS-CoV-1. N. Engl. J. Med. *382*, 1564-1567. 10.1056/nejmc2004973.

424. Meselson, M. (2020). Droplets and Aerosols in the Transmission of SARS-CoV-2. N. Engl. J. Med. *382*, 2063-2063. 10.1056/nejmc2009324.

425. Ahn, J.H., Kim, J., Hong, S.P., Choi, S.Y., Yang, M.J., Ju, Y.S., Kim, Y.T., Kim, H.M., Rahman, M.D.T., Chung, M.K., et al. (2021). Nasal ciliated cells are primary targets for SARS-CoV-2 replication in early stage of COVID-19. J Clin Invest *131*. 10.1172/jci148517.

426. Hou, Y.J., Okuda, K., Edwards, C.E., Martinez, D.R., Asakura, T., Dinnon, K.H., Kato, T., Lee, R.E., Yount, B.L., Mascenik, T.M., et al. (2020). SARS-CoV-2 Reverse Genetics Reveals a Variable Infection Gradient in the Respiratory Tract. Cell *182*, 429-446.e414. 10.1016/j.cell.2020.05.042.

427. Hoffmann, M., Kleine-Weber, H., Schroeder, S., Krüger, N., Herrler, T., Erichsen, S., Schiergens, T.S., Herrler, G., Wu, N.-H., Nitsche, A., et al. (2020). SARS-CoV-2 Cell Entry Depends on ACE2 and TMPRSS2 and Is Blocked by a Clinically Proven Protease Inhibitor. Cell *181*, 271-280.e278. 10.1016/j.cell.2020.02.052.

428. Zhao, M.-M., Yang, W.-L., Yang, F.-Y., Zhang, L., Huang, W.-J., Hou, W., Fan, C.-F., Jin, R.-H., Feng, Y.-M., Wang, Y.-C., and Yang, J.-K. (2021). Cathepsin L plays a key role in SARS-CoV-2 infection in humans and humanized mice and is a promising target for new drug development. Signal Transduct. Target. Ther. *6*, 134. 10.1038/s41392-021-00558-8.

429. Walker, A.P., Fan, H., Keown, J.R., Knight, M.L., Grimes, J.M., and Fodor, E. (2021). The SARS-CoV-2 RNA polymerase is a viral RNA capping enzyme. Nucleic Acids Res. *49*, 13019-13030. 10.1093/nar/gkab1160.

430. Pan, R., Kindler, E., Cao, L., Zhou, Y., Zhang, Z., Liu, Q., Ebert, N., Züst, R., Sun, Y., Gorbalenya, A.E., et al. (2022). N7-Methylation of the Coronavirus RNA Cap Is Required for Maximal Virulence by Preventing Innate Immune Recognition. Mbio *13*, e03662-03621. 10.1128/mbio.03662-21.

431. Kim, D., Lee, J.-Y., Yang, J.-S., Kim, J.W., Kim, V.N., and Chang, H. (2020). The Architecture of SARS-CoV-2 Transcriptome. Cell *181*, 914-921 e910. 10.1016/j.cell.2020.04.011.

432. Brant, A.C., Tian, W., Majerciak, V., Yang, W., and Zheng, Z.-M. (2021). SARS-CoV-2: from its discovery to genome structure, transcription, and replication. Cell Biosci. *11*, 136. 10.1186/s13578-021-00643-z.

433. Klein, S., Cortese, M., Winter, S.L., Wachsmuth-Melm, M., Neufeldt, C.J., Cerikan, B., Stanifer, M.L., Boulant, S., Bartenschlager, R., and Chlanda, P. (2020). SARS-CoV-2 structure and replication characterized by in situ cryo-electron tomography. Nat. Commun. *11*, 5885. 10.1038/s41467-020-19619-7.

434. Wolff, G., Limpens, R.W.A.L., Zevenhoven-Dobbe, J.C., Laugks, U., Zheng, S., Jong, A.W.M.d., Koning, R.I., Agard, D.A., Grünewald, K., Koster, A.J., et al. (2020). A molecular pore spans the double membrane of the coronavirus replication organelle. Science *369*, 1395-1398. 10.1126/science.abd3629.

435. Finkel, Y., Mizrahi, O., Nachshon, A., Weingarten-Gabbay, S., Morgenstern, D., Yahalom-Ronen, Y., Tamir, H., Achdout, H., Stein, D., Israeli, O., et al. (2021).

The coding capacity of SARS-CoV-2. Nature *589*, 125-130. 10.1038/s41586-020-2739-1.

436. Sola, I., Almazán, F., Zúñiga, S., and Enjuanes, L. (2015). Continuous and Discontinuous RNA Synthesis in Coronaviruses. Annu. Rev. Virol. *2*, 265-288. 10.1146/annurev-virology-100114-055218.

437. Bravo, M.S., Berengua, C., Marín, P., Esteban, M., Rodriguez, C., Cuerpo, M.d., Miró, E., Cuesta, G., Mosquera, M., Sánchez-Palomino, S., et al. (2021). Viral Culture Confirmed SARS-CoV-2 Subgenomic RNA Value as a Good Surrogate Marker of Infectivity. J. Clin. Microbiol. *60*, e01609-01621. 10.1128/jcm.01609-21.

438. Zhang, Y., Huang, K., Xie, D., Lau, J.Y., Shen, W., Li, P., Wang, D., Zou, Z., Shi, S., Ren, H., et al. (2021). In vivo structure and dynamics of the SARS-CoV-2 RNA genome. Nat. Commun. *12*, 5695. 10.1038/s41467-021-25999-1.

439. Hartenian, E., Nandakumar, D., Lari, A., Ly, M., Tucker, J.M., and Glaunsinger, B.A. (2020). The molecular virology of coronaviruses. J. Biol. Chem. *295*, 12910-12934. 10.1074/jbc.rev120.013930.

440. Cong, Y., Ulasli, M., Schepers, H., Mauthe, M., V'kovski, P., Kriegenburg, F., Thiel, V., Haan, C.A.M.d., and Reggiori, F. (2019). Nucleocapsid Protein Recruitment to Replication-Transcription Complexes Plays a Crucial Role in Coronaviral Life Cycle. J Virol *94*, 10.1128/jvi.01925-01919. 10.1128/jvi.01925-19.

441. Yao, H., Song, Y., Chen, Y., Wu, N., Xu, J., Sun, C., Zhang, J., Weng, T., Zhang, Z., Wu, Z., et al. (2020). Molecular Architecture of the SARS-CoV-2 Virus. Cell *183*, 730-738.e713. 10.1016/j.cell.2020.09.018.

442. Bracquemond, D., and Muriaux, D. (2021). Betacoronavirus Assembly: Clues and Perspectives for Elucidating SARS-CoV-2 Particle Formation and Egress. Mbio *12*, 10.1128/mbio.02371-02321. 10.1128/mbio.02371-21.

443. Lu, M. (2021). Single-Molecule FRET Imaging of Virus Spike–Host Interactions. Viruses *13*, 332. 10.3390/v13020332.

444. Jackson, C.B., Farzan, M., Chen, B., and Choe, H. (2022). Mechanisms of SARS-CoV-2 entry into cells. Nat Rev Mol Cell Bio *23*, 3-20. 10.1038/s41580-021-00418-x.

445. Mykytyn, A.Z., Breugem, T.I., Riesebosch, S., Schipper, D., Doel, P.B.v.d., Rottier, R.J., Lamers, M.M., and Haagmans, B.L. (2021). SARS-CoV-2 entry into human airway organoids is serine protease-mediated and facilitated by the multibasic cleavage site. eLife *10*, e64508. 10.7554/elife.64508.

446. Huang, I.C., Bosch, B.J., Li, F., Li, W., Lee, K.H., Ghiran, S., Vasilieva, N., Dermody, T.S., Harrison, S.C., Dormitzer, P.R., et al. (2006). SARS Coronavirus, but Not Human Coronavirus NL63, Utilizes Cathepsin L to Infect ACE2-expressing Cells*. J. Biol. Chem. *281*, 3198-3203. 10.1074/jbc.m508381200.

447. Simmons, G., Gosalia, D.N., Rennekamp, A.J., Reeves, J.D., Diamond, S.L., and Bates, P. (2005). Inhibitors of cathepsin L prevent severe acute respiratory syndrome coronavirus entry. Proc National Acad Sci *102*, 11876-11881. 10.1073/pnas.0505577102.

448. Beumer, J., Geurts, M.H., Lamers, M.M., Puschhof, J., Zhang, J., Vaart, J.v.d., Mykytyn, A.Z., Breugem, T.I., Riesebosch, S., Schipper, D., et al. (2021). A CRISPR/Cas9 genetically engineered organoid biobank reveals essential host

factors for coronaviruses. Nat. Commun. *12*, 5498. 10.1038/s41467-021-25729-7.

449. Pujadas, E., Chaudhry, F., McBride, R., Richter, F., Zhao, S., Wajnberg, A., Nadkarni, G., Glicksberg, B.S., Houldsworth, J., and Cordon-Cardo, C. (2020). SARS-CoV-2 viral load predicts COVID-19 mortality. Lancet Respir. Med. *8*, e70. 10.1016/s2213-2600(20)30354-4.

450. Hadjadj, J., Yatim, N., Barnabei, L., Corneau, A., Boussier, J., Smith, N., Péré, H., Charbit, B., Bondet, V., Chenevier-Gobeaux, C., et al. (2020). Impaired type I interferon activity and inflammatory responses in severe COVID-19 patients. Science *369*, 718-724. 10.1126/science.abc6027.

451. Lucas, C., Wong, P., Klein, J., Castro, T.B.R., Silva, J., Sundaram, M., Ellingson, M.K., Mao, T., Oh, J.E., Israelow, B., et al. (2020). Longitudinal analyses reveal immunological misfiring in severe COVID-19. Nature *584*, 463-469. 10.1038/s41586-020-2588-y.

452. Hoang, T.N., Pino, M., Boddapati, A.K., Viox, E.G., Starke, C.E., Upadhyay, A.A., Gumber, S., Nekorchuk, M., Busman-Sahay, K., Strongin, Z., et al. (2021). Baricitinib treatment resolves lower-airway macrophage inflammation and neutrophil recruitment in SARS-CoV-2-infected rhesus macaques. Cell *184*, 460-475.e421. 10.1016/j.cell.2020.11.007.

453. Knoll, R., Schultze, J.L., and Schulte-Schrepping, J. (2021). Monocytes and Macrophages in COVID-19. Front Immunol *12*, 720109. 10.3389/fimmu.2021.720109.

454. Khanmohammadi, S., and Rezaei, N. (2021). Role of Toll-like receptors in the pathogenesis of COVID-19. J. Méd. Virol. *93*, 2735-2739. 10.1002/jmv.26826.

455. Yang, Y., Wang, S., Xie, X., Li, J., and Zhang, R. (2021). Change of gene expression profiles in human cardiomyocytes and macrophages infected with SARS-CoV-2 and its significance. Zhong nan da xue xue bao Yi xue ban J. Cent. S. Univ. Méd. Sci. *46*, 1203-1211. 10.11817/j.issn.1672-7347.2021.210221.

456. Lester, S.N., and Li, K. (2014). Toll-Like Receptors in Antiviral Innate Immunity. J. Mol. Biol. *426*, 1246-1264. 10.1016/j.jmb.2013.11.024.

457. Schulz, C., Perdiguero, E.G., Chorro, L., Szabo-Rogers, H., Cagnard, N., Kierdorf, K., Prinz, M., Wu, B., Jacobsen, S.E.W., Pollard, J.W., et al. (2012). A Lineage of Myeloid Cells Independent of Myb and Hematopoietic Stem Cells. Science *336*, 86-90. 10.1126/science.1219179.

458. Woo, Y.D., Jeong, D., and Chung, D.H. (2021). Development and Functions of Alveolar Macrophages. Mol. Cells *44*, 292-300. 10.14348/molcells.2021.0058.

459. Hou, F., Xiao, K., Tang, L., and Xie, L. (2021). Diversity of Macrophages in Lung Homeostasis and Diseases. Front Immunol *12*, 753940. 10.3389/fimmu.2021.753940.

460. Reddy, S.P., and Mehta, D. (2017). Lung Interstitial Macrophages Redefined: It Is Not That Simple Anymore. Am J Resp Cell Mol *57*, 135-136. 10.1165/rcmb.2017-0158ed.

461. Upadhyay, A.A., Viox, E.G., Hoang, T.N., Boddapati, A.K., Pino, M., Lee, M.Y., Corry, J., Strongin, Z., Cowan, D.A., Beagle, E.N., et al. (2023). TREM2(+) and interstitial-like macrophages orchestrate airway inflammation in SARS-CoV-2

infection in rhesus macaques. Nat Commun *14*, 1914. 10.1038/s41467-023-37425-9.

462. Hou, F., Wang, H., Zheng, K., Yang, W., Xiao, K., Rong, Z., Xiao, J., Li, J., Cheng, B., Tang, L., and Xie, L. (2023). Distinct Transcriptional and Functional Differences of Lung Resident and Monocyte-Derived Alveolar Macrophages During the Recovery Period of Acute Lung Injury. Immune Netw. *23*, e24. 10.4110/in.2023.23.e24.

463. Chu, X., Zhang, B., Koeken, V.A.C.M., Gupta, M.K., and Li, Y. (2021). Multi-Omics Approaches in Immunological Research. Front Immunol *12*, 2312. 10.3389/fimmu.2021.668045.

464. Kopf, M., Schneider, C., and Nobs, S.P. (2015). The development and function of lung-resident macrophages and dendritic cells. Nat Immunol *16*, 36-44. 10.1038/ni.3052.

465. Pöpperl, P., Stoff, M., and Beineke, A. (2025). Alveolar Macrophages in Viral Respiratory Infections: Sentinels and Saboteurs of Lung Defense. Int. J. Mol. Sci. *26*, 407. 10.3390/ijms26010407.

466. Li, X., Kolling, F.W., Aridgides, D., Mellinger, D., Ashare, A., and Jakubzick, C.V. (2022). ScRNA-seq expression of IFI27 and APOC2 identifies four alveolar macrophage superclusters in healthy BALF. Life Sci. Alliance *5*, e202201458. 10.26508/lsa.202201458.

467. Grant, R.A., Morales-Nebreda, L., Markov, N.S., Swaminathan, S., Querrey, M., Guzman, E.R., Abbott, D.A., Donnelly, H.K., Donayre, A., Goldberg, I.A., et al.

(2021). Circuits between infected macrophages and T cells in SARS-CoV-2 pneumonia. Nature *590*, 635-641. 10.1038/s41586-020-03148-w.

468. Liao, M., Liu, Y., Yuan, J., Wen, Y., Xu, G., Zhao, J., Cheng, L., Li, J., Wang, X., Wang, F., et al. (2020). Single-cell landscape of bronchoalveolar immune cells in patients with COVID-19. Nat Med *26*, 842-844. 10.1038/s41591-020-0901-9.

469. Minutti, C.M., Jackson-Jones, L.H., García-Fojeda, B., Knipper, J.A., Sutherland, T.E., Logan, N., Ringqvist, E., Guillamat-Prats, R., Ferenbach, D.A., Artigas, A., et al. (2017). Local amplifiers of IL-4Rα–mediated macrophage activation promote repair in lung and liver. Science *356*, 1076-1080. 10.1126/science.aaj2067.

470. Mould, K.J., Jackson, N.D., Henson, P.M., Seibold, M.A., and Janssen, W.J. (2019). Single cell RNA sequencing identifies unique inflammatory airspace macrophage subsets. JCI Insight *4*. 10.1172/jci.insight.126556.

471. Gschwend, J., Sherman, S.P.M., Ridder, F., Feng, X., Liang, H.-E., Locksley, R.M., Becher, B., and Schneider, C. (2021). Alveolar macrophages rely on GM-CSF from alveolar epithelial type 2 cells before and after birth. J. Exp. Med. *218*, e20210745. 10.1084/jem.20210745.

472. Mould, K.J., Barthel, L., Mohning, M.P., Thomas, S.M., McCubbrey, A.L., Danhorn, T., Leach, S.M., Fingerlin, T.E., O'Connor, B.P., Reisz, J.A., et al. (2017). Cell Origin Dictates Programming of Resident versus Recruited Macrophages during Acute Lung Injury. Am J Resp Cell Mol *57*, 294-306. 10.1165/rcmb.2017-0061oc.

473. Ural, B.B., Yeung, S.T., Damani-Yokota, P., Devlin, J.C., Vries, M.d., Vera-Licona, P., Samji, T., Sawai, C.M., Jang, G., Perez, O.A., et al. (2020). Identification of a nerve-associated, lung-resident interstitial macrophage subset with distinct localization and immunoregulatory properties. Sci Immunol *5*. 10.1126/sciimmunol.aax8756.

474. Westphalen, K., Gusarova, G.A., Islam, M.N., Subramanian, M., Cohen, T.S., Prince, A.S., and Bhattacharya, J. (2014). Sessile alveolar macrophages communicate with alveolar epithelium to modulate immunity. Nature *506*, 503-506. 10.1038/nature12902.

475. Hung, L.-Y., Sen, D., Oniskey, T.K., Katzen, J., Cohen, N.A., Vaughan, A.E., Nieves, W., Urisman, A., Beers, M.F., Krummel, M.F., and Herbert, D.B.R. (2019). Macrophages promote epithelial proliferation following infectious and non-infectious lung injury through a Trefoil factor 2-dependent mechanism. Mucosal Immunol *12*, 64-76. 10.1038/s41385-018-0096-2.

476. Lv, J., Wang, Z., Qu, Y., Zhu, H., Zhu, Q., Tong, W., Bao, L., Lv, Q., Cong, J., Li, D., et al. (2021). Distinct uptake, amplification, and release of SARS-CoV-2 by M1 and M2 alveolar macrophages. Cell Discov. *7*, 24. 10.1038/s41421-021-00258-1.

477. Bassler, K., Schulte-Schrepping, J., Warnat-Herresthal, S., Aschenbrenner, A.C., and Schultze, J.L. (2019). The Myeloid Cell Compartment—Cell by Cell. Annu Rev Immunol *37*, 1-25. 10.1146/annurev-immunol-042718-041728.

478. Dick, S.A., Wong, A., Hamidzada, H., Nejat, S., Nechanitzky, R., Vohra, S., Mueller, B., Zaman, R., Kantores, C., Aronoff, L., et al. (2022). Three tissue

resident macrophage subsets coexist across organs with conserved origins and life cycles. Sci Immunol *7*, eabf7777. 10.1126/sciimmunol.abf7777.

479. Gibbings, S.L., Thomas, S.M., Atif, S.M., McCubbrey, A.L., Desch, A.N., Danhorn, T., Leach, S.M., Bratton, D.L., Henson, P.M., Janssen, W.J., and Jakubzick, C.V. (2017). Three Unique Interstitial Macrophages in the Murine Lung at Steady State. Am J Resp Cell Mol *57*, 66-76. 10.1165/rcmb.2016-0361oc.

480. Fu, Y., Pajulas, A., Wang, J., Zhou, B., Cannon, A., Cheung, C.C.L., Zhang, J., Zhou, H., Fisher, A.J., Omstead, D.T., et al. (2022). Mouse pulmonary interstitial macrophages mediate the pro-tumorigenic effects of IL-9. Nat. Commun. *13*, 3811. 10.1038/s41467-022-31596-7.

481. Guilliams, M., Mildner, A., and Yona, S. (2018). Developmental and Functional Heterogeneity of Monocytes. Immunity *49*, 595-613. 10.1016/j.immuni.2018.10.005.

482. Alefishat, E., Jelinek, H.F., Mousa, M., Tay, G.K., and Alsafar, H.S. (2022). Immune response to SARS-CoV-2 variants: A focus on severity, susceptibility, and preexisting immunity. J. Infect. Public Heal. *15*, 277-288. 10.1016/j.jiph.2022.01.007.

483. Silvin, A., Chapuis, N., Dunsmore, G., Goubet, A.-G., Dubuisson, A., Derosa, L., Almire, C., Hénon, C., Kosmider, O., Droin, N., et al. (2020). Elevated Calprotectin and Abnormal Myeloid Cell Subsets Discriminate Severe from Mild COVID-19. Cell *182*, 1401-1418.e1418. 10.1016/j.cell.2020.08.002.

484. Schulte-Schrepping, J., Reusch, N., Paclik, D., Baßler, K., Schlickeiser, S., Zhang, B., Krämer, B., Krammer, T., Brumhard, S., Bonaguro, L., et al. (2020).

Severe COVID-19 Is Marked by a Dysregulated Myeloid Cell Compartment. Cell *182*, 1419-1440.e1423. 10.1016/j.cell.2020.08.001.

485. Graham, L.C., Harder, J.M., Soto, I., Vries, W.N.d., John, S.W.M., and Howell, G.R. (2016). Chronic consumption of a western diet induces robust glial activation in aging mice and in a mouse model of Alzheimer's disease. Sci Rep-uk *6*, 21568. 10.1038/srep21568.

486. Stettler, K., Beltramello, M., Espinosa, D.A., Graham, V., Cassotta, A., Bianchi, S., Vanzetta, F., Minola, A., Jaconi, S., Mele, F., et al. (2016). Specificity, cross-reactivity, and function of antibodies elicited by Zika virus infection. Science *353*, 823-826. 10.1126/science.aaf8505.

487. Wang, T.T., Sewatanon, J., Memoli, M.J., Wrammert, J., Bournazos, S., Bhaumik, S.K., Pinsky, B.A., Chokephaibulkit, K., Onlamoon, N., Pattanapanyasat, K., et al. (2017). IgG antibodies to dengue enhanced for FcγRIIIA binding determine disease severity. Science *355*, 395-398. 10.1126/science.aai8128.

488. Bournazos, S., Gupta, A., and Ravetch, J.V. (2020). The role of IgG Fc receptors in antibody-dependent enhancement. Nat Rev Immunol *20*, 633-643. 10.1038/s41577-020-00410-0.

489. Maemura, T., Kuroda, M., Armbrust, T., Yamayoshi, S., Halfmann, P.J., and Kawaoka, Y. (2021). Antibody-Dependent Enhancement of SARS-CoV-2 Infection Is Mediated by the IgG Receptors FcγRIIA and FcγRIIIA but Does Not Contribute to Aberrant Cytokine Production by Macrophages. Mbio *12*, e01987-01921. 10.1128/mbio.01987-21.

490. Saletti, G., Gerlach, T., Jansen, J.M., Molle, A., Elbahesh, H., Ludlow, M., Li, W., Bosch, B.-J., Osterhaus, A.D.M.E., and Rimmelzwaan, G.F. (2020). Older adults lack SARS CoV-2 cross-reactive T lymphocytes directed to human coronaviruses OC43 and NL63. Sci Rep-uk *10*, 21447. 10.1038/s41598-020-78506-9.

491. Bert, N.L., Tan, A.T., Kunasegaran, K., Tham, C.Y.L., Hafezi, M., Chia, A., Chng, M.H.Y., Lin, M., Tan, N., Linster, M., et al. (2020). SARS-CoV-2-specific T cell immunity in cases of COVID-19 and SARS, and uninfected controls. Nature *584*, 457-462. 10.1038/s41586-020-2550-z.

492. Tang, F., Quan, Y., Xin, Z.-T., Wrammert, J., Ma, M.-J., Lv, H., Wang, T.-B., Yang, H., Richardus, J.H., Liu, W., and Cao, W.-C. (2011). Lack of Peripheral Memory B Cell Responses in Recovered Patients with Severe Acute Respiratory Syndrome: A Six-Year Follow-Up Study. J Immunol *186*, 7264-7268. 10.4049/jimmunol.0903490.

493. Özüdoğru, O., Bahçe, Y.G., and Acer, Ö. (2023). SARS CoV-2 reinfection rate is higher in the Omicron variant than in the Alpha and Delta variants. Ir. J. Méd. Sci. (1971 -) *192*, 751-756. 10.1007/s11845-022-03060-4.

494. Hall, V.J., Foulkes, S., Charlett, A., Atti, A., Monk, E.J.M., Simmons, R., Wellington, E., Cole, M.J., Saei, A., Oguti, B., et al. (2021). SARS-CoV-2 infection rates of antibody-positive compared with antibody-negative health-care workers in England: a large, multicentre, prospective cohort study (SIREN). Lancet *397*, 1459-1469. 10.1016/s0140-6736(21)00675-9.

495. Murchu, E.O., Byrne, P., Carty, P.G., Gascun, C.D., Keogan, M., O'Neill, M., Harrington, P., and Ryan, M. (2022). Quantifying the risk of SARS-CoV-2 reinfection over time. Rev. Méd. Virol. *32*, e2260. 10.1002/rmv.2260.

496. Zhao, M., Zhang, H., Liu, K., Gao, G.F., and Liu, W.J. (2017). Human T-cell immunity against the emerging and re-emerging viruses. Sci. China Life Sci. *60*, 1307-1316. 10.1007/s11427-017-9241-3.

497. Liu, L., Wei, Q., Lin, Q., Fang, J., Wang, H., Kwok, H., Tang, H., Nishiura, K., Peng, J., Tan, Z., et al. (2019). Anti–spike IgG causes severe acute lung injury by skewing macrophage responses during acute SARS-CoV infection. JCI Insight *4*, e123158. 10.1172/jci.insight.123158.

498. Bergamaschi, L., Mescia, F., Turner, L., Hanson, A.L., Kotagiri, P., Dunmore, B.J., Ruffieux, H., Sa, A.D., Huhn, O., Morgan, M.D., et al. (2021). Longitudinal analysis reveals that delayed bystander CD8+ T cell activation and early immune pathology distinguish severe COVID-19 from mild disease. Immunity *54*, 1257-1275.e1258. 10.1016/j.immuni.2021.05.010.

499. Laing, A.G., Lorenc, A., Barrio, I.d.M.d., Das, A., Fish, M., Monin, L., Muñoz-Ruiz, M., McKenzie, D.R., Hayday, T.S., Francos-Quijorna, I., et al. (2020). A dynamic COVID-19 immune signature includes associations with poor prognosis. Nat Med *26*, 1623-1635. 10.1038/s41591-020-1038-6.

500. Kuri-Cervantes, L., Pampena, M.B., Meng, W., Rosenfeld, A.M., Ittner, C.A.G., Weisman, A.R., Agyekum, R.S., Mathew, D., Baxter, A.E., Vella, L.A., et al. (2020). Comprehensive mapping of immune perturbations associated with severe COVID-19. Sci Immunol *5*, eabd7114. 10.1126/sciimmunol.abd7114.

501. Diao, B., Wang, C., Tan, Y., Chen, X., Liu, Y., Ning, L., Chen, L., Li, M., Liu, Y., Wang, G., et al. (2020). Reduction and Functional Exhaustion of T Cells in Patients With Coronavirus Disease 2019 (COVID-19). Front Immunol *11*, 827. 10.3389/fimmu.2020.00827.

502. Notarbartolo, S., Ranzani, V., Bandera, A., Gruarin, P., Bevilacqua, V., Putignano, A.R., Gobbini, A., Galeota, E., Manara, C., Bombaci, M., et al. (2021). Integrated longitudinal immunophenotypic, transcriptional, and repertoire analyses delineate immune responses in patients with COVID-19. Sci Immunol *6*. 10.1126/sciimmunol.abg5021.

503. Mathew, D., Giles, J.R., Baxter, A.E., Oldridge, D.A., Greenplate, A.R., Wu, J.E., Alanio, C., Kuri-Cervantes, L., Pampena, M.B., D'Andrea, K., et al. (2020). Deep immune profiling of COVID-19 patients reveals distinct immunotypes with therapeutic implications. Science *369*, eabc8511. 10.1126/science.abc8511.

504. Moss, P. (2022). The T cell immune response against SARS-CoV-2. Nat Immunol *23*, 186-193. 10.1038/s41590-021-01122-w.

505. Deinhardt-Emmer, S., Böttcher, S., Häring, C., Giebeler, L., Henke, A., Zell, R., Jungwirth, J., Jordan, P.M., Werz, O., Hornung, F., et al. (2021). SARS-CoV-2 Causes Severe Epithelial Inflammation and Barrier Dysfunction. J Virol *95*, 10.1128/jvi.00110-00121. 10.1128/jvi.00110-21.

506. Song, J.-W., Zhang, C., Fan, X., Meng, F.-P., Xu, Z., Xia, P., Cao, W.-J., Yang, T., Dai, X.-P., Wang, S.-Y., et al. (2020). Immunological and inflammatory profiles in mild and severe cases of COVID-19. Nat. Commun. *11*, 3410. 10.1038/s41467-020-17240-2.

507. Tarke, A., Sidney, J., Kidd, C.K., Dan, J.M., Ramirez, S.I., Yu, E.D., Mateus, J., Antunes, R.d.S., Moore, E., Rubiro, P., et al. (2021). Comprehensive analysis of T cell immunodominance and immunoprevalence of SARS-CoV-2 epitopes in COVID-19 cases. Cell Rep. Med. *2*, 100204. 10.1016/j.xcrm.2021.100204.

508. Stephenson, E., Reynolds, G., Botting, R.A., Calero-Nieto, F.J., Morgan, M.D., Tuong, Z.K., Bach, K., Sungnak, W., Worlock, K.B., Yoshida, M., et al. (2021). Single-cell multi-omics analysis of the immune response in COVID-19. Nat Med *27*, 904-916. 10.1038/s41591-021-01329-2.

509. Boppana, S., Qin, K., Files, J.K., Russell, R.M., Stoltz, R., Bibollet-Ruche, F., Bansal, A., Erdmann, N., Hahn, B.H., and Goepfert, P.A. (2021). SARS-CoV-2-specific circulating T follicular helper cells correlate with neutralizing antibodies and increase during early convalescence. PLoS Pathog. *17*, e1009761. 10.1371/journal.ppat.1009761.

510. Peng, Y., Felce, S.L., Dong, D., Penkava, F., Mentzer, A.J., Yao, X., Liu, G., Yin, Z., Chen, J.-L., Lu, Y., et al. (2022). An immunodominant NP105–113-B*07:02 cytotoxic T cell response controls viral replication and is associated with less severe COVID-19 disease. Nat Immunol *23*, 50-61. 10.1038/s41590-021-01084-z.

511. Wheatley, A.K., Juno, J.A., Wang, J.J., Selva, K.J., Reynaldi, A., Tan, H.-X., Lee, W.S., Wragg, K.M., Kelly, H.G., Esterbauer, R., et al. (2021). Evolution of immune responses to SARS-CoV-2 in mild-moderate COVID-19. Nat. Commun. *12*, 1162. 10.1038/s41467-021-21444-5.

512. Yang, G., Cao, J., Qin, J., Mei, X., Deng, S., Xia, Y., Zhao, J., Wang, J., Luan, T., Chen, D., et al. (2024). Initial COVID-19 severity influenced by SARS-CoV-2-specific T cells imprints T-cell memory and inversely affects reinfection. Signal Transduct. Target. Ther. *9*, 141. 10.1038/s41392-024-01867-4.

513. Gray-Gaillard, S.L., Solis, S.M., Chen, H.M., Monteiro, C., Ciabattoni, G., Samanovic, M.I., Cornelius, A.R., Williams, T., Geesey, E., Rodriguez, M., et al. (2024). SARS-CoV-2 inflammation durably imprints memory CD4 T cells. Sci Immunol *9*, eadj8526. 10.1126/sciimmunol.adj8526.

514. Cohen, K.W., Linderman, S.L., Moodie, Z., Czartoski, J., Lai, L., Mantus, G., Norwood, C., Nyhoff, L.E., Edara, V.V., Floyd, K., et al. (2021). Longitudinal analysis shows durable and broad immune memory after SARS-CoV-2 infection with persisting antibody responses and memory B and T cells. Cell Rep. Med. *2*, 100354. 10.1016/j.xcrm.2021.100354.

515. Jung, M.K., and Shin, E.-C. (2021). Phenotypes and Functions of SARS-CoV-2-Reactive T Cells. Mol. Cells *44*, 401-407. 10.14348/molcells.2021.0079.

516. Adamo, S., Michler, J., Zurbuchen, Y., Cervia, C., Taeschler, P., Raeber, M.E., Sain, S.B., Nilsson, J., Moor, A.E., and Boyman, O. (2022). Signature of long-lived memory CD8+ T cells in acute SARS-CoV-2 infection. Nature *602*, 148-155. 10.1038/s41586-021-04280-x.

517. Tarke, A., Coelho, C.H., Zhang, Z., Dan, J.M., Yu, E.D., Methot, N., Bloom, N.I., Goodwin, B., Phillips, E., Mallal, S., et al. (2021). SARS-CoV-2 vaccination induces immunological memory able to cross-recognize variants from Alpha to Omicron. Biorxiv, 2021.2012.2028.474333. 10.1101/2021.12.28.474333.

518. Szabo, P.A., Dogra, P., Gray, J.I., Wells, S.B., Connors, T.J., Weisberg, S.P., Krupska, I., Matsumoto, R., Poon, M.M.L., Idzikowski, E., et al. (2021). Longitudinal profiling of respiratory and systemic immune responses reveals myeloid cell-driven lung inflammation in severe COVID-19. Immunity *54*, 797-814.e796. 10.1016/j.immuni.2021.03.005.

519. Nielsen, S.C.A., Yang, F., Jackson, K.J.L., Hoh, R.A., Röltgen, K., Jean, G.H., Stevens, B.A., Lee, J.-Y., Rustagi, A., Rogers, A.J., et al. (2020). Human B Cell Clonal Expansion and Convergent Antibody Responses to SARS-CoV-2. Cell Host Microbe *28*, 516-525.e515. 10.1016/j.chom.2020.09.002.

520. Dan, J.M., Mateus, J., Kato, Y., Hastie, K.M., Yu, E.D., Faliti, C.E., Grifoni, A., Ramirez, S.I., Haupt, S., Frazier, A., et al. (2021). Immunological memory to SARS-CoV-2 assessed for up to 8 months after infection. Science *371*, eabf4063. 10.1126/science.abf4063.

521. Sokal, A., Chappert, P., Barba-Spaeth, G., Roeser, A., Fourati, S., Azzaoui, I., Vandenberghe, A., Fernandez, I., Meola, A., Bouvier-Alias, M., et al. (2021). Maturation and persistence of the anti-SARS-CoV-2 memory B cell response. Cell *184*, 1201-1213.e1214. 10.1016/j.cell.2021.01.050.

522. Hartley, G.E., Zelm, M.C.v., and Robinson, M.J. (2022). The benefit of boosters: diversity and inclusion in the COVID-19 memory response. Immunol. Cell Biol. *100*, 15-17. 10.1111/imcb.12511.

523. Long, Q.-X., Liu, B.-Z., Deng, H.-J., Wu, G.-C., Deng, K., Chen, Y.-K., Liao, P., Qiu, J.-F., Lin, Y., Cai, X.-F., et al. (2020). Antibody responses to SARS-CoV-2 in patients with COVID-19. Nat Med *26*, 845-848. 10.1038/s41591-020-0897-1.

524. Anderson, E.M., Goodwin, E.C., Verma, A., Arevalo, C.P., Bolton, M.J., Weirick, M.E., Gouma, S., McAllister, C.M., Christensen, S.R., Weaver, J., et al. (2021). Seasonal human coronavirus antibodies are boosted upon SARS-CoV-2 infection but not associated with protection. Cell *184*, 1858-1864.e1810. 10.1016/j.cell.2021.02.010.

525. Röltgen, K., and Boyd, S.D. (2021). Antibody and B cell responses to SARS-CoV-2 infection and vaccination. Cell Host Microbe *29*, 1063-1075. 10.1016/j.chom.2021.06.009.

526. Temperton, N.J., Chan, P.K., Simmons, G., Zambon, M.C., Tedder, R.S., Takeuchi, Y., and Weiss, R.A. (2005). Longitudinally Profiling Neutralizing Antibody Response to SARS Coronavirus with Pseudotypes - Volume 11, Number 3—March 2005 - Emerging Infectious Diseases journal - CDC. Emerg. Infect. Dis. *11*, 411-416. 10.3201/eid1103.040906.

527. Piccoli, L., Park, Y.-J., Tortorici, M.A., Czudnochowski, N., Walls, A.C., Beltramello, M., Silacci-Fregni, C., Pinto, D., Rosen, L.E., Bowen, J.E., et al. (2020). Mapping Neutralizing and Immunodominant Sites on the SARS-CoV-2 Spike Receptor-Binding Domain by Structure-Guided High-Resolution Serology. Cell *183*, 1024-+. 10.1016/j.cell.2020.09.037.

528. Röltgen, K., Powell, A.E., Wirz, O.F., Stevens, B.A., Hogan, C.A., Najeeb, J., Hunter, M., Wang, H., Sahoo, M.K., Huang, C., et al. (2020). Defining the features and duration of antibody responses to SARS-CoV-2 infection associated with disease severity and outcome. Sci Immunol *5*, eabe0240. 10.1126/sciimmunol.abe0240.

529. Shrock, E., Fujimura, E., Kula, T., Timms, R.T., Lee, I.H., Leng, Y., Robinson, M.L., Sie, B.M., Li, M.Z., Chen, Y., et al. (2020). Viral epitope profiling of COVID-19 patients reveals cross-reactivity and correlates of severity. Science *370*, eabd4250. 10.1126/science.abd4250.

530. Zhu, A., Liu, M., Li, Y., Lei, Q., Wu, Q., Lin, M., Lai, D., Lu, L., Yu, S., Guo, S., et al. (2022). Age- and Severity-Associated Humoral Immunity Response in COVID-19 Patients: A Cohort Study from Wuhan, China. J. Clin. Med. *11*, 5974. 10.3390/jcm11195974.

531. Hansen, C.B., Jarlhelt, I., Pérez-Alós, L., Landsy, L.H., Loftager, M., Rosbjerg, A., Helgstrand, C., Bjelke, J.R., Egebjerg, T., Jardine, J.G., et al. (2020). SARS-CoV-2 Antibody Responses Are Correlated to Disease Severity in COVID-19 Convalescent Individuals. J Immunol *206*, ji2000898. 10.4049/jimmunol.2000898.

532. Cohen, C.A., Li, A.P.Y., Hachim, A., Hui, D.S.C., Kwan, M.Y.W., Tsang, O.T.Y., Chiu, S.S., Chan, W.H., Yau, Y.S., Kavian, N., et al. (2021). SARS-CoV-2 specific T cell responses are lower in children and increase with age and time after infection. Nat. Commun. *12*, 4678. 10.1038/s41467-021-24938-4.

533. Hachim, A., Gu, H., Kavian, O., Mori, M., Kwan, M.Y.W., Chan, W.H., Yau, Y.S., Chiu, S.S., Tsang, O.T.Y., Hui, D.S.C., et al. (2022). SARS-CoV-2 accessory proteins reveal distinct serological signatures in children. Nat. Commun. *13*, 2951. 10.1038/s41467-022-30699-5.

534. Larsen, M.D., Graaf, E.L.d., Sonneveld, M.E., Plomp, H.R., Nouta, J., Hoepel, W., Chen, H.-J., Linty, F., Visser, R., Brinkhaus, M., et al. (2021). Afucosylated

IgG characterizes enveloped viral responses and correlates with COVID-19 severity. Science *371*, eabc8378. 10.1126/science.abc8378.

535. Butler, S.E., Crowley, A.R., Natarajan, H., Xu, S., Weiner, J.A., Bobak, C.A., Mattox, D.E., Lee, J., Wieland-Alter, W., Connor, R.I., et al. (2021). Distinct Features and Functions of Systemic and Mucosal Humoral Immunity Among SARS-CoV-2 Convalescent Individuals. Front Immunol *11*, 618685. 10.3389/fimmu.2020.618685.

536. Wang, Z., Lorenzi, J.C.C., Muecksch, F., Finkin, S., Viant, C., Gaebler, C., Cipolla, M., Hoffmann, H.-H., Oliveira, T.Y., Oren, D.A., et al. (2021). Enhanced SARS-CoV-2 neutralization by dimeric IgA. Sci Transl Med *13*, eabf1555. 10.1126/scitranslmed.abf1555.

537. Leekha, A., Saeedi, A., Sefat, K.M.S.R., Kumar, M., Martinez-Paniagua, M., Damian, A., Kulkarni, R., Reichel, K., Rezvan, A., Masoumi, S., et al. (2024). Multi-antigen intranasal vaccine protects against challenge with sarbecoviruses and prevents transmission in hamsters. Nat. Commun. *15*, 6193. 10.1038/s41467-024-50133-2.

538. Leekha, A., Saeedi, A., Kumar, M., Sefat, K.M.S.R., Martinez-Paniagua, M., Meng, H., Fathi, M., Kulkarni, R., Reichel, K., Biswas, S., et al. (2024). An intranasal nanoparticle STING agonist protects against respiratory viruses in animal models. Nat. Commun. *15*, 6053. 10.1038/s41467-024-50234-y.

539. Hastie, K.M., Li, H., Bedinger, D., Schendel, S.L., Dennison, S.M., Li, K., Rayaprolu, V., Yu, X., Mann, C., Zandonatti, M., et al. (2021). Defining variant-

resistant epitopes targeted by SARS-CoV-2 antibodies: A global consortium study. Science *374*, 472-478. 10.1126/science.abh2315.

540. Tong, P., Gautam, A., Windsor, I.W., Travers, M., Chen, Y., Garcia, N., Whiteman, N.B., McKay, L.G.A., Storm, N., Malsick, L.E., et al. (2021). Memory B cell repertoire for recognition of evolving SARS-CoV-2 spike. Cell *184*, 4969-4980.e4915. 10.1016/j.cell.2021.07.025.

541. Yuan, M., Liu, H., Wu, N.C., and Wilson, I.A. (2021). Recognition of the SARS-CoV-2 receptor binding domain by neutralizing antibodies. Biochem Bioph Res Co *538*, 192-203. 10.1016/j.bbrc.2020.10.012.

542. Suryadevara, N., Shrihari, S., Gilchuk, P., VanBlargan, L.A., Binshtein, E., Zost, S.J., Nargi, R.S., Sutton, R.E., Winkler, E.S., Chen, E.C., et al. (2021). Neutralizing and protective human monoclonal antibodies recognizing the N-terminal domain of the SARS-CoV-2 spike protein. Cell *184*, 2316-2331.e2315. 10.1016/j.cell.2021.03.029.

543. Administration, F., and Drug Fact Sheet for Patients, Parents, and Caregivers Emergency Use Authorization (EUA) of PEMGARDA (pemivibart) for Coronavirus Disease 2019 (COVID-19).

544. Administration, F., and Drug (2024). EMERGENCY USE AUTHORIZATION OF PEMGARDA (PEMIVIBART).

545. Rappazzo, C.G., Tse, L.V., Kaku, C.I., Wrapp, D., Sakharkar, M., Huang, D., Deveau, L.M., Yockachonis, T.J., Herbert, A.S., Battles, M.B., et al. (2021). Broad and potent activity against SARS-like viruses by an engineered human monoclonal antibody. Science *371*, 823-829. 10.1126/science.abf4830.

546. Pinto, D., Park, Y.-J., Beltramello, M., Walls, A.C., Tortorici, M.A., Bianchi, S., Jaconi, S., Culap, K., Zatta, F., Marco, A.D., et al. (2020). Cross-neutralization of SARS-CoV-2 by a human monoclonal SARS-CoV antibody. Nature *583*, 290-295. 10.1038/s41586-020-2349-y.

547. Addetia, A., Park, Y.-J., Starr, T., Greaney, A.J., Sprouse, K.R., Bowen, J.E., Tiles, S.W., Voorhis, W.C.V., Bloom, J.D., Corti, D., et al. (2023). Structural changes in the SARS-CoV-2 spike E406W mutant escaping a clinical monoclonal antibody cocktail. Cell Reports *42*, 112621. 10.1016/j.celrep.2023.112621.

548. Rosen, L.E., Tortorici, M.A., Marco, A.D., Pinto, D., Foreman, W.B., Taylor, A.L., Park, Y.-J., Bohan, D., Rietz, T., Errico, J.M., et al. (2024). A potent pan-sarbecovirus neutralizing antibody resilient to epitope diversification. Cell *187*, 7196-7213.e7126. 10.1016/j.cell.2024.09.026.

549. Starr, T.N., Czudnochowski, N., Liu, Z., Zatta, F., Park, Y.-J., Addetia, A., Pinto, D., Beltramello, M., Hernandez, P., Greaney, A.J., et al. (2021). SARS-CoV-2 RBD antibodies that maximize breadth and resistance to escape. Nature *597*, 97-102. 10.1038/s41586-021-03807-6.

550. Tortorici, M.A., Czudnochowski, N., Starr, T.N., Marzi, R., Walls, A.C., Zatta, F., Bowen, J.E., Jaconi, S., Iulio, J.D., Wang, Z., et al. (2021). Broad sarbecovirus neutralization by a human monoclonal antibody. Nature *597*, 103-108. 10.1038/s41586-021-03817-4.

551. Pinto, D., Sauer, M.M., Czudnochowski, N., Low, J.S., Tortorici, M.A., Housley, M.P., Noack, J., Walls, A.C., Bowen, J.E., Guarino, B., et al. (2021). Broad

betacoronavirus neutralization by a stem helix–specific human antibody. Science *373*, 1109-1116. 10.1126/science.abj3321.

552. Dacon, C., Peng, L., Lin, T.-H., Tucker, C., Lee, C.-C.D., Cong, Y., Wang, L., Purser, L., Cooper, A.J.R., Williams, J.K., et al. (2023). Rare, convergent antibodies targeting the stem helix broadly neutralize diverse betacoronaviruses. Cell Host Microbe *31*, 97-111.e112. 10.1016/j.chom.2022.10.010.

553. Low, J.S., Jerak, J., Tortorici, M.A., McCallum, M., Pinto, D., Cassotta, A., Foglierini, M., Mele, F., Abdelnabi, R., Weynand, B., et al. (2022). ACE2-binding exposes the SARS-CoV-2 fusion peptide to broadly neutralizing coronavirus antibodies. Science *377*, eabq2679. 10.1126/science.abq2679.

554. Dacon, C., Tucker, C., Peng, L., Lee, C.-C.D., Lin, T.-H., Yuan, M., Cong, Y., Wang, L., Purser, L., Williams, J.K., et al. (2022). Broadly neutralizing antibodies target the coronavirus fusion peptide. Science *377*, eabq3773. 10.1126/science.abq3773.

555. Zhou, P., Yuan, M., Song, G., Beutler, N., Shaabani, N., Huang, D., He, W.-t., Zhu, X., Callaghan, S., Yong, P., et al. (2022). A human antibody reveals a conserved site on beta-coronavirus spike proteins and confers protection against SARS-CoV-2 infection. Sci Transl Med *14*, eabi9215. 10.1126/scitranslmed.abi9215.

556. Zhou, B., Zhou, R., Tang, B., Chan, J.F.-W., Luo, M., Peng, Q., Yuan, S., Liu, H., Mok, B.W.-Y., Chen, B., et al. (2022). A broadly neutralizing antibody protects Syrian hamsters against SARS-CoV-2 Omicron challenge. Nat. Commun. *13*, 3589. 10.1038/s41467-022-31259-7.

557. Edwards, C.T., Karunakaran, K.A., Garcia, E., Beutler, N., Gagne, M., Golden, N., Aoued, H., Pellegrini, K.L., Burnett, M.R., Honeycutt, C.C., et al. (2024). Passive infusion of an S2-Stem broadly neutralizing antibody protects against SARS-CoV-2 infection and lower airway inflammation in rhesus macaques. Biorxiv. 10.1101/2024.07.30.605768.

558. Sette, A., and Crotty, S. (2022). Immunological memory to SARS-CoV-2 infection and COVID-19 vaccines. Immunol Rev *310*, 27-46. 10.1111/imr.13089.

559. Mathieu, E., Ritchie, H., Rodés-Guirao, L., Appel, C., Gavrilov, D., Giattino, C., Hasell, J., Macdonald, B., Dattani, S., Beltekian, D., et al. Coronavirus (COVID-19) Vaccinations - Our World in Data. Coronavirus (COVID-19) Vaccinations.

560. Administration, F., and Drug (2021). FDA Approves First COVID-19 Vaccine.

561. Thomas, S.J., Moreira, E.D., Kitchin, N., Absalon, J., Gurtman, A., Lockhart, S., Perez, J.L., Marc, G.P., Polack, F.P., Zerbini, C., et al. (2021). Safety and Efficacy of the BNT162b2 mRNA Covid-19 Vaccine through 6 Months. N. Engl. J. Med. *385*, 1761-1773. 10.1056/nejmoa2110345.

562. Administration, U.S.F., and Drug (2020). Moderna COVID-19 Vaccine EUA Letter of Authorization.

563. Zinatizadeh, M.R., Zarandi, P.K., Zinatizadeh, M., Yousefi, M.H., Amani, J., and Rezaei, N. (2022). Efficacy of mRNA, adenoviral vector, and perfusion protein COVID-19 vaccines. Biomed. Pharmacother. *146*, 112527. 10.1016/j.biopha.2021.112527.

564. Atmar, R.L., Lyke, K.E., Deming, M.E., Jackson, L.A., Branche, A.R., Sahly, H.M.E., Rostad, C.A., Martin, J.M., Johnston, C., Rupp, R.E., et al. (2022).

Homologous and Heterologous Covid-19 Booster Vaccinations. N. Engl. J. Med. *386*, 1046-1057. 10.1056/nejmoa2116414.

565. Administration, F., and Drug (2023). Revocation of EUA 27205 - Janssen COVID-19 Vaccine.

566. MacNeil, J.R., Su, J.R., Broder, K.R., Guh, A.Y., Gargano, J.W., Wallace, M., Hadler, S.C., Scobie, H.M., Blain, A.E., Moulia, D., et al. (2021). Updated Recommendations from the Advisory Committee on Immunization Practices for Use of the Janssen (Johnson & Johnson) COVID-19 Vaccine After Reports of Thrombosis with Thrombocytopenia Syndrome Among Vaccine Recipients — United States, April 2021. Morb. Mortal. Wkly. Rep. *70*, 651-656. 10.15585/mmwr.mm7017e4.

567. Administration, F., and Drug (2023). Coronavirus (COVID-19) Update: FDA Authorizes Changes to Simplify Use of Bivalent mRNA COVID-19 Vaccines.

568. Administration, F., and Drug (2023). Recommendation for the 2023-2024 Formula of COVID-19 vaccines in the U.S.

569. Tartof, S.Y., Slezak, J.M., Puzniak, L., Frankland, T.B., Ackerson, B.K., Jodar, L., and McLaughlin, J.M. (2024). Effectiveness of BNT162b2 XBB Vaccine Against XBB and JN.1 Sublineages. Open Forum Infect. Dis. *11*, ofae370. 10.1093/ofid/ofae370.

570. Ma, K.C., Castro, J., Lambrou, A.S., Rose, E.B., Cook, P.W., Batra, D., Cubenas, C., Hughes, L.J., MacCannell, D.R., Mandal, P., et al. (2024). Genomic Surveillance for SARS-CoV-2 Variants: Circulation of Omicron XBB and JN.1

Lineages — United States, May 2023–September 2024. Morb. Mortal. Wkly. Rep. *73*, 938-945. 10.15585/mmwr.mm7342a1.

571. Patel, N., Trost, J.F., Guebre-Xabier, M., Zhou, H., Norton, J., Jiang, D., Cai, Z., Zhu, M., Marchese, A.M., Greene, A.M., et al. (2023). XBB.1.5 spike protein COVID-19 vaccine induces broadly neutralizing and cellular immune responses against EG.5.1 and emerging XBB variants. Sci Rep-uk *13*, 19176. 10.1038/s41598-023-46025-y.

572. Hadfield, J., Megill, C., Bell, S.M., et al. (2025). Nextstrain: real-time tracking of pathogen evolution. Nextstrain / ncov / gisaid / global / 6m.

573. Reynolds, C.J., Gibbons, J.M., Pade, C., Lin, K.-M., Sandoval, D.M., Pieper, F., Butler, D.K., Liu, S., Otter, A.D., Joy, G., et al. (2022). Heterologous infection and vaccination shapes immunity against SARS-CoV-2 variants. Science *375*, 183-192. 10.1126/science.abm0811.

574. Collier, A.-r.Y., Miller, J., Hachmann, N.P., McMahan, K., Liu, J., Bondzie, E.A., Gallup, L., Rowe, M., Schonberg, E., Thai, S., et al. (2023). Immunogenicity of BA.5 Bivalent mRNA Vaccine Boosters. N. Engl. J. Med. *388*, 565-567. 10.1056/nejmc2213948.

575. Aydillo, T., Rombauts, A., Stadlbauer, D., Aslam, S., Abelenda-Alonso, G., Escalera, A., Amanat, F., Jiang, K., Krammer, F., Carratala, J., and García-Sastre, A. (2021). Immunological imprinting of the antibody response in COVID-19 patients. Nat. Commun. *12*, 3781. 10.1038/s41467-021-23977-1.

576. Dunkle, L.M., Kotloff, K.L., Gay, C.L., Áñez, G., Adelglass, J.M., Hernández, A.Q.B., Harper, W.L., Duncanson, D.M., McArthur, M.A., Florescu, D.F., et al.

(2021). Efficacy and Safety of NVX-CoV2373 in Adults in the United States and Mexico. N. Engl. J. Med. *386*, 531-543. 10.1056/nejmoa2116185.

577. Committee, F., Drug Administration, V., and Related Biological Products, A. (2023). Novavax COVID-19 Vaccine, Adjuvanted.

578. Heath, P.T., Galiza, E.P., Baxter, D.N., Boffito, M., Browne, D., Burns, F., Chadwick, D.R., Clark, R., Cosgrove, C., Galloway, J., et al. (2021). Safety and Efficacy of NVX-CoV2373 Covid-19 Vaccine. N. Engl. J. Med. *385*, 1172-1183. 10.1056/nejmoa2107659.

579. Administration, F., and Drug (2023). FDA Authorizes Updated Novavax COVID-19 Vaccine Formulated to Better Protect Against Currently Circulating Variants.

580. Administration, F., and Drug (2024). Novavax-LOA-2024-2025.

581. Inc, N. (2022). FDA Grants Emergency Use Authorization for Novavax COVID-19 Vaccine, Adjuvanted for Adolescents Aged 12 Through 17.

582. Sheng, W.-H., Lin, P.-H., Cheng, Y.-C., Wu, Y.-Y., Hsieh, M.-J., Yang, H.-C., Chang, S.-Y., and Chang, S.-C. (2024). Immunogenicity and safety of heterologous booster with protein-based COVID-19 vaccine (NVX-CoV2373) in healthy adults: A comparative analysis with mRNA vaccines. J. Formos. Méd. Assoc. *123*, 340-346. 10.1016/j.jfma.2023.10.012.

583. Mallory, R.M., Formica, N., Pfeiffer, S., Wilkinson, B., Marcheschi, A., Albert, G., McFall, H., Robinson, M., Plested, J.S., Zhu, M., et al. (2022). Safety and immunogenicity following a homologous booster dose of a SARS-CoV-2 recombinant spike protein vaccine (NVX-CoV2373): a secondary analysis of a

randomised, placebo-controlled, phase 2 trial. Lancet Infect. Dis. *22*, 1565-1576. 10.1016/s1473-3099(22)00420-0.

584. Tan, W., Zhao, X., Ma, X., Wang, W., Niu, P., Xu, W., Gao, G.F., and Wu, G. (2020). A Novel Coronavirus Genome Identified in a Cluster of Pneumonia Cases - Wuhan, China 2019-2020. China CDC Wkly. *2*, 61-62.

585. Cui, J., Li, F., and Shi, Z.-L. (2019). Origin and evolution of pathogenic coronaviruses. Nat Rev Microbiol *17*, 181-192. 10.1038/s41579-018-0118-9.

586. Forni, D., Cagliani, R., Clerici, M., and Sironi, M. (2017). Molecular Evolution of Human Coronavirus Genomes. Trends Microbiol. *25*, 35-48. 10.1016/j.tim.2016.09.001.

587. Mackay, I.M., and Arden, K.E. (2015). MERS coronavirus: diagnostics, epidemiology and transmission. Virol. J. *12*, 222. 10.1186/s12985-015-0439-5.

588. Stadler, K., Masignani, V., Eickmann, M., Becker, S., Abrignani, S., Klenk, H.-D., and Rappuoli, R. (2003). SARS — beginning to understand a new virus. Nat Rev Microbiol *1*, 209-218. 10.1038/nrmicro775.

589. Walsh, E.E., Jr, R.W.F., Falsey, A.R., Kitchin, N., Absalon, J., Gurtman, A., Lockhart, S., Neuzil, K., Mulligan, M.J., Bailey, R., et al. (2020). Safety and Immunogenicity of Two RNA-Based Covid-19 Vaccine Candidates. N. Engl. J. Med. *383*, 2439-2450. 10.1056/nejmoa2027906.

590. Anderson, E.J., Rouphael, N.G., Widge, A.T., Jackson, L.A., Roberts, P.C., Makhene, M., Chappell, J.D., Denison, M.R., Stevens, L.J., Pruijssers, A.J., et al. (2020). Safety and Immunogenicity of SARS-CoV-2 mRNA-1273 Vaccine in Older Adults. N. Engl. J. Med. *383*, 2427-2438. 10.1056/nejmoa2028436.

591. Folegatti, P.M., Ewer, K.J., Aley, P.K., Angus, B., Becker, S., Belij-Rammerstorfer, S., Bellamy, D., Bibi, S., Bittaye, M., Clutterbuck, E.A., et al. (2020). Safety and immunogenicity of the ChAdOx1 nCoV-19 vaccine against SARS-CoV-2: a preliminary report of a phase 1/2, single-blind, randomised controlled trial. Lancet *396*, 467-478. 10.1016/s0140-6736(20)31604-4.

592. Ramasamy, M.N., Minassian, A.M., Ewer, K.J., Flaxman, A.L., Folegatti, P.M., Owens, D.R., Voysey, M., Aley, P.K., Angus, B., Babbage, G., et al. (2021). Safety and immunogenicity of ChAdOx1 nCoV-19 vaccine administered in a prime-boost regimen in young and old adults (COV002): a single-blind, randomised, controlled, phase 2/3 trial. Lancet *396*, 1979-1993. 10.1016/s0140-6736(20)32466-1.

593. Zhu, F.-C., Guan, X.-H., Li, Y.-H., Huang, J.-Y., Jiang, T., Hou, L.-H., Li, J.-X., Yang, B.-F., Wang, L., Wang, W.-J., et al. (2020). Immunogenicity and safety of a recombinant adenovirus type-5-vectored COVID-19 vaccine in healthy adults aged 18 years or older: a randomised, double-blind, placebo-controlled, phase 2 trial. Lancet *396*, 479-488. 10.1016/s0140-6736(20)31605-6.

594. Voysey, M., Clemens, S.A.C., Madhi, S.A., Weckx, L.Y., Folegatti, P.M., Aley, P.K., Angus, B., Baillie, V.L., Barnabas, S.L., Bhorat, Q.E., et al. (2021). Safety and efficacy of the ChAdOx1 nCoV-19 vaccine (AZD1222) against SARS-CoV-2: an interim analysis of four randomised controlled trials in Brazil, South Africa, and the UK. Lancet *397*, 99-111. 10.1016/s0140-6736(20)32661-1.

595. Sahin, U., Muik, A., Vogler, I., Derhovanessian, E., Kranz, L.M., Vormehr, M., Quandt, J., Bidmon, N., Ulges, A., Baum, A., et al. (2021). BNT162b2 vaccine

induces neutralizing antibodies and poly-specific T cells in humans. Nature *595*, 572-577. 10.1038/s41586-021-03653-6.

596. Sahin, U., Muik, A., Derhovanessian, E., Vogler, I., Kranz, L.M., Vormehr, M., Baum, A., Pascal, K., Quandt, J., Maurus, D., et al. (2020). COVID-19 vaccine BNT162b1 elicits human antibody and TH1 T cell responses. Nature *586*, 594-599. 10.1038/s41586-020-2814-7.

597. Frater, J., Ewer, K.J., Ogbe, A., Pace, M., Adele, S., Adland, E., Alagaratnam, J., Aley, P.K., Ali, M., Ansari, M.A., et al. (2021). Safety and immunogenicity of the ChAdOx1 nCoV-19 (AZD1222) vaccine against SARS-CoV-2 in HIV infection: a single-arm substudy of a phase 2/3 clinical trial. Lancet HIV *8*, e474-e485. 10.1016/s2352-3018(21)00103-x.

598. Stephenson, K.E., Gars, M.L., Sadoff, J., Groot, A.M.d., Heerwegh, D., Truyers, C., Atyeo, C., Loos, C., Chandrashekar, A., McMahan, K., et al. (2021). Immunogenicity of the Ad26.COV2.S Vaccine for COVID-19. JAMA *325*, 1535-1544. 10.1001/jama.2021.3645.

599. Keech, C., Albert, G., Cho, I., Robertson, A., Reed, P., Neal, S., Plested, J.S., Zhu, M., Cloney-Clark, S., Zhou, H., et al. (2020). Phase 1–2 Trial of a SARS-CoV-2 Recombinant Spike Protein Nanoparticle Vaccine. N. Engl. J. Med. *383*, 2320-2332. 10.1056/nejmoa2026920.

600. Tai, W., Zhang, X., Drelich, A., Shi, J., Hsu, J.C., Luchsinger, L., Hillyer, C.D., Tseng, C.-T.K., Jiang, S., and Du, L. (2020). A novel receptor-binding domain (RBD)-based mRNA vaccine against SARS-CoV-2. Cell Res. *30*, 932-935. 10.1038/s41422-020-0387-5.

601. Pardi, N., Hogan, M.J., and Weissman, D. (2020). Recent advances in mRNA vaccine technology. Curr. Opin. Immunol. *65*, 14-20. 10.1016/j.coi.2020.01.008.

602. Szabó, G.T., Mahiny, A.J., and Vlatkovic, I. (2022). COVID-19 mRNA vaccines: Platforms and current developments. Mol. Ther. *30*, 1850-1868. 10.1016/j.ymthe.2022.02.016.

603. Baden, L.R., Sahly, H.M.E., Essink, B., Kotloff, K., Frey, S., Novak, R., Diemert, D., Spector, S.A., Rouphael, N., Creech, C.B., et al. (2020). Efficacy and Safety of the mRNA-1273 SARS-CoV-2 Vaccine. N. Engl. J. Med. *384*, 403-416. 10.1056/nejmoa2035389.

604. Bellino, S. (2021). COVID-19 vaccines approved in the European Union: current evidence and perspectives. Expert Rev. Vaccines *20*, 1195-1199. 10.1080/14760584.2021.1962304.

605. Agency, E.M. (2021). EMA recommends COVID-19 Vaccine AstraZeneca for authorisation in the EU.

606. Serra, N., Andriolo, M., Butera, I., Mazzola, G., Sergi, C.M., Fasciana, T.M.A., Giammanco, A., Gagliano, M.C., Cascio, A., and Carlo, P.D. (2023). A Serological Analysis of the Humoral Immune Responses of Anti-RBD IgG, Anti-S1 IgG, and Anti-S2 IgG Levels Correlated to Anti-N IgG Positivity and Negativity in Sicilian Healthcare Workers (HCWs) with Third Doses of the mRNA-Based SARS-CoV-2 Vaccine: A Retrospective Cohort Study. Nato Adv Sci Inst Se *11*, 1136. 10.3390/vaccines11071136.

607. Błaszczuk, A., Michalski, A., Malm, M., Drop, B., and Polz-Dacewicz, M. (2022). Antibodies to NCP, RBD and S2 SARS-CoV-2 in Vaccinated and Unvaccinated Healthcare Workers. Nato Adv Sci Inst Se *10*, 1169. 10.3390/vaccines10081169.

608. Agnihothram, S., Gopal, R., Yount, B.L., Donaldson, E.F., Menachery, V.D., Graham, R.L., Scobey, T.D., Gralinski, L.E., Denison, M.R., Zambon, M., and Baric, R.S. (2014). Evaluation of Serologic and Antigenic Relationships Between Middle Eastern Respiratory Syndrome Coronavirus and Other Coronaviruses to Develop Vaccine Platforms for the Rapid Response to Emerging Coronaviruses. J. Infect. Dis. *209*, 995-1006. 10.1093/infdis/jit609.

609. Huang, A.T., Garcia-Carreras, B., Hitchings, M.D.T., Yang, B., Katzelnick, L.C., Rattigan, S.M., Borgert, B.A., Moreno, C.A., Solomon, B.D., Trimmer-Smith, L., et al. (2020). A systematic review of antibody mediated immunity to coronaviruses: kinetics, correlates of protection, and association with severity. Nat. Commun. *11*, 4704. 10.1038/s41467-020-18450-4.

610. Li, Y., Ma, M.-l., Lei, Q., Wang, F., Hong, W., Lai, D.-y., Hou, H., Xu, Z.-w., Zhang, B., Chen, H., et al. (2021). Linear epitope landscape of the SARS-CoV-2 Spike protein constructed from 1,051 COVID-19 patients. Cell Reports *34*, 108915-108915. 10.1016/j.celrep.2021.108915.

611. Ladner, J.T., Henson, S.N., Boyle, A.S., Engelbrektson, A.L., Fink, Z.W., Rahee, F., D'ambrozio, J., Schaecher, K.E., Stone, M., Dong, W., et al. (2021). Epitope-resolved profiling of the SARS-CoV-2 antibody response identifies cross-reactivity with endemic human coronaviruses. Cell Rep. Med. *2*, 100189. 10.1016/j.xcrm.2020.100189.

612. Aguilar-Bretones, M., Fouchier, R.A.M., Koopmans, M.P.G., and Nierop, G.P.v. (2023). Impact of antigenic evolution and original antigenic sin on SARS-CoV-2 immunity. J Clin Invest *133*, e162192. 10.1172/jci162192.

613. Sauer, M.M., Tortorici, M.A., Park, Y.-J., Walls, A.C., Homad, L., Acton, O., Bowen, J., Wang, C., Xiong, X., Schueren, W.d.v.d., et al. (2021). Structural basis for broad coronavirus neutralization. Biorxiv, 2020.2012.2029.424482. 10.1101/2020.12.29.424482.

614. Wang, C., Haperen, R.v., Gutiérrez-Álvarez, J., Li, W., Okba, N.M.A., Albulescu, I., Widjaja, I., Dieren, B.v., Fernandez-Delgado, R., Sola, I., et al. (2021). A conserved immunogenic and vulnerable site on the coronavirus spike protein delineated by cross-reactive monoclonal antibodies. Nat. Commun. *12*, 1715. 10.1038/s41467-021-21968-w.

615. Dejnirattisai, W., Huo, J., Zhou, D., Zahradník, J., Supasa, P., Liu, C., Duyvesteyn, H.M.E., Ginn, H.M., Mentzer, A.J., Tuekprakhon, A., et al. (2022). SARS-CoV-2 Omicron-B.1.1.529 leads to widespread escape from neutralizing antibody responses. Cell *185*, 467-484.e415. 10.1016/j.cell.2021.12.046.

616. Leung, K., Shum, M.H.H., Leung, G.M., Lam, T.T.Y., and Wu, J.T. (2021). Early transmissibility assessment of the N501Y mutant strains of SARS-CoV-2 in the United Kingdom, October to November 2020. Eurosurveillance *26*, 2002106. 10.2807/1560-7917.es.2020.26.1.2002106.

617. Makoni, M. (2021). South Africa responds to new SARS-CoV-2 variant. Lancet (Lond., Engl.) *397*, 267-267. 10.1016/s0140-6736(21)00144-6.

618. Faria, N.R., Mellan, T.A., Whittaker, C., Claro, I.M., Candido, D.d.S., Mishra, S., Crispim, M.A.E., Sales, F.C.S., Hawryluk, I., McCrone, J.T., et al. (2021). Genomics and epidemiology of the P.1 SARS-CoV-2 lineage in Manaus, Brazil. Sci. (N. York, Ny) *372*, 815-821. 10.1126/science.abh2644.

619. Singh, J., Rahman, S.A., Ehtesham, N.Z., Hira, S., and Hasnain, S.E. (2021). SARS-CoV-2 variants of concern are emerging in India. Nat Med *27*, 1131-1133. 10.1038/s41591-021-01397-4.

620. Zhou, Y., Zhi, H., and Teng, Y. (2023). The outbreak of SARS-CoV-2 Omicron lineages, immune escape, and vaccine effectivity. J. Méd. Virol. *95*, 10.1002/jmv.28138. 10.1002/jmv.28138.

621. Rambaut, A., Holmes, E.C., O'Toole, Á., Hill, V., McCrone, J.T., Ruis, C., Plessis, L.d., and Pybus, O.G. (2020). A dynamic nomenclature proposal for SARS-CoV-2 lineages to assist genomic epidemiology. Nat. Microbiol. *5*, 1403-1407. 10.1038/s41564-020-0770-5.

622. Pastorio, C., Zech, F., Noettger, S., Jung, C., Jacob, T., Sanderson, T., Sparrer, K.M.J., and Kirchhoff, F. (2022). Determinants of Spike infectivity, processing, and neutralization in SARS-CoV-2 Omicron subvariants BA.1 and BA.2. Cell Host Microbe *30*, 1255-1268.e1255. 10.1016/j.chom.2022.07.006.

623. Liu, Y., and Rocklöv, J. (2022). The effective reproductive number of the Omicron variant of SARS-CoV-2 is several times relative to Delta. J. Travel Med. *29*, taac037. 10.1093/jtm/taac037.

624. Willett, B.J., Grove, J., MacLean, O.A., Wilkie, C., Lorenzo, G.D., Furnon, W., Cantoni, D., Scott, S., Logan, N., Ashraf, S., et al. (2022). SARS-CoV-2 Omicron

is an immune escape variant with an altered cell entry pathway. Nat. Microbiol. *7*, 1161-1179. 10.1038/s41564-022-01143-7.

625. Rogers, T.F., Zhao, F., Huang, D., Beutler, N., Burns, A., He, W.-t., Limbo, O., Smith, C., Song, G., Woehl, J., et al. (2020). Isolation of potent SARS-CoV-2 neutralizing antibodies and protection from disease in a small animal model. Sci. (N. York, Ny) *369*, 956-963. 10.1126/science.abc7520.

626. Robbiani, D.F., Gaebler, C., Muecksch, F., Lorenzi, J.C.C., Wang, Z., Cho, A., Agudelo, M., Barnes, C.O., Gazumyan, A., Finkin, S., et al. (2020). Convergent Antibody Responses to SARS-CoV-2 in Convalescent Individuals. Nature *584*, 437-442. 10.1038/s41586-020-2456-9.

627. Li, F. (2015). Structure, Function, and Evolution of Coronavirus Spike Proteins. Annu. Rev. Virol. *3*, 1-25. 10.1146/annurev-virology-110615-042301.

628. Walls, A.C., Park, Y.-J., Tortorici, M.A., Wall, A., McGuire, A.T., and Veesler, D. (2020). Structure, Function, and Antigenicity of the SARS-CoV-2 Spike Glycoprotein. Cell *181*, 281-292.e286. 10.1016/j.cell.2020.02.058.

629. Wrapp, D., Wang, N., Corbett, K.S., Goldsmith, J.A., Hsieh, C.-L., Abiona, O., Graham, B.S., and McLellan, J.S. (2020). Cryo-EM structure of the 2019-nCoV spike in the prefusion conformation. Sci. (N. York, Ny) *367*, 1260-1263. 10.1126/science.abb2507.

630. Mascola, J.R., Graham, B.S., and Fauci, A.S. (2021). SARS-CoV-2 Viral Variants—Tackling a Moving Target. JAMA *325*, 1261-1262. 10.1001/jama.2021.2088.

631. Wang, P., Nair, M.S., Liu, L., Iketani, S., Luo, Y., Guo, Y., Wang, M., Yu, J., Zhang, B., Kwong, P.D., et al. (2021). Antibody resistance of SARS-CoV-2 variants B.1.351 and B.1.1.7. Nature *593*, 130-135. 10.1038/s41586-021-03398-2.

632. Guo, L., Lin, S., Chen, Z., Cao, Y., He, B., and Lu, G. (2023). Targetable elements in SARS-CoV-2 S2 subunit for the design of pan-coronavirus fusion inhibitors and vaccines. Signal Transduct. Target. Ther. *8*, 197. 10.1038/s41392-023-01472-x.

633. Chen, Y., Zhao, X., Zhou, H., Zhu, H., Jiang, S., and Wang, P. (2023). Broadly neutralizing antibodies to SARS-CoV-2 and other human coronaviruses. Nat Rev Immunol *23*, 189-199. 10.1038/s41577-022-00784-3.

634. Song, G., He, W.-t., Callaghan, S., Anzanello, F., Huang, D., Ricketts, J., Torres, J.L., Beutler, N., Peng, L., Vargas, S., et al. (2021). Cross-reactive serum and memory B-cell responses to spike protein in SARS-CoV-2 and endemic coronavirus infection. Nat. Commun. *12*, 2938. 10.1038/s41467-021-23074-3.

635. Nelson, C.E., Namasivayam, S., Foreman, T.W., Kauffman, K.D., Sakai, S., Dorosky, D.E., Lora, N.E., Brooks, K., Potter, E.L., Garza, N.L., et al. (2022). Mild SARS-CoV-2 infection in rhesus macaques is associated with viral control prior to antigen-specific T cell responses in tissues. Sci Immunol *7*, eabo0535. 10.1126/sciimmunol.abo0535.

636. Ziegler, C.G.K., Allon, S.J., Nyquist, S.K., Mbano, I.M., Miao, V.N., Tzouanas, C.N., Cao, Y., Yousif, A.S., Bals, J., Hauser, B.M., et al. (2020). SARS-CoV-2 Receptor ACE2 Is an Interferon-Stimulated Gene in Human Airway Epithelial

Cells and Is Detected in Specific Cell Subsets across Tissues. Cell *181*, 1016-1035.e1019. 10.1016/j.cell.2020.04.035.

637. Muñoz-Fontela, C., Widerspick, L., Albrecht, R.A., Beer, M., Carroll, M.W., Wit, E.d., Diamond, M.S., Dowling, W.E., Funnell, S.G.P., García-Sastre, A., et al. (2022). Advances and gaps in SARS-CoV-2 infection models. PLoS Pathog. *18*, e1010161. 10.1371/journal.ppat.1010161.

638. Gagne, M., Moliva, J.I., Foulds, K.E., Andrew, S.F., Flynn, B.J., Werner, A.P., Wagner, D.A., Teng, I.T., Lin, B.C., Moore, C., et al. (2022). mRNA-1273 or mRNA-Omicron boost in vaccinated macaques elicits similar B cell expansion, neutralizing responses, and protection from Omicron. Cell *185*, 1556-1571.e1518. 10.1016/j.cell.2022.03.038.

639. Waickman, A.T., Victor, K., Newell, K., Li, T., Friberg, H., Foulds, K.E., Roederer, M., Bolton, D.L., Currier, J.R., and Seder, R. (2022). mRNA-1273 vaccination protects against SARS-CoV-2–elicited lung inflammation in nonhuman primates. JCI Insight *7*, e160039. 10.1172/jci.insight.160039.

640. Viox, E.G., Hoang, T.N., Upadhyay, A.A., Nchioua, R., Hirschenberger, M., Strongin, Z., Tharp, G.K., Pino, M., Nguyen, K., Harper, J.L., et al. (2023). Modulation of type I interferon responses potently inhibits SARS-CoV-2 replication and inflammation in rhesus macaques. Sci Immunol *8*, eadg0033. 10.1126/sciimmunol.adg0033.

641. Singh, D.K., Singh, B., Ganatra, S.R., Gazi, M., Cole, J., Thippeshappa, R., Alfson, K.J., Clemmons, E., Gonzalez, O., Escobedo, R., et al. (2021).

Responses to acute infection with SARS-CoV-2 in the lungs of rhesus macaques, baboons and marmosets. Nat. Microbiol. *6*, 73-78. 10.1038/s41564-020-00841-4.

642. Fahlberg, M.D., Blair, R.V., Doyle-Meyers, L.A., Midkiff, C.C., Zenere, G., Russell-Lodrigue, K.E., Monjure, C.J., Haupt, E.H., Penney, T.P., Lehmicke, G., et al. (2020). Cellular events of acute, resolving or progressive COVID-19 in SARS-CoV-2 infected non-human primates. Nat. Commun. *11*, 6078. 10.1038/s41467-020-19967-4.

643. Aid, M., Busman-Sahay, K., Vidal, S.J., Maliga, Z., Bondoc, S., Starke, C., Terry, M., Jacobson, C.A., Wrijil, L., Ducat, S., et al. (2020). Vascular Disease and Thrombosis in SARS-CoV-2-Infected Rhesus Macaques. Cell *183*, 1354-1366.e1313. 10.1016/j.cell.2020.10.005.

644. Esaulova, E., Das, S., Singh, D.K., Choreño-Parra, J.A., Swain, A., Arthur, L., Rangel-Moreno, J., Ahmed, M., Singh, B., Gupta, A., et al. (2021). The immune landscape in tuberculosis reveals populations linked to disease and latency. Cell Host Microbe *29*, 165-178. 10.1016/j.chom.2020.11.013.

645. Yang, Y., Shen, C., Li, J., Yuan, J., Wei, J., Huang, F., Wang, F., Li, G., Li, Y., Xing, L., et al. (2020). Plasma IP-10 and MCP-3 levels are highly associated with disease severity and predict the progression of COVID-19. J Allergy Clin Immunol *146*, 119-127 e114. 10.1016/j.jaci.2020.04.027.

646. Kelley, N., Jeltema, D., Duan, Y., and He, Y. (2019). The NLRP3 Inflammasome: An Overview of Mechanisms of Activation and Regulation. Int J Mol Sci *20*. 10.3390/ijms20133328.

647. Andrews, N., Stowe, J., Kirsebom, F., Toffa, S., Rickeard, T., Gallagher, E., Gower, C., Kall, M., Groves, N., O'Connell, A.-M., et al. (2022). Covid-19 Vaccine Effectiveness against the Omicron (B.1.1.529) Variant. N. Engl. J. Med. *386*, 1532-1546. 10.1056/nejmoa2119451.

648. Sauer, M.M., Tortorici, M.A., Park, Y.-J., Walls, A.C., Homad, L., Acton, O.J., Bowen, J.E., Wang, C., Xiong, X., Schueren, W.d.v.d., et al. (2021). Structural basis for broad coronavirus neutralization. Nat. Struct. Mol. Biol. *28*, 478-486. 10.1038/s41594-021-00596-4.

649. Shah, P., Canziani, G.A., Carter, E.P., and Chaiken, I. (2021). The Case for S2: The Potential Benefits of the S2 Subunit of the SARS-CoV-2 Spike Protein as an Immunogen in Fighting the COVID-19 Pandemic. Front Immunol *12*, 637651. 10.3389/fimmu.2021.637651.

650. Singh, D.K., Aladyeva, E., Das, S., Singh, B., Esaulova, E., Swain, A., Ahmed, M., Cole, J., Moodley, C., Mehra, S., et al. (2022). Myeloid cell interferon responses correlate with clearance of SARS-CoV-2. Nat. Commun. *13*, 679. 10.1038/s41467-022-28315-7.

651. Chen, S.T., Park, M.D., Valle, D.M.D., Buckup, M., Tabachnikova, A., Thompson, R.C., Simons, N.W., Mouskas, K., Lee, B., Geanon, D., et al. (2022). A shift in lung macrophage composition is associated with COVID-19 severity and recovery. Sci Transl Med *14*, eabn5168-eabn5168. 10.1126/scitranslmed.abn5168.

652. Vidarsson, G., Dekkers, G., and Rispens, T. (2014). IgG Subclasses and Allotypes: From Structure to Effector Functions. Front Immunol *5*, 520. 10.3389/fimmu.2014.00520.

653. Wei, H., and Wang, J.-Y. (2021). Role of Polymeric Immunoglobulin Receptor in IgA and IgM Transcytosis. Int. J. Mol. Sci. *22*, 2284. 10.3390/ijms22052284.

654. Tan, S.T., Kwan, A.T., Rodríguez-Barraquer, I., Singer, B.J., Park, H.J., Lewnard, J.A., Sears, D., and Lo, N.C. (2023). Infectiousness of SARS-CoV-2 breakthrough infections and reinfections during the Omicron wave. Nat Med *29*, 358-365. 10.1038/s41591-022-02138-x.

655. Prunas, O., Warren, J.L., Crawford, F.W., Gazit, S., Patalon, T., Weinberger, D.M., and Pitzer, V.E. (2022). Vaccination with BNT162b2 reduces transmission of SARS-CoV-2 to household contacts in Israel. Science *375*, eabl4292. 10.1126/science.abl4292.

656. Jung, J., Kim, J.Y., Park, H., Park, S., Lim, J.S., Lim, S.Y., Bae, S., Lim, Y.-J., Kim, E.O., Kim, J., et al. (2022). Transmission and Infectious SARS-CoV-2 Shedding Kinetics in Vaccinated and Unvaccinated Individuals. JAMA Netw. Open *5*, e2213606. 10.1001/jamanetworkopen.2022.13606.

657. Abu-Raddad, L.J., Chemaitelly, H., Ayoub, H.H., Tang, P., Coyle, P., Hasan, M.R., Yassine, H.M., Benslimane, F.M., Al-Khatib, H.A., Al-Kanaani, Z., et al. (2022). Relative infectiousness of SARS-CoV-2 vaccine breakthrough infections, reinfections, and primary infections. Nat. Commun. *13*, 532. 10.1038/s41467-022-28199-7.

658. Chen, P.Z., Bobrovitz, N., Premji, Z.A., Koopmans, M., Fisman, D.N., and Gu, F.X. (2021). SARS-CoV-2 shedding dynamics across the respiratory tract, sex, and disease severity for adult and pediatric COVID-19. eLife *10*, e70458. 10.7554/elife.70458.

659. Chen, P.Z., Koopmans, M., Fisman, D.N., and Gu, F.X. (2021). Understanding why superspreading drives the COVID-19 pandemic but not the H1N1 pandemic. Lancet Infect. Dis. *21*, 1203-1204. 10.1016/s1473-3099(21)00406-0.

660. Marks, M., Millat-Martinez, P., Ouchi, D., Roberts, C.h., Alemany, A., Corbacho-Monné, M., Ubals, M., Tobias, A., Tebé, C., Ballana, E., et al. (2021). Transmission of COVID-19 in 282 clusters in Catalonia, Spain: a cohort study. Lancet Infect. Dis. *21*, 629-636. 10.1016/s1473-3099(20)30985-3.

661. Kampen, J.J.A.v., Vijver, D.A.M.C.v.d., Fraaij, P.L.A., Haagmans, B.L., Lamers, M.M., Okba, N., Akker, J.P.C.v.d., Endeman, H., Gommers, D.A.M.P.J., Cornelissen, J.J., et al. (2021). Duration and key determinants of infectious virus shedding in hospitalized patients with coronavirus disease-2019 (COVID-19). Nat. Commun. *12*, 267. 10.1038/s41467-020-20568-4.

662. Castro, V.T., Chardin, H., Santos, J.A.d., Barra, G.B., Castilho, G.R., Souza, P.M., Magalhães, P.d.O., Acevedo, A.C., and Guerra, E.N.S. (2023). Detection of anti-SARS-CoV-2 salivary antibodies in vaccinated adults. Front Immunol *14*, 1296603. 10.3389/fimmu.2023.1296603.

663. Stolovich-Rain, M., Kumari, S., Friedman, A., Kirillov, S., Socol, Y., Billan, M., Pal, R.R., Das, K., Golding, P., Oiknine-Djian, E., et al. (2023). Intramuscular mRNA

BNT162b2 vaccine against SARS-CoV-2 induces neutralizing salivary IgA. Front Immunol *13*, 933347. 10.3389/fimmu.2022.933347.

664. Cao, K.T., Cobos-Uribe, C., Knight, N., Jonnalagadda, R., Robinette, C., Jaspers, I., and Rebuli, M.E. (2023). SARS-CoV-2 mRNA vaccination induces an intranasal mucosal response characterized by neutralizing antibodies. J. Allergy Clin. Immunol.: Glob. *2*, 100129. 10.1016/j.jacig.2023.100129.

665. Gorochov, G., Ropers, J., Launay, O., Dorgham, K., Mata-Jardin, O.d., Lebbah, S., Durier, C., Bauer, R., Radenne, A., Desaint, C., et al. (2024). Serum and Salivary IgG and IgA Response After COVID-19 Messenger RNA Vaccination. JAMA Netw. Open *7*, e248051. 10.1001/jamanetworkopen.2024.8051.

666. Pooley, N., Karim, S.S.A., Combadière, B., Ooi, E.E., Harris, R.C., Seblain, C.E.G., Kisomi, M., and Shaikh, N. (2023). Durability of Vaccine-Induced and Natural Immunity Against COVID-19: A Narrative Review. Infect. Dis. Ther. *12*, 367-387. 10.1007/s40121-022-00753-2.

667. Fabiani, M., Puopolo, M., Morciano, C., Spuri, M., Alegiani, S.S., Filia, A., D'Ancona, F., Manso, M.D., Riccardo, F., Tallon, M., et al. (2022). Effectiveness of mRNA vaccines and waning of protection against SARS-CoV-2 infection and severe covid-19 during predominant circulation of the delta variant in Italy: retrospective cohort study. BMJ *376*, e069052. 10.1136/bmj-2021-069052.

668. Wang, Q., Guo, Y., Iketani, S., Nair, M.S., Li, Z., Mohri, H., Wang, M., Yu, J., Bowen, A.D., Chang, J.Y., et al. (2022). Antibody evasion by SARS-CoV-2 Omicron subvariants BA.2.12.1, BA.4 and BA.5. Nature *608*, 603-608. 10.1038/s41586-022-05053-w.

669. Feikin, D.R., Higdon, M.M., Abu-Raddad, L.J., Andrews, N., Araos, R., Goldberg, Y., Groome, M.J., Huppert, A., O'Brien, K.L., Smith, P.G., et al. (2022). Duration of effectiveness of vaccines against SARS-CoV-2 infection and COVID-19 disease: results of a systematic review and meta-regression. Lancet *399*, 924-944. 10.1016/s0140-6736(22)00152-0.

670. Britton, A., Fleming-Dutra, K.E., Shang, N., Smith, Z.R., Dorji, T., Derado, G., Accorsi, E.K., Ajani, U.A., Miller, J., Schrag, S.J., and Verani, J.R. (2022). Association of COVID-19 Vaccination With Symptomatic SARS-CoV-2 Infection by Time Since Vaccination and Delta Variant Predominance. JAMA *327*, 1032-1041. 10.1001/jama.2022.2068.

671. Bar-On, Y.M., Goldberg, Y., Mandel, M., Bodenheimer, O., Amir, O., Freedman, L., Alroy-Preis, S., Ash, N., Huppert, A., and Milo, R. (2022). Protection by a Fourth Dose of BNT162b2 against Omicron in Israel. N. Engl. J. Med. *386*, 1712-1720. 10.1056/nejmoa2201570.

672. Gazit, S., Saciuk, Y., Perez, G., Peretz, A., Pitzer, V.E., and Patalon, T. (2022). Short term, relative effectiveness of four doses versus three doses of BNT162b2 vaccine in people aged 60 years and older in Israel: retrospective, test negative, case-control study. BMJ *377*, e071113. 10.1136/bmj-2022-071113.

673. Winokur, P., Gayed, J., Fitz-Patrick, D., Thomas, S.J., Diya, O., Lockhart, S., Xu, X., Zhang, Y., Bangad, V., Schwartz, H.I., et al. (2023). Bivalent Omicron BA.1–Adapted BNT162b2 Booster in Adults Older than 55 Years. N. Engl. J. Med. *388*, 214-227. 10.1056/nejmoa2213082.

674. Mateo-Urdiales, A., Sacco, C., Fotakis, E.A., Manso, M.D., Bella, A., Riccardo, F., Bressi, M., Rota, M.C., Petrone, D., Siddu, A., et al. (2023). Relative effectiveness of monovalent and bivalent mRNA boosters in preventing severe COVID-19 due to omicron BA.5 infection up to 4 months post-administration in people aged 60 years or older in Italy: a retrospective matched cohort study. Lancet Infect. Dis. *23*, 1349-1359. 10.1016/s1473-3099(23)00374-2.

675. Usdan, L., Patel, S., Rodriguez, H., Xu, X., Lee, D.-Y., Finn, D., Wyper, H., Lowry, F.S., Mensa, F.J., Lu, C., et al. (2023). A Bivalent Omicron-BA.4/BA.5-Adapted BNT162b2 Booster in ≥12-Year-Olds. Clin. Infect. Dis., ciad718. 10.1093/cid/ciad718.

676. Khoury, D.S., Docken, S.S., Subbarao, K., Kent, S.J., Davenport, M.P., and Cromer, D. (2023). Predicting the efficacy of variant-modified COVID-19 vaccine boosters. Nat Med *29*, 574-578. 10.1038/s41591-023-02228-4.

677. Li, Y., Lai, D.-y., Zhang, H.-n., Jiang, H.-w., Tian, X., Ma, M.-l., Qi, H., Meng, Q.-f., Guo, S.-j., Wu, Y., et al. (2020). Linear epitopes of SARS-CoV-2 spike protein elicit neutralizing antibodies in COVID-19 patients. Cell. Mol. Immunol. *17*, 1095-1097. 10.1038/s41423-020-00523-5.

678. Imai, M., Ito, M., Kiso, M., Yamayoshi, S., Uraki, R., Fukushi, S., Watanabe, S., Suzuki, T., Maeda, K., Sakai-Tagawa, Y., et al. (2022). Efficacy of Antiviral Agents against Omicron Subvariants BQ.1.1 and XBB. N. Engl. J. Med. *388*, 89-91. 10.1056/nejmc2214302.

679. Wang, Q., Iketani, S., Li, Z., Liu, L., Guo, Y., Huang, Y., Bowen, A.D., Liu, M., Wang, M., Yu, J., et al. (2023). Alarming antibody evasion properties of rising

SARS-CoV-2 BQ and XBB subvariants. Cell *186*, 279-286.e278. 10.1016/j.cell.2022.12.018.

680. Takashita, E., Yamayoshi, S., Halfmann, P., Wilson, N., Ries, H., Richardson, A., Bobholz, M., Vuyk, W., Maddox, R., Baker, D.A., et al. (2022). In Vitro Efficacy of Antiviral Agents against Omicron Subvariant BA.4.6. N. Engl. J. Med. *387*, 2094-2097. 10.1056/nejmc2211845.

681. Wang, Q., Li, Z., Ho, J., Guo, Y., Yeh, A.Y., Mohri, H., Liu, M., Wang, M., Yu, J., Shah, J.G., et al. (2022). Resistance of SARS-CoV-2 omicron subvariant BA.4.6 to antibody neutralisation. Lancet Infect. Dis. *22*, 1666-1668. 10.1016/s1473-3099(22)00694-6.

682. Takashita, E., Yamayoshi, S., Simon, V., Bakel, H.v., Sordillo, E.M., Pekosz, A., Fukushi, S., Suzuki, T., Maeda, K., Halfmann, P., et al. (2022). Efficacy of Antibodies and Antiviral Drugs against Omicron BA.2.12.1, BA.4, and BA.5 Subvariants. N. Engl. J. Med. *387*, 468-470. 10.1056/nejmc2207519.

683. Administration, F.a.D. (2022). Fact sheet for healthcare providers: Emergency Use Authorization (EUA) of sotrovimab.

684. Administration, F.a.D. (2023). Fact sheet for healthcare providers: Emergency Use Authorization for Evusheld (tixagevimab co-packaged with cilgavimab).

685. Administration, F.a.D. (2022). Fact sheet for healthcare providers: Emergency Use Authorization (EUA) of bebtelovimab.

686. Scherer, E.M., Babiker, A., Adelman, M.W., Allman, B., Key, A., Kleinhenz, J.M., Langsjoen, R.M., Nguyen, P.-V., Onyechi, I., Sherman, J.D., et al. (2022). SARS-

CoV-2 Evolution and Immune Escape in Immunocompromised Patients. N. Engl. J. Med. *386*. 10.1056/nejmc2202861.

687. Bock, A. (2024). New Guidance Helps Clinicians Use Pemivibart to Protect Immunocompromised Patients From COVID-19. JAMA. 10.1001/jama.2024.18589.

688. Mullick, B., Magar, R., Jhunjhunwala, A., and Barati Farimani, A. (2021). Understanding mutation hotspots for the SARS-CoV-2 spike protein using Shannon Entropy and K-means clustering. Comput Biol Med *138*, 104915. 10.1016/j.compbiomed.2021.104915.

689. Rowe, L.A., Beddingfield, B.J., Goff, K., Killeen, S.Z., Chirichella, N.R., Melton, A., Roy, C.J., and Maness, N.J. (2022). Intra-Host SARS-CoV-2 Evolution in the Gut of Mucosally-Infected Chlorocebus aethiops (African Green Monkeys). Viruses *14*, 77. 10.3390/v14010077.

690. Choudhary, M.C., Deo, R., Evering, T.H., Chew, K.W., Giganti, M.J., Moser, C., Ritz, J., Regan, J., Flynn, J.P., Crain, C.R., et al. (2024). Characterization of Treatment Resistance and Viral Kinetics in the Setting of Single-Active Versus Dual-Active Monoclonal Antibodies Against Severe Acute Respiratory Syndrome Coronavirus 2. J. Infect. Dis. *230*, 394-402. 10.1093/infdis/jiae192.

691. Munster, V.J., Flagg, M., Singh, M., Yinda, C.K., Williamson, B.N., Feldmann, F., Pérez-Pérez, L., Schulz, J., Brumbaugh, B., Holbrook, M.G., et al. (2023). Subtle differences in the pathogenicity of SARS-CoV-2 variants of concern B.1.1.7 and B.1.351 in rhesus macaques. Sci Immunol *8*, eadg7015. 10.1126/sciimmunol.adg7015.

692. Routhu, N.K., Stampfer, S.D., Lai, L., Akhtar, A., Tong, X., Yuan, D., Chicz, T.M., McNamara, R.P., Jakkala, K., Davis-Gardner, M.E., et al. (2021). Efficacy of mRNA-1273 and Novavax ancestral or BA.1 spike booster vaccines against SARS-CoV-2 BA.5 infection in non-human primates. Science Advances *7*, eabj3627. 10.1126/sciadv.abj3627.

693. Zhou, P., Song, G., Liu, H., Yuan, M., He, W.-t., Beutler, N., Zhu, X., Tse, L.V., Martinez, D.R., Schäfer, A., et al. (2023). Broadly neutralizing anti-S2 antibodies protect against all three human betacoronaviruses that cause deadly disease. Immunity *56*, 669-686.e667. 10.1016/j.immuni.2023.02.005.

694. Corbett, K.S., Nason, M.C., Flach, B., Gagne, M., O'Connell, S., Johnston, T.S., Shah, S.N., Edara, V.V., Floyd, K., Lai, L., et al. (2021). Immune correlates of protection by mRNA-1273 vaccine against SARS-CoV-2 in nonhuman primates. Science *373*, eabj0299. 10.1126/science.abj0299.

695. Corbett, K.S., Flynn, B., Foulds, K.E., Francica, J.R., Boyoglu-Barnum, S., Werner, A.P., Flach, B., O'Connell, S., Bock, K.W., Minai, M., et al. (2020). Evaluation of the mRNA-1273 Vaccine against SARS-CoV-2 in Nonhuman Primates. N Engl J Med *383*, 1544-1555. 10.1056/NEJMoa2024671.

696. Rogers, T.F., Zhao, F., Huang, D., Beutler, N., Burns, A., He, W.-t., Limbo, O., Smith, C., Song, G., Woehl, J., et al. (2020). Isolation of potent SARS-CoV-2 neutralizing antibodies and protection from disease in a small animal model. Science *369*, 956-963. 10.1126/science.abc7520.

697. Integrated DNA Technologies, I. (2024). ARTIC SARS-CoV-2 Amplicon Panel; 10011442. https://www.idtdna.com/pages/products/next-generation-

sequencing/workflow/xgen-ngs-amplicon-sequencing/predesigned-amplicon-panels/artic-sc2-amp-panel.

698. Zheng, G.X.Y., Terry, J.M., Belgrader, P., Ryvkin, P., Bent, Z.W., Wilson, R., Ziraldo, S.B., Wheeler, T.D., McDermott, G.P., Zhu, J.J., et al. (2017). Massively parallel digital transcriptional profiling of single cells. Nat. Commun. *8*. ARTN 14049

10.1038/ncomms14049.

699. Hafemeister, C., and Satija, R. (2019). Normalization and variance stabilization of single-cell RNA-seq data using regularized negative binomial regression. Genome Biology *20*, 296. 10.1186/s13059-019-1874-1.

700. Stuart, T., Butler, A., Hoffman, P., Hafemeister, C., Papalexi, E., Mauck, W.M., Hao, Y., Stoeckius, M., Smibert, P., and Satija, R. (2019). Comprehensive Integration of Single-Cell Data. Cell *177*, 1888-1902.e1821. 10.1016/j.cell.2019.05.031.

701. Finak, G., McDavid, A., Yajima, M., Deng, J., Gersuk, V., Shalek, A.K., Slichter, C.K., Miller, H.W., McElrath, M.J., Prlic, M., et al. (2015). MAST: a flexible statistical framework for assessing transcriptional changes and characterizing heterogeneity in single-cell RNA sequencing data. Genome Biology *16*, 278. 10.1186/s13059-015-0844-5.

702. Travaglini, K.J., Nabhan, A.N., Penland, L., Sinha, R., Gillich, A., Sit, R.V., Chang, S., Conley, S.D., Mori, Y., Seita, J., et al. (2020). A molecular cell atlas of the human lung from single-cell RNA sequencing. Nature *587*, 619-625. 10.1038/s41586-020-2922-4.

703. Hao, Y., Hao, S., Andersen-Nissen, E., Mauck, W.M., Zheng, S., Butler, A., Lee, M.J., Wilk, A.J., Darby, C., Zager, M., et al. (2021). Integrated analysis of multimodal single-cell data. Cell *184*, 3573-3587.e3529. 10.1016/j.cell.2021.04.048.

704. Wu, T., Hu, E., Xu, S., Chen, M., Guo, P., Dai, Z., Feng, T., Zhou, L., Tang, W., Zhan, L., et al. (2021). clusterProfiler 4.0: A universal enrichment tool for interpreting omics data. Innov. *2*, 100141. 10.1016/j.xinn.2021.100141.

705. Subramanian, A., Tamayo, P., Mootha, V.K., Mukherjee, S., Ebert, B.L., Gillette, M.A., Paulovich, A., Pomeroy, S.L., Golub, T.R., Lander, E.S., and Mesirov, J.P. (2005). Gene set enrichment analysis: A knowledge-based approach for interpreting genome-wide expression profiles. Proc National Acad Sci *102*, 15545-15550. 10.1073/pnas.0506580102.

706. Liberzon, A., Birger, C., Thorvaldsdóttir, H., Ghandi, M., Mesirov, Jill P., and Tamayo, P. (2015). The Molecular Signatures Database Hallmark Gene Set Collection. Cell Syst. *1*, 417-425. 10.1016/j.cels.2015.12.004.

707. Liberzon, A., Birger, C., Thorvaldsdottir, H., Ghandi, M., Mesirov, J.P., and Tamayo, P. (2015). The Molecular Signatures Database (MSigDB) hallmark gene set collection. Cell Syst *1*, 417-425. 10.1016/j.cels.2015.12.004.

708. Liberzon, A., Subramanian, A., Pinchback, R., Thorvaldsdóttir, H., Tamayo, P., and Mesirov, J.P. (2011). Molecular signatures database (MSigDB) 3.0. Bioinformatics *27*, 1739-1740. 10.1093/bioinformatics/btr260.

709. Haynes, B.F., and Burton, D.R. (2017). Developing an HIV vaccine. Science *355*, 1129-1130. 10.1126/science.aan0662.

710. Flynn, N.M., Forthal, D.N., Harro, C.D., Judson, F.N., Mayer, K.H., Para, M.F., and Group, r.H.I.V.V.S. (2005). Placebo-Controlled Phase 3 Trial of a Recombinant Glycoprotein 120 Vaccine to Prevent HIV-1 Infection. J. Infect. Dis. *191*, 654-665. 10.1086/428404.

711. Pitisuttithum, P., Gilbert, P., Gurwith, M., Heyward, W., Martin, M., van Griensven, F., Hu, D., Tappero, Jordan W., Choopanya, K., and Group, B.V.E. (2006). Randomized, Double-Blind, Placebo-Controlled Efficacy Trial of a Bivalent Recombinant Glycoprotein 120 HIV-1 Vaccine among Injection Drug Users in Bangkok, Thailand. J. Infect. Dis. *194*, 1661-1671. 10.1086/508748.

712. Buchbinder, S.P., Mehrotra, D.V., Duerr, A., Fitzgerald, D.W., Mogg, R., Li, D., Gilbert, P.B., Lama, J.R., Marmor, M., Rio, C.d., et al. (2008). Efficacy assessment of a cell-mediated immunity HIV-1 vaccine (the Step Study): a double-blind, randomised, placebo-controlled, test-of-concept trial. Lancet *372*, 1881-1893. 10.1016/s0140-6736(08)61591-3.

713. Gray, G.E., Allen, M., Moodie, Z., Churchyard, G., Bekker, L.-G., Nchabeleng, M., Mlisana, K., Metch, B., Bruyn, G.d., Latka, M.H., et al. (2011). Safety and efficacy of the HVTN 503/Phambili Study of a clade-B-based HIV-1 vaccine in South Africa: a double-blind, randomised, placebo-controlled test-of-concept phase 2b study. Lancet Infect. Dis. *11*, 507-515. 10.1016/s1473-3099(11)70098-6.

714. Graham, B.S., Gilman, M.S.A., and McLellan, J.S. (2019). Structure-Based Vaccine Antigen Design. Annu. Rev. Med. *70*, 91-104. 10.1146/annurev-med-121217-094234.

715. Pegu, A., Hessell, A.J., Mascola, J.R., and Haigwood, N.L. (2017). Use of broadly neutralizing antibodies for HIV-1 prevention. Immunol Rev *275*, 296-312. 10.1111/imr.12511.

716. Caskey, M., Klein, F., Lorenzi, J.C.C., Seaman, M.S., West, A.P., Buckley, N., Kremer, G., Nogueira, L., Braunschweig, M., Scheid, J.F., et al. (2015). Viraemia suppressed in HIV-1-infected humans by broadly neutralizing antibody 3BNC117. Nature *522*, 487-491. 10.1038/nature14411.

717. Mascola, J.R., Lewis, M.G., Stiegler, G., Harris, D., VanCott, T.C., Hayes, D., Louder, M.K., Brown, C.R., Sapan, C.V., Frankel, S.S., et al. (1999). Protection of Macaques against Pathogenic Simian/Human Immunodeficiency Virus 89.6PD by Passive Transfer of Neutralizing Antibodies. J Virol *73*, 4009-4018. 10.1128/jvi.73.5.4009-4018.1999.

718. Mascola, J.R., Stiegler, G., VanCott, T.C., Katinger, H., Carpenter, C.B., Hanson, C.E., Beary, H., Hayes, D., Frankel, S.S., Birx, D.L., and Lewis, M.G. (2000). Protection of macaques against vaginal transmission of a pathogenic HIV-1/SIV chimeric virus by passive infusion of neutralizing antibodies. Nat Med *6*, 207-210. 10.1038/72318.

719. Baba, T.W., Liska, V., Hofmann-Lehmann, R., Vlasak, J., Xu, W., Ayehunie, S., Cavacini, L.A., Posner, M.R., Katinger, H., Stiegler, G., et al. (2000). Human neutralizing monoclonal antibodies of the IgG1 subtype protect against mucosal simian–human immunodeficiency virus infection. Nat Med *6*, 200-206. 10.1038/72309.

720. Hessell, A.J., Poignard, P., Hunter, M., Hangartner, L., Tehrani, D.M., Bleeker, W.K., Parren, P.W.H.I., Marx, P.A., and Burton, D.R. (2009). Effective, low-titer antibody protection against low-dose repeated mucosal SHIV challenge in macaques. Nat Med *15*, 951-954. 10.1038/nm.1974.

721. Parren, P.W.H.I., Marx, P.A., Hessell, A.J., Luckay, A., Harouse, J., Cheng-Mayer, C., Moore, J.P., and Burton, D.R. (2001). Antibody Protects Macaques against Vaginal Challenge with a Pathogenic R5 Simian/Human Immunodeficiency Virus at Serum Levels Giving Complete Neutralization In Vitro. J Virol *75*, 8340-8347. 10.1128/jvi.75.17.8340-8347.2001.

722. Hessell, A.J., Rakasz, E.G., Poignard, P., Hangartner, L., Landucci, G., Forthal, D.N., Koff, W.C., Watkins, D.I., and Burton, D.R. (2009). Broadly Neutralizing Human Anti-HIV Antibody 2G12 Is Effective in Protection against Mucosal SHIV Challenge Even at Low Serum Neutralizing Titers. PLoS Pathog. *5*, e1000433. 10.1371/journal.ppat.1000433.

723. Doria-Rose, N.A., Klein, R.M., Manion, M.M., O'Dell, S., Phogat, A., Chakrabarti, B., Hallahan, C.W., Migueles, S.A., Wrammert, J., Ahmed, R., et al. (2009). Frequency and Phenotype of Human Immunodeficiency Virus Envelope-Specific B Cells from Patients with Broadly Cross-Neutralizing Antibodies. J Virol *83*, 188-199. 10.1128/jvi.01583-08.

724. Dhillon, A.K., Donners, H., Pantophlet, R., Johnson, W.E., Decker, J.M., Shaw, G.M., Lee, F.-H., Richman, D.D., Doms, R.W., Vanham, G., and Burton, D.R. (2007). Dissecting the Neutralizing Antibody Specificities of Broadly Neutralizing

Sera from Human Immunodeficiency Virus Type 1-Infected Donors. J Virol *81*, 6548-6562. 10.1128/jvi.02749-06.

725. Sanders, R.W., and Moore, J.P. (2017). Native-like Env trimers as a platform for HIV-1 vaccine design. Immunol Rev *275*, 161-182. 10.1111/imr.12481.

726. Ringe, R.P., Sanders, R.W., Yasmeen, A., Kim, H.J., Lee, J.H., Cupo, A., Korzun, J., Derking, R., Montfort, T.v., Julien, J.-P., et al. (2013). Cleavage strongly influences whether soluble HIV-1 envelope glycoprotein trimers adopt a native-like conformation. Proc National Acad Sci *110*, 18256-18261. 10.1073/pnas.1314351110.

727. Pauthner, M., Havenar-Daughton, C., Sok, D., Nkolola, J.P., Bastidas, R., Boopathy, A.V., Carnathan, D.G., Chandrashekar, A., Cirelli, K.M., Cottrell, C.A., et al. (2017). Elicitation of Robust Tier 2 Neutralizing Antibody Responses in Nonhuman Primates by HIV Envelope Trimer Immunization Using Optimized Approaches. Immunity *46*, 1073-1088.e1076. 10.1016/j.immuni.2017.05.007.

728. Vukovich, M.J., Raju, N., Kgagudi, P., Manamela, N.P., Abu-Shmais, A.A., Gripenstraw, K.R., Wasdin, P.T., Shen, X.Y., Dwyer, B., Akoad, J., et al. (2024). Development of LIBRA-seq for the guinea pig model system as a tool for the evaluation of antibody responses to multivalent HIV-1 vaccines. J Virol *98*. 10.1128/jvi.01478-23.

729. Shiakolas, A.R., Kramer, K.J., Johnson, N.V., Wall, S.C., Suryadevara, N., Wrapp, D., Periasamy, S., Pilewski, K.A., Raju, N., Nargi, R., et al. (2022). Efficient discovery of SARS-CoV-2-neutralizing antibodies via B cell receptor

sequencing and ligand blocking. Nat Biotechnol *40*, 1270-1275. 10.1038/s41587-022-01232-2.

730. Johnson, N.V., Wall, S.C., Kramer, K.J., Holt, C.M., Periasamy, S., Richardson, S., Suryadevara, N., Andreano, E., Paciello, I., Pierleoni, G., et al. (2024). Discovery and Characterization of a Pan-betacoronavirus S2-binding antibody. Biorxiv, 2024.2001.2015.575741. 10.1101/2024.01.15.575741.

731. Vukovich, M.J., Shiakolas, A.R., Lindenberger, J., Richardson, R.A., Bass, L.E., Barr, M., Liu, Y., Go, E.P., Park, C.S., May, A.J., et al. (2024). Isolation and characterization of IgG3 glycan-targeting antibodies with exceptional cross-reactivity for diverse viral families. PLoS Pathog. *20*, e1012499. 10.1371/journal.ppat.1012499.

732. Galeota, E., Bevilacqua, V., Gobbini, A., Gruarin, P., Bombaci, M., Pesce, E., Favalli, A., Lombardi, A., Vincenti, F., Ongaro, J., et al. (2024). Tracking the immune response profiles elicited by the BNT162b2 vaccine in COVID-19 unexperienced and experienced individuals. Clin. Immunol. *261*, 110164. 10.1016/j.clim.2024.110164.

733. He, B., Liu, S., Wang, Y., Xu, M., Cai, W., Liu, J., Bai, W., Ye, S., Ma, Y., Hu, H., et al. (2021). Rapid isolation and immune profiling of SARS-CoV-2 specific memory B cell in convalescent COVID-19 patients via LIBRA-seq. Signal Transduct. Target. Ther. *6*, 195. 10.1038/s41392-021-00610-7.

734. Walker, L.M., Shiakolas, A.R., Venkat, R., Liu, Z.A., Wall, S., Raju, N., Pilewski, K.A., Setliff, I., Murji, A.A., Gillespie, R., et al. (2022). High-Throughput B Cell

Epitope Determination by Next-Generation Sequencing. Front Immunol *13*, 855772. 10.3389/fimmu.2022.855772.

735. Abu-Shmais, A.A., Vukovich, M.J., Wasdin, P.T., Suresh, Y.P., Marinov, T.M., Rush, S.A., Gillespie, R.A., Sankhala, R.S., Choe, M., Joyce, M.G., et al. (2024). Antibody sequence determinants of viral antigen specificity. Mbio *15*, e01560-01524. 10.1128/mbio.01560-24.

736. Pilewski, K.A., Wall, S., Richardson, S.I., Manamela, N.P., Clark, K., Hermanus, T., Binshtein, E., Venkat, R., Sautto, G.A., Kramer, K.J., et al. (2023). Functional HIV-1/HCV cross-reactive antibodies isolated from a chronically co-infected donor. Cell Reports *42*, 112044. 10.1016/j.celrep.2023.112044.

737. Song, Y., Wang, J., Yang, Z., He, Q., Bao, C., Xie, Y., Sun, Y., Li, S., Quan, Y., Yang, H., and Li, C. (2024). Heterologous booster vaccination enhances antibody responses to SARS-CoV-2 by improving Tfh function and increasing B-cell clonotype SHM frequency. Front Immunol *15*, 1406138. 10.3389/fimmu.2024.1406138.

738. Shiakolas, A.R., Kramer, K.J., Wrapp, D., Richardson, S.I., Schäfer, A., Wall, S., Wang, N., Janowska, K., Pilewski, K.A., Venkat, R., et al. (2021). Cross-reactive coronavirus antibodies with diverse epitope specificities and Fc effector functions. Cell Rep. Med. *2*, 100313. 10.1016/j.xcrm.2021.100313.

739. Suryadevara, N., Shiakolas, A.R., VanBlargan, L.A., Binshtein, E., Chen, R.E., Case, J.B., Kramer, K.J., Armstrong, E.C., Myers, L., Trivette, A., et al. (2022). An antibody targeting the N-terminal domain of SARS-CoV-2 disrupts the spike trimer. J Clin Invest *132*, e159062. 10.1172/jci159062.

740. Weaver, G.C., Villar, R.F., Kanekiyo, M., Nabel, G.J., Mascola, J.R., and Lingwood, D. (2016). In vitro reconstitution of B cell receptor–antigen interactions to evaluate potential vaccine candidates. Nat Protoc *11*, 193-213. 10.1038/nprot.2016.009.

741. Schooten, J.v., Haaren, M.M.v., Li, H., McCoy, L.E., Havenar-Daughton, C., Cottrell, C.A., Burger, J.A., Woude, P.v.d., Helgers, L.C., Tomris, I., et al. (2021). Antibody responses induced by SHIV infection are more focused than those induced by soluble native HIV-1 envelope trimers in non-human primates. PLoS Pathog. *17*, e1009736. 10.1371/journal.ppat.1009736.

742. Sanders, R.W., Gils, M.J.v., Derking, R., Sok, D., Ketas, T.J., Burger, J.A., Ozorowski, G., Cupo, A., Simonich, C., Goo, L., et al. (2015). HIV-1 neutralizing antibodies induced by native-like envelope trimers. Science *349*, aac4223. 10.1126/science.aac4223.

743. Havenar-Daughton, C., Carnathan, D.G., Peña, A.T.d.l., Pauthner, M., Briney, B., Reiss, S.M., Wood, J.S., Kaushik, K., Gils, M.J.v., Rosales, S.L., et al. (2016). Direct Probing of Germinal Center Responses Reveals Immunological Features and Bottlenecks for Neutralizing Antibody Responses to HIV Env Trimer. Cell Reports *17*, 2195-2209. 10.1016/j.celrep.2016.10.085.

744. Zhang, P., Narayanan, E., Liu, Q., Tsybovsky, Y., Boswell, K., Ding, S., Hu, Z., Follmann, D., Lin, Y., Miao, H., et al. (2021). A multiclade env–gag VLP mRNA vaccine elicits tier-2 HIV-1-neutralizing antibodies and reduces the risk of heterologous SHIV infection in macaques. Nat Med *27*, 2234-2245. 10.1038/s41591-021-01574-5.

745. Sahoo, A., Hodge, E.A., LaBranche, C.C., Styles, T.M., Shen, X., Cheedarla, N., Shiferaw, A., Ozorowski, G., Lee, W.-H., Ward, A.B., et al. (2022). Structure-guided changes at the V2 apex of HIV-1 clade C trimer enhance elicitation of autologous neutralizing and broad V1V2-scaffold antibodies. Cell Reports *38*, 110436. 10.1016/j.celrep.2022.110436.

746. Petitdemange, C., Kasturi, S.P., Kozlowski, P.A., Nabi, R., Quarnstrom, C.F., Reddy, P.B.J., Derdeyn, C.A., Spicer, L.M., Patel, P., Legere, T., et al. (2019). Vaccine induction of antibodies and tissue-resident CD8+ T cells enhances protection against mucosal SHIV-infection in young macaques. JCI Insight *4*, e126047. 10.1172/jci.insight.126047.

747. Ramesh, A., Darko, S., Hua, A., Overman, G., Ransier, A., Francica, J.R., Trama, A., Tomaras, G.D., Haynes, B.F., Douek, D.C., and Kepler, T.B. (2017). Structure and Diversity of the Rhesus Macaque Immunoglobulin Loci through Multiple De Novo Genome Assemblies. Front Immunol *8*, 1407. 10.3389/fimmu.2017.01407.

748. Manso, T., Folch, G., Giudicelli, V., Jabado-Michaloud, J., Kushwaha, A., Ngoune, V.N., Georga, M., Papadaki, A., Debbagh, C., Pégorier, P., et al. (2021). IMGT® databases, related tools and web resources through three main axes of research and development. Nucleic Acids Res. *50*, D1262-D1272. 10.1093/nar/gkab1136.

749. Cirelli, K.M., Carnathan, D.G., Nogal, B., Martin, J.T., Rodriguez, O.L., Upadhyay, A.A., Enemuo, C.A., Gebru, E.H., Choe, Y., Viviano, F., et al. (2019). Slow Delivery Immunization Enhances HIV Neutralizing Antibody and Germinal Center

Responses via Modulation of Immunodominance. Cell *177*, 1153-1171.e1128. 10.1016/j.cell.2019.04.012.

750. Bernat, N.V., Corcoran, M., Nowak, I., Kaduk, M., Dopico, X.C., Narang, S., Maisonasse, P., Dereuddre-Bosquet, N., Murrell, B., and Hedestam, G.B.K. (2021). Rhesus and cynomolgus macaque immunoglobulin heavy-chain genotyping yields comprehensive databases of germline VDJ alleles. Immunity *54*, 355-366.e354. 10.1016/j.immuni.2020.12.018.

751. Zhang, W., Wang, I.M., Wang, C., Lin, L., Chai, X., Wu, J., Bett, A.J., Dhanasekaran, G., Casimiro, D.R., and Liu, X. (2016). IMPre: An Accurate and Efficient Software for Prediction of T- and B-Cell Receptor Germline Genes and Alleles from Rearranged Repertoire Data. Front Immunol *7*, 457. 10.3389/fimmu.2016.00457.

752. Ye, J., Ma, N., Madden, T.L., and Ostell, J.M. (2013). IgBLAST: an immunoglobulin variable domain sequence analysis tool. Nucleic Acids Res. *41*, W34-W40. 10.1093/nar/gkt382.

753. Hao, Y., Stuart, T., Kowalski, M.H., Choudhary, S., Hoffman, P., Hartman, A., Srivastava, A., Molla, G., Madad, S., Fernandez-Granda, C., and Satija, R. (2024). Dictionary learning for integrative, multimodal and scalable single-cell analysis. Nat Biotechnol *42*, 293-304. 10.1038/s41587-023-01767-y.

754. Gupta, N.T., Heiden, J.A.V., Uduman, M., Gadala-Maria, D., Yaari, G., and Kleinstein, S.H. (2015). Change-O: a toolkit for analyzing large-scale B cell immunoglobulin repertoire sequencing data. Bioinformatics *31*, 3356-3358. 10.1093/bioinformatics/btv359.

755. Krzywinski, M., Schein, J., Birol, İ., Connors, J., Gascoyne, R., Horsman, D., Jones, S.J., and Marra, M.A. (2009). Circos: An information aesthetic for comparative genomics. Genome Res *19*, 1639-1645. 10.1101/gr.092759.109.

756. Peres, A., Upadhyay, A.A., Klein, V., Saha, S., Rodriguez, O.L., Vanwinkle, Z.M., Karunakaran, K., Metz, A., Lauer, W., Lin, M.C., et al. (2025). A Broad Survey and Functional Analysis of Immunoglobulin Loci Variation in Rhesus Macaques. Biorxiv, 2025.2001.2007.631319. 10.1101/2025.01.07.631319.

757. Li, P., Faraone, J.N., Hsu, C.C., Chamblee, M., Liu, Y., Zheng, Y.M., Xu, Y., Carlin, C., Horowitz, J.C., Mallampalli, R.K., et al. (2024). Neutralization and Stability of JN.1-derived LB.1, KP.2.3, KP.3 and KP.3.1.1 Subvariants. Biorxiv. 10.1101/2024.09.04.611219.

758. Usdan, L., Patel, S., Rodriguez, H., Xu, X., Lee, D.Y., Finn, D., Wyper, H., Lowry, F.S., Mensa, F.J., Lu, C., et al. (2024). A Bivalent Omicron-BA.4/BA.5-Adapted BNT162b2 Booster in >/=12-Year-Olds. Clin Infect Dis *78*, 1194-1203. 10.1093/cid/ciad718.

759. Xie, Y., Choi, T., and Al-Aly, Z. (2024). Postacute Sequelae of SARS-CoV-2 Infection in the Pre-Delta, Delta, and Omicron Eras. N. Engl. J. Med. *391*, 515-525. 10.1056/nejmoa2403211.

760. Ozonoff, A., Jayavelu, N.D., Liu, S., Melamed, E., Milliren, C.E., Qi, J., Geng, L.N., McComsey, G.A., Cairns, C.B., Baden, L.R., et al. (2024). Features of acute COVID-19 associated with post-acute sequelae of SARS-CoV-2 phenotypes: results from the IMPACC study. Nat. Commun. *15*, 216. 10.1038/s41467-023-44090-5.

761. Kwon, T. (2024). Utilizing non-human primate models to combat recent COVID-19/SARS-CoV-2 and viral infectious disease outbreaks. J. Méd. Primatol. *53*, e12689. 10.1111/jmp.12689.

762. Yinda, C.K., Port, J.R., Bushmaker, T., Owusu, I.O., Purushotham, J.N., Avanzato, V.A., Fischer, R.J., Schulz, J.E., Holbrook, M.G., Hebner, M.J., et al. (2021). K18-hACE2 mice develop respiratory disease resembling severe COVID-19. PLoS Pathog. *17*, e1009195. 10.1371/journal.ppat.1009195.

763. Seehusen, F., Clark, J.J., Sharma, P., Bentley, E.G., Kirby, A., Subramaniam, K., Wunderlin-Giuliani, S., Hughes, G.L., Patterson, E.I., Michael, B.D., et al. (2022). Neuroinvasion and Neurotropism by SARS-CoV-2 Variants in the K18-hACE2 Mouse. Viruses *14*, 1020. 10.3390/v14051020.

764. Avnir, Y., Watson, C.T., Glanville, J., Peterson, E.C., Tallarico, A.S., Bennett, A.S., Qin, K., Fu, Y., Huang, C.-Y., Beigel, J.H., et al. (2016). IGHV1-69 polymorphism modulates anti-influenza antibody repertoires, correlates with IGHV utilization shifts and varies by ethnicity. Sci Rep-uk *6*, 20842. 10.1038/srep20842.

765. Wheatley, A.K., and Kent, S.J. (2015). Prospects for antibody-based universal influenza vaccines in the context of widespread pre-existing immunity. Expert Rev. Vaccines *14*, 1227-1239. 10.1586/14760584.2015.1068125.

766. Pushparaj, P., Nicoletto, A., Sheward, D.J., Das, H., Dopico, X.C., Vidakovics, L.P., Hanke, L., Chernyshev, M., Narang, S., Kim, S., et al. (2023). Immunoglobulin germline gene polymorphisms influence the function of SARS-CoV-2 neutralizing antibodies. Immunity *56*, 193-206.e197. 10.1016/j.immuni.2022.12.005.

767. Leggat, D.J., Cohen, K.W., Willis, J.R., Fulp, W.J., deCamp, A.C., Kalyuzhniy, O., Cottrell, C.A., Menis, S., Finak, G., Ballweber-Fleming, L., et al. (2022). Vaccination induces HIV broadly neutralizing antibody precursors in humans. Science *378*, eadd6502. 10.1126/science.add6502.

768. Mahobe, R. (2022). U.S. FDA approves Gilead's long-acting HIV drug Sunlenca. Reuters.